Three-Dimensional Simulation Of River Flood Flows

Volume II: Figures

Hervé P. Morvan
(Eng. ESTP Paris, M.Sc.)

Thesis submitted for the degree of
Doctor of Philosophy
in the department of Civil Engineering,
The University of Glasgow

Department of Civil Engineering,
The University of Glasgow
Rankine Building
Oakfield Avenue
Glasgow G12 8LT

June 2001

Conventions

The following conventions are used consistently in the following thesis:

- Cross-sectional figures are plotted looking in the downstream direction.
- Velocity figures display the velocity magnitude or norm, calculated as the square root of the three spatial components of the velocity elevated to the power of 2.
- Angle plots refer to the direction of the velocity vector in the horizontal plane, with respect to the normal to the cross-section (which represents the 0°). Positive angles are measured when the velocity direction is heading towards the left with respect to the normal (0°), and the value of the angle is that between the velocity direction and the normal. When the velocity is heading towards the right hand side, this is considered a negative angle and measured using the same convention. These were the conventions used by the FCF experimentalists.
- All units are SI units unless stated otherwise.

List of Figures

Chapter 4:
Grids, Boundary Conditions, Solution Techniques and other Numerical Issues

Figures for Chapter 4

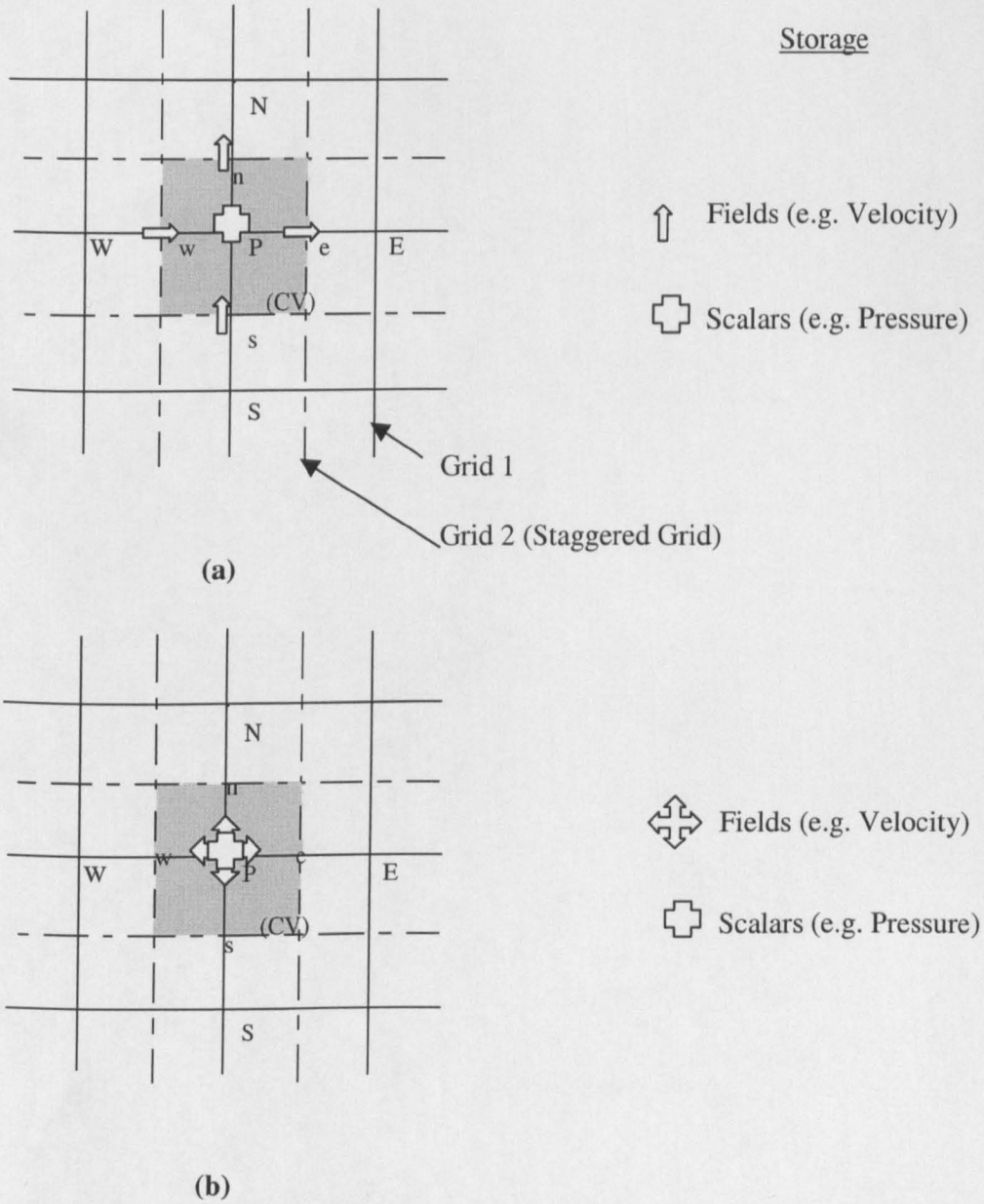

Fig. 4.1 – Finite Volume Grids: (a) Staggered Grid, (b) Non-Staggered Grid

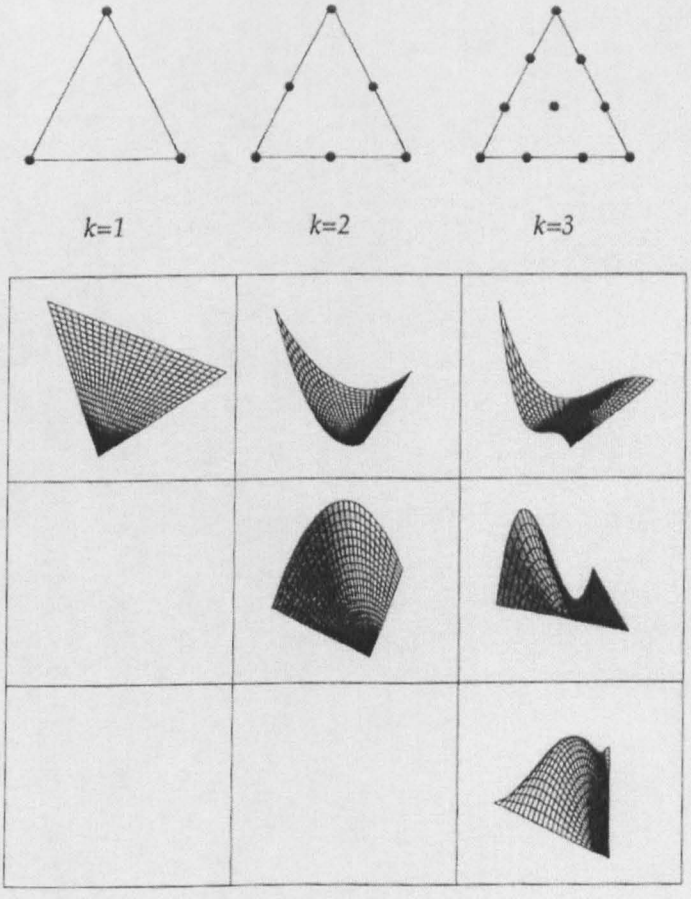

Fig. 4.2 – Shape Functions: Linear, Parabolic and Cubic (After Quarteroni and Valli, 1994)

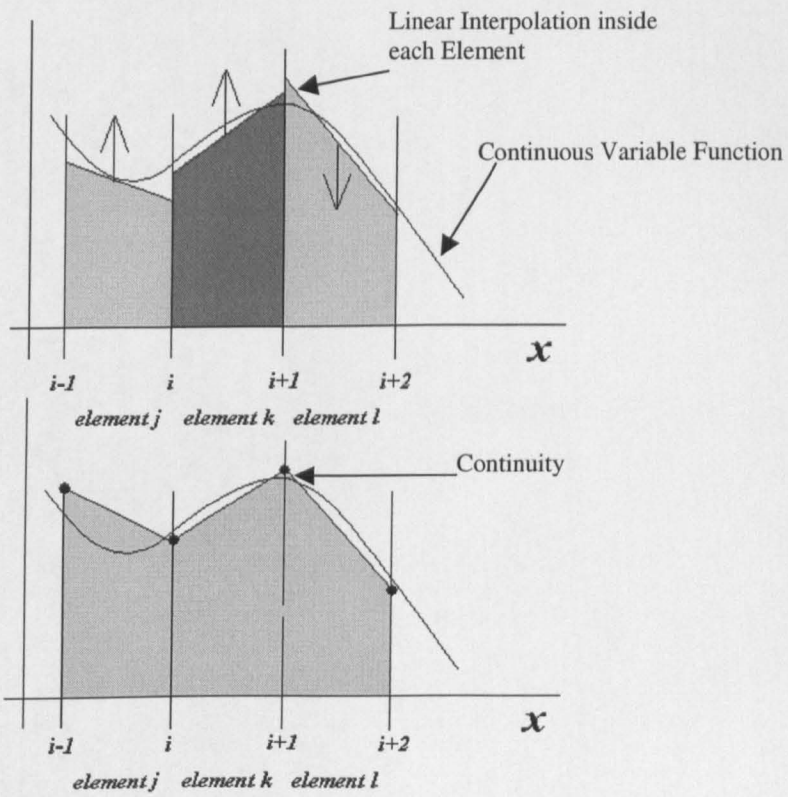

Fig. 4.3 – Illustration of A Finite Element Approximation

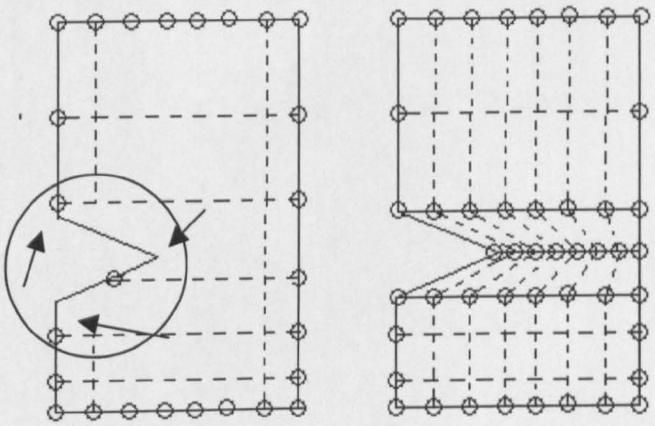

Fig. 4.4 – Multiblock Geometry and Meshing

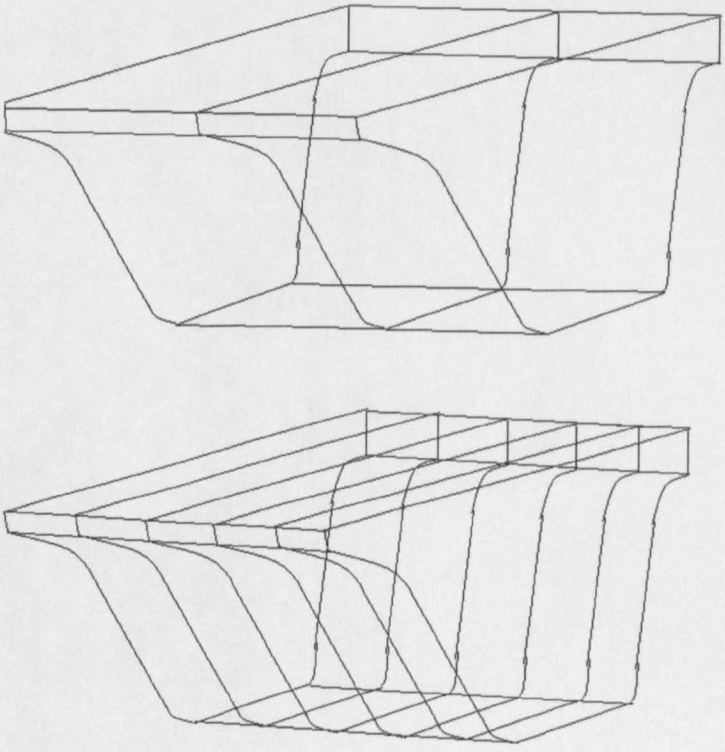

Fig. 4.5 - Three-Dimensional Geometrical Representation of a Channel:

(a) Two-Solid Representation,

(b) Five-Solid Representation.

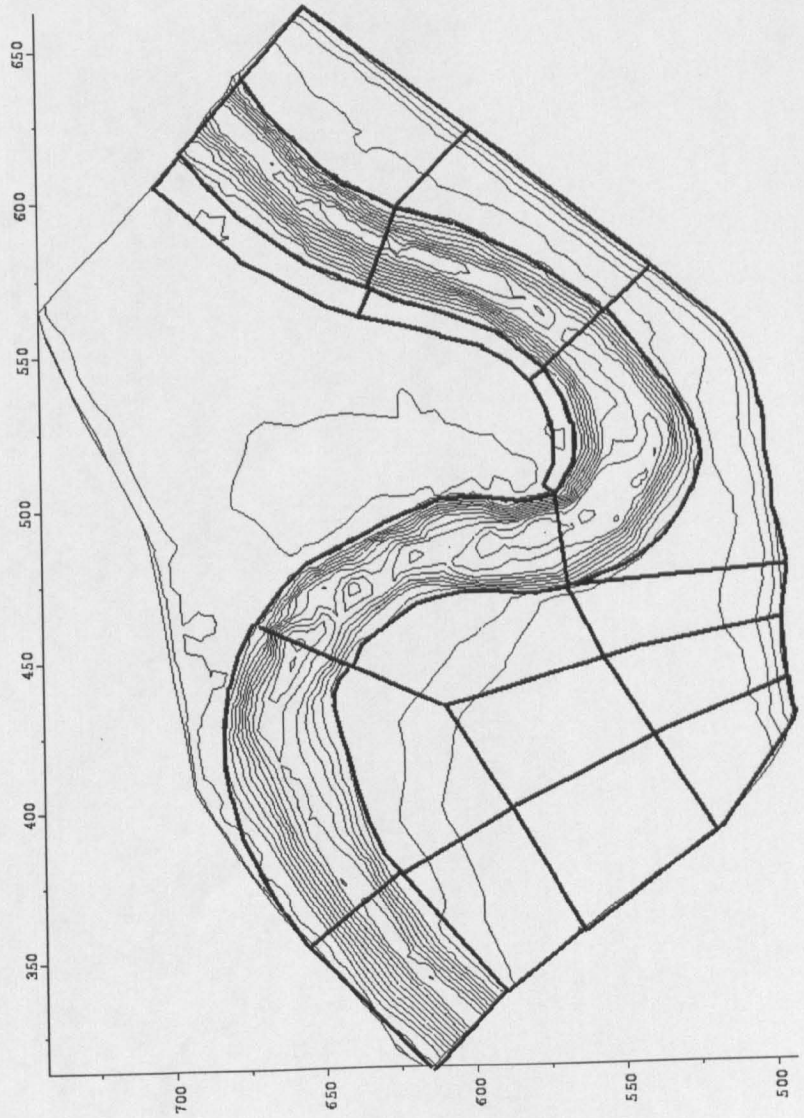

Fig. 4.6 – Severn Plan View Multi-Block Structure for CFX Mesh Generation

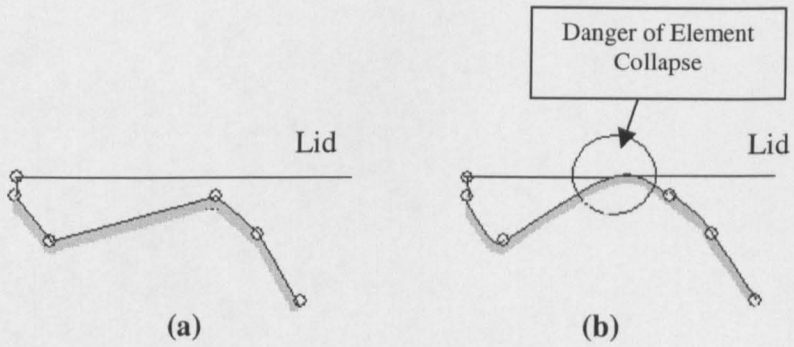

Fig. 4.7 – Cross-Sectional Representation of the Bottom Topography

(a) Composite Edge made of Linear Interpolation;

(b) Quadratic Interpolation or Spline.

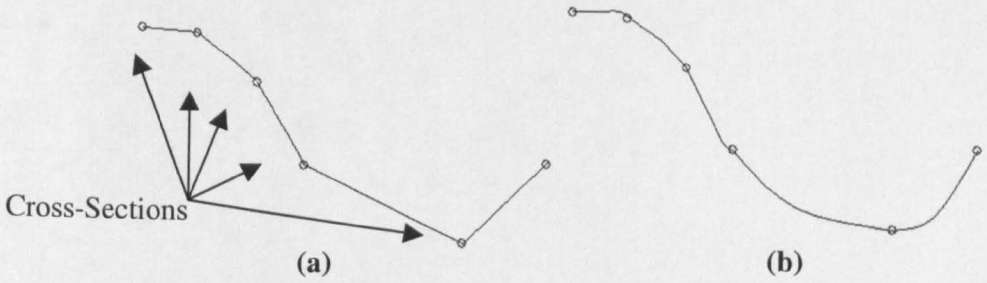

Fig. 4.8 – Plan View Representation of a Meander: (a) Linear, (b) Spline.

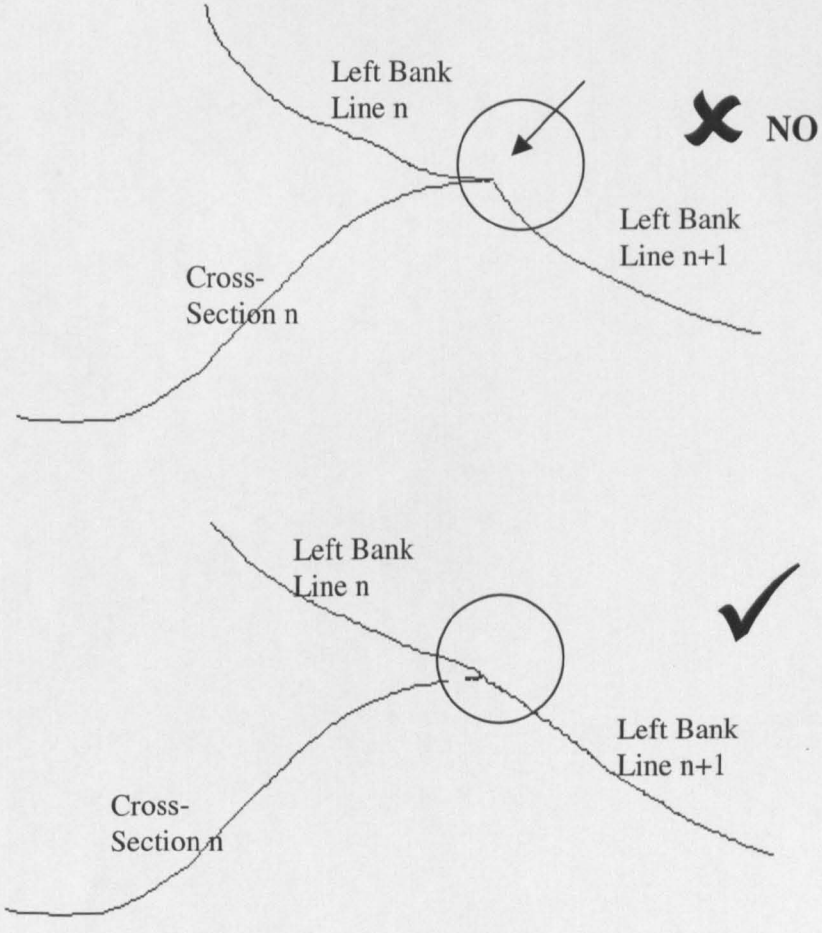

Fig. 4.9 –Bank Line Inter-Block Connection in CFX

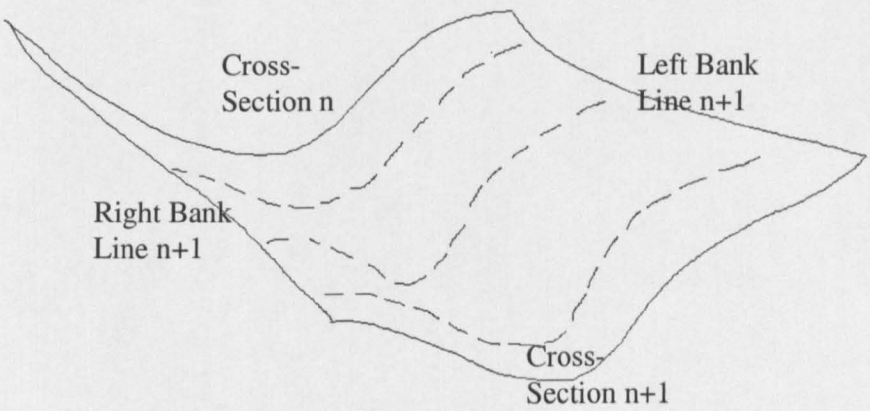

Fig. 4.10 – Bed Surface for a Natural Channel Block in CFX

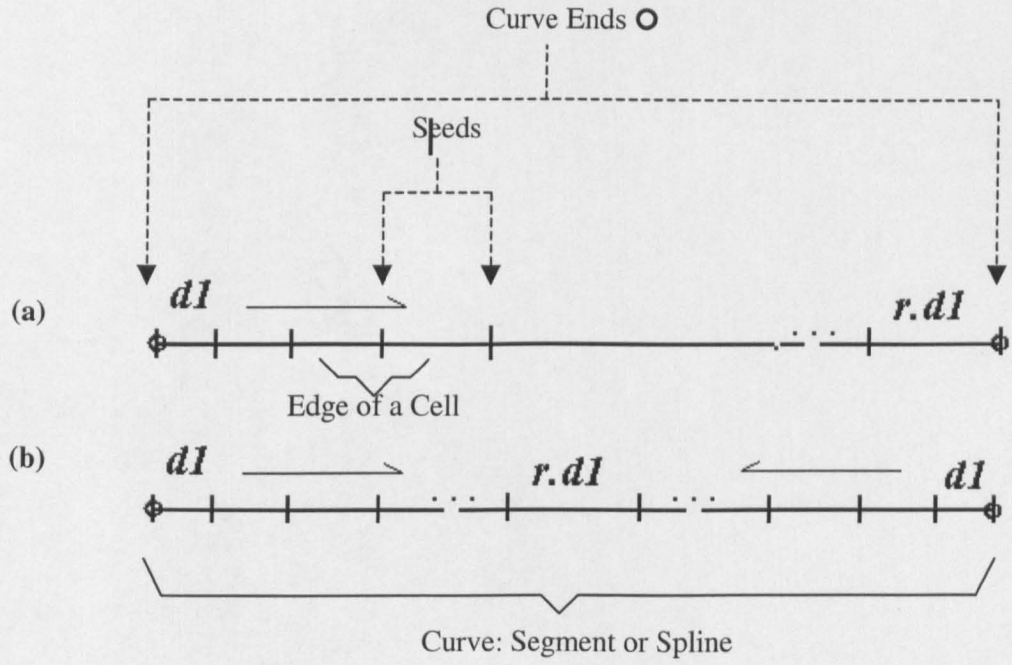

Fig. 4.11 – Mesh Point Generation along a Curve in CFX: (a) one-directional, (b) bi-directional

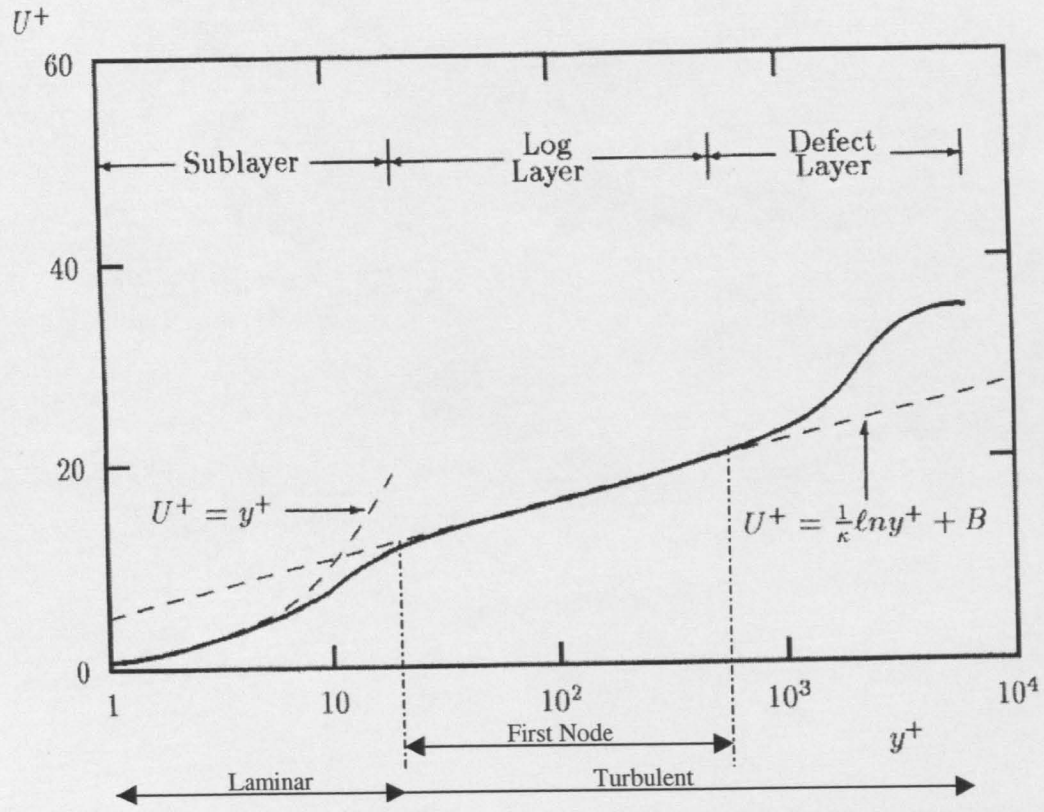

Fig. 4.12 –Velocity Profile for a Turbulent Boundary Layer (adapted from Wilcox, 1993)

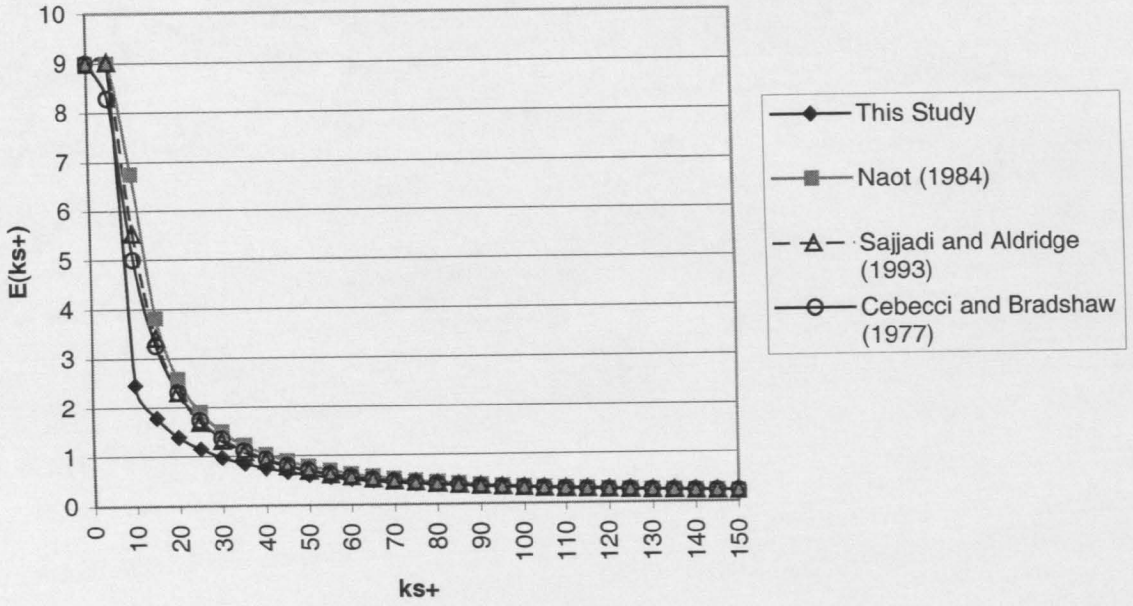

Fig. 4.13 – Law of the Wall *E* Value as a Function of the Non-dimensional Roughness

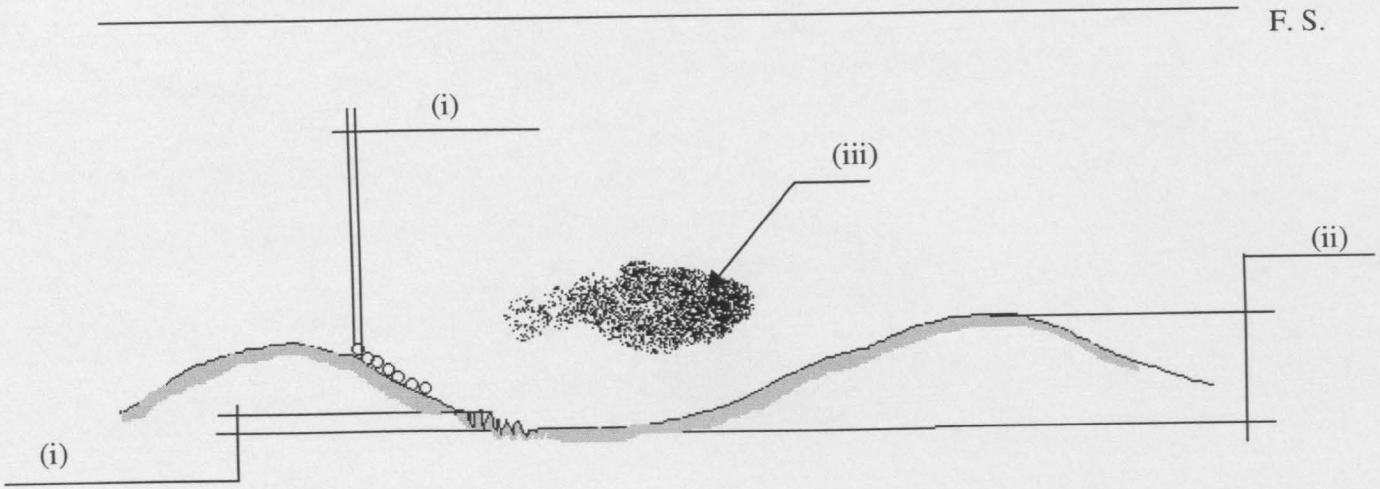

4.14 – Parameters Influencing Roughness Height at the Walls:
(i) Grain Roughness, (ii) Bedform Roughness, and (iii) Suspended Particle Roughness

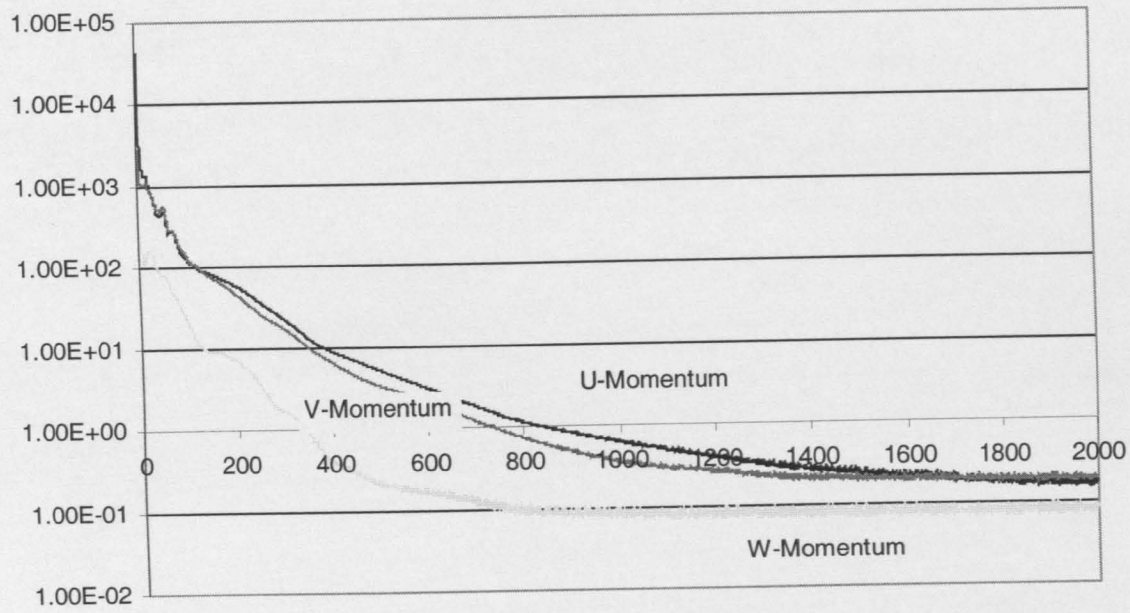

Fig. 4.15 - Convergence History
(FCF Model, Grid FCF-3, K-Epsilon Model, *ks* = 0.2 mm)

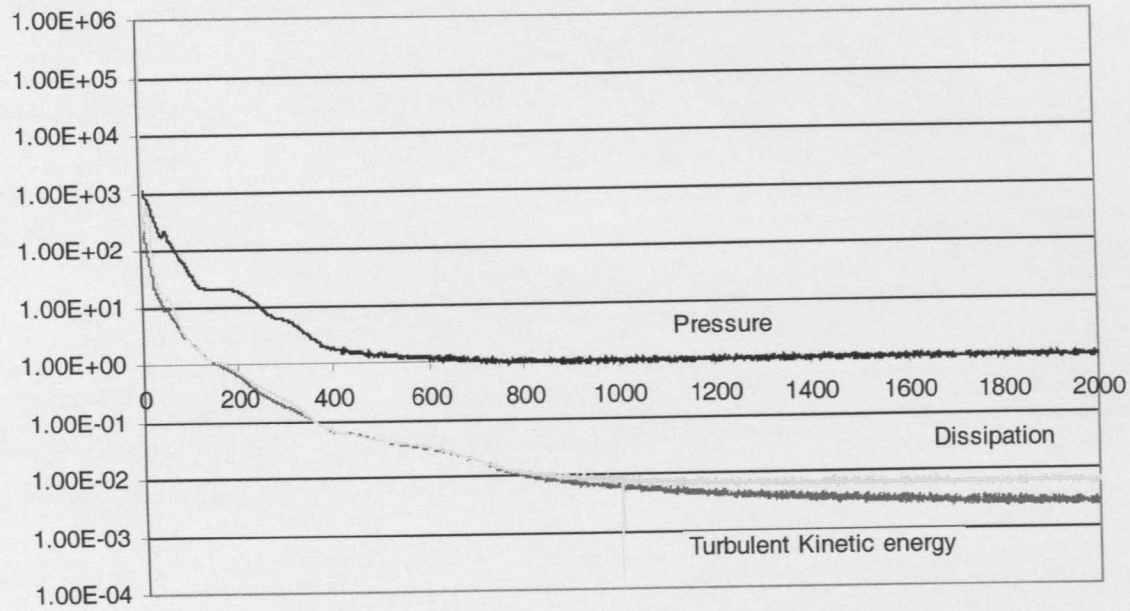

Fig. 4.16 - Convergence History
(FCF Model, Grid FCF-3, K-Epsilon Model, *ks* = 0.2 mm)

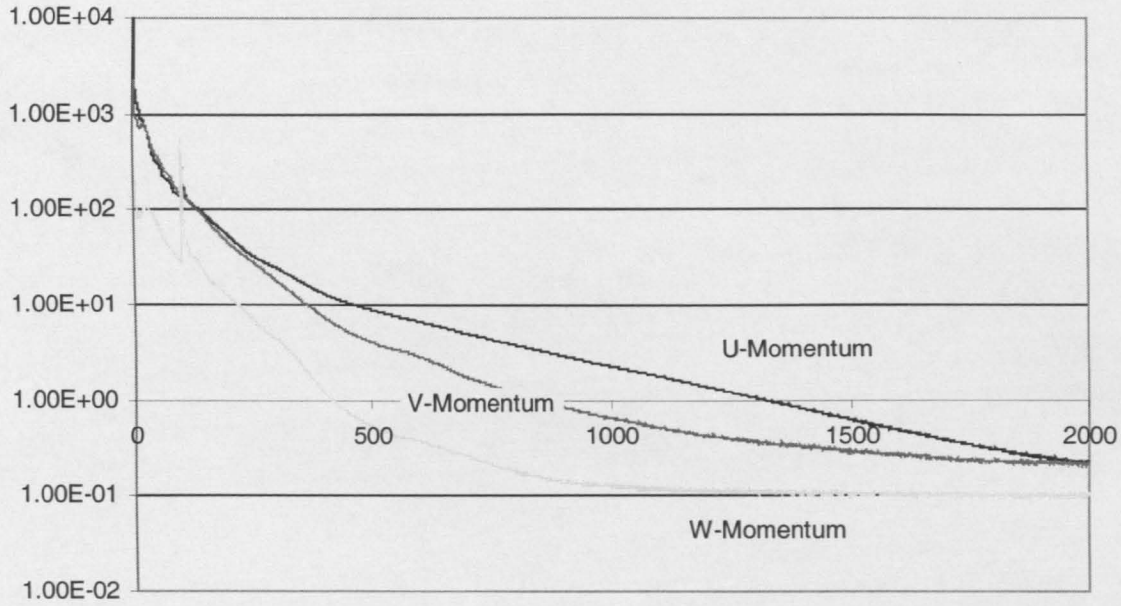

Fig. 4.17 - Convergence History
(FCF Model, Grid FCF-3, RSM, *ks* = 0.8 mm)

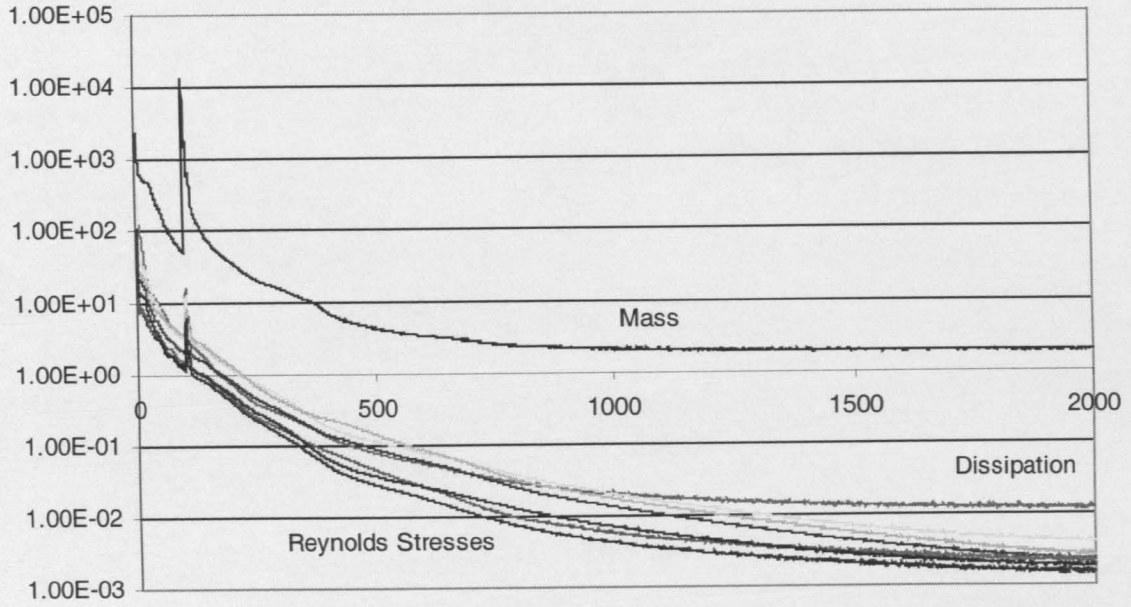

Fig. 4.18 - Convergence History
(FCF Model, Grid FCF-3, RSM, *ks* = 0.8 mm)

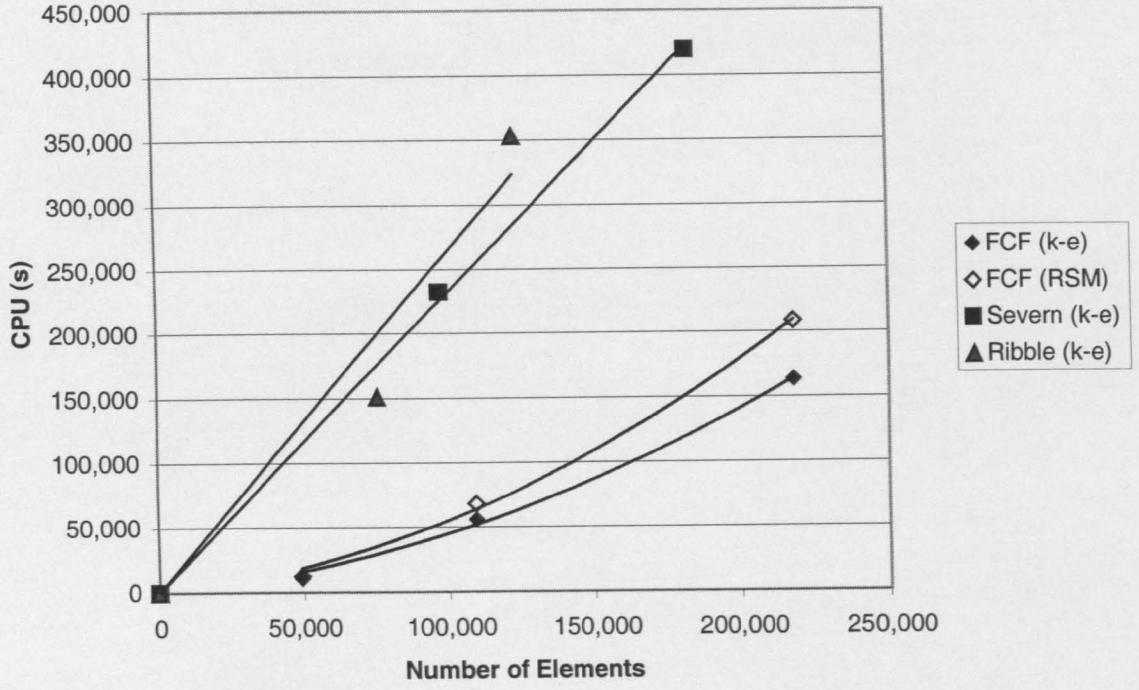

Fig. 4.19 – Scalability of CFX 4.2 for FCF Experiment B23 and River Applications

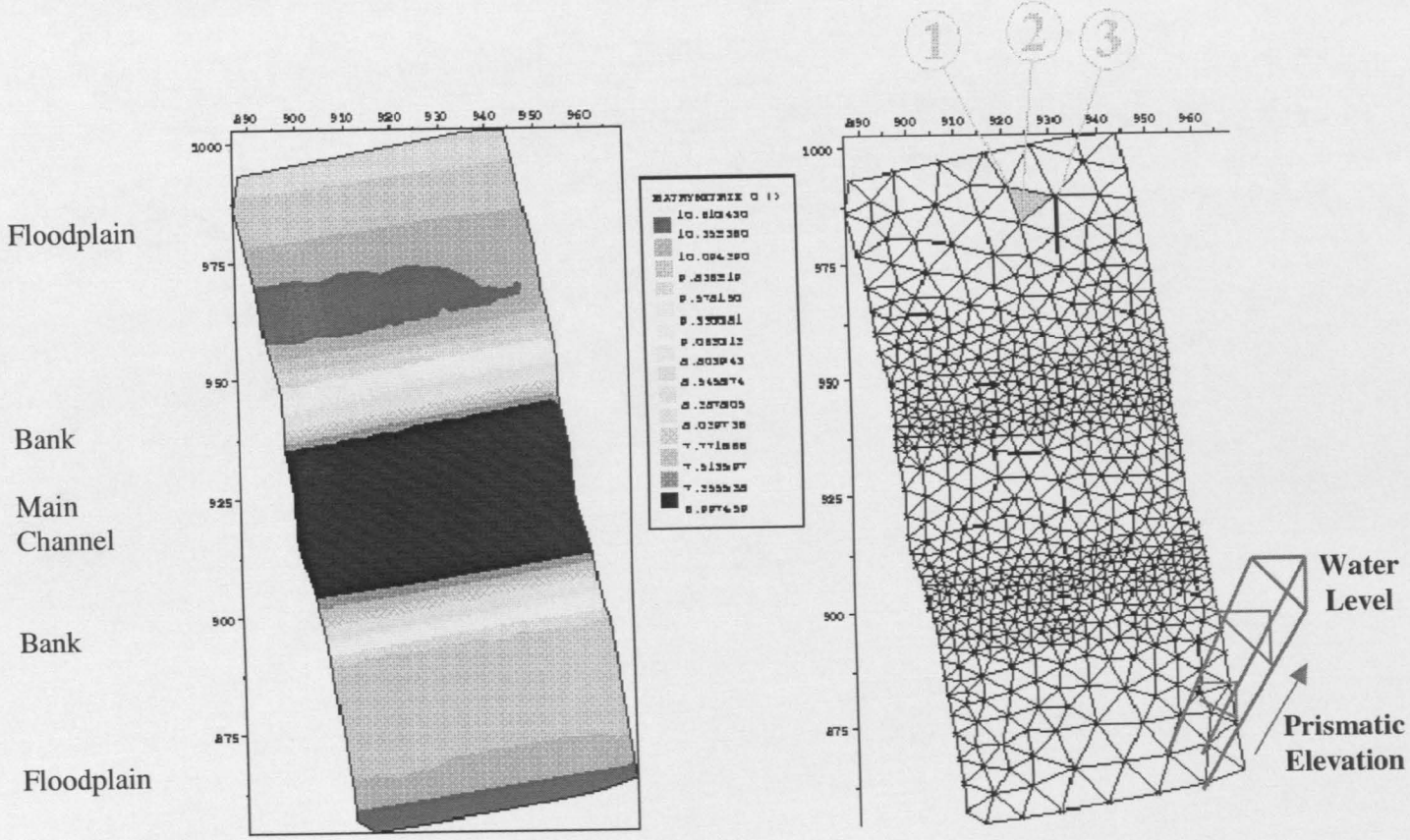

Fig. 4.20 – Topographical Representation and Mesh for a Channel Section in TELEMAC

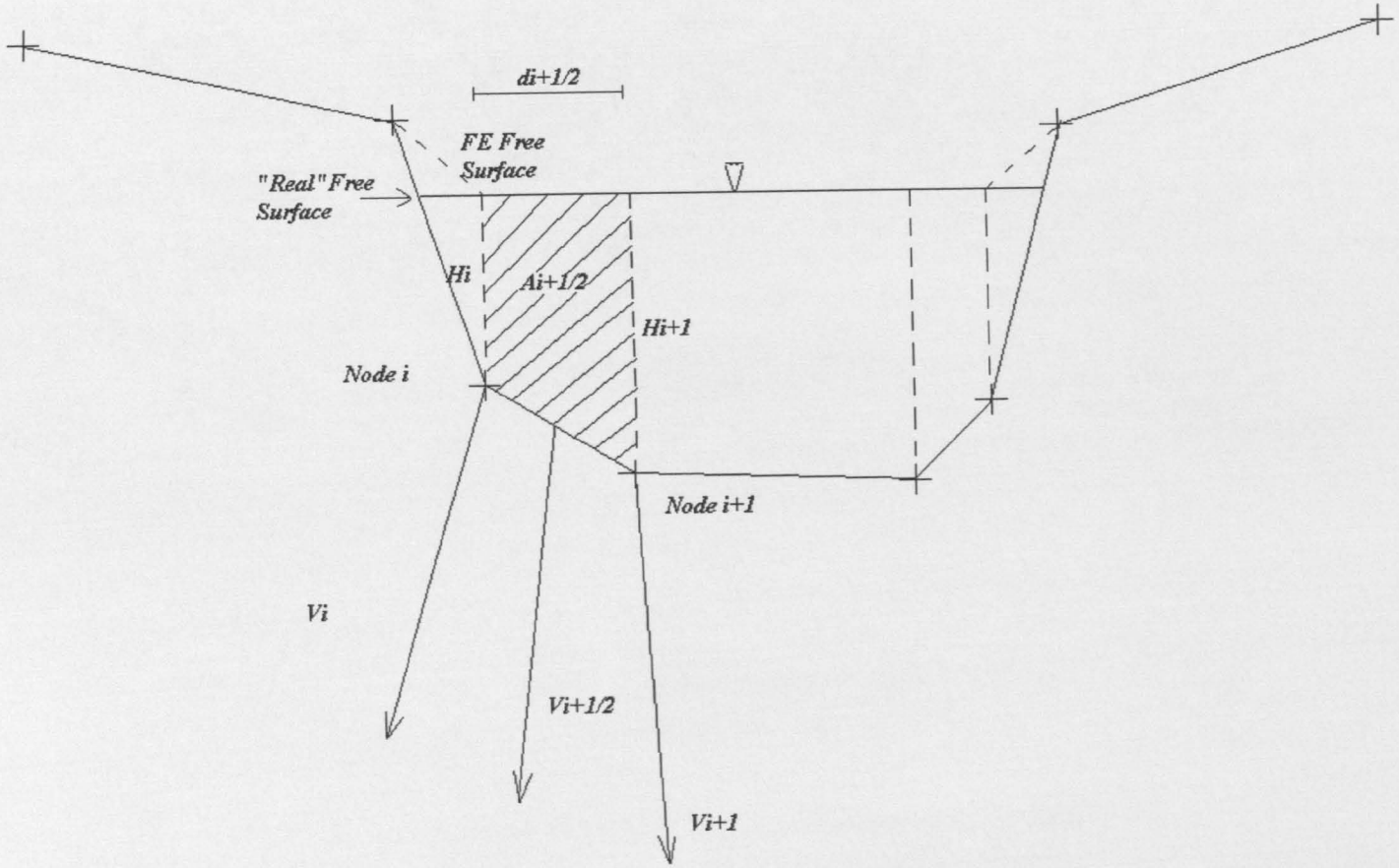

Fig. 4.21 – Schematic Representation of the Outlet Cross-Section used to Implement the Subroutine Q3DSORTIE in TELEMAC

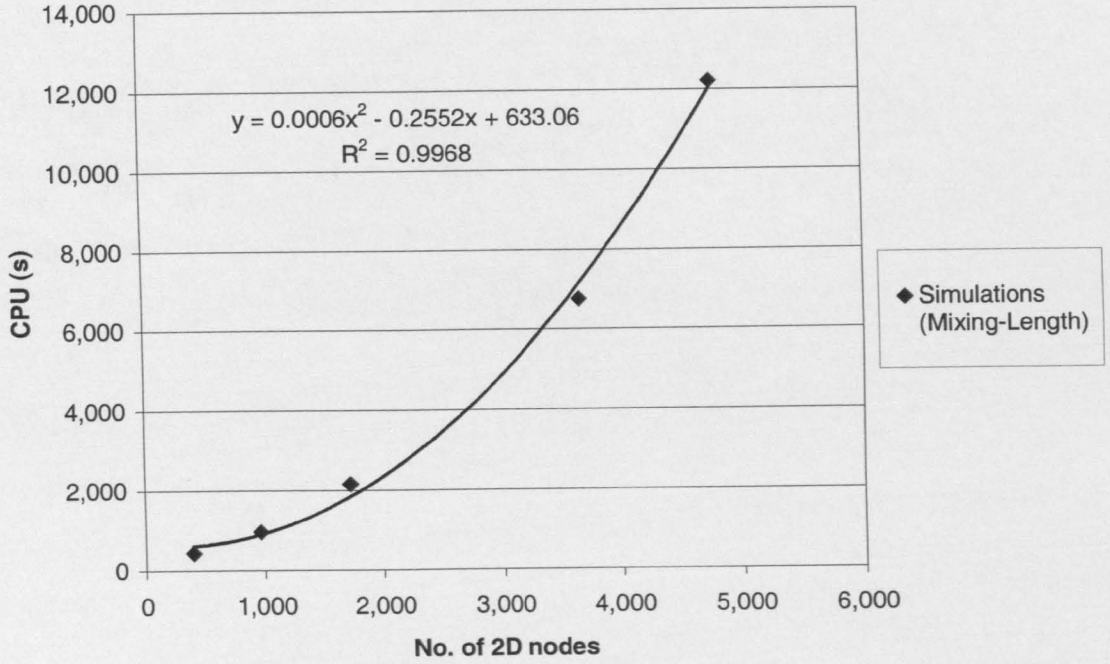

Fig. 4.22 – Scalability of TELEMAC-2D for Simulations of the Ribble Reach

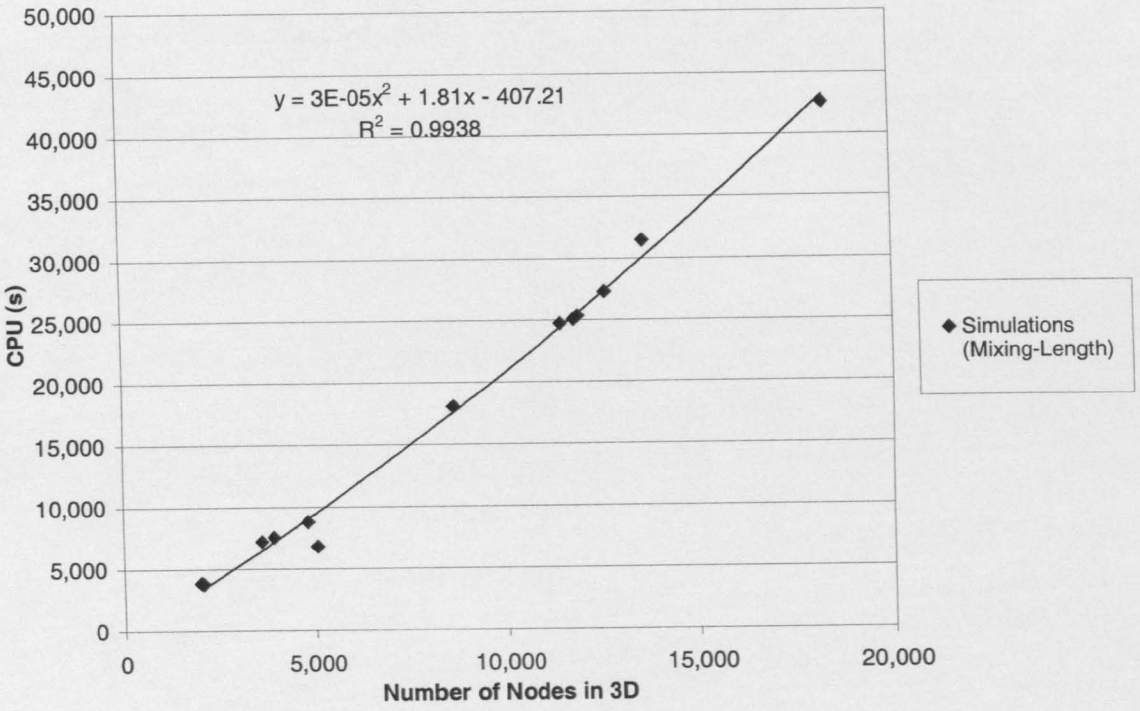

Fig. 4.23 – Scalability of TELEMAC-3D for Simulations of Ribble Reach

Chapter 5:
Numerical Models Evaluation
- The Flood Channel Facility Test Case

Figures for Chapter 5

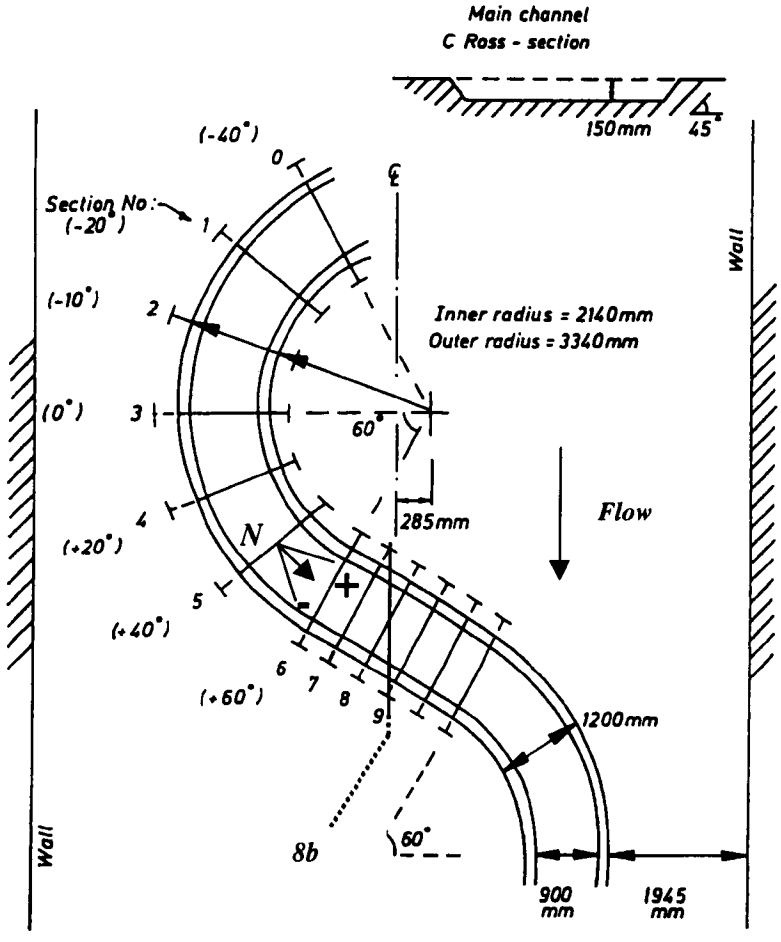

Fig. 5.1. – Plan View Design of the 60 Degree Flood Channel Facility Programme Series B Flume (modified from Ervine et al., 1993)

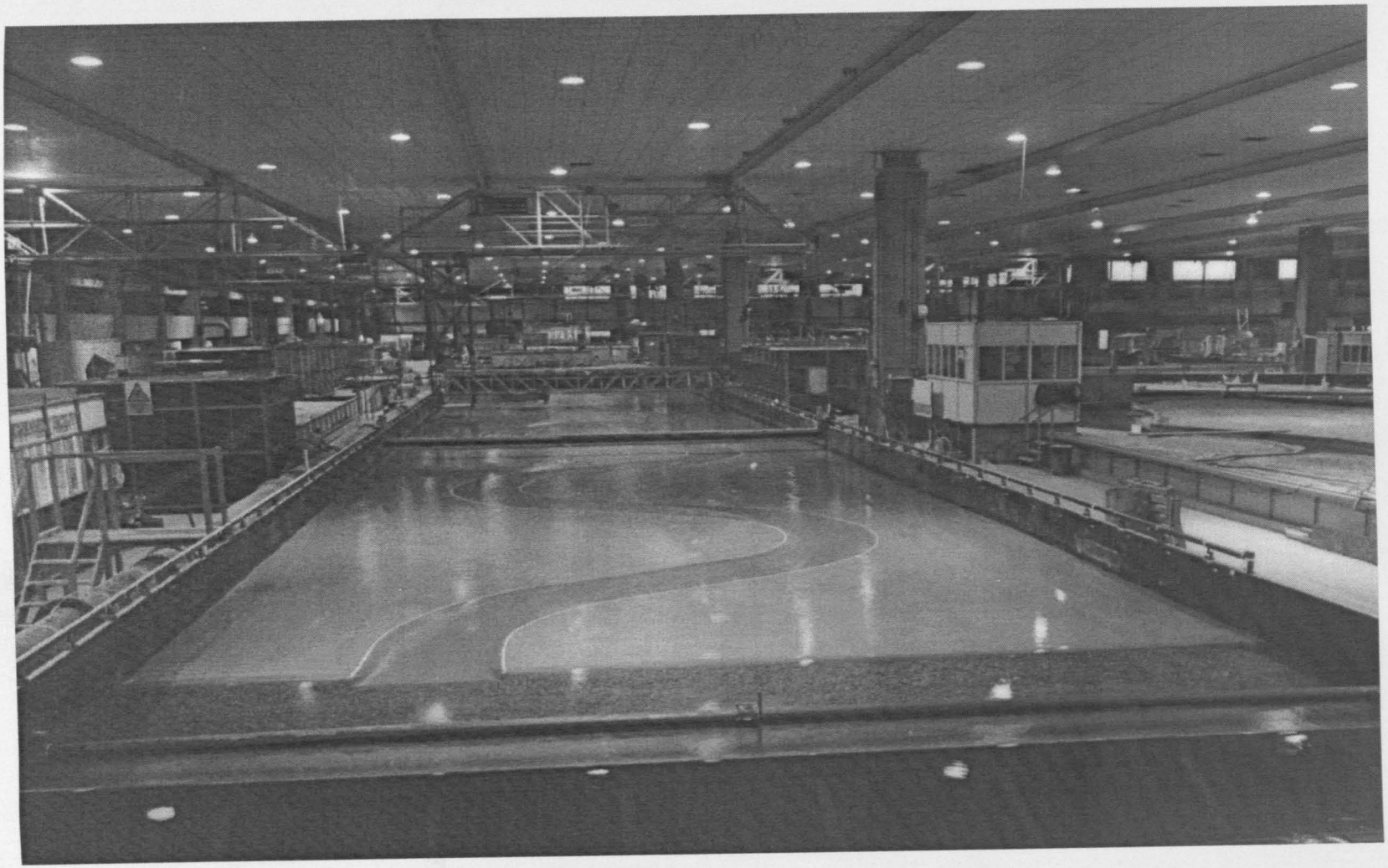

Fig. 5.2 – Photograph of 60 Degree Flood Channel Facility Programme Series B Flume

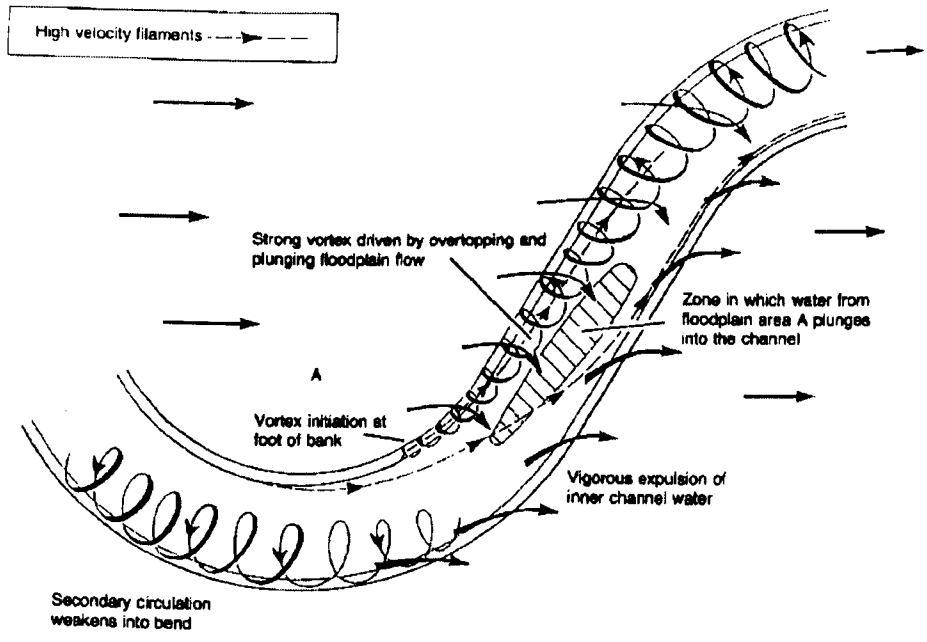

Fig. 5.3 – Flow Structure at a Bend in a Meandering Compound Channel Flow (after Willetts and Hardwick, 1993)

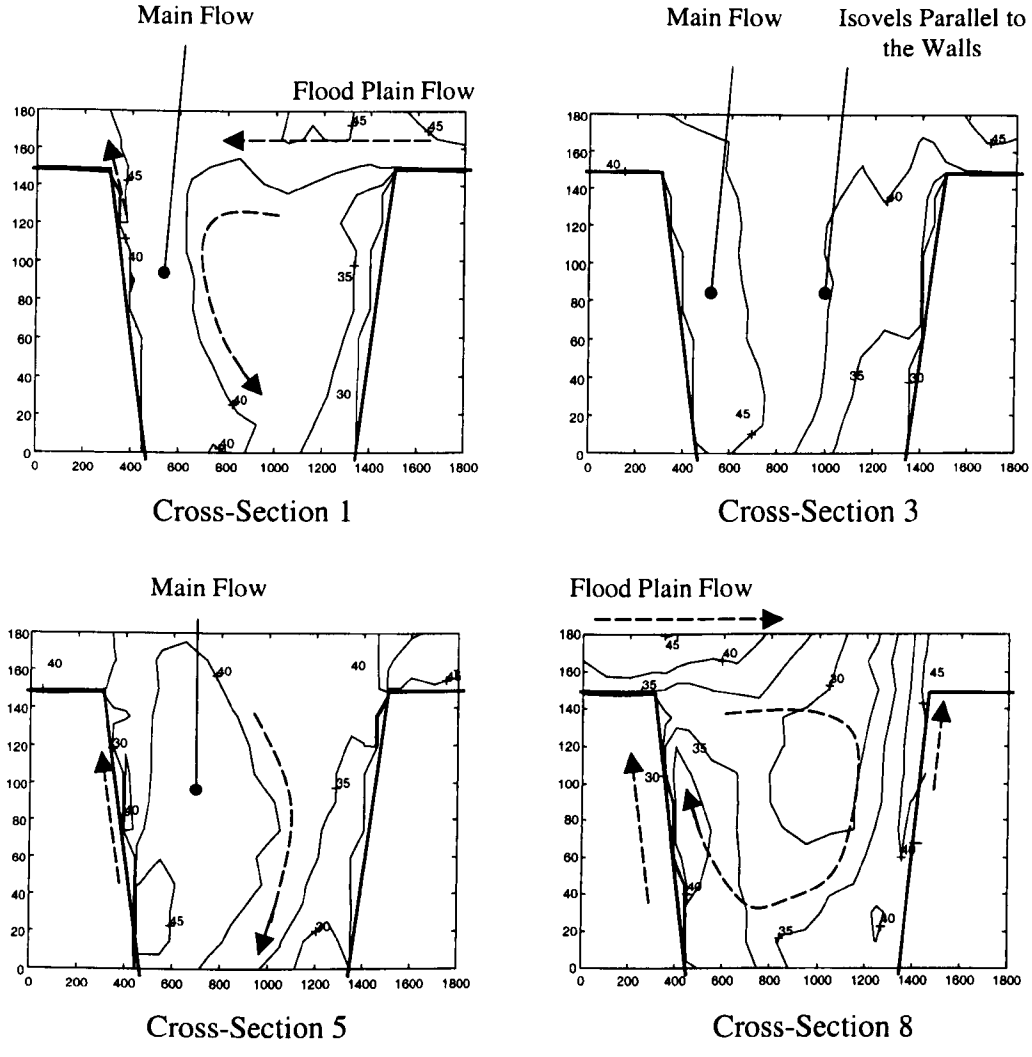

Fig. 5.4 – FCF B23 Velocity Norm Data (cm/s) at Cross-Sections 1, 3, 5 and 8 (looking downstream)

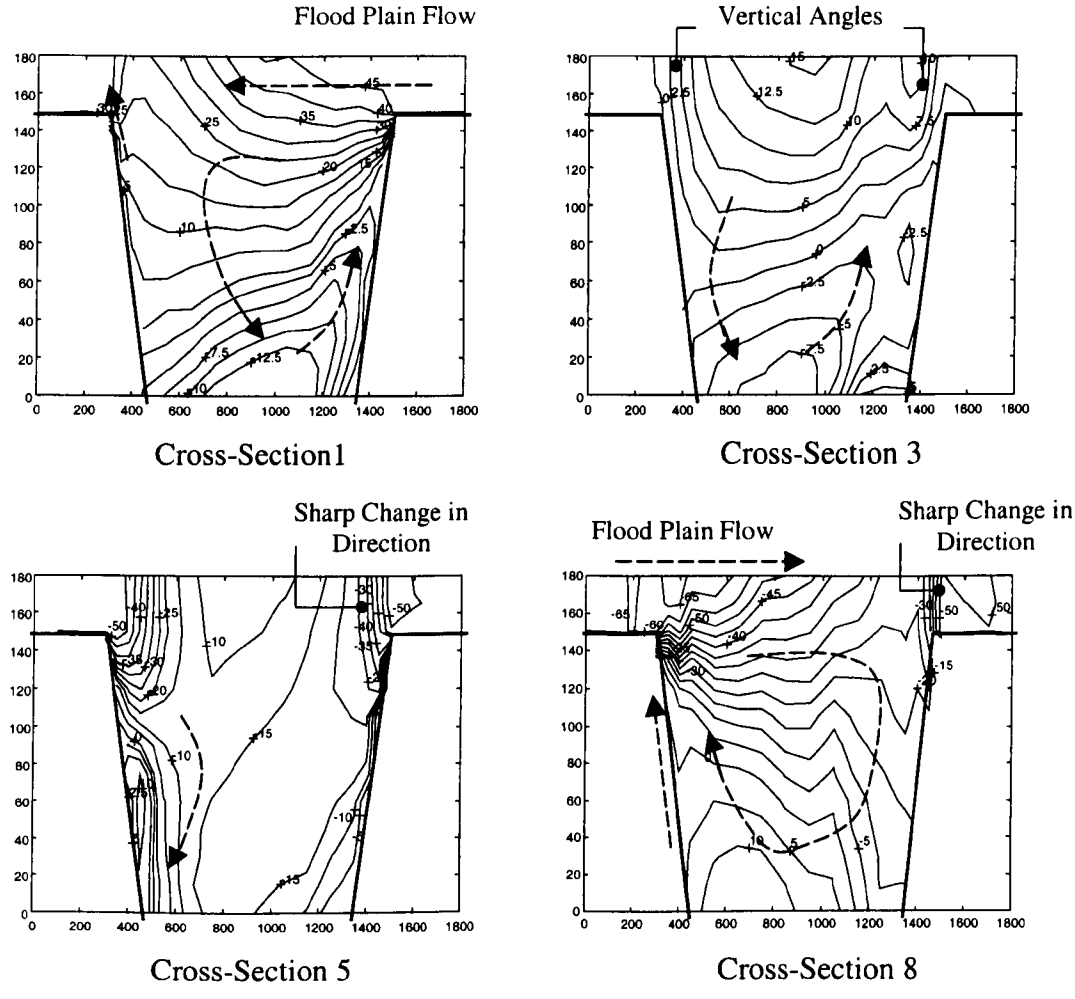

Fig. 5.5 – FCF B23 Direction Angle Data (deg.) at Cross-Sections 1, 3, 5 and 8 (looking downstream)

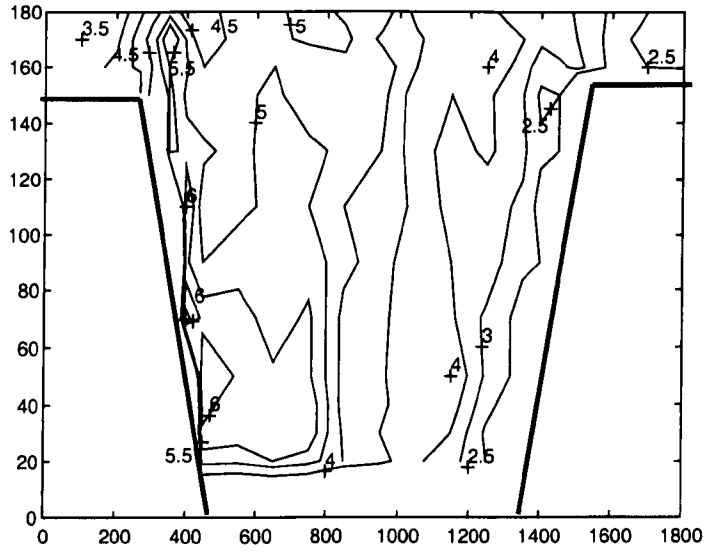

Fig. 5.6 - FCF B23 Turbulence Data at Cross-Section 3: u' (cm/s)

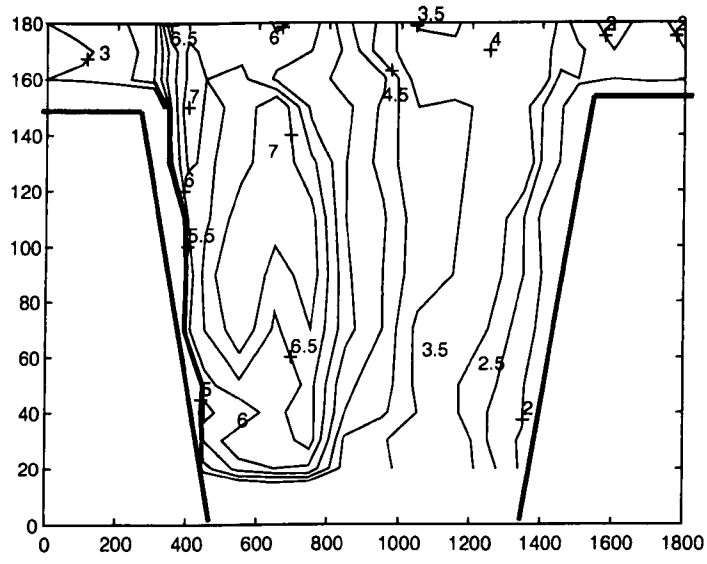

Fig. 5.7 - FCF B23 Turbulence Data at Cross-Section 3: v' (cm/s)

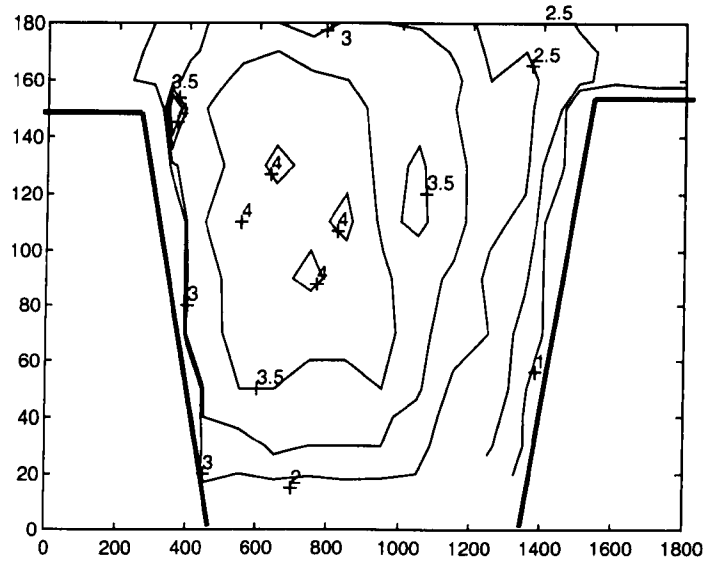

Fig. 5.8 – FCF B23 Turbulence Data at Cross-Section 3: w' (cm/s)

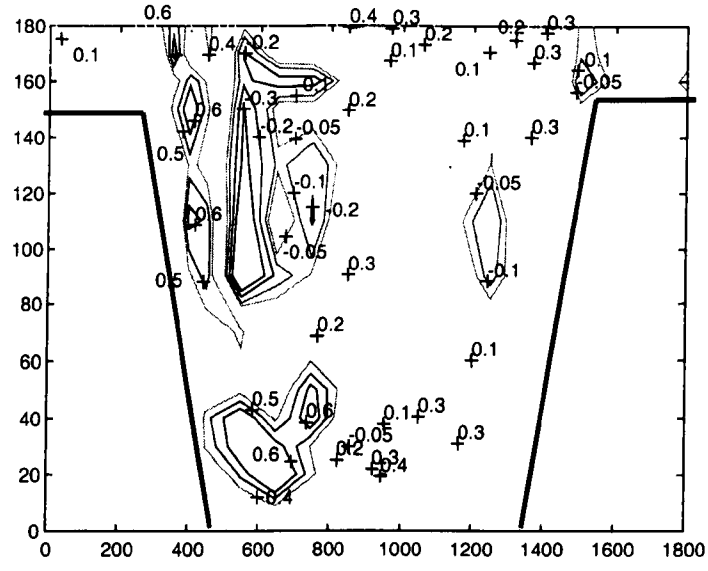

Fig. 5.9 - FCF B23 Turbulence Data at Cross-Section 3: $T_{yx}(N/m^2)$

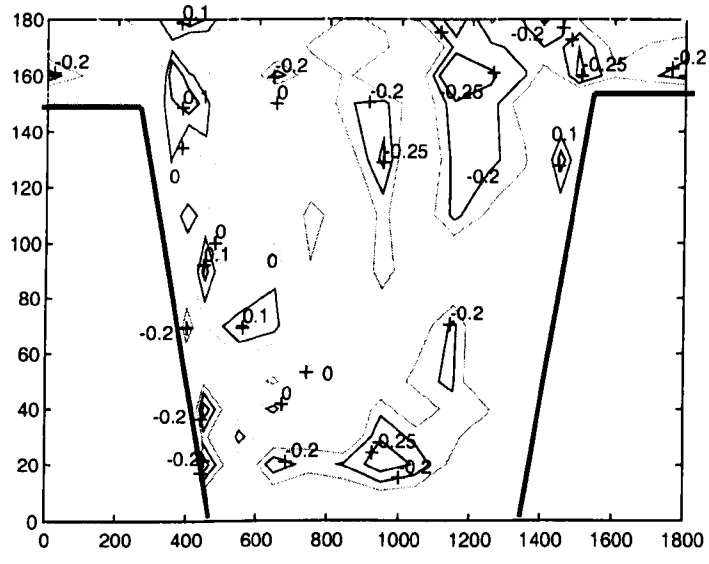

Fig. 5.10 - FCF B23 Turbulence Data at Cross-Section 3: $T_{zx}(N/m^2)$

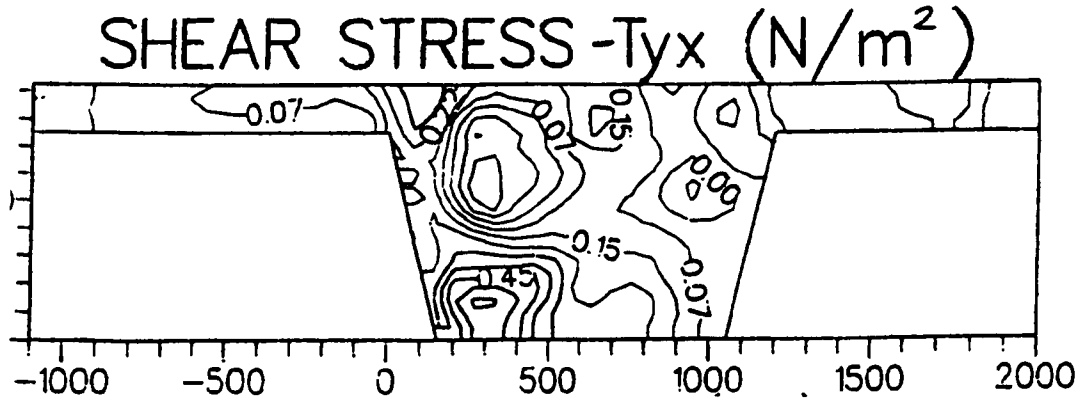

Fig. 5.11 – Interpretation of FCF B23 Turbulence Data at the Cross-Over: $T_{yx}(N/m^2)$

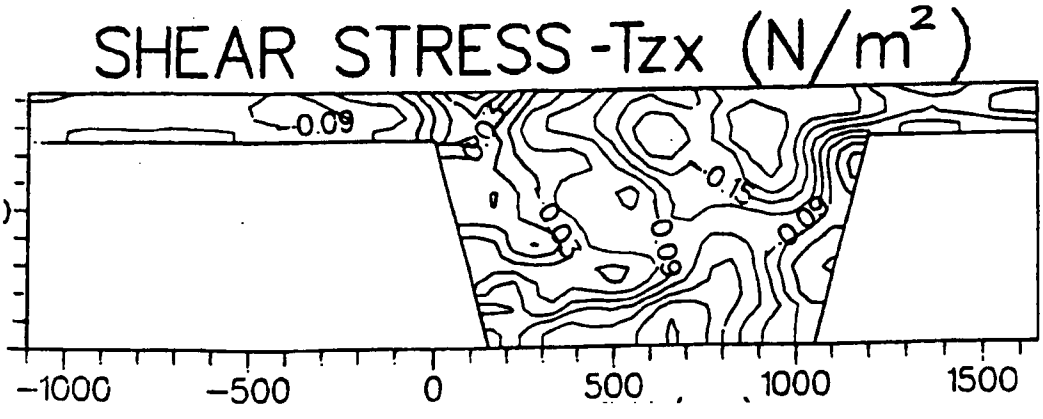

Fig. 5.12 – Interpretation of FCF B23 Turbulence Data at Cross-Section 3: $T_{zx}(N/m^2)$

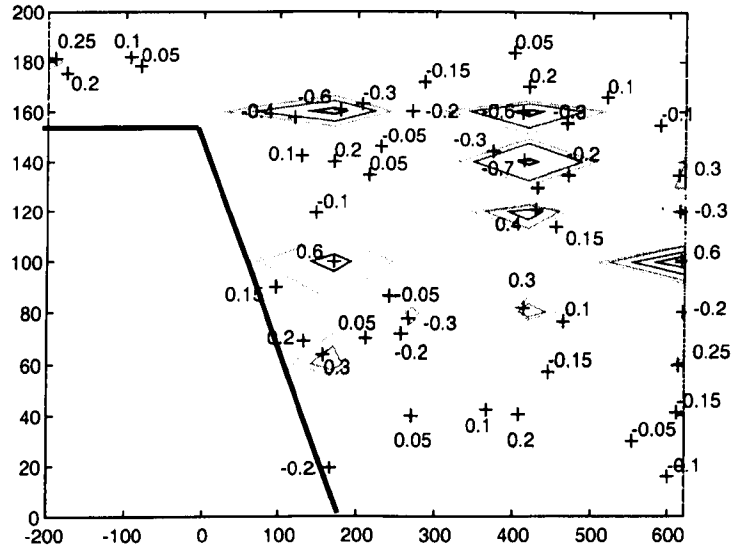

Fig. 5.13 - FCF B23 Turbulence Data at the Cross-Over: $T_{yx}(N/m^2)$

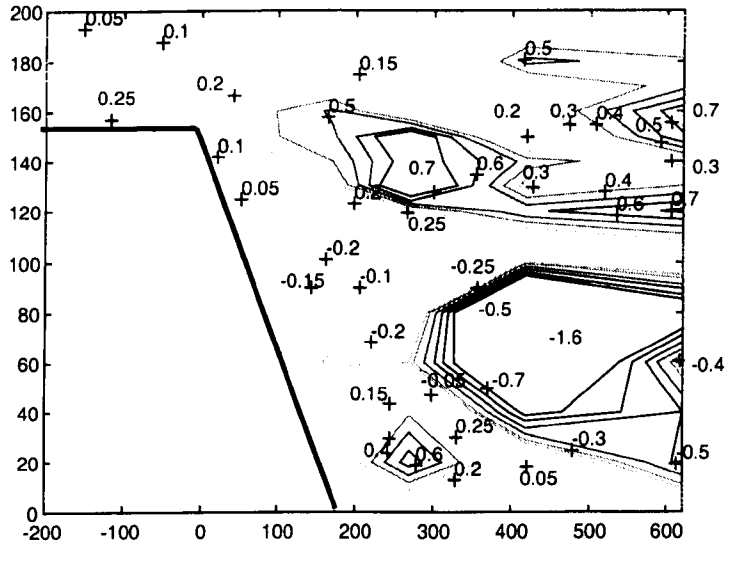

Fig. 5.14 - FCF B23 Turbulence Data at Cross-Section 3: $T_{zx}(N/m^2)$

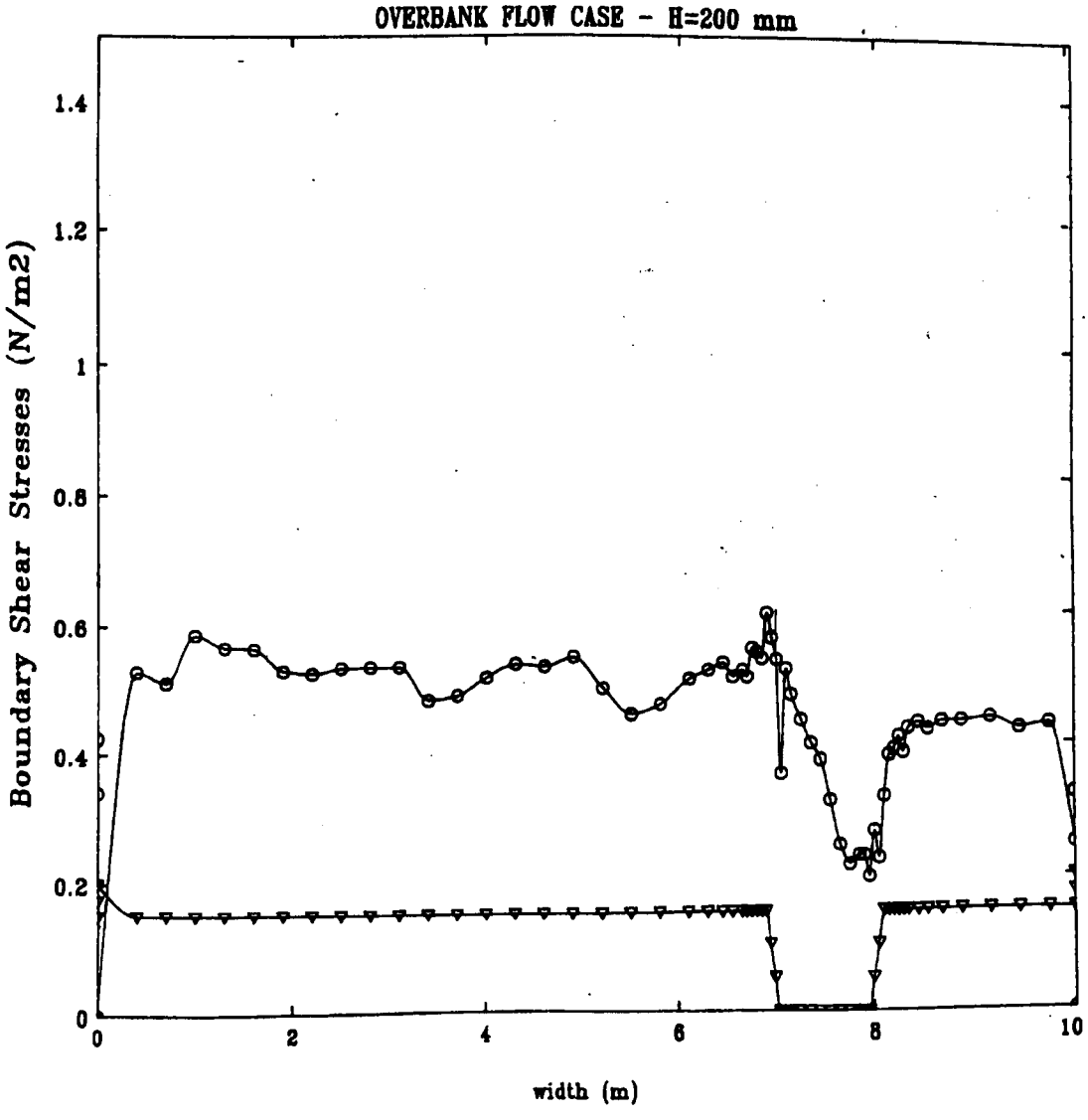

Fig. 5.15 – FCF B23 Bed Shear Stress Data at Cross-Section 3 (N/m^2)

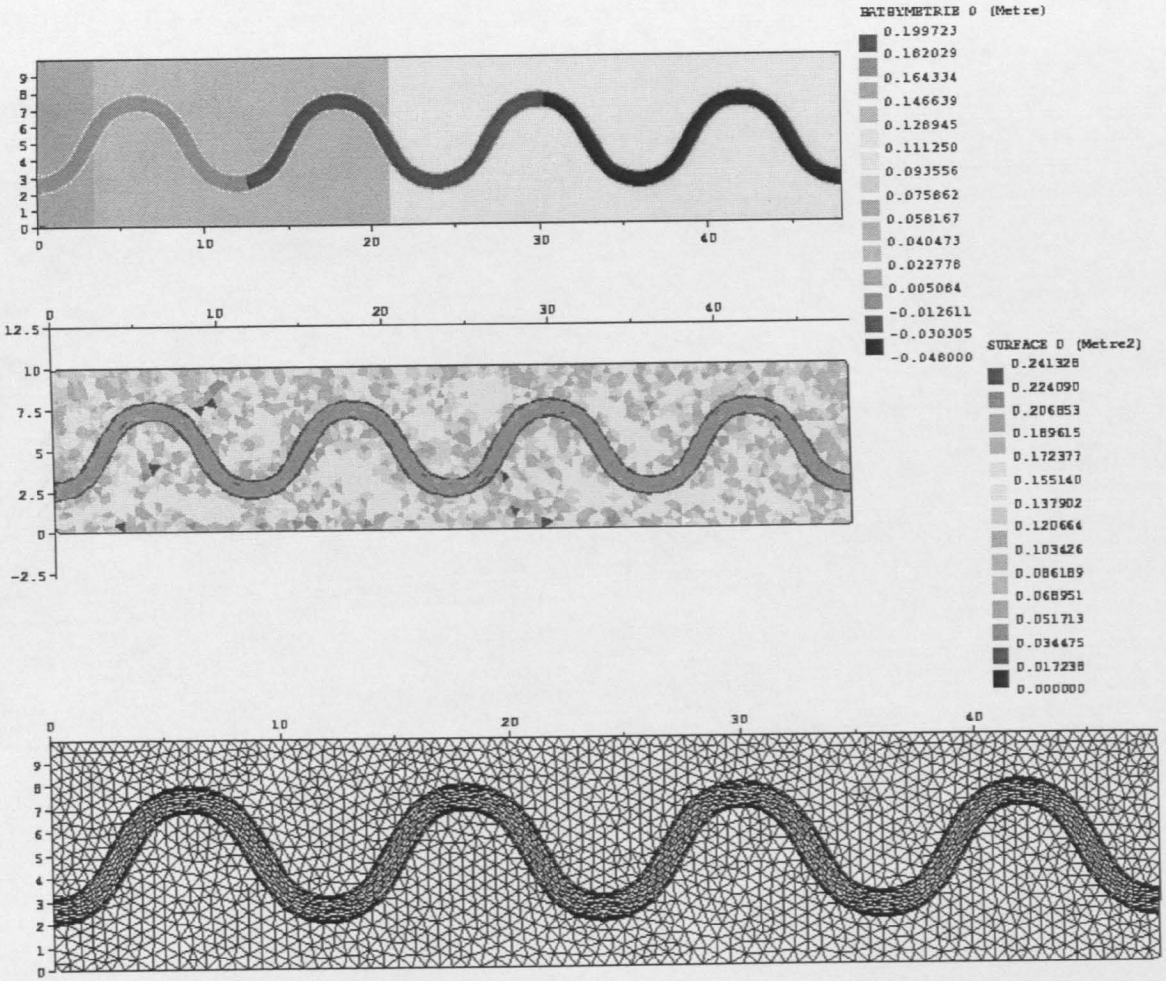

Fig. 5.16 – FCF Series B Geometry and Mesh Characteristics for TELEMAC

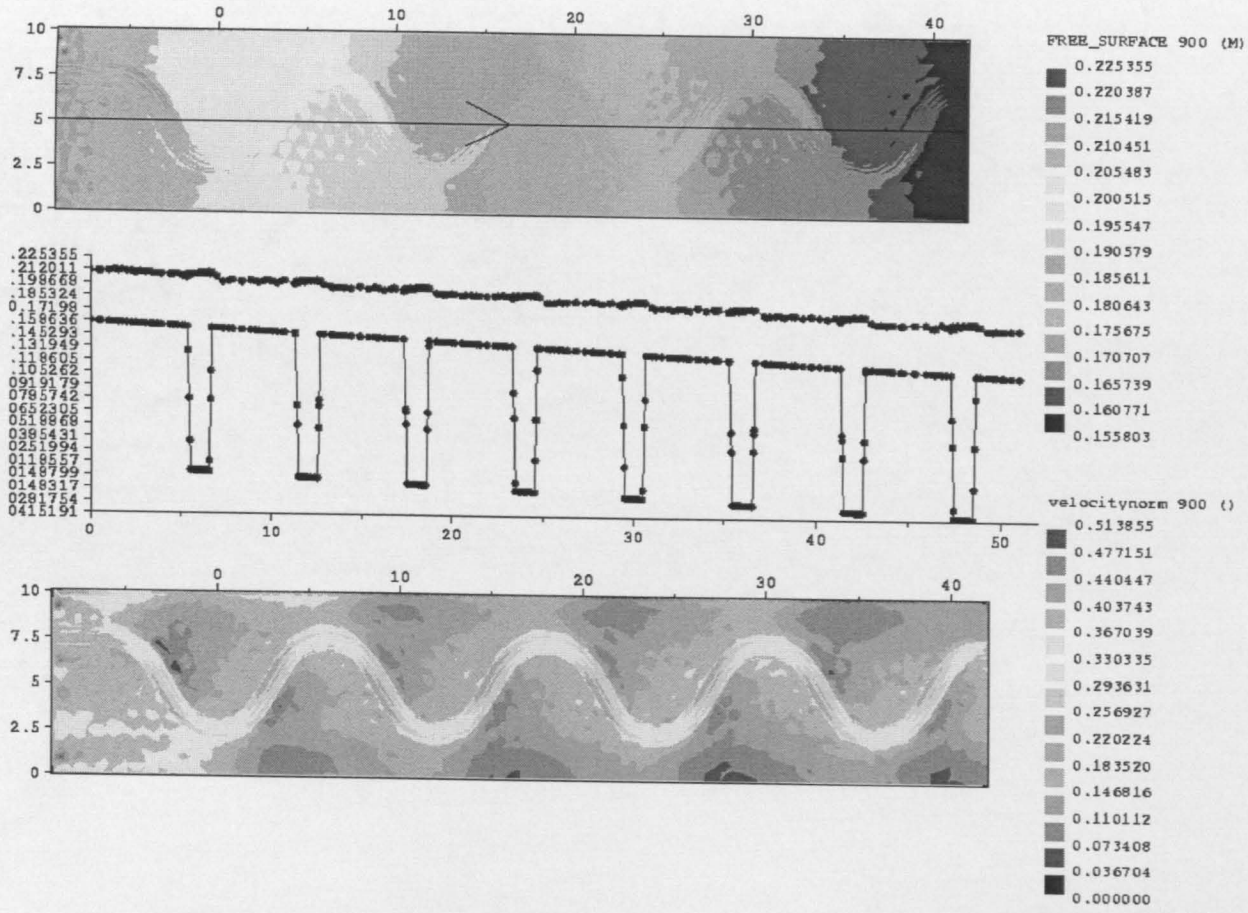

Fig. 5.17 – FCF B23 TELEMAC Free-Surface Profile and Dept-Averaged Velocity (C = 68 $m^{1/2}/s$, Mixing-Length Model)

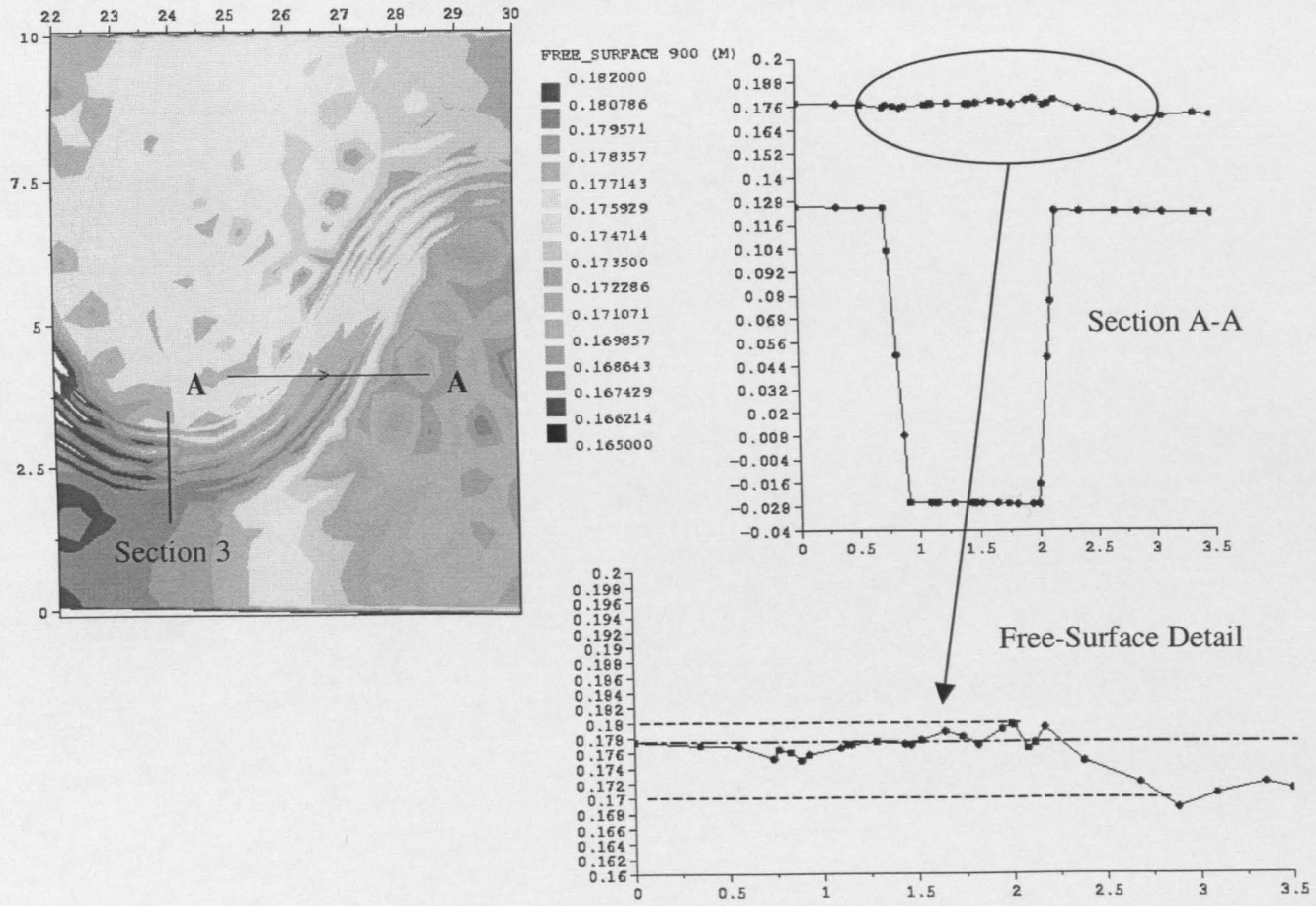

Fig. 5.18 – FCF B23 TELEMAC Free-Surface Contraction and Expansion past the Bend (C = 68 $m^{1/2}/s$, Mixing-Length Model)

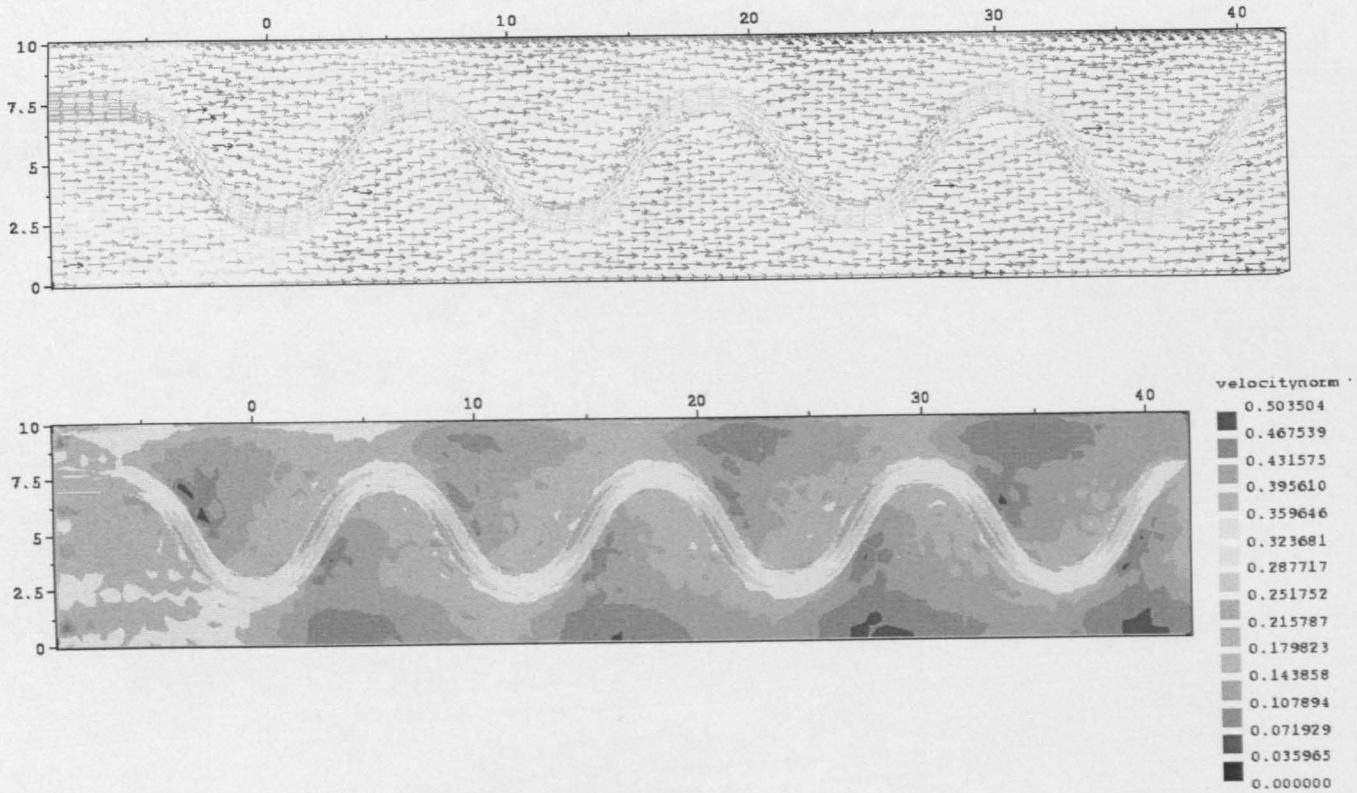

Fig. 5.19 – FCF B23 TELEMAC Depth Averaged Velocity Field (C = 68 $m^{1/2}/s$, Mixing Length Model)

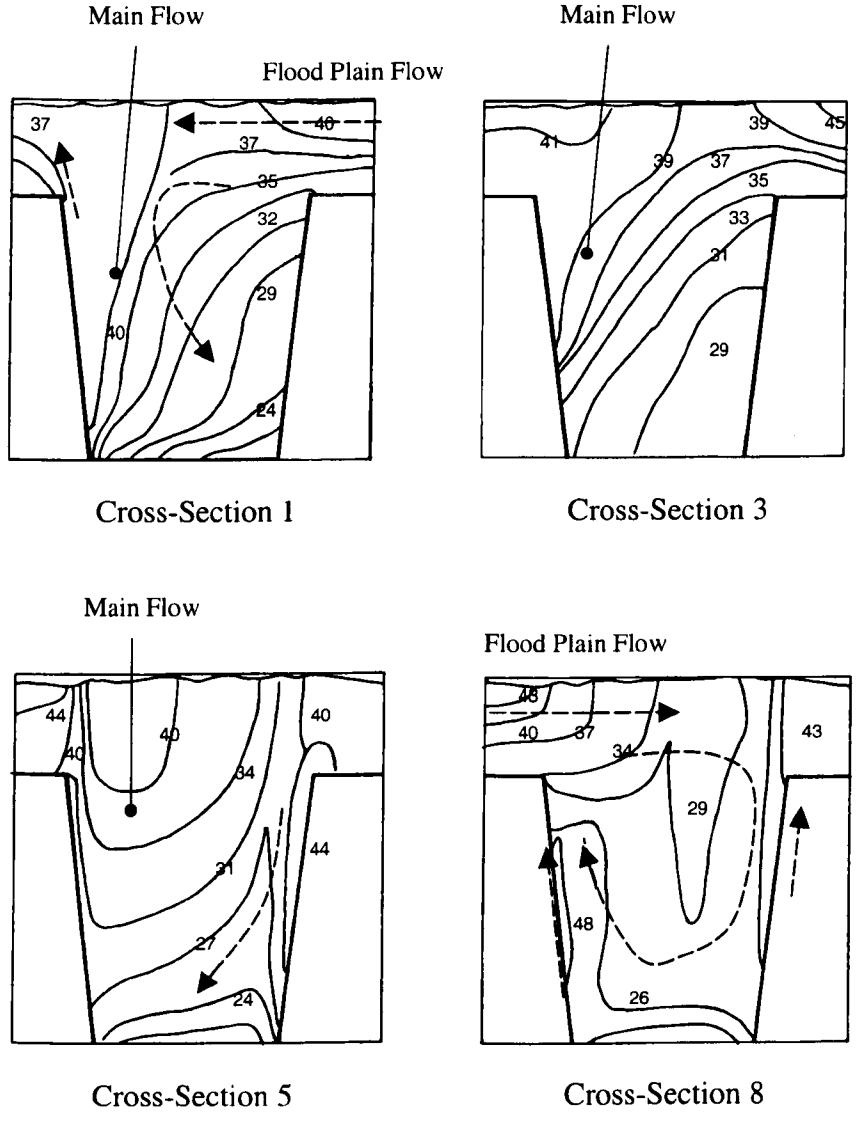

Fig. 5.20 – FCF B23 TELEMAC Velocity Norm Predictions (cm/s) at Cross-Sections 1, 3, 5 and 8 (C = 68 $m^{1/2}/s$, Mesh TELEMAC FCF-1, Mixing-Length Model)

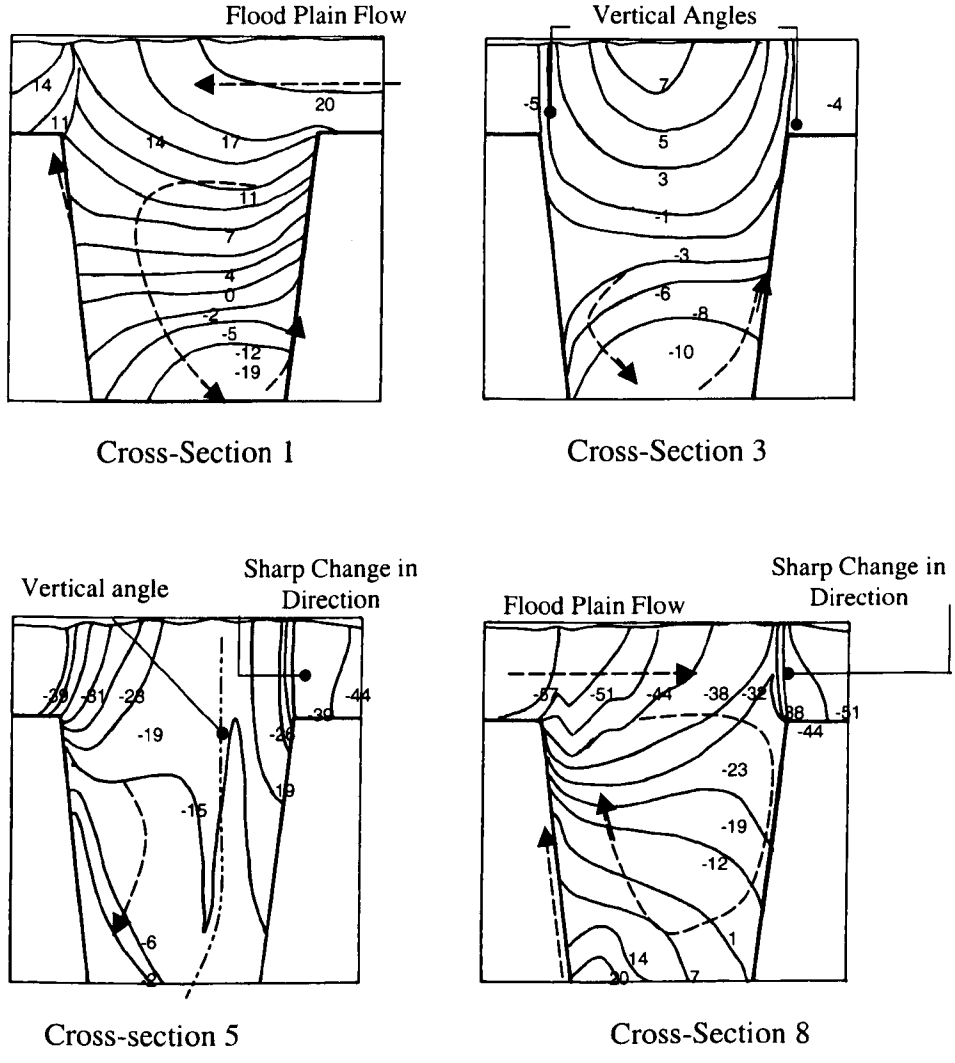

Fig. 5.21 – FCF B23 TELEMAC Velocity Angle Predictions (deg.) at Cross-Sections 1, 3, 5 and 8 (C = 68 $m^{1/2}/s$, Mesh TELEMAC FCF-1, Mixing-Length Model)

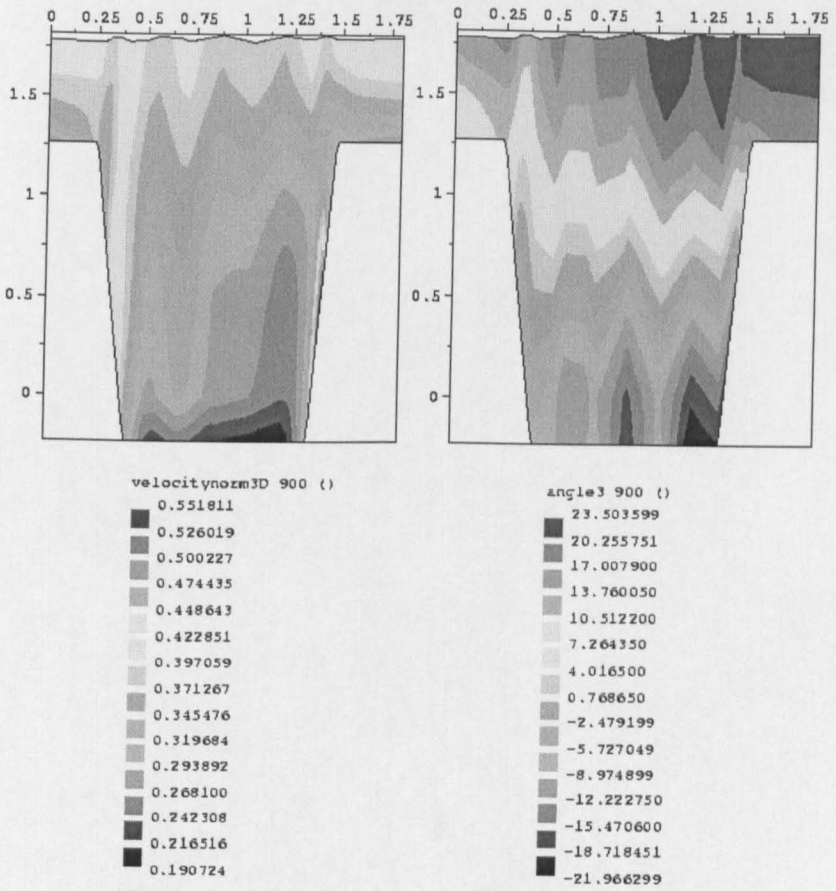

Fig. 5.22 – FCF B23 TELEMAC Outputs for Cross-Section 1:
(a)Velocity Norm (left; m/s)
(b) Angle (deg.)
(C = 68 $m^{1/2}/s$, Mesh TELEMAC FCF-1, Mixing-Length Model)

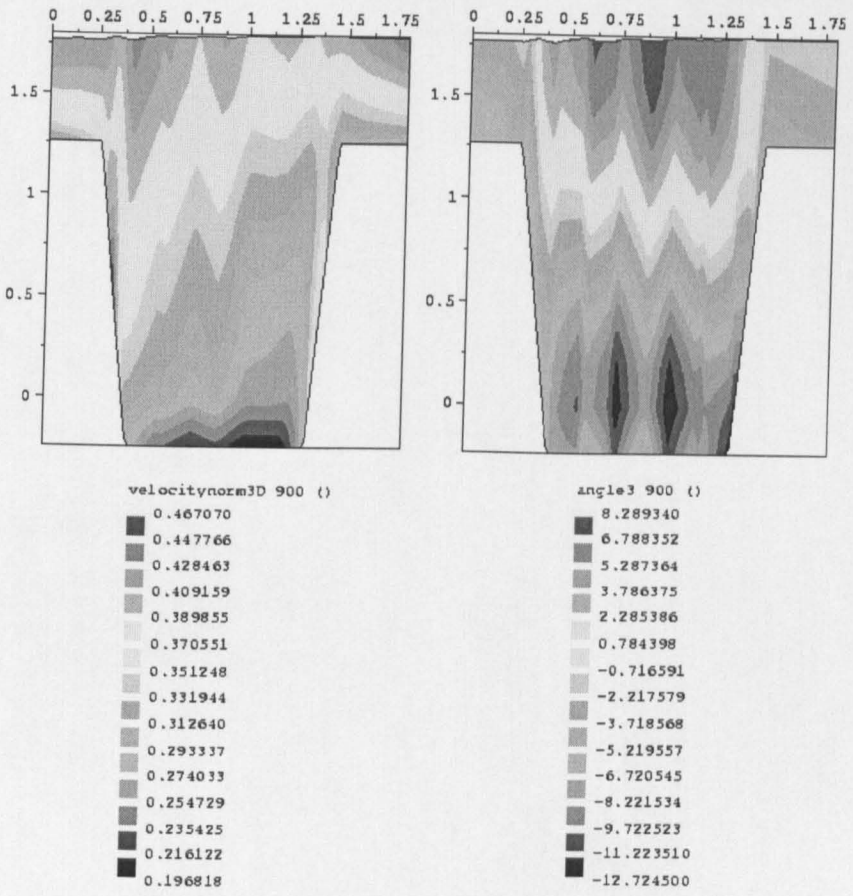

(a) (b)

Fig. 5.23 – FCF B23 TELEMAC Outputs for Cross-Section 3:
(a)Velocity Norm (left; m/s)
(b) Angle (deg.)
(C = 68 $m^{1/2}/s$, Mesh TELEMAC FCF-1, Mixing-Length Model)

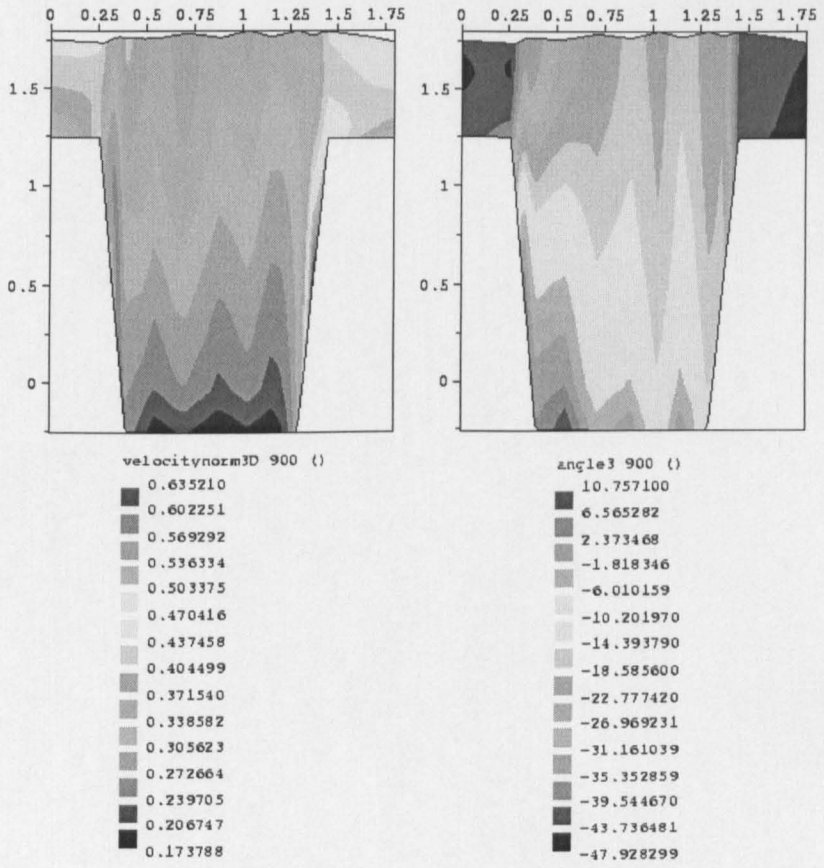

Fig. 5.24 – FCF B23 TELEMAC Outputs for Cross-Section 5:
(a)Velocity Norm (left; m/s)
(b) Angle (deg.)
(C = 68 $m^{1/2}/s$, Mesh TELEMAC FCF-1, Mixing-Length Model)

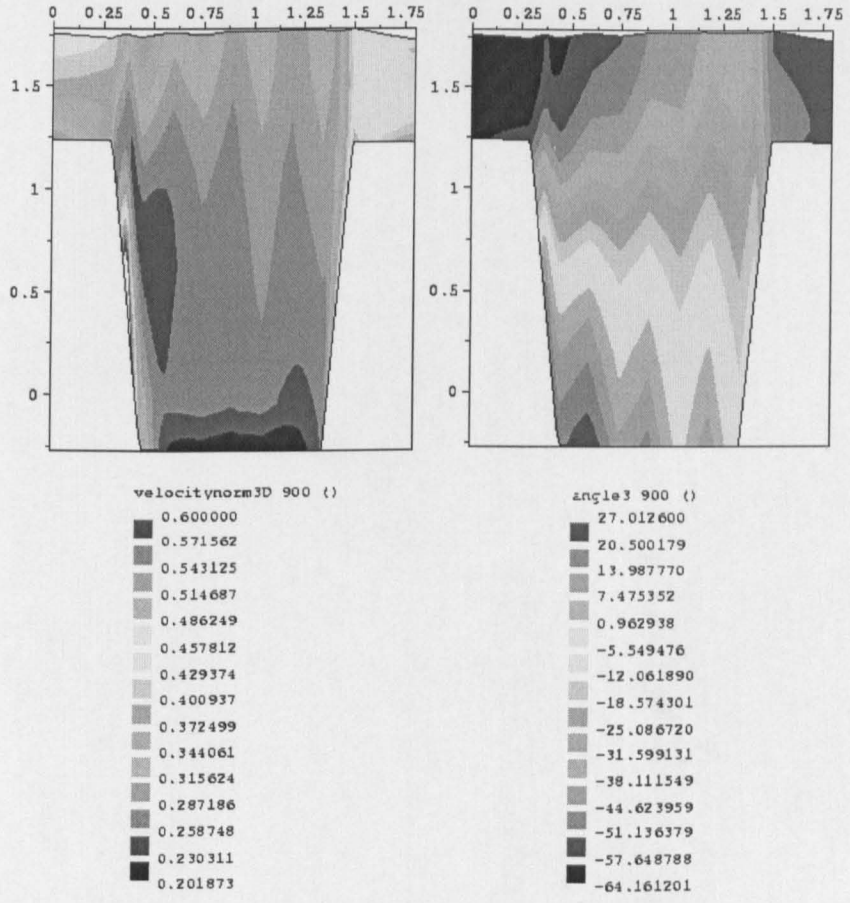

Fig. 5.25 – FCF B23 TELEMAC Outputs for Cross-Section 8:
(a)Velocity Norm (left; m/s)
(b) Angle (deg.)
(C = 68 $m^{1/2}/s$, Mesh TELEMAC FCF-1, Mixing-Length Model)

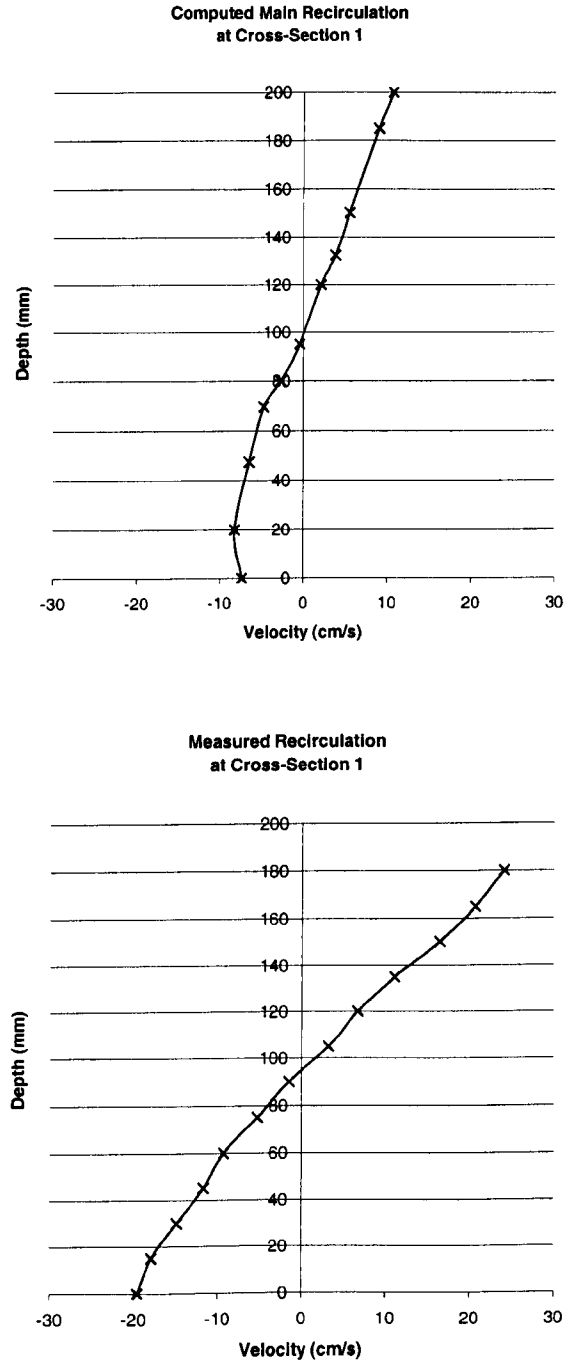

Fig. 5.26 – FCF B23 TELEMAC Model: Recirculation at Cross-Section 1

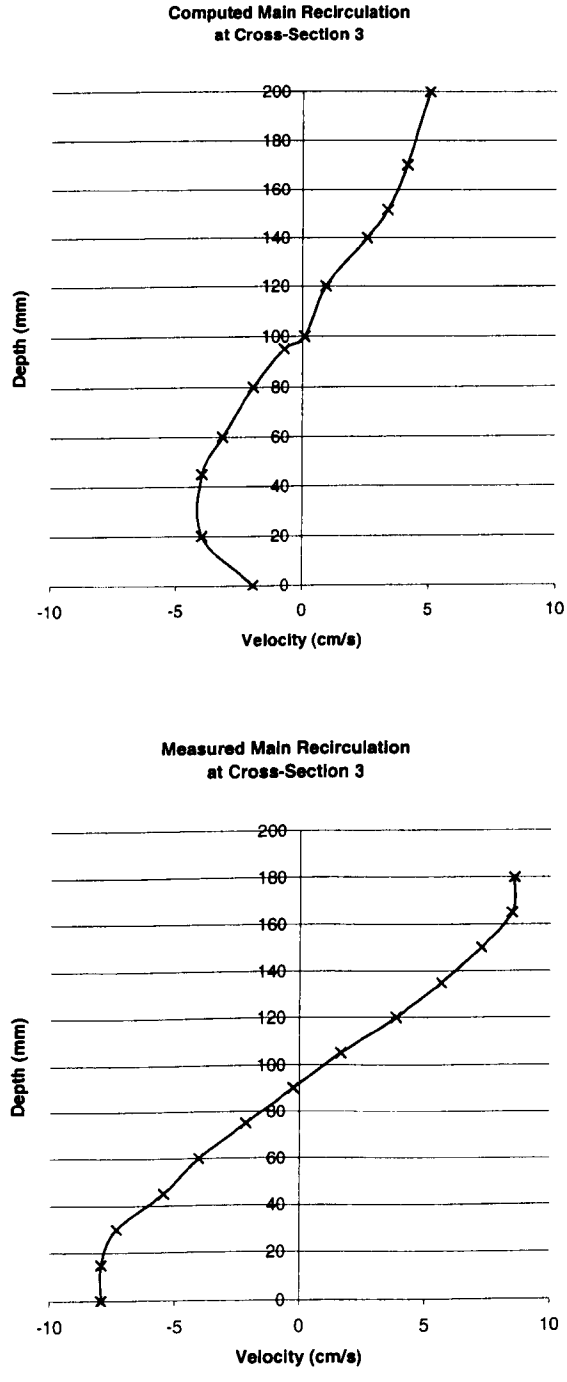

Fig. 5.27 – FCF B23 TELEMAC Model: Recirculation at Cross-Section 3

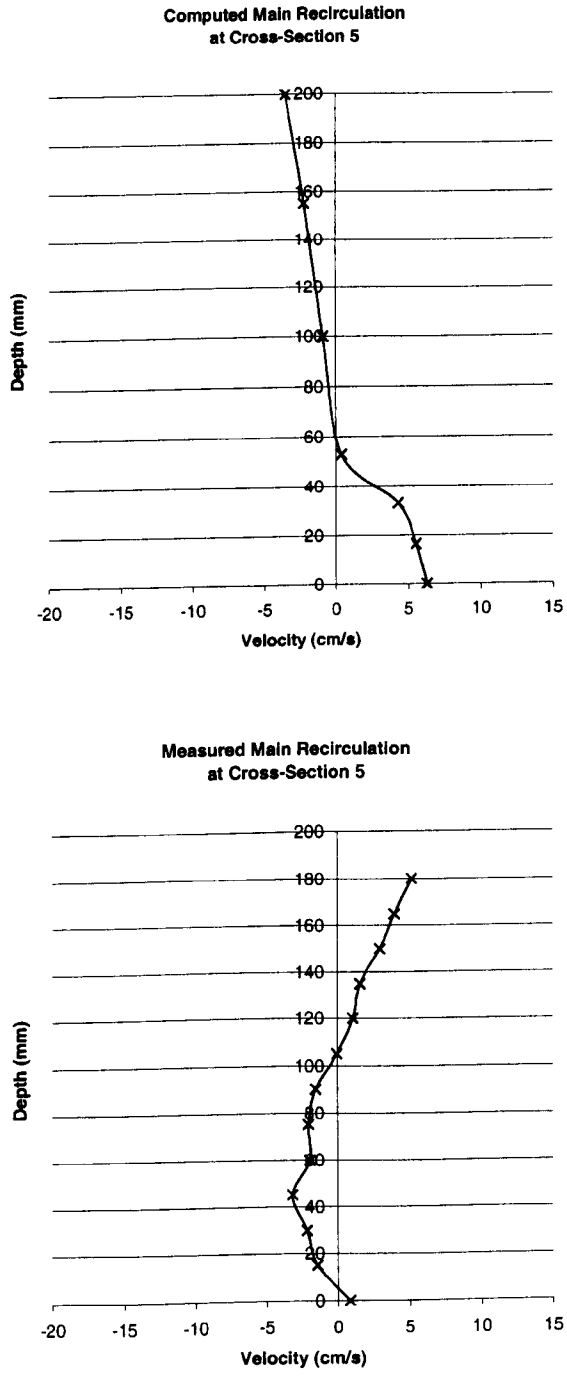

Fig. 5.28 – FCF B23 TELEMAC Model: Recirculation at Cross-Section 5

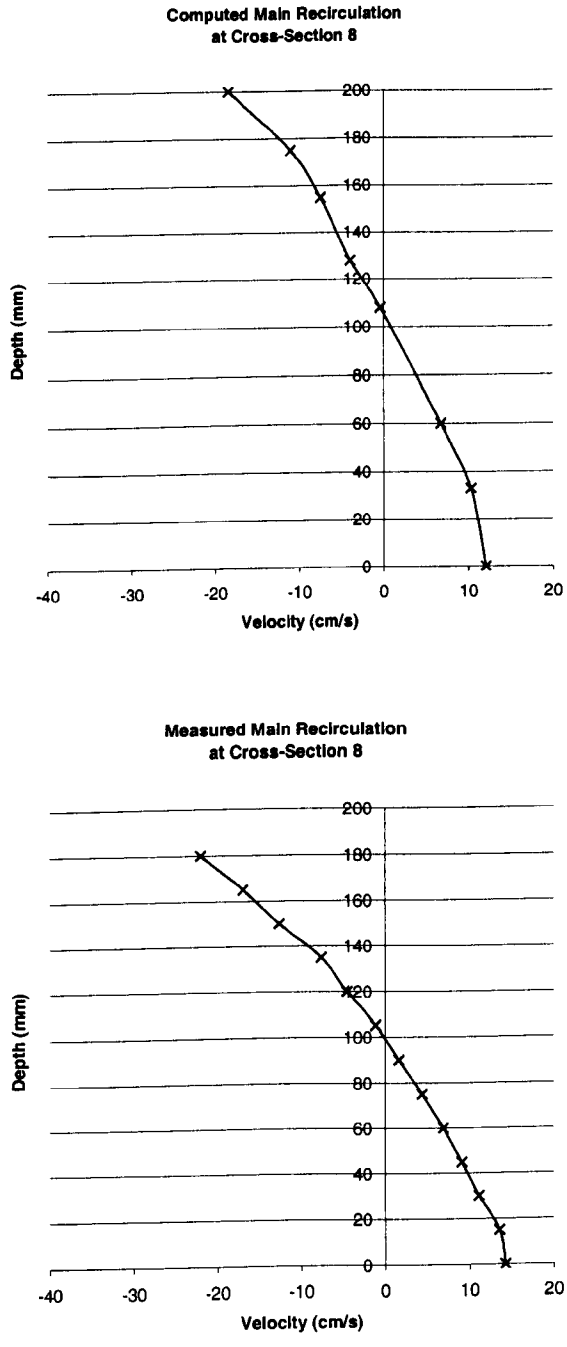

Fig. 5.29 – FCF B23 TELEMAC Model: Recirculation at Cross-Section 8

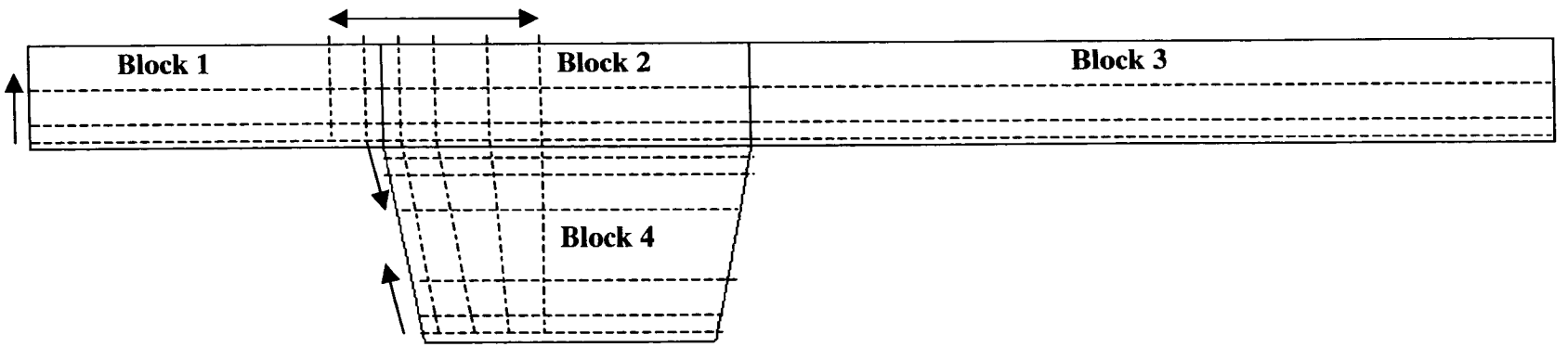

Fig. 5.30 – Construction of the CFX Numerical Grid of the FCF

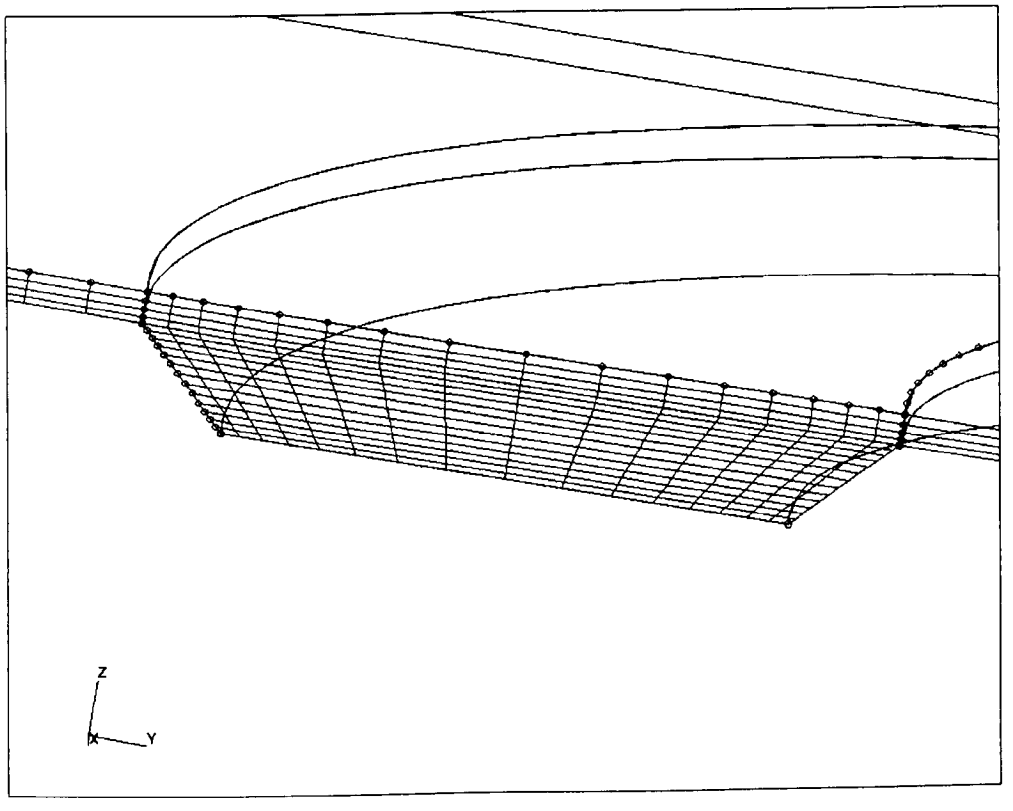

Fig. 5.31 – CFX Grid FCF-1

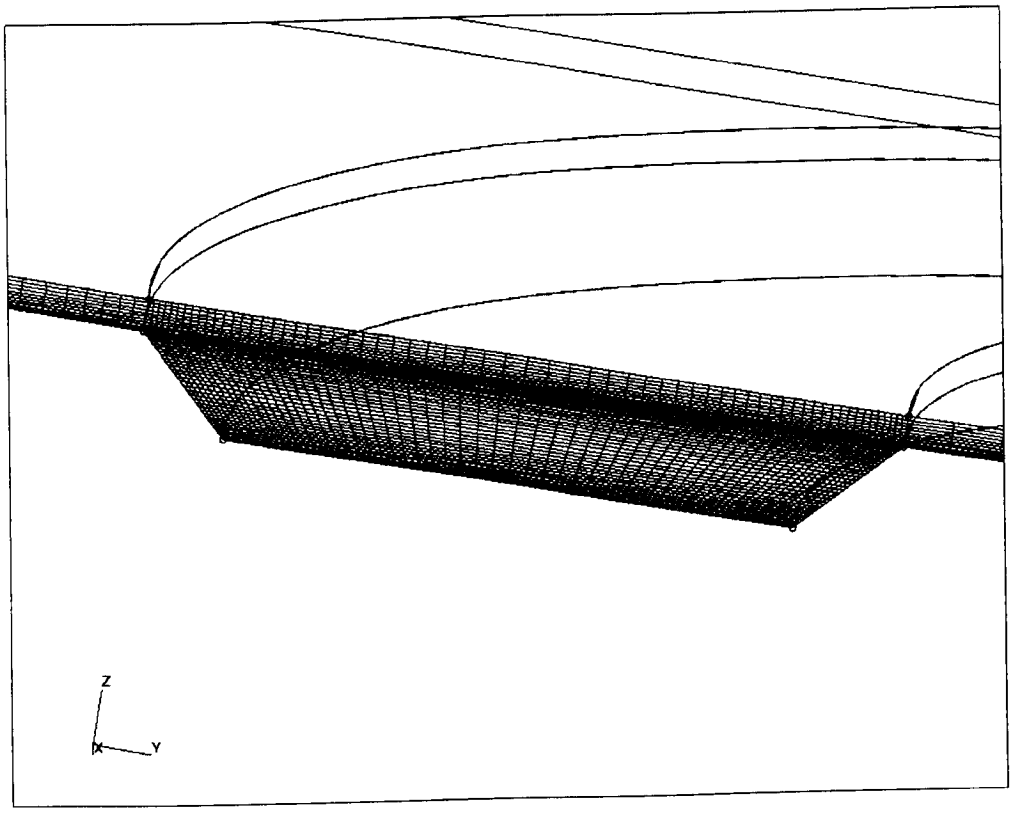

Fig. 5.32 – CFX Grid FCF-3

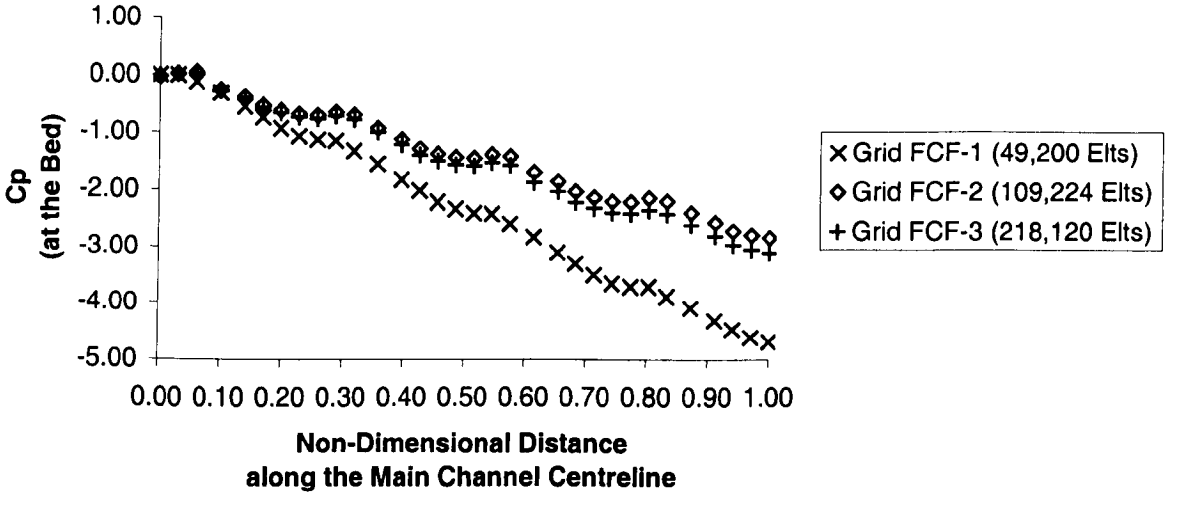

Fig. 5.33 – Mesh Independence: Comparison of the Non-dimensionalized Pressure Term C_p for Different Mesh Resolution in CFX

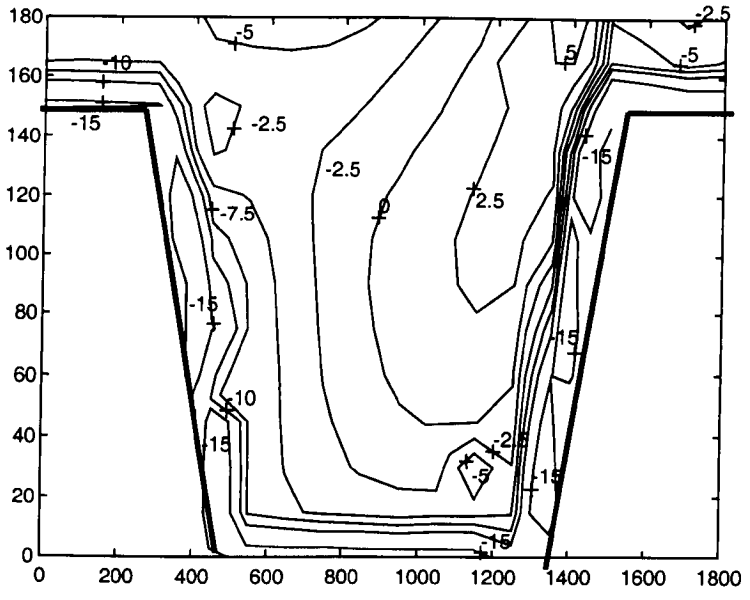

Fig. 5.34 –Difference in Velocity at Cross-Section 8 between CFX FCF-1 and FCF-3 (cm/s)

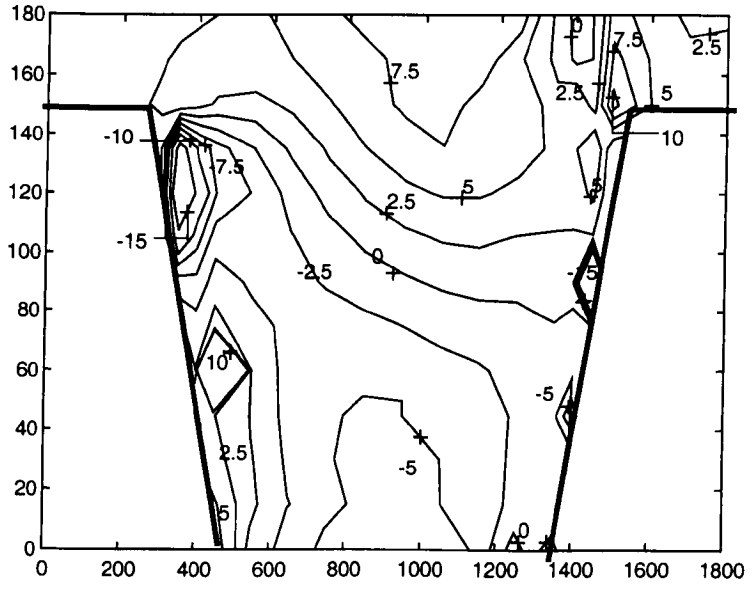

Fig. 5.35 –Difference in Angle at Cross-Section 8 between CFX FCF-1 and FCF-3 (deg.)

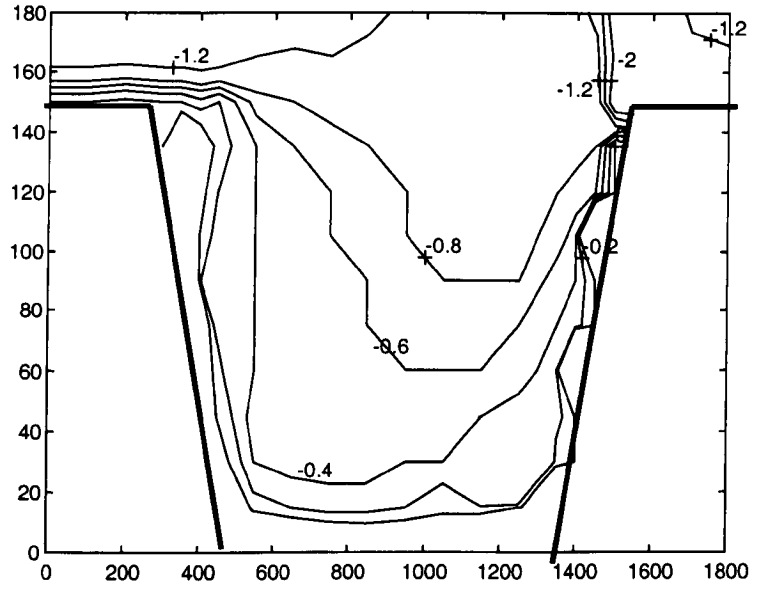

Fig. 5.36 –Difference in Velocity at Cross-Section 8 between CFX FCF-2 and FCF-3 (cm/s)

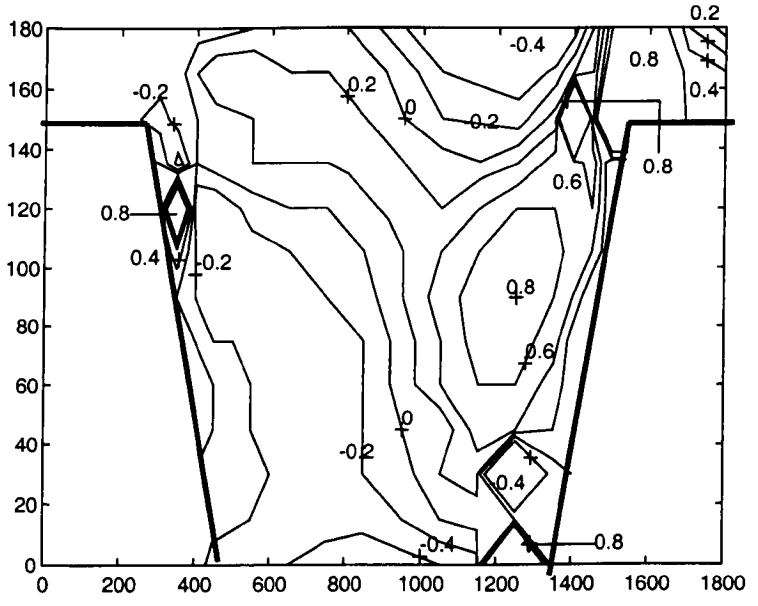

Fig. 5.37 –Difference in Angle at Cross-Section 8 between CFX FCF-2 and FCF-3 (deg.)

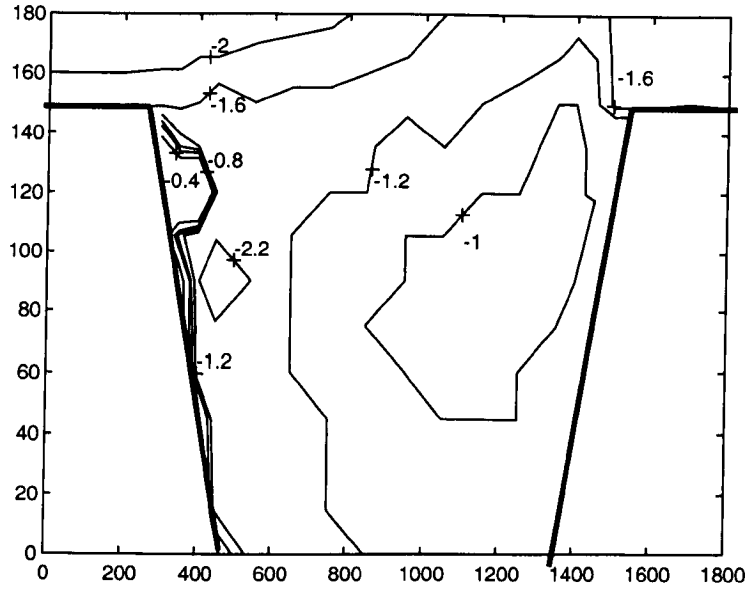

Fig. 5.38 –Difference in Velocity at Cross-Section 8 between Model using an I/O Boundary Condition and a Model using Periodic Boundary Conditions (FCF-2)

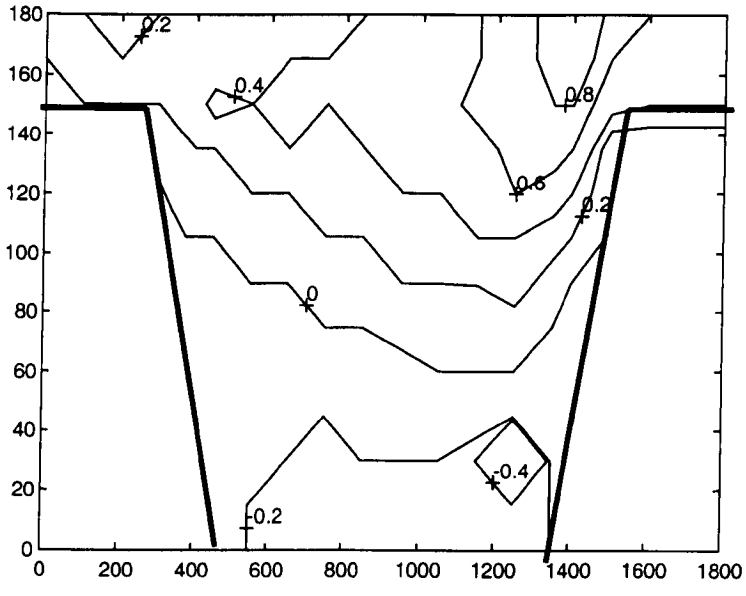

Fig. 5.39 –Difference in Angle at Cross-Section 8 between Model using an I/O Boundary Condition and a Model using Periodic Boundary Conditions (FCF-2)

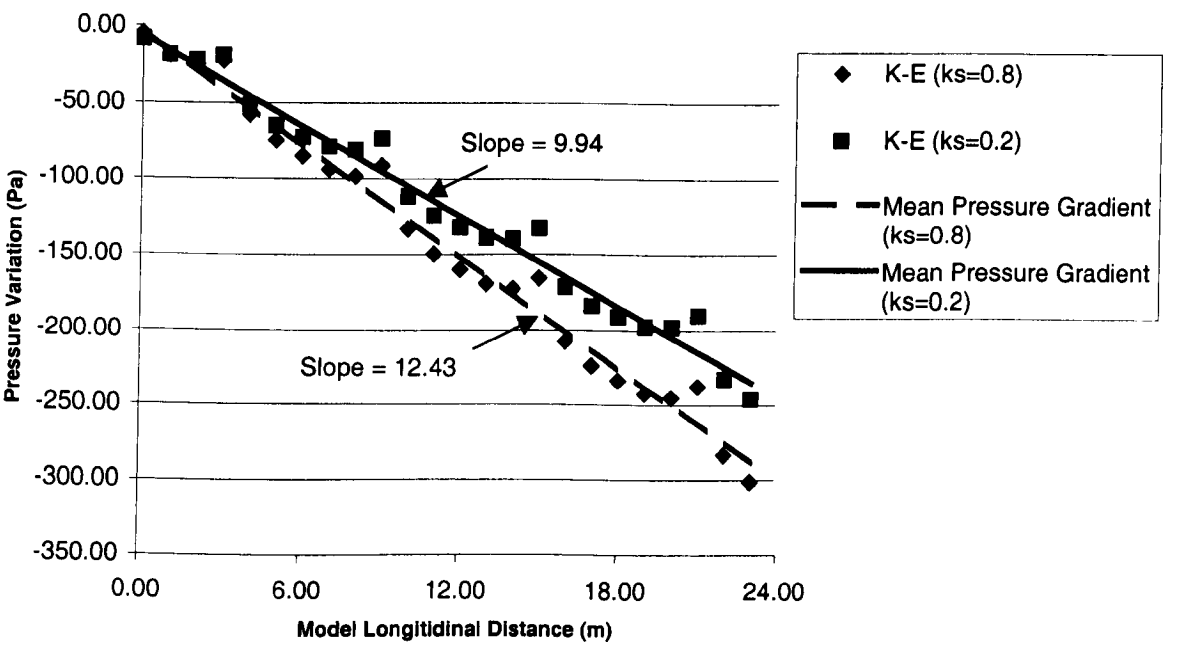

Fig. 5.40 – Sensitivity Analysis for the CFX Model of FCF B23 Experiment: Variation of the Pressure Slope with Roughness

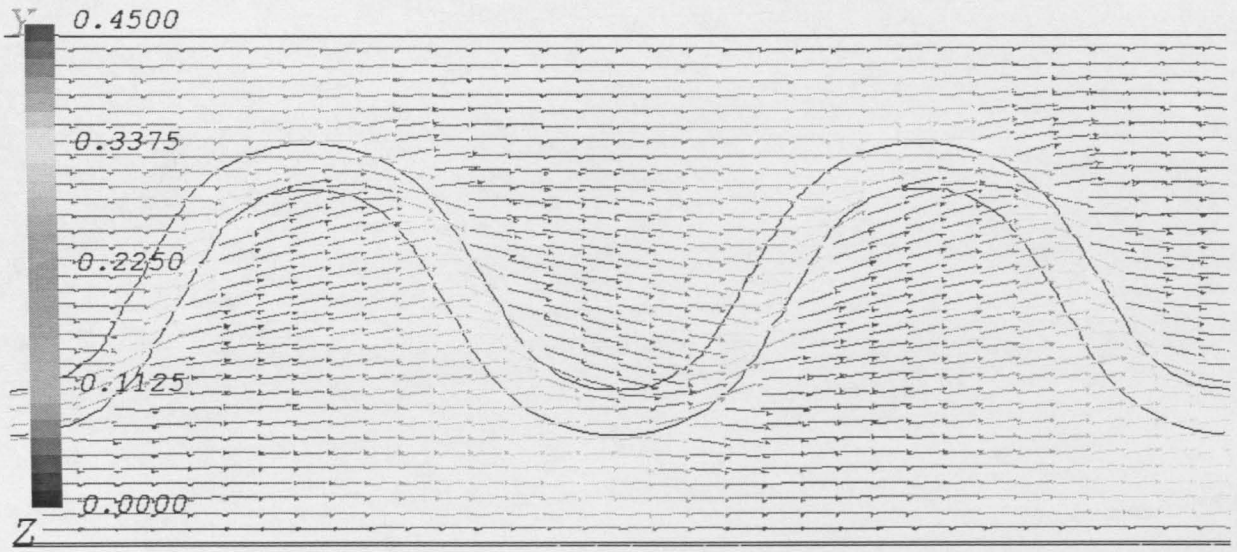

Fig. 5.41 – CFX Surface Velocity for FCF B23 Experiment (k_s = 0.2 mm, Mesh FCF-2, k-ε Model)

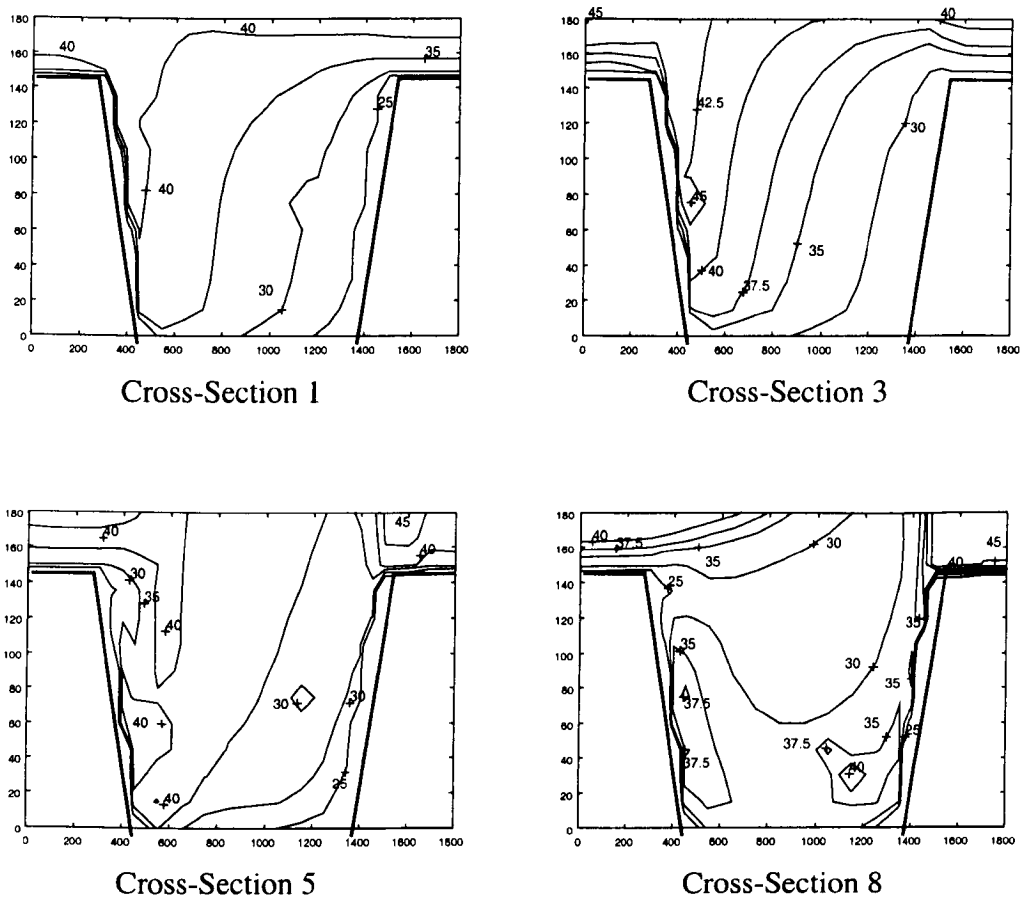

Fig. 5.42 – FCF B23 CFX Velocity Norm Predictions (cm/s) at Cross-Sections 1, 3, 5 and 8 (k_s = 0.8 mm, Grid FCF-3, k-ε Model)

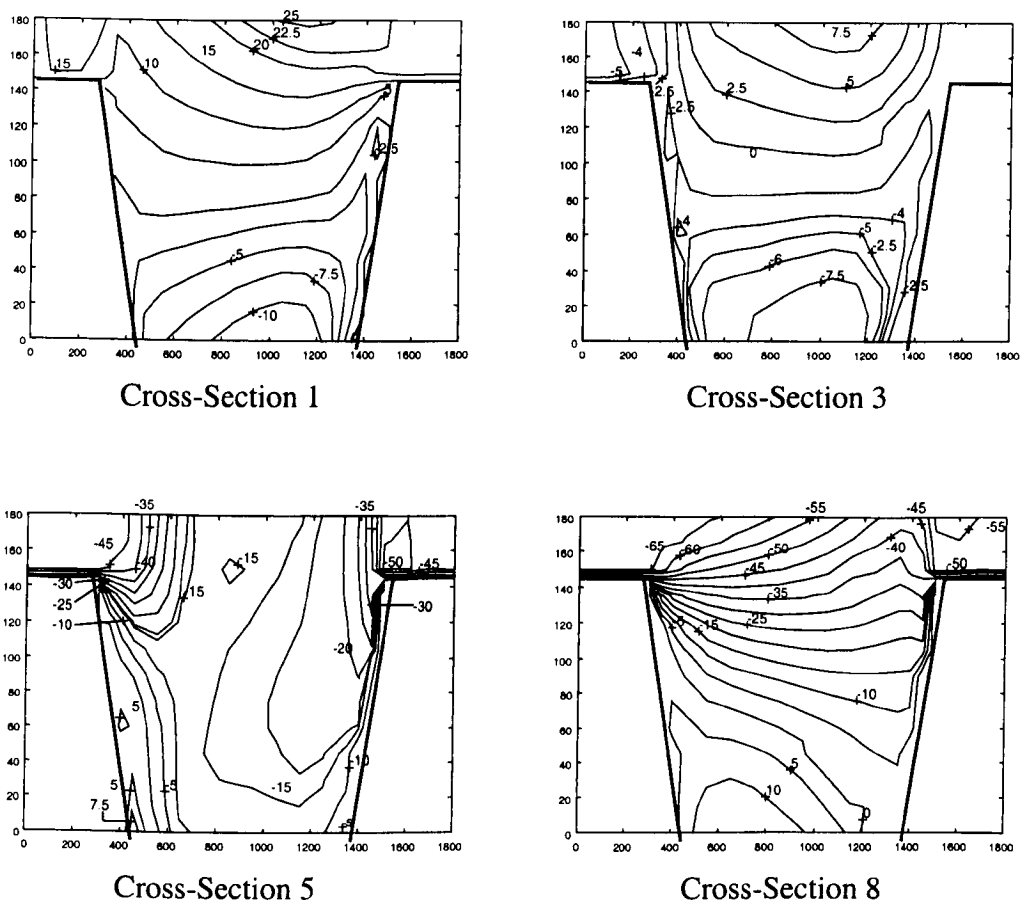

Fig. 5.43 - FCF B23 CFX Velocity Angle Predictions (deg.) at Cross-Sections 1, 3, 5 and 8 (k_s = 0.8 mm, Grid FCF-3, k-ε Model)

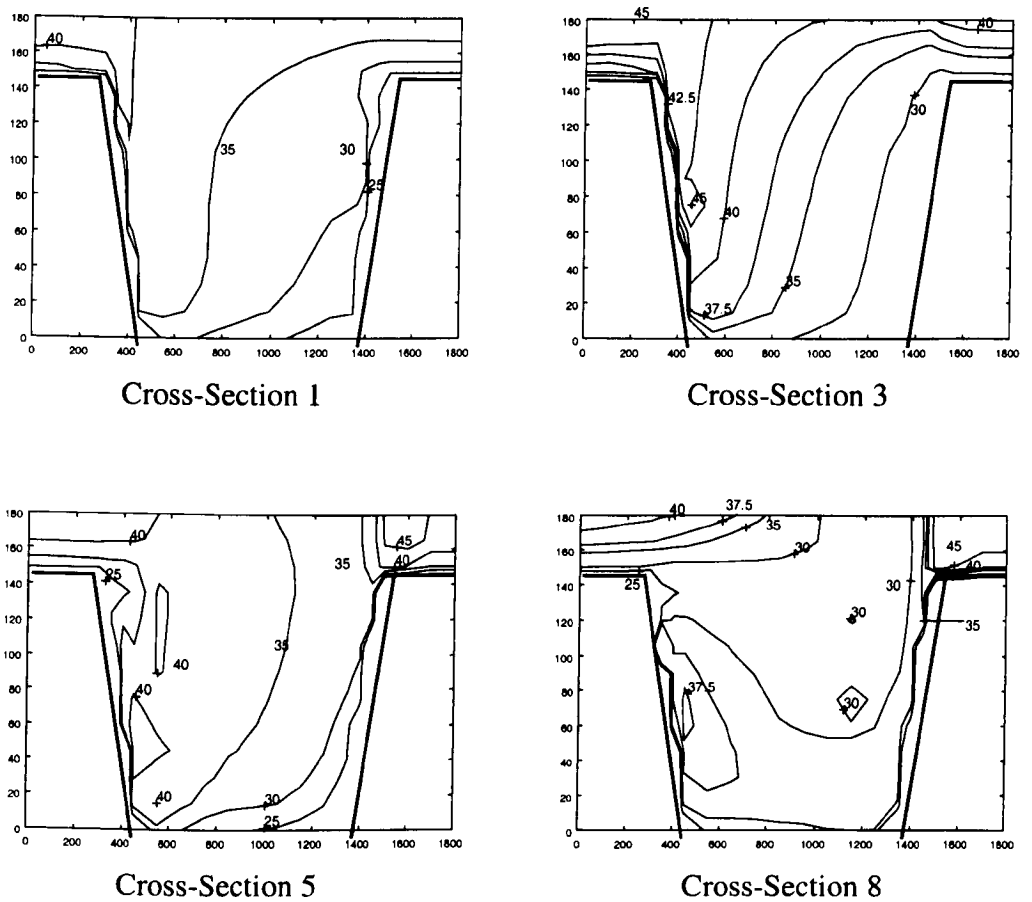

Fig. 5.44 – FCF B23 CFX Velocity Norm Predictions (cm/s) at Cross-Sections 1, 3, 5 and 8 (k_s = 0.8 mm, Grid FCF-3, RSM Model)

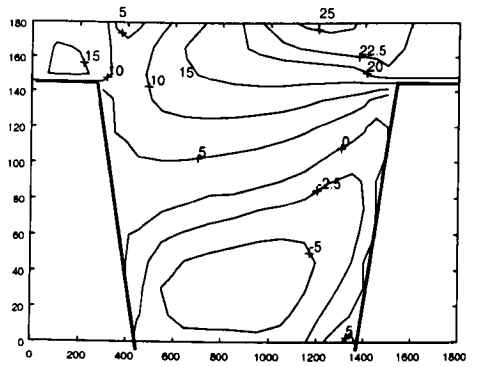

Cross-Section 1

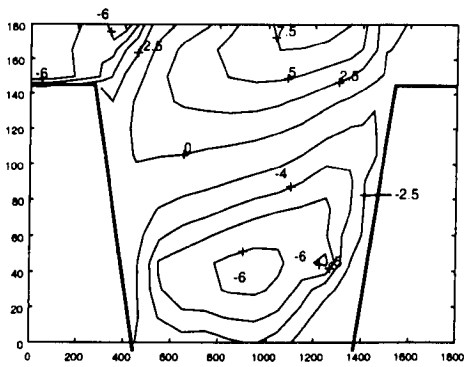

Cross-Section 3

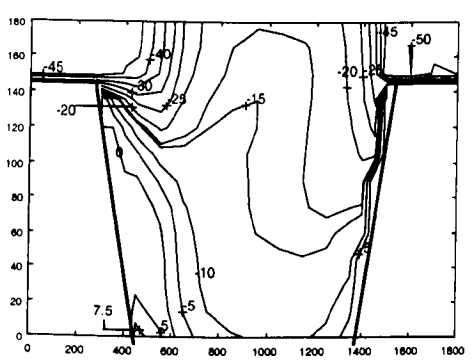

Cross-Section 5

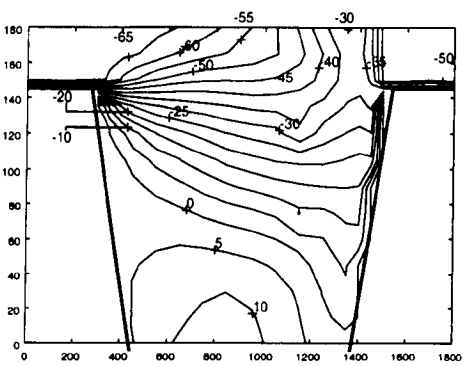

Cross-Section 5

Fig. 5.45 – FCF B23 CFX Velocity Angle Predictions (deg.) at Cross-Sections 1, 3, 5 and 8 (k_s = 0.8 mm, Grid FCF-3, RSM Model)

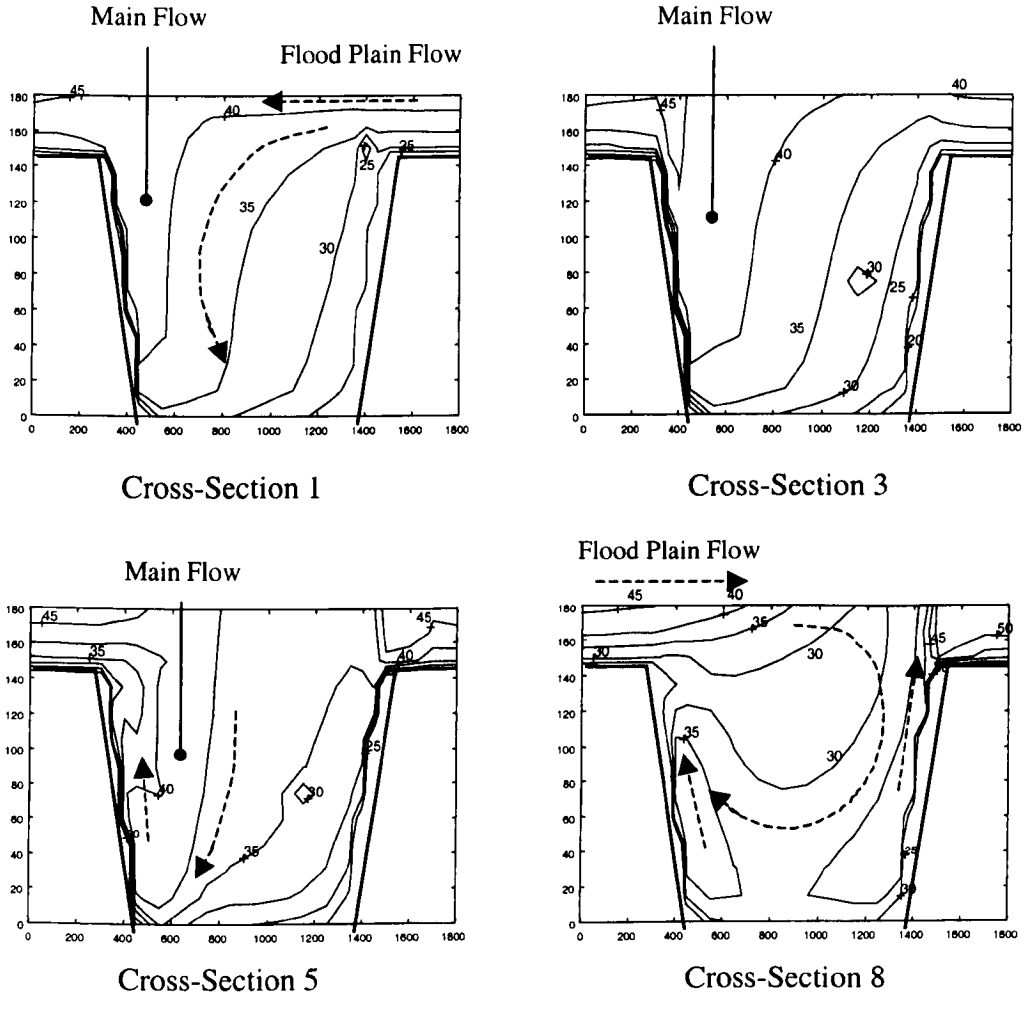

Fig. 5.46 – FCF B23 CFX Velocity Norm Predictions (cm/s) at Cross-Sections 1, 3, 5 and 8 (k_s = 0.2 mm, Grid FCF-3, k-ε Model)

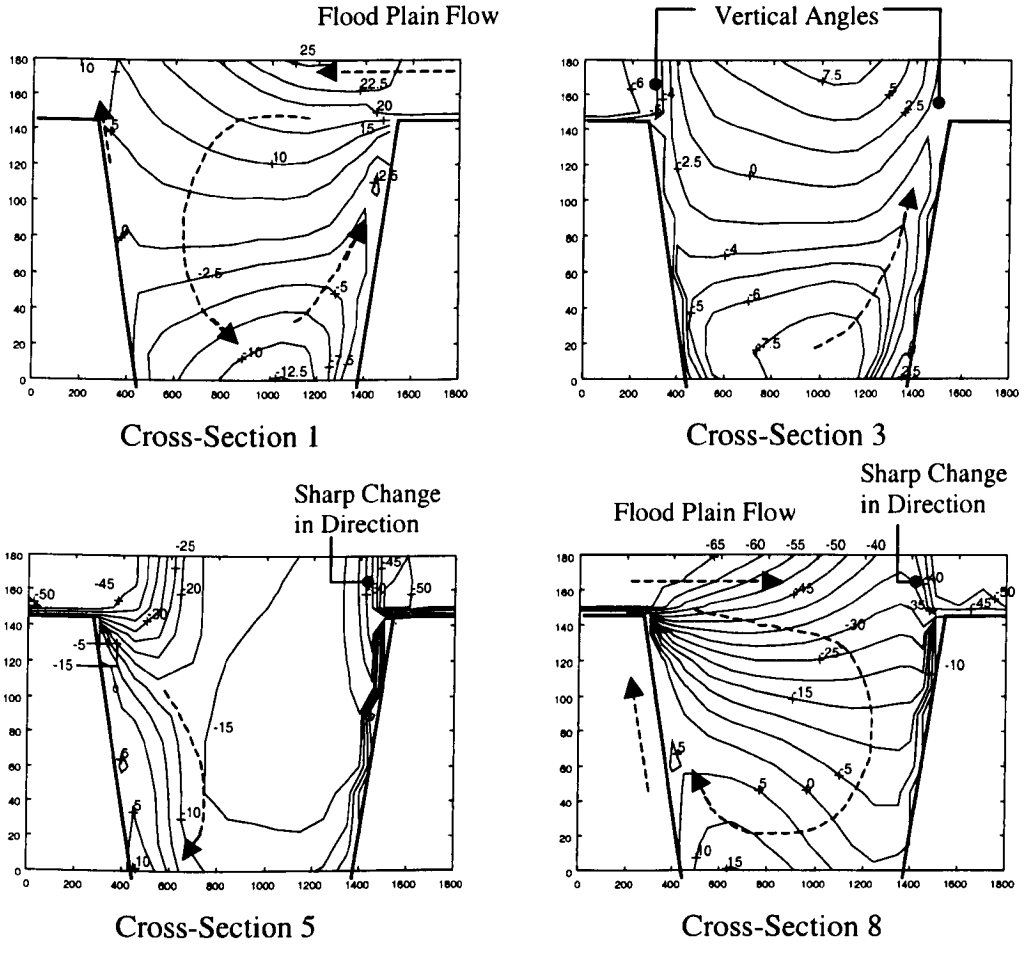

Fig. 5.47 - FCF B23 CFX Velocity Angle Predictions (deg.) at Cross-Sections 1, 3, 5 and 8 (k_s = 0.2 mm, Grid FCF-3, RSM)

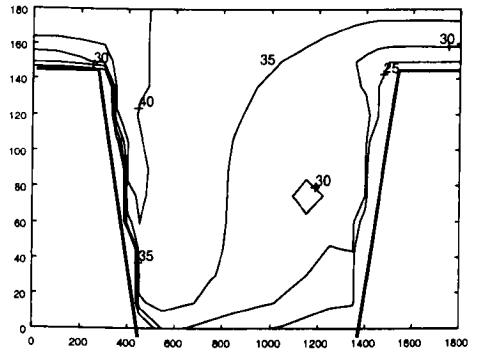

Cross-Section 1

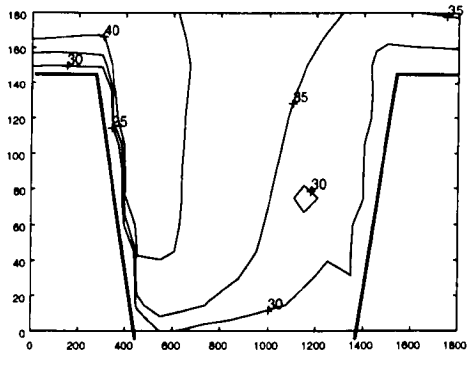

Cross-Section 3

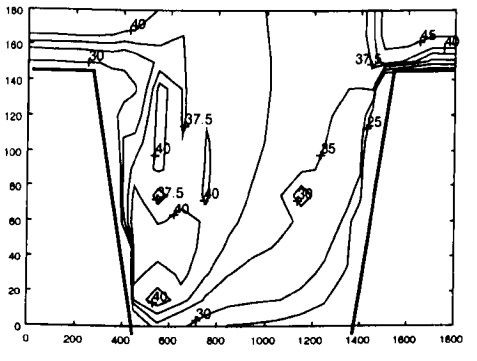

Cross-Section 5

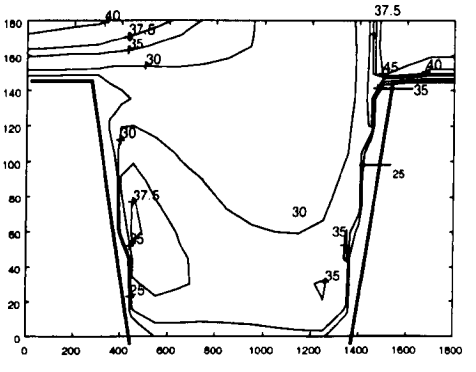

Cross-Section 8

Fig. 5.48 – FCF B23 CFX Velocity Norm Predictions (cm/s) at Cross-Sections 1, 3, 5 and 8 (k_s = 0.2 mm, Grid FCF-3, RSM)

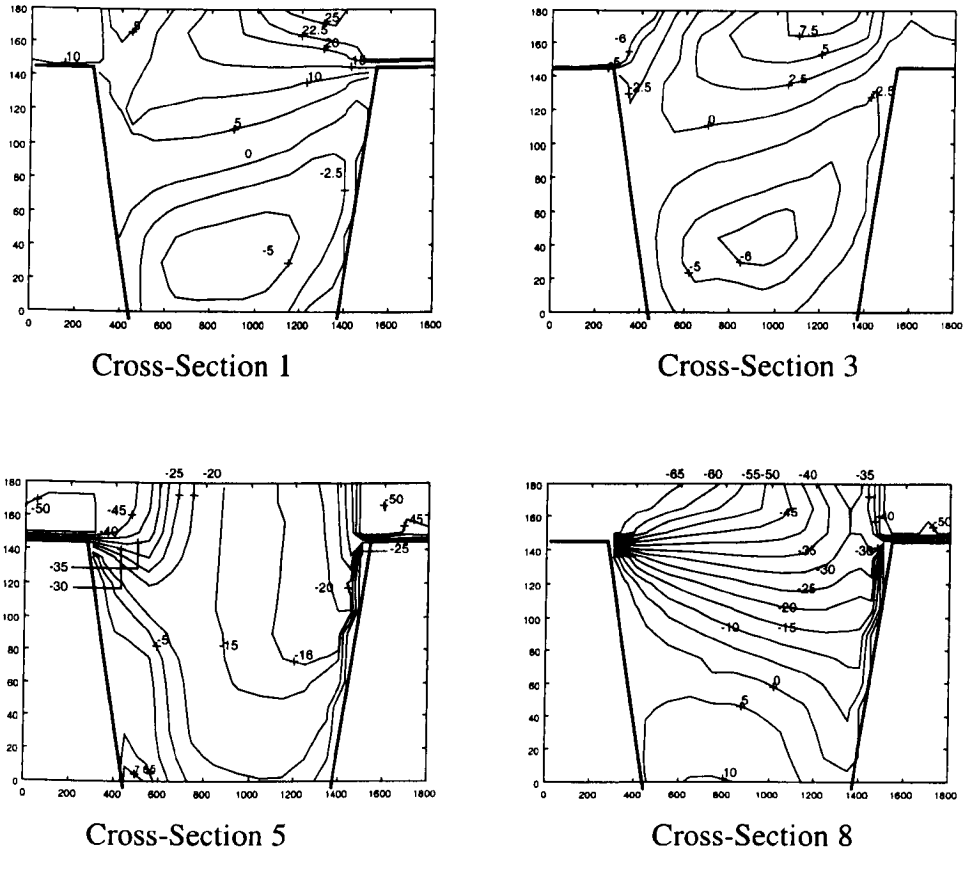

Fig. 5.49 - FCF B23 CFX Velocity Angle Predictions (deg.) ay Cross-Sections 1, 3, 5 and 8 (k_s = 0.2 mm, Grid FCF-3, RSM)

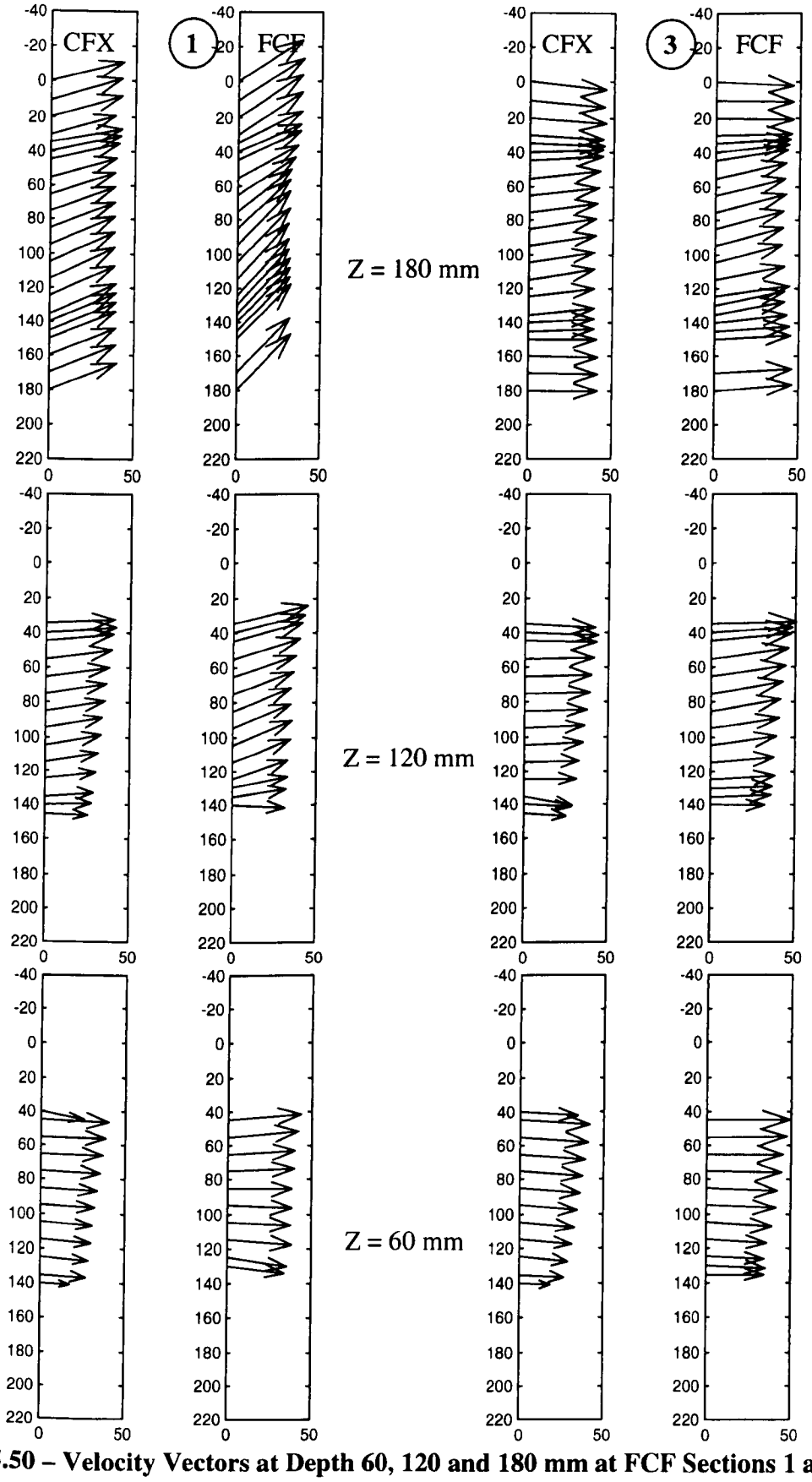

Fig. 5.50 – Velocity Vectors at Depth 60, 120 and 180 mm at FCF Sections 1 and 3

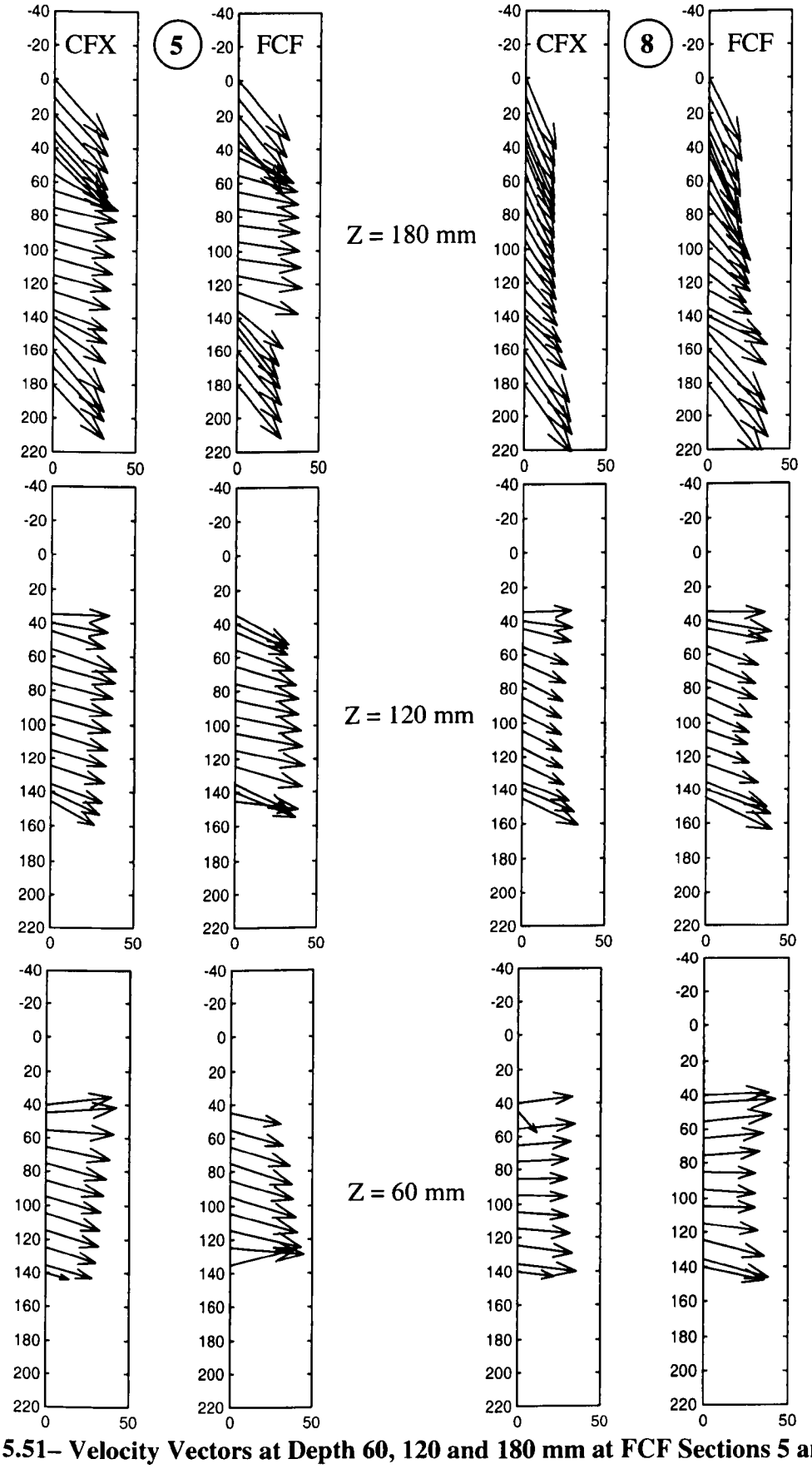

Fig. 5.51– Velocity Vectors at Depth 60, 120 and 180 mm at FCF Sections 5 and 8

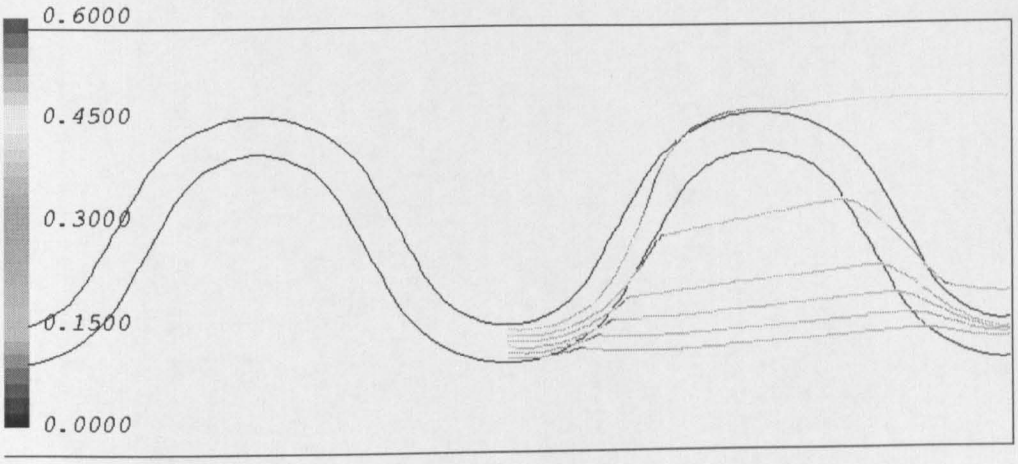

(a)

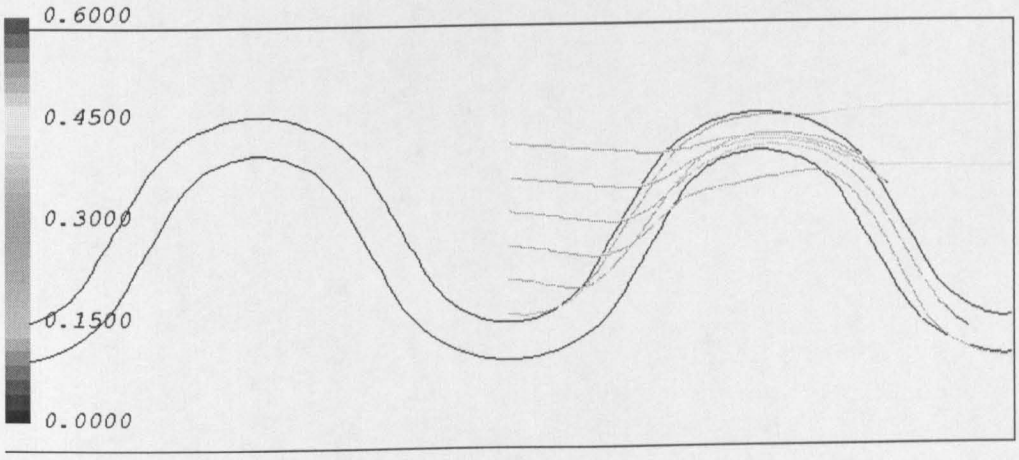

(b)

Fig. 5.52 – FCF B23 CFX Numerical Tracer Experiment:
(a) Release in Main Channel at Mid-Depth (100 mm)
(b) Release on the Floodplain at Mid-Depth (175 mm)

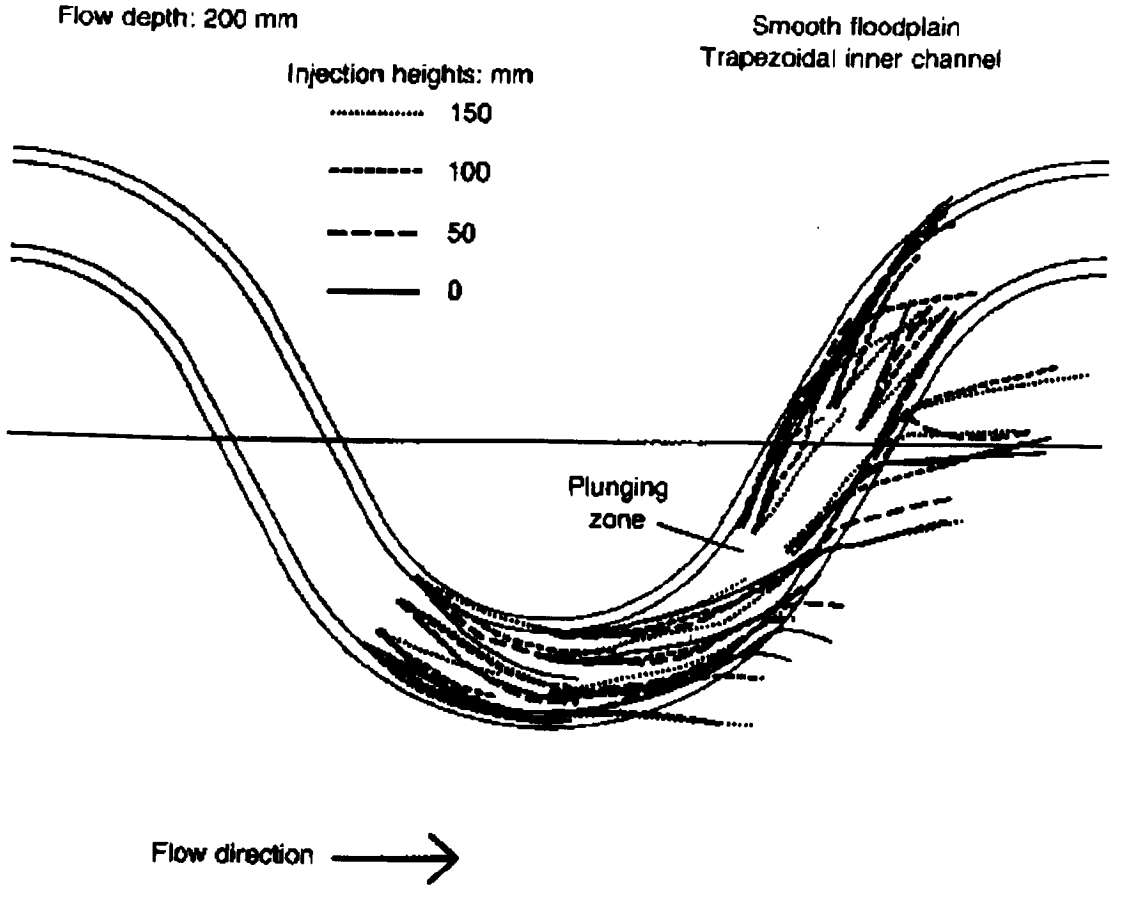

Fig. 5.53 – Tracer Experimental Data in FCF B23
(after Willetts and Hardwick, 1993)

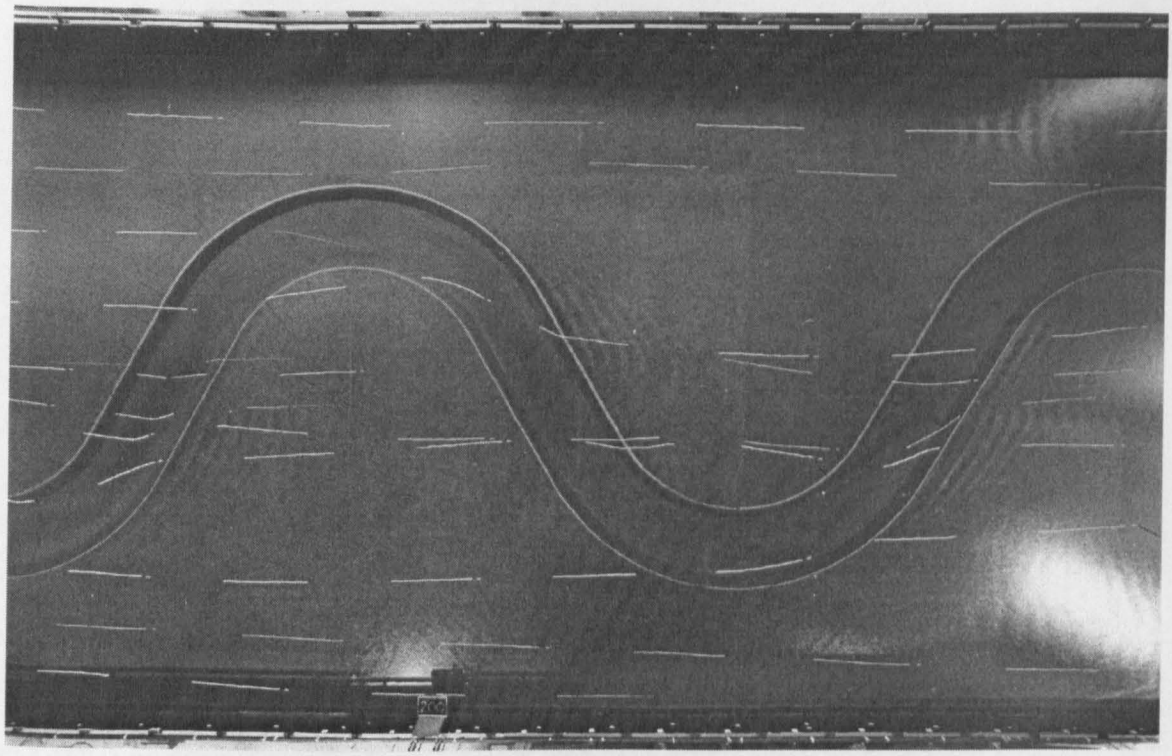

(a)

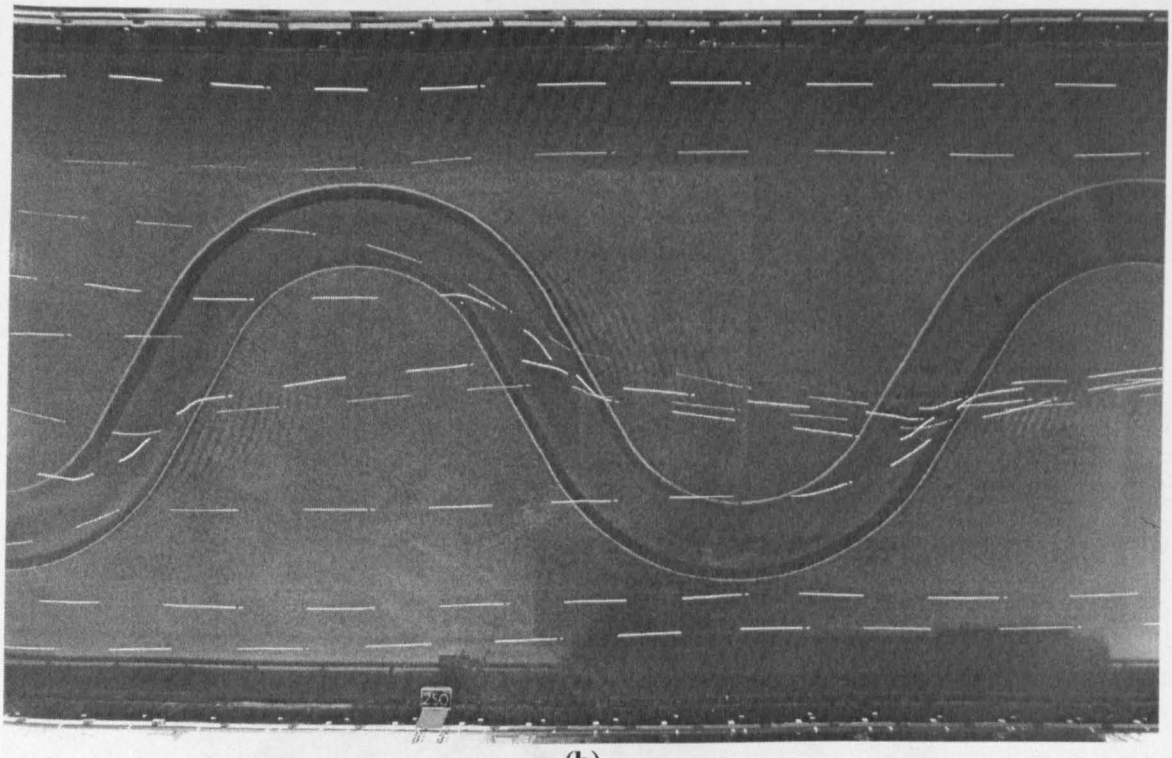

(b)

Fig. 5.54 – Surface Tracer Experiment Photographs in FCF Series B: (a) Dr = 0.25, (b) Dr = 0.40
(Courtesy of Professor Ervine, Univ. of Glasgow)

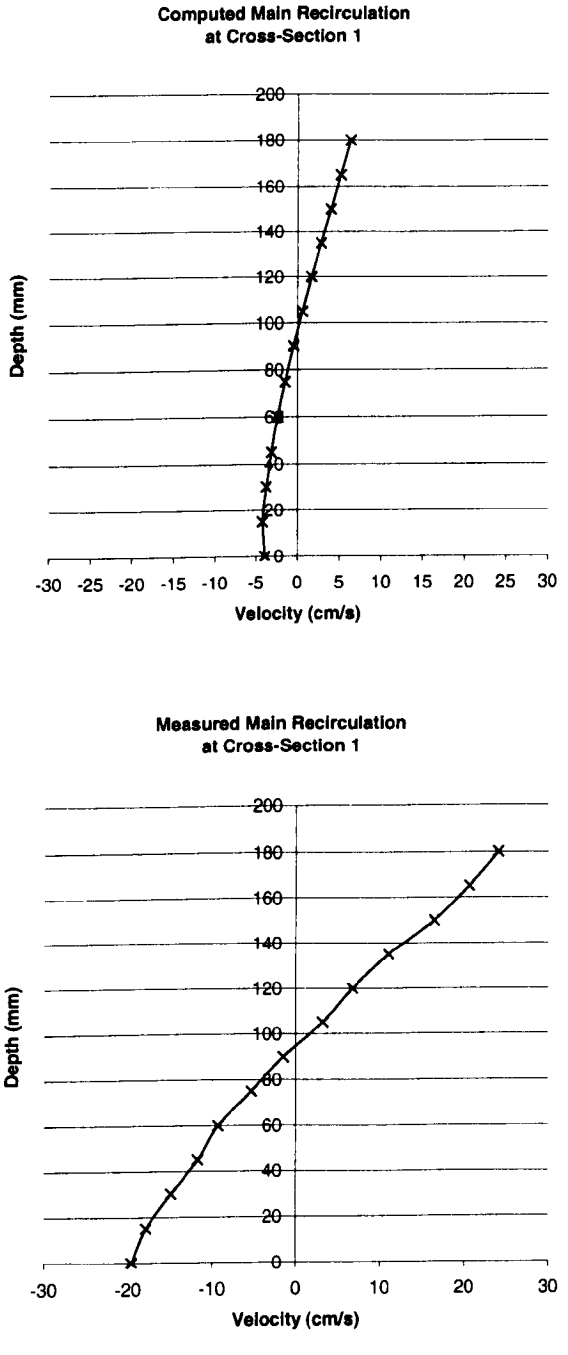

Fig. 5.55 – FCF B23 CFX Model: Recirculation at Cross-Section 1

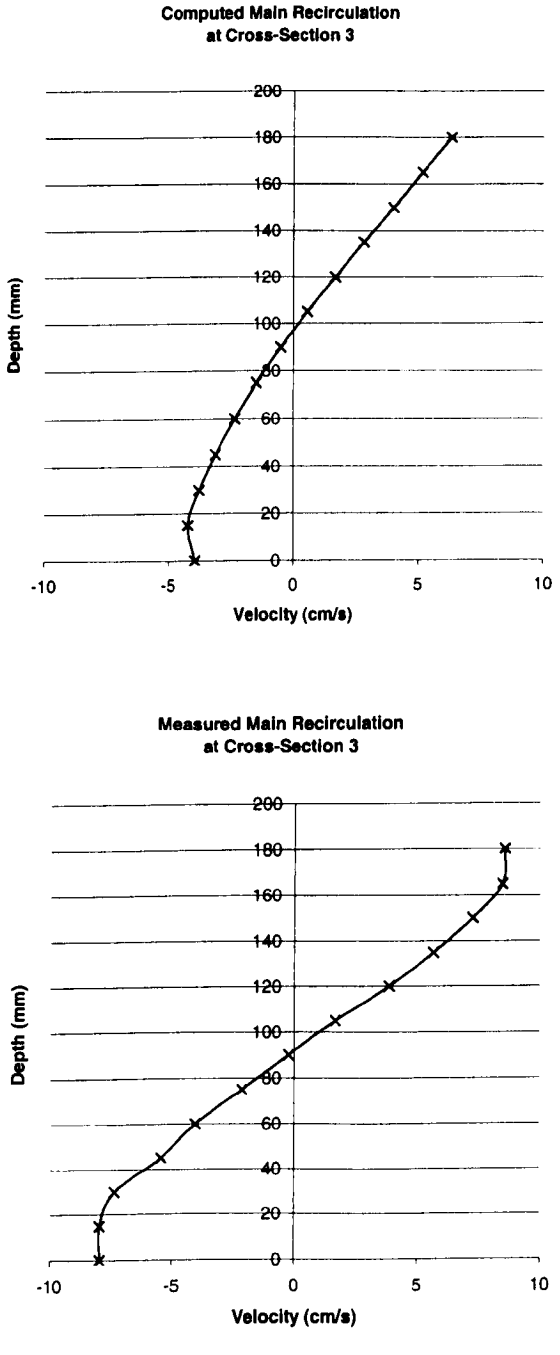

Fig. 5.56 – FCF B23 CFX Model: Recirculation at Cross-Section 3

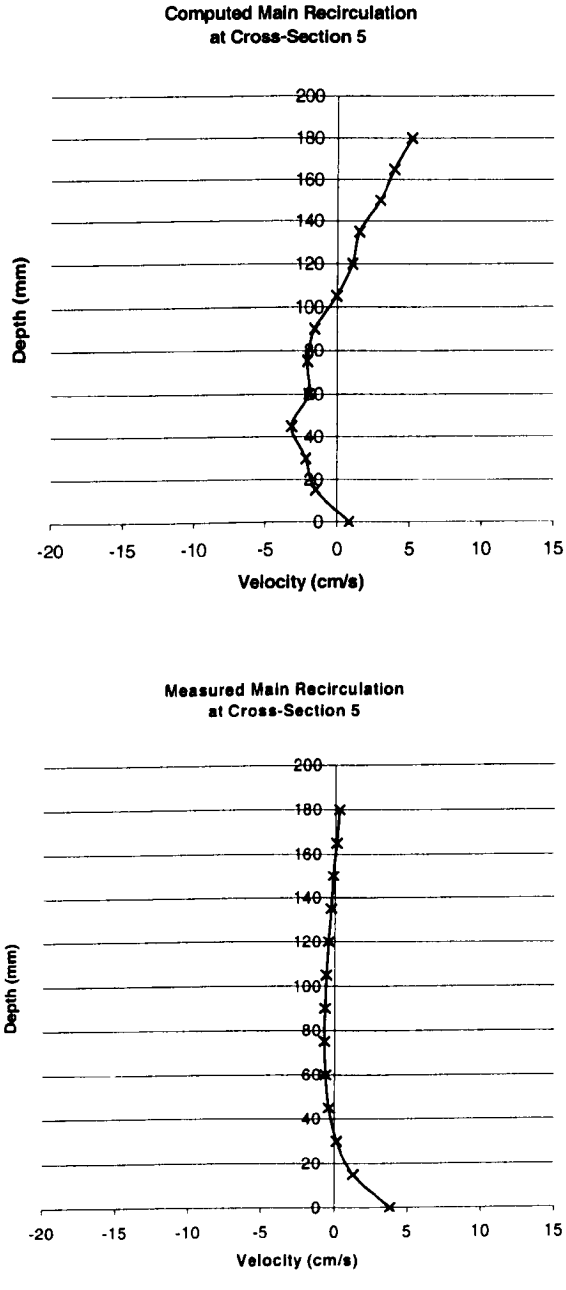

Fig. 5.57 – FCF B23 CFX Model: Recirculation at Cross-Section 5

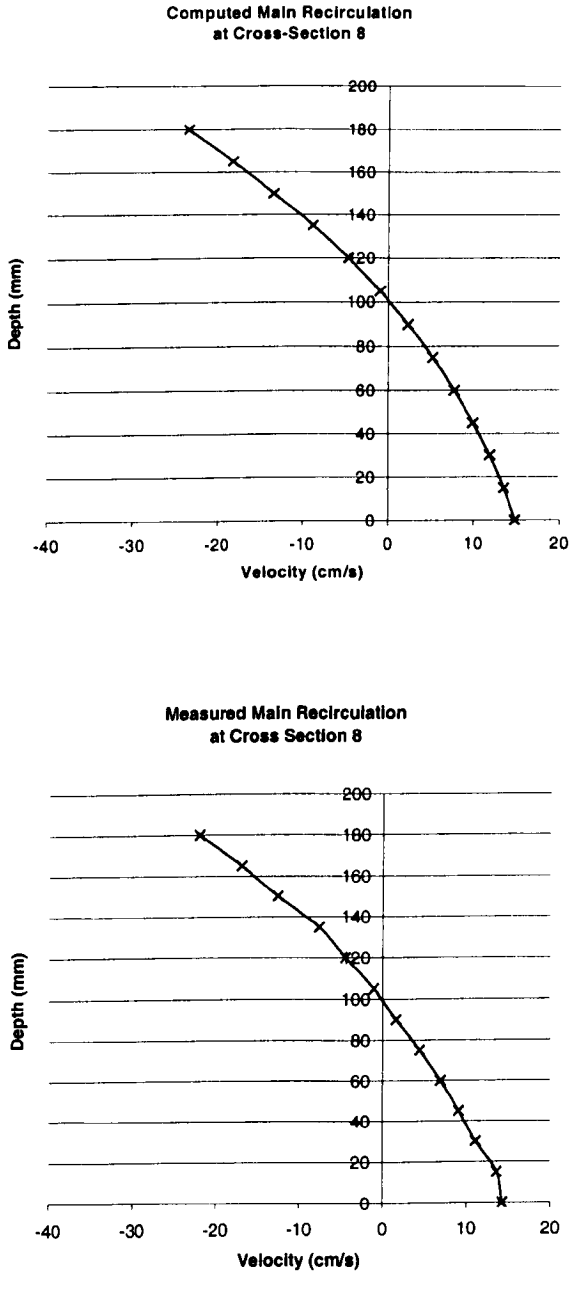

Fig. 5.59 – FCF B23 CFX Model: Recirculation at Cross-Section 8

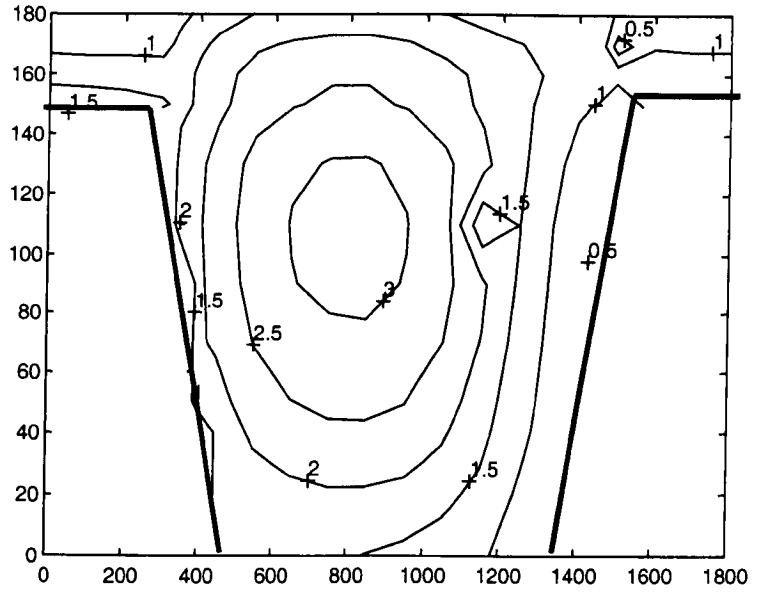

(a)

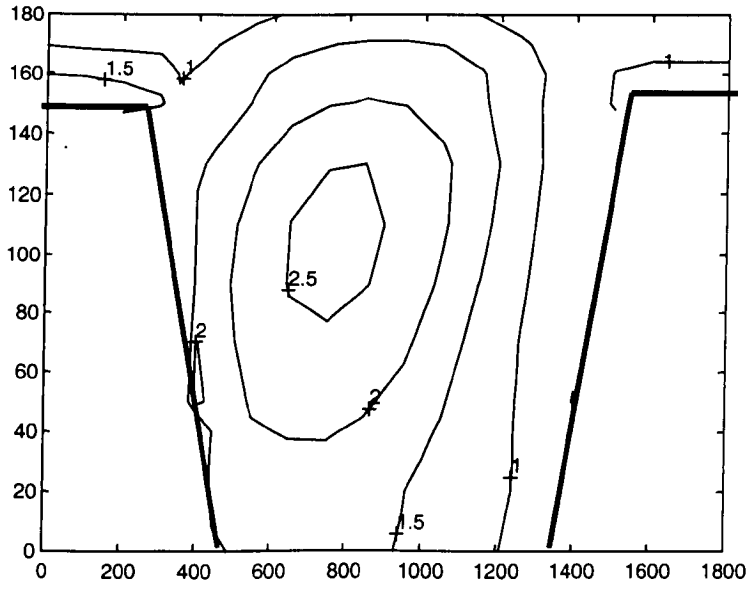

(b)

Fig. 5.60 - CFX Predicted Turbulence Kinetic Energy ($\times 10^{-3}$ m^2/s^2) at Cross-Section 3:

(a) k-ε Model

(b) RSM

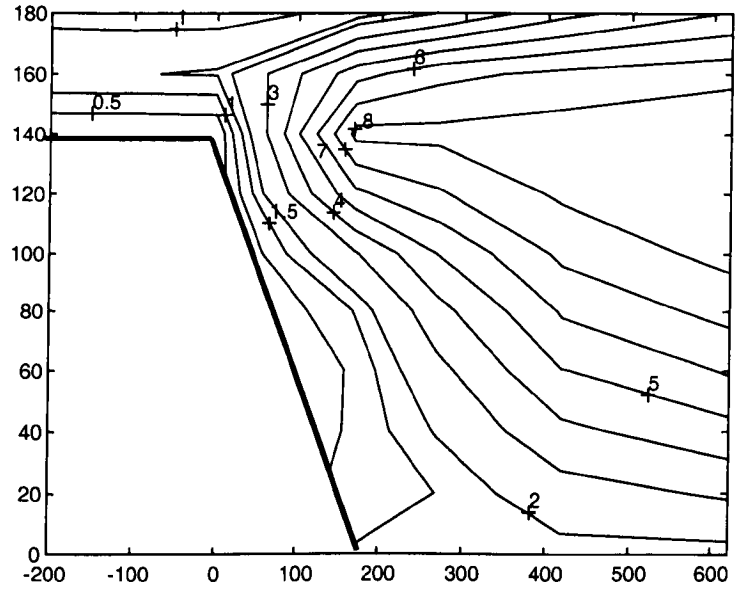

(a)

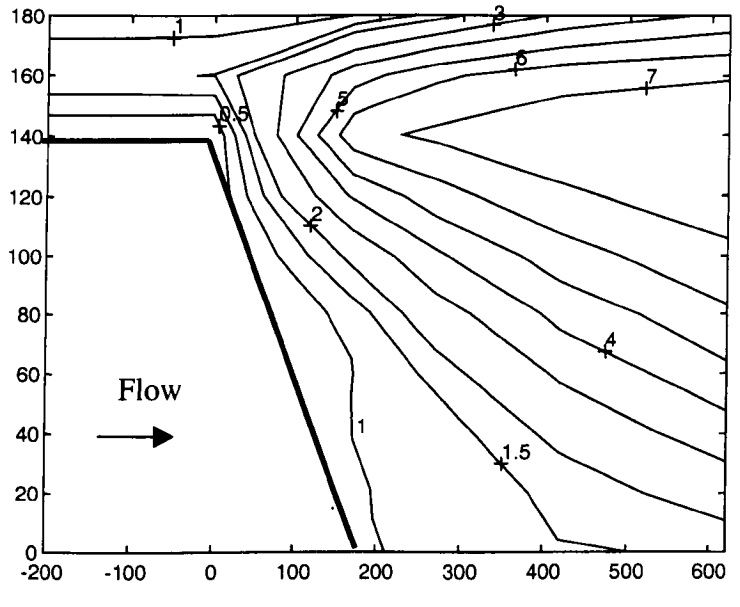

(b)

Fig. 5.61 – CFX Predicted Turbulence Kinetic Energy ($\times 10^{-3}$ m^2/s^2) at Cross-Section 8b:

(a) k-ε Model

(b) RSM

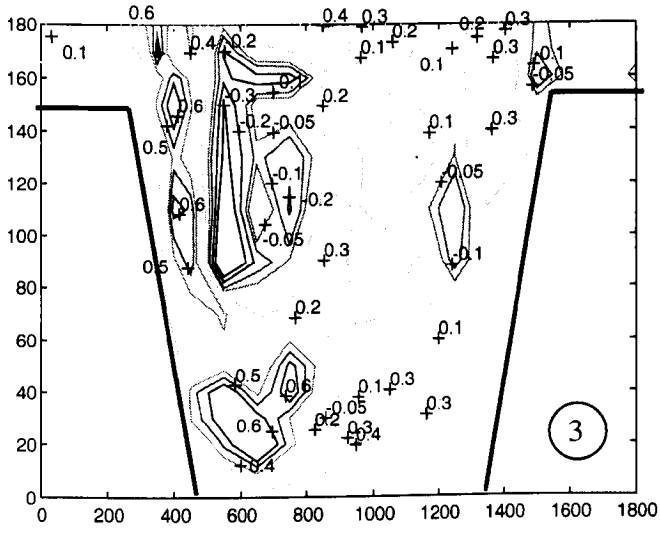

FCF Turbulence Data at Cross-Section 3: $T_{yx}(N/m^2)$

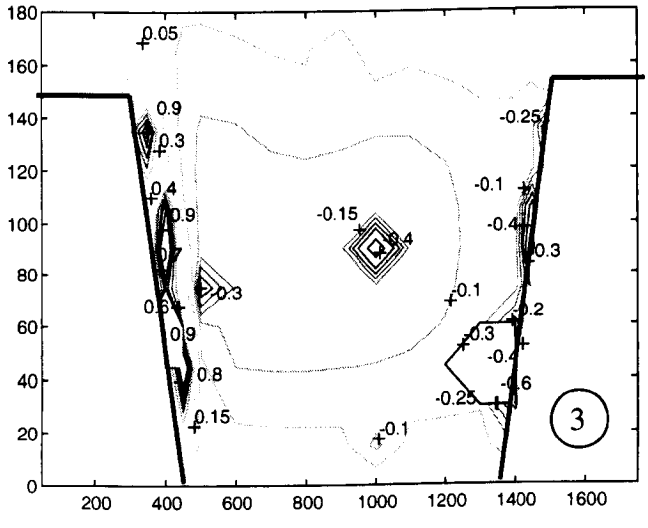

Processed T_{yx} (N/m^2) at Cross-Section 3, using CFX k-ε Data

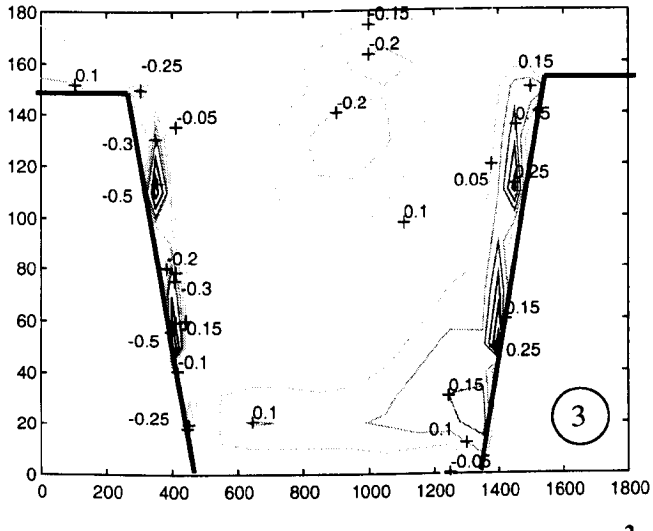

Calculated T_{yx} (N/m^2) at Cross-Section 3 with RSM

Fig. 5.62 – Comparison of T_{yx} (N/m^2) at Cross-Section 3

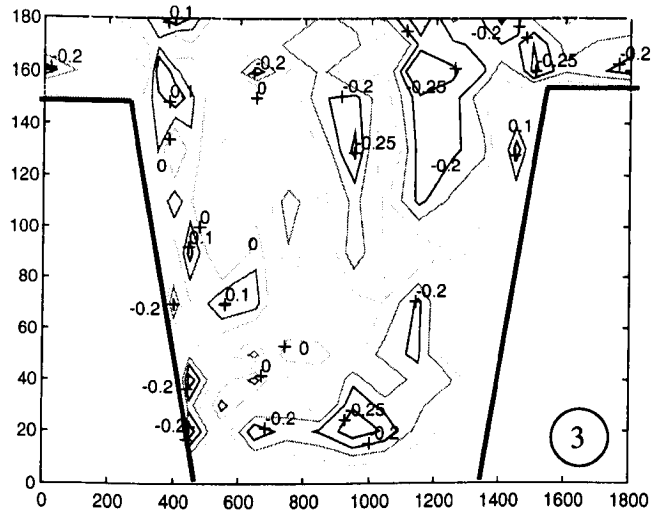

FCF Turbulence Data at Cross-Section 3: $T_{zx}(N/m^2)$

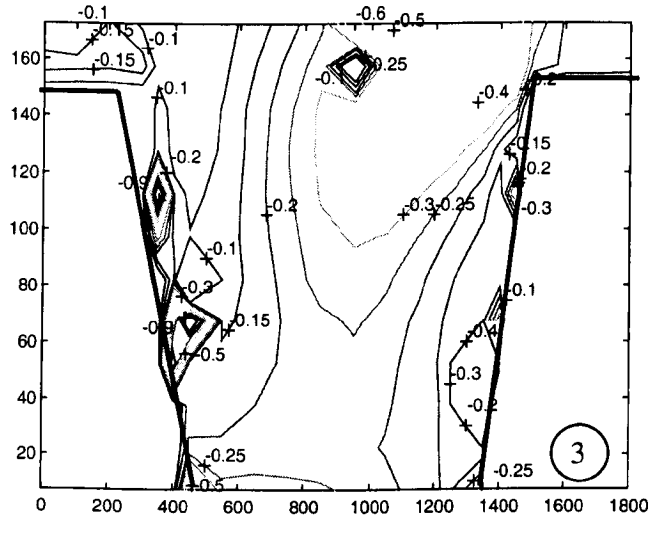

Processed $T_{zx}(N/m^2)$ at Cross-Section 3, using k-ε Data

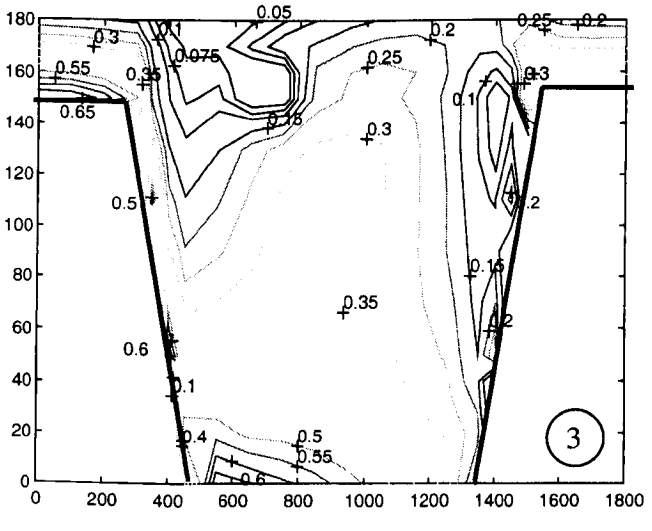

Calculated $T_{zx}(N/m^2)$ at Cross-Section 3 with RSM

Fig. 5.63 - Comparison of T_{zx} (N/m^2) at Cross-Section 3

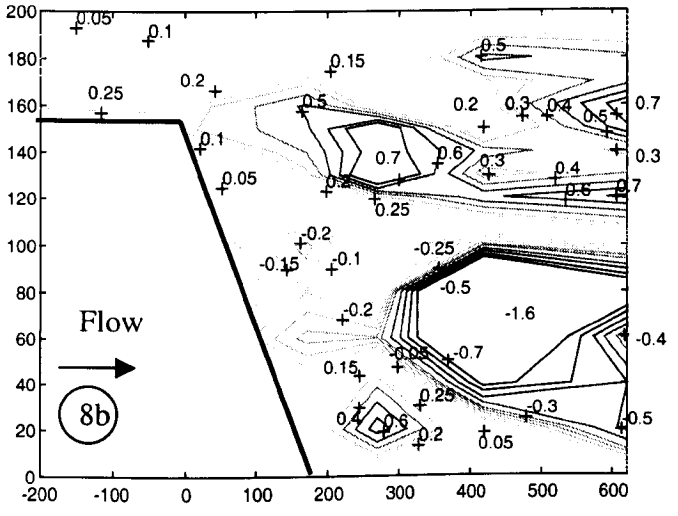

FCF Turbulence Data at the Cross-Over: $T_{zx}(N/m^2)$

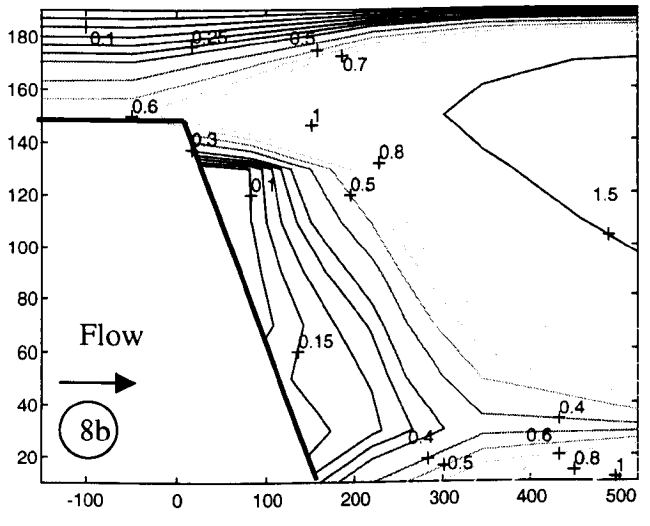

Processed $T_{zx}(N/m^2)$ at the Cross-Over, using k-ε Data

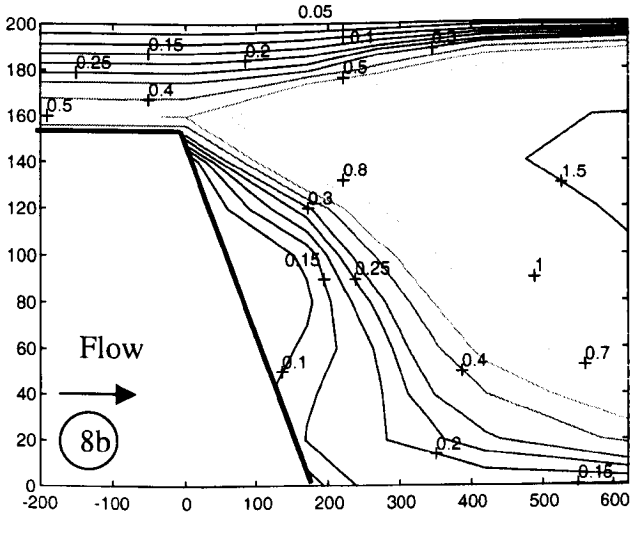

Calculated $T_{zx}(N/m^2)$ at the Cross-Over with RSM

Fig. 5.64 - Comparison of $T_{zx}(N/m^2)$ at the Cross-Over

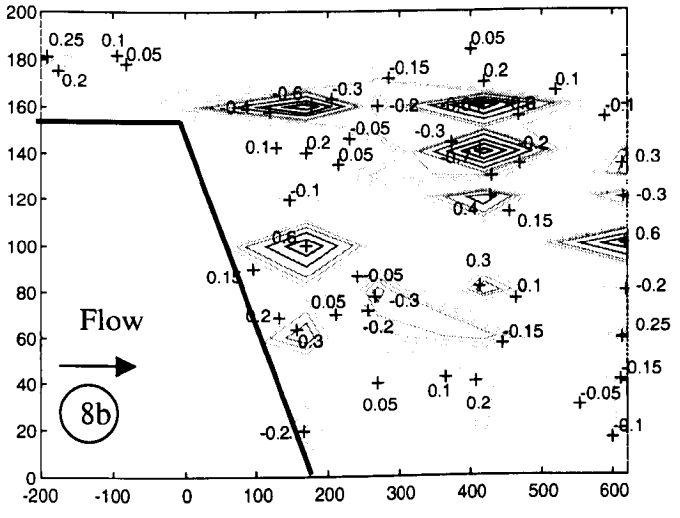

FCF Turbulence Data at the Cross-Over: $T_{yx}(N/m^2)$

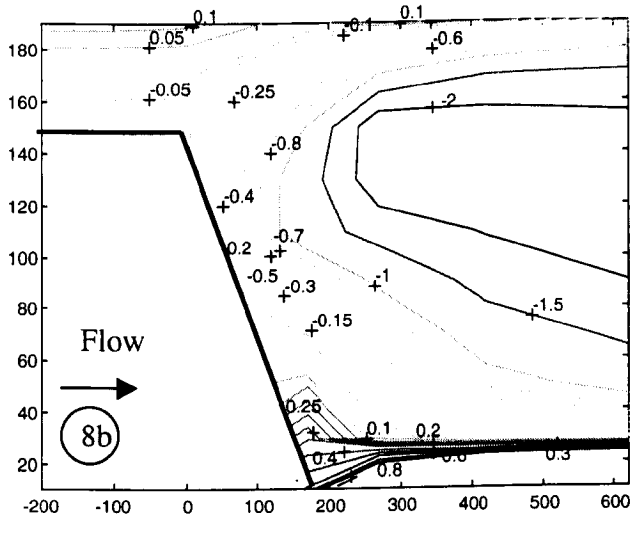

Processed $T_{yz}(N/m^2)$ at the Cross-Over, using k-ε Data

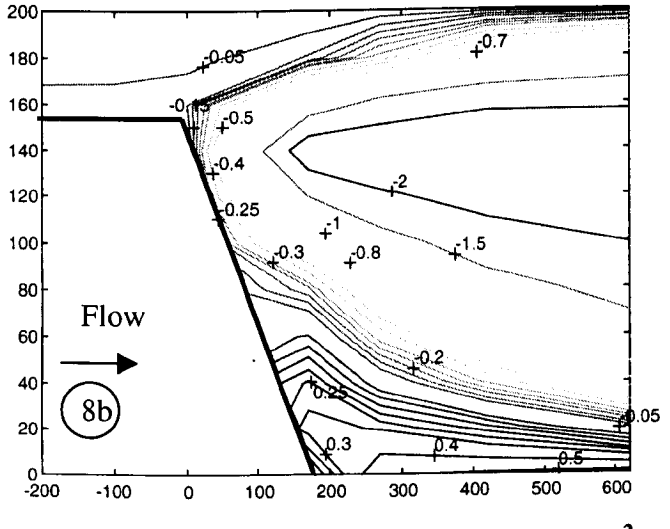

Calculated $T_{yz}(N/m^2)$ at the Cross-Over with RSM

Fig. 5.65 - Comparison of T_{yz} (N/m^2) at the Cross-Over

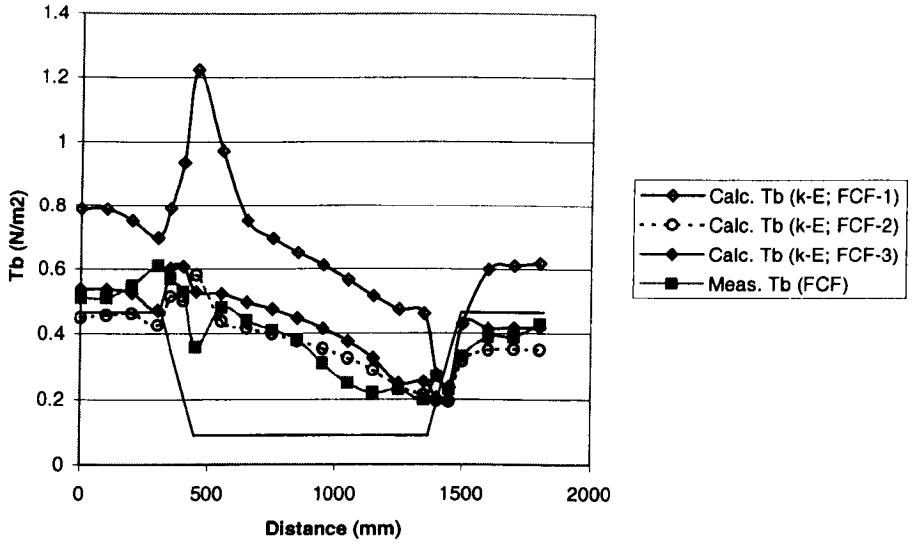

(a)

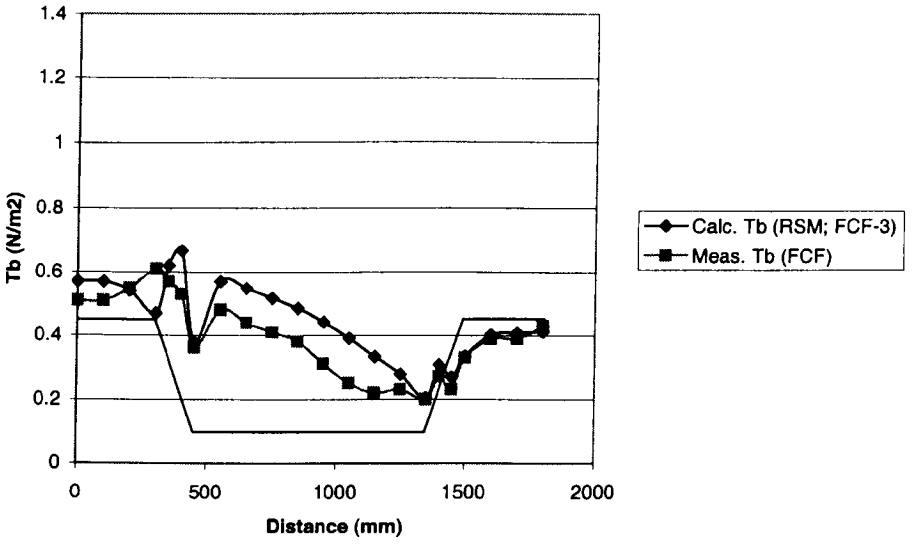

(b)

Fig. 5.66 – Comparison of Bed Shear Stress Profiles at Cross-Section 3 from CFX FCF B23 Model:
(a) with k-ε turbulence model;
(b) with LRR-RSM.

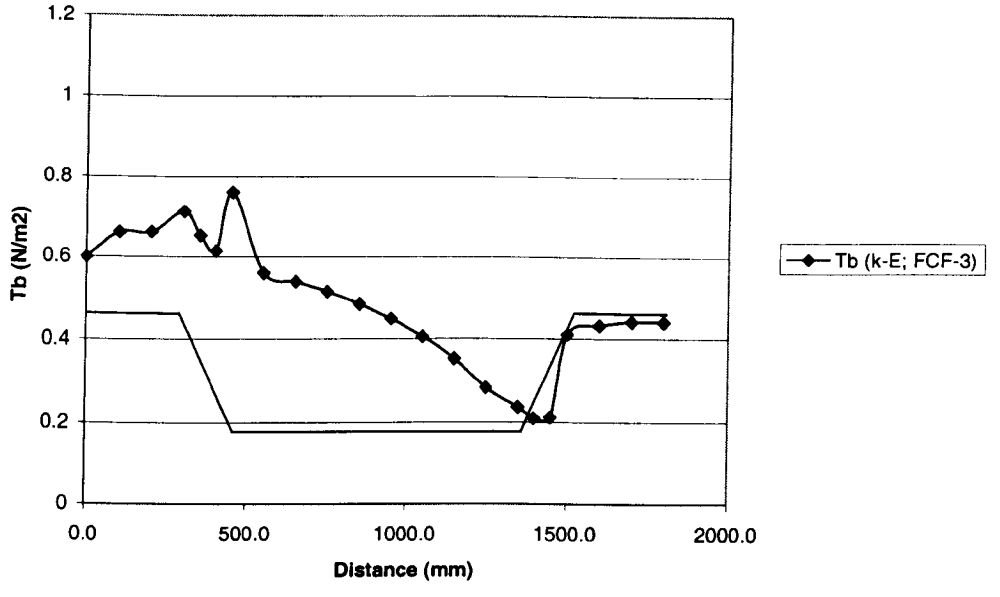

Fig. 5.67 – Calculated Bed Shear Stress Profile at Cross-Section 1 from CFX FCF B23 Model

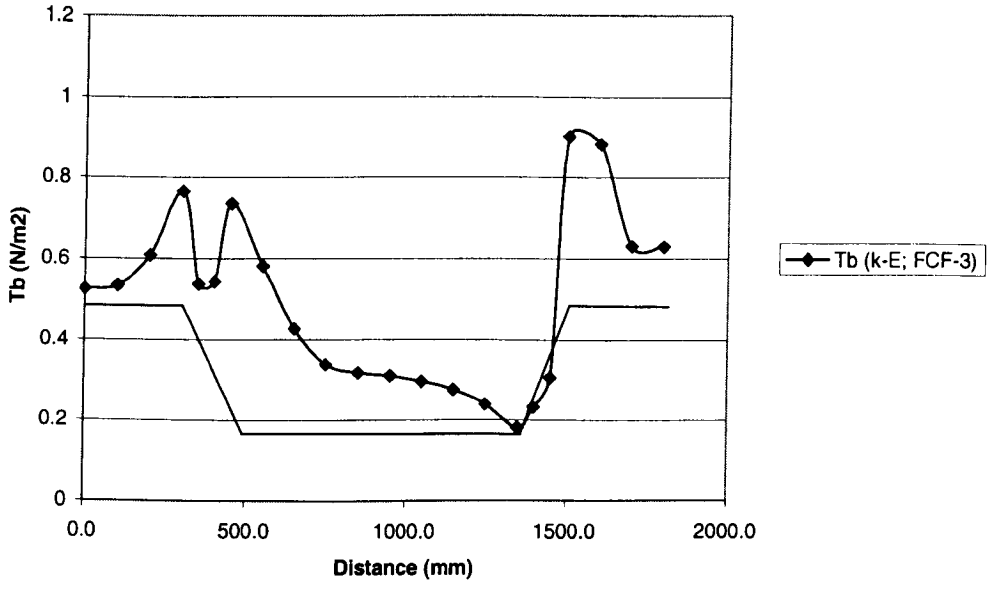

Fig. 5.68 – Calculated Bed Shear Stress Profile at Cross-Section 5 from CFX FCF B23 Model

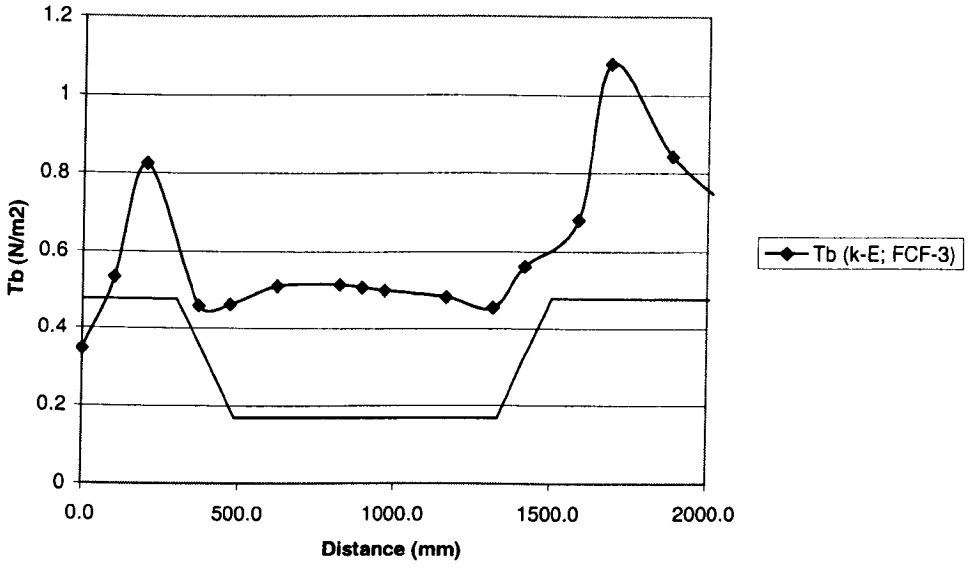

Fig. 5.69 – Calculated Bed Shear Stress Profile at Cross-Section 8 from CFX FCF B23 Model

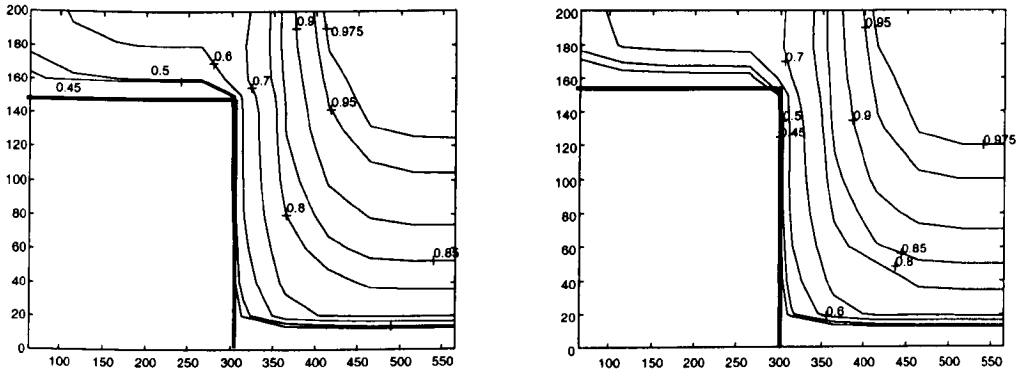

Fig. 5.70 – Comparison of Velocity Profile in Tominaga's Model For Different Grid Resolutions (54,000 and 109,200 Elements)

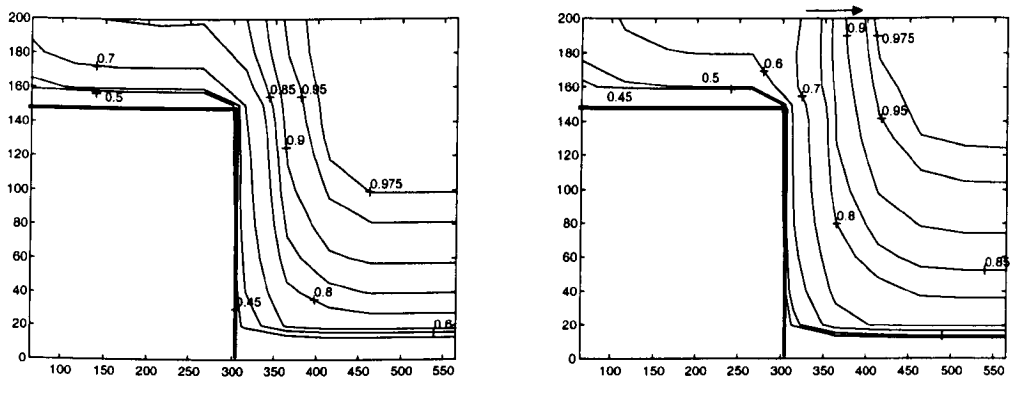

(a) (b)

Fig. 5.71 – Predicted Velocity Profiles in Tominaga's Experiment (CFX):

(a) k-ε Model

(b) LRR-RSM

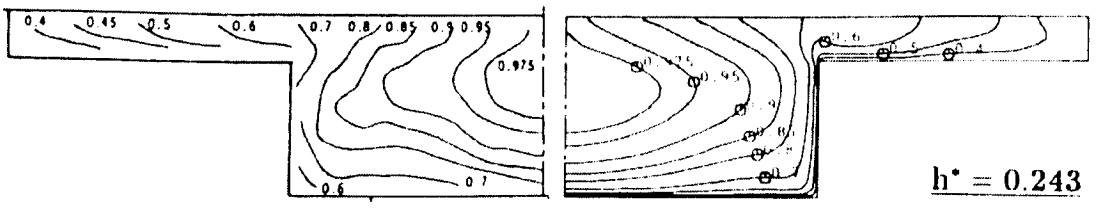

(a) (b)

Fig. 5.72 – Tominga's Experiment Results:
(a) Laboratory Data (Tominaga et al., 1989)
(b) LRR-RSM Numerical Model (Cokljat, 1993)

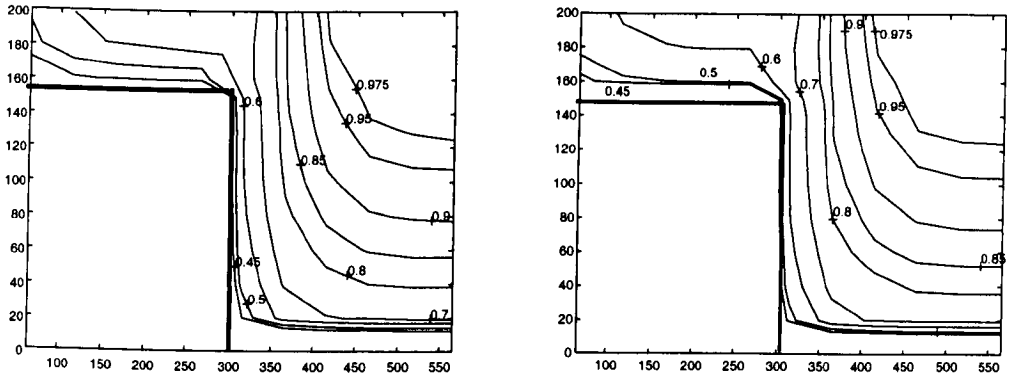

(a) (b)

Fig. 5.73 – Impact of Reynolds Number in Tominaga's Experiment (CFX):

(a) Re = 3.5×10^4

(b) Re = 7.0×10^4

Chapter 6:
Application of CFD to Flooded Rivers
– Rivers Severn and Ribble

Figures for Chapter 6

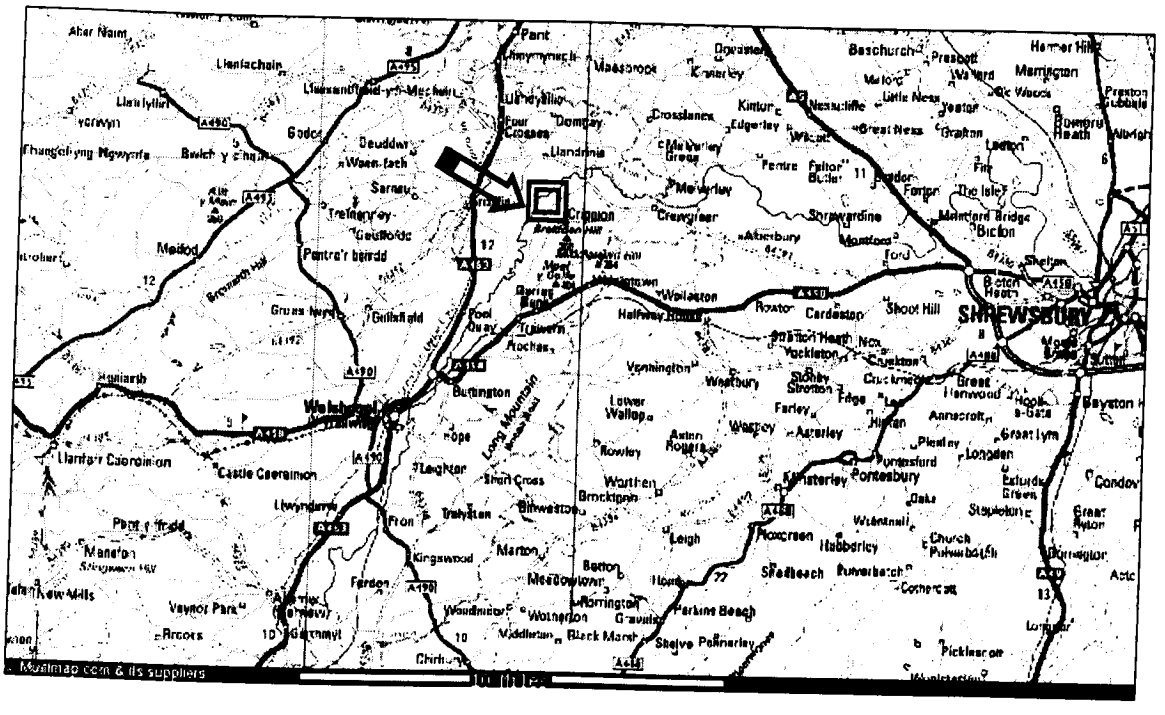

(a)

(b)

Fig. 6.1 – Location of the River Severn Site (MultiMap.Com)

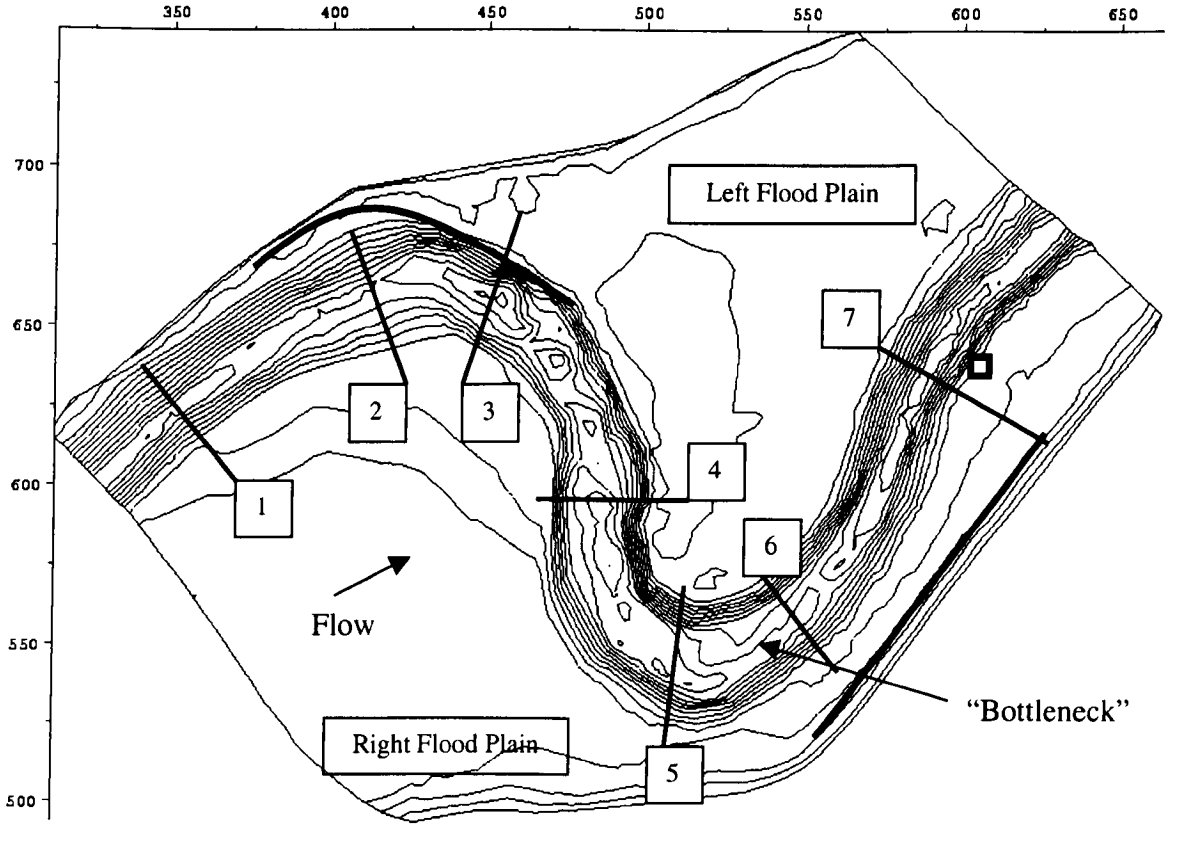

Fig. 6.2 – Plan View of the Severn, Location of the Cross-Sections, Path of the Free Surface Measurements ▬ and Location of the Measurement Tower ◘

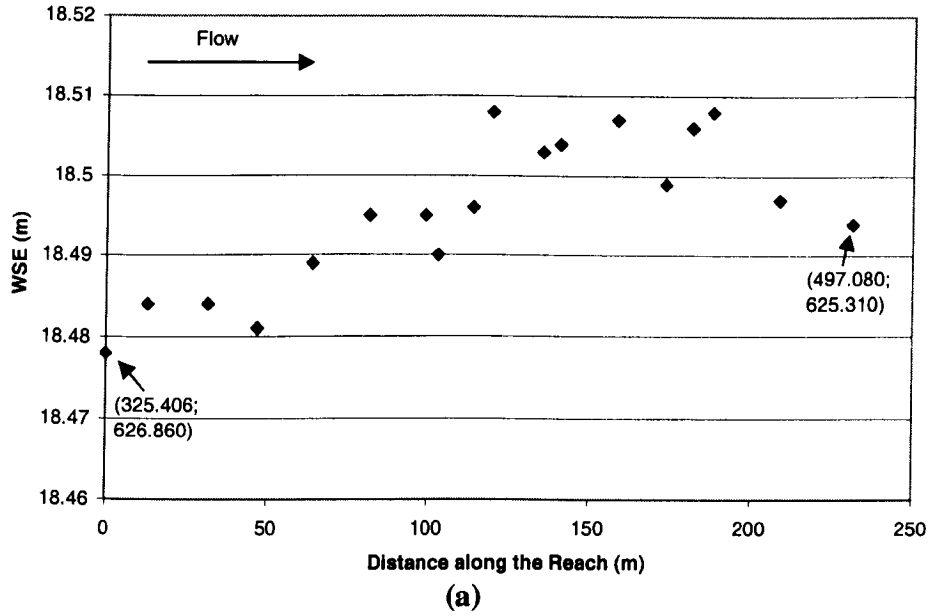

(a)

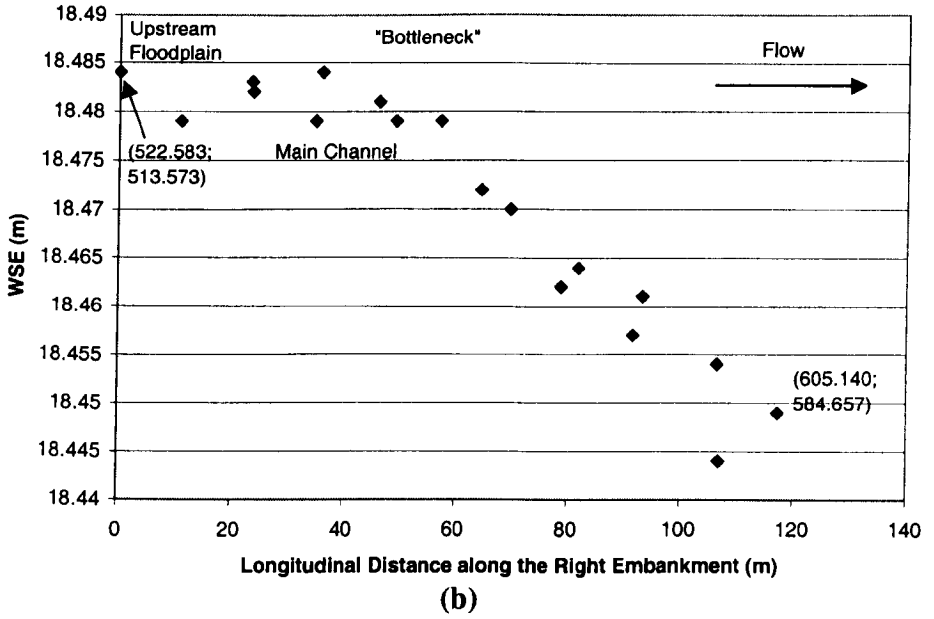

(b)

Fig. 6.3 – Observed Water Surface Elevation for the Event of 14 December 1999:
(a) Along the First Bend
(b) Along the Right Bund
(point planview coordinates in brackets)

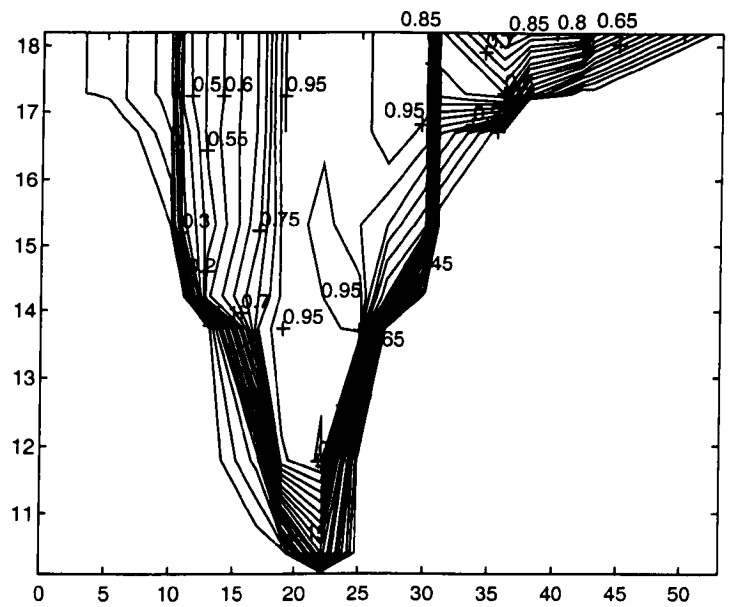

Fig. 6.4 – Measured Velocity Profile at Cross-Section 7 in the Severn (m/s; December 1999)

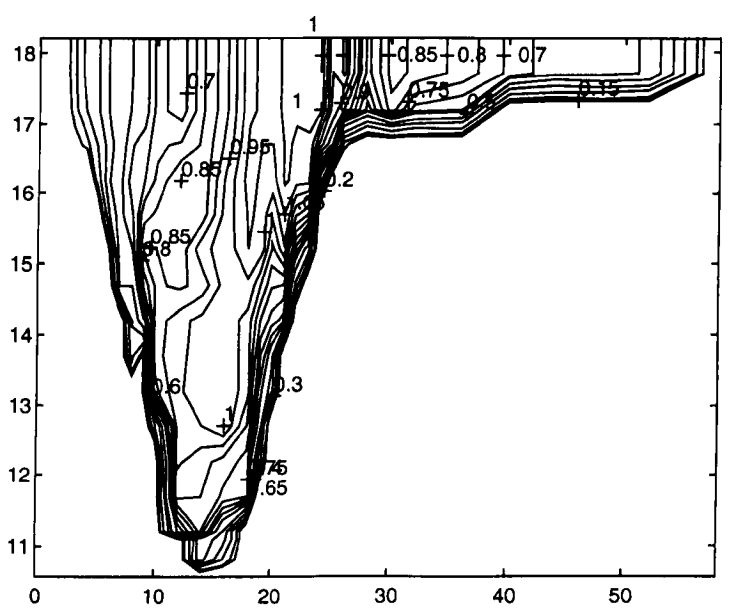

Fig. 6.5 – Measured Velocity Profile at Cross-Section 7 in the Severn (m/s; March 2000)

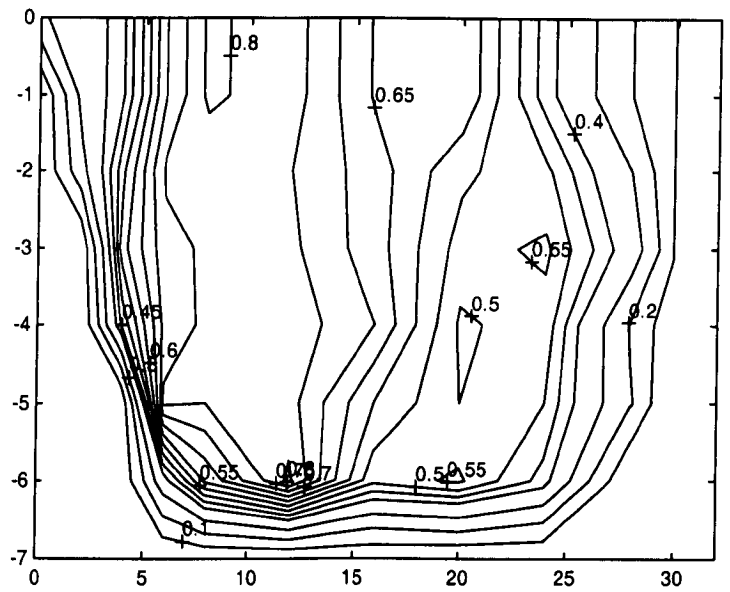

Fig. 6.6 – Measured velocity Profile at Cross-Section 5 in the Severn (m/s; October 2000)

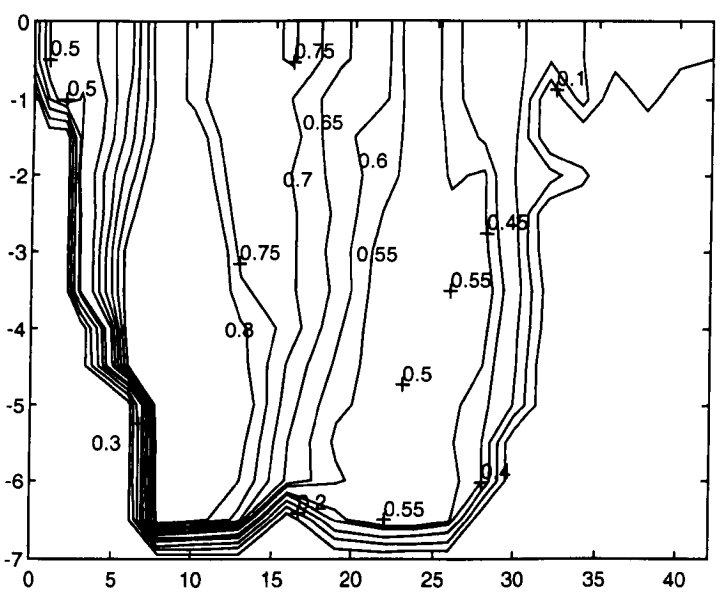

Fig. 6.7 – Measured Velocity Profile at Cross-Section 5 in the Severn (m/s; November 2000)

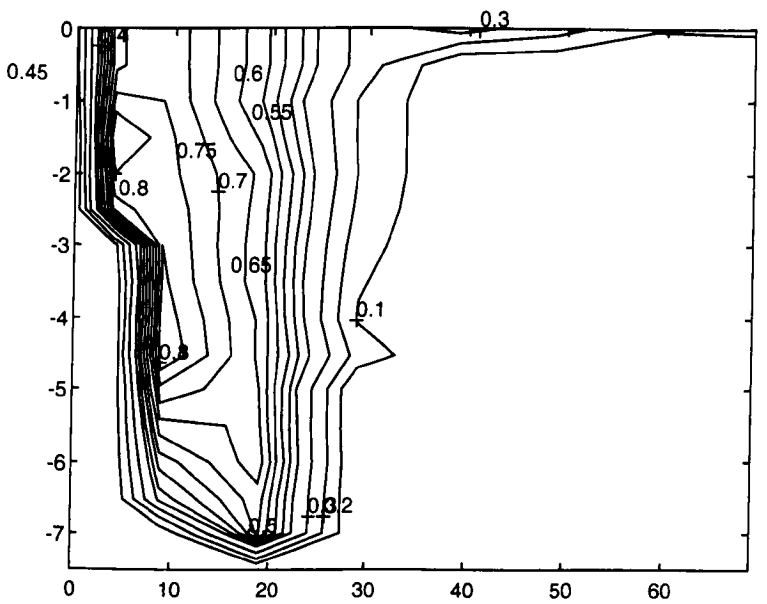

Fig. 6.8 – Measured velocity Profile Between Cross-Sections 4 and 5 in the Severn (m/s; December 2000)

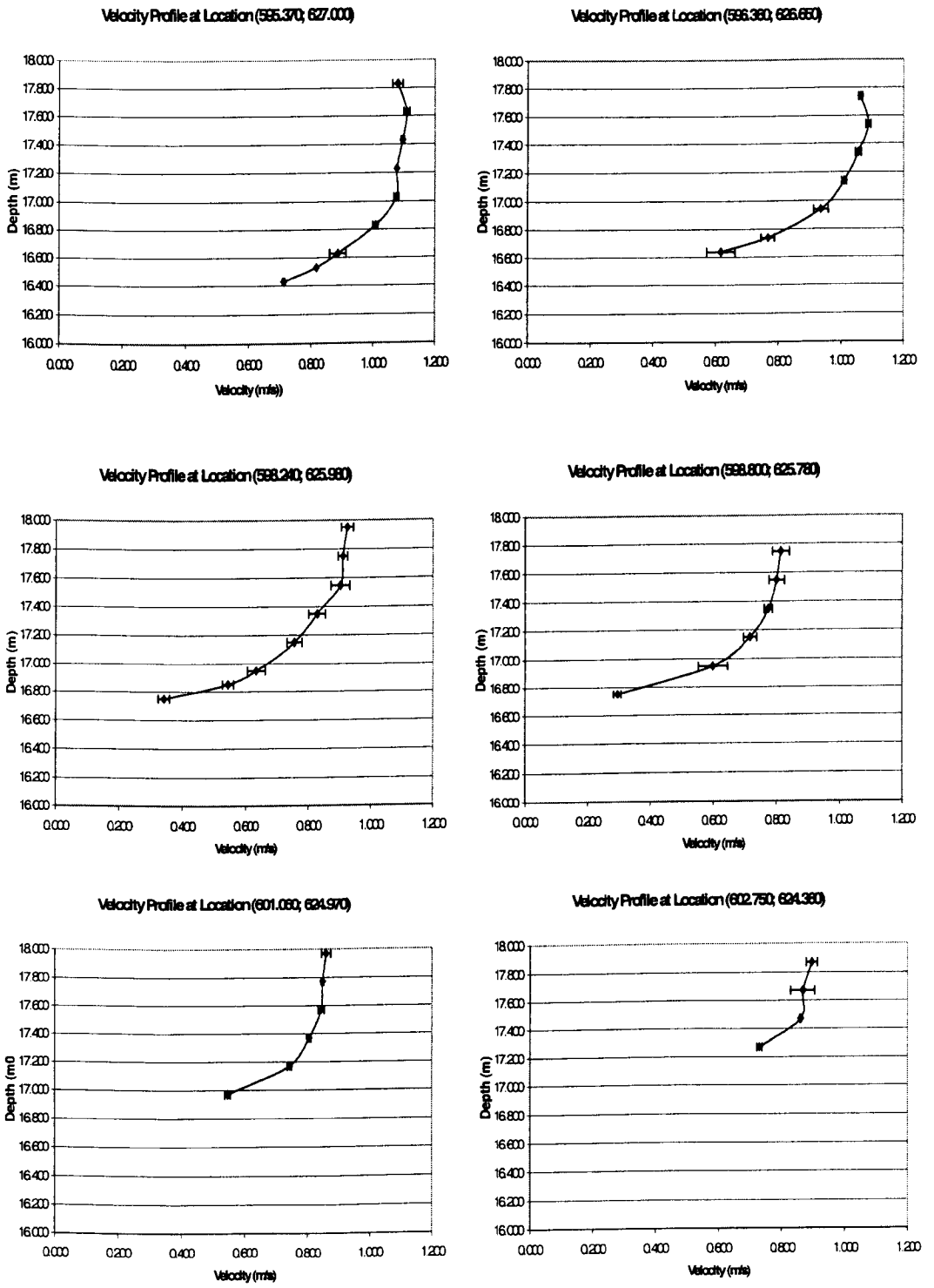

Fig. 6.9 – Velocity Profiles along the Right Main Channel Bank of the River Severn at the Tower (m/s; March 2000)

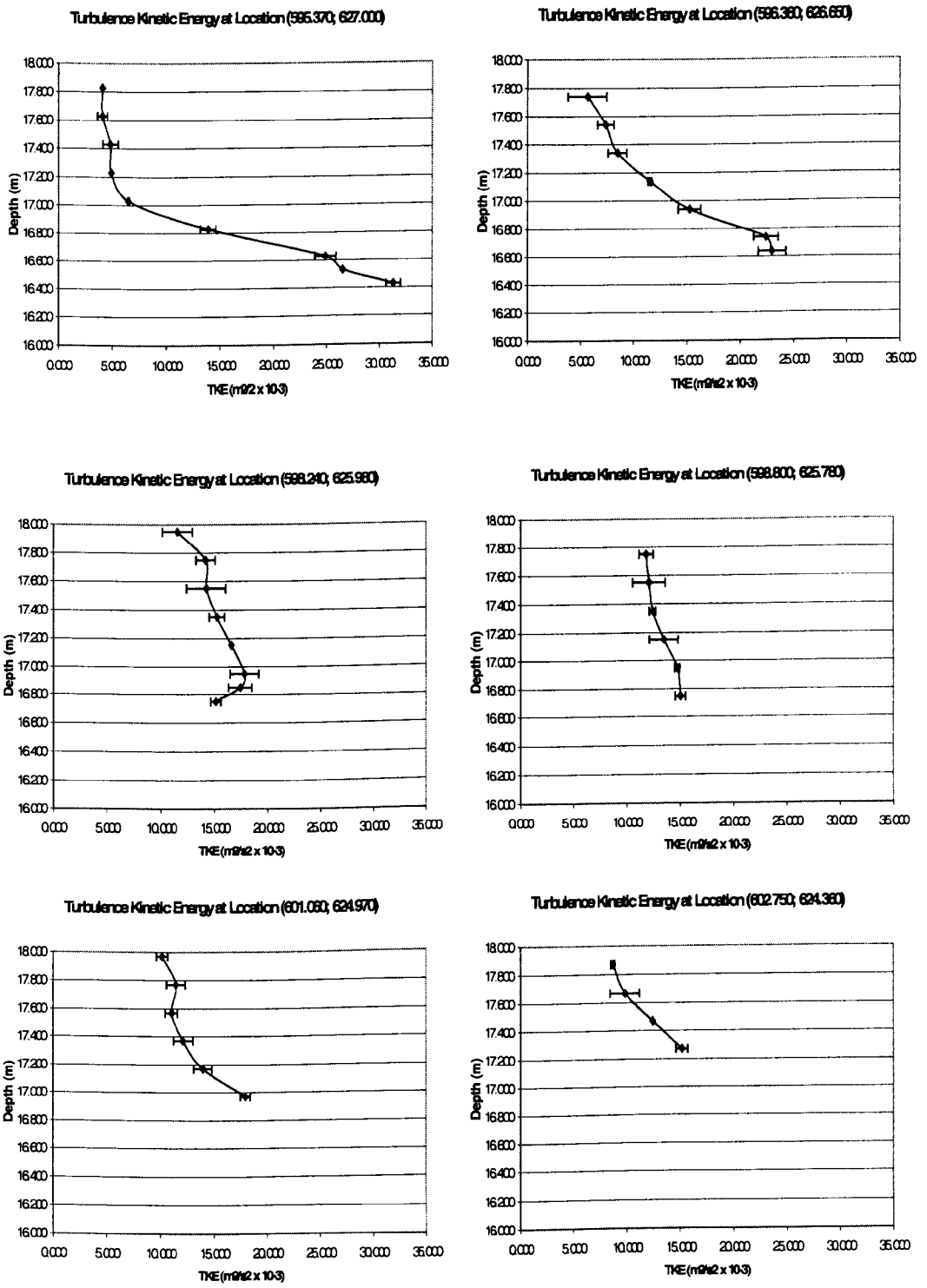

Fig. 6.10 – Turbulence Kinetic Energy Profiles along the Right Main Channel Bank of the River Severn at the Tower (m^2/s^2; March 2000)

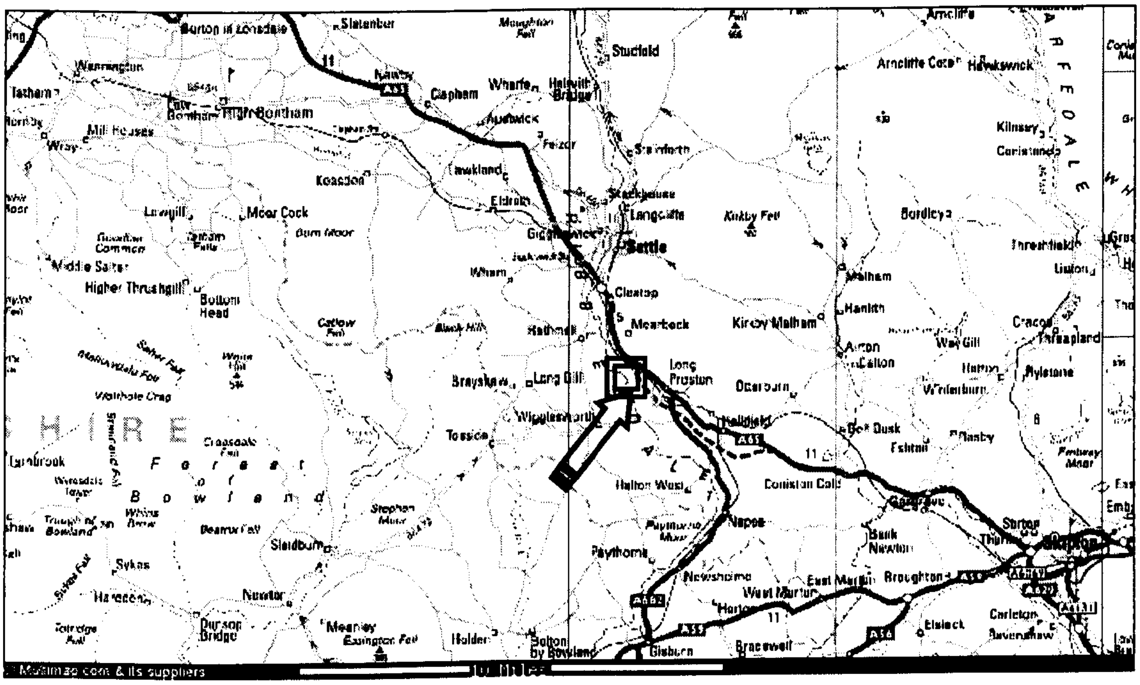

(a)

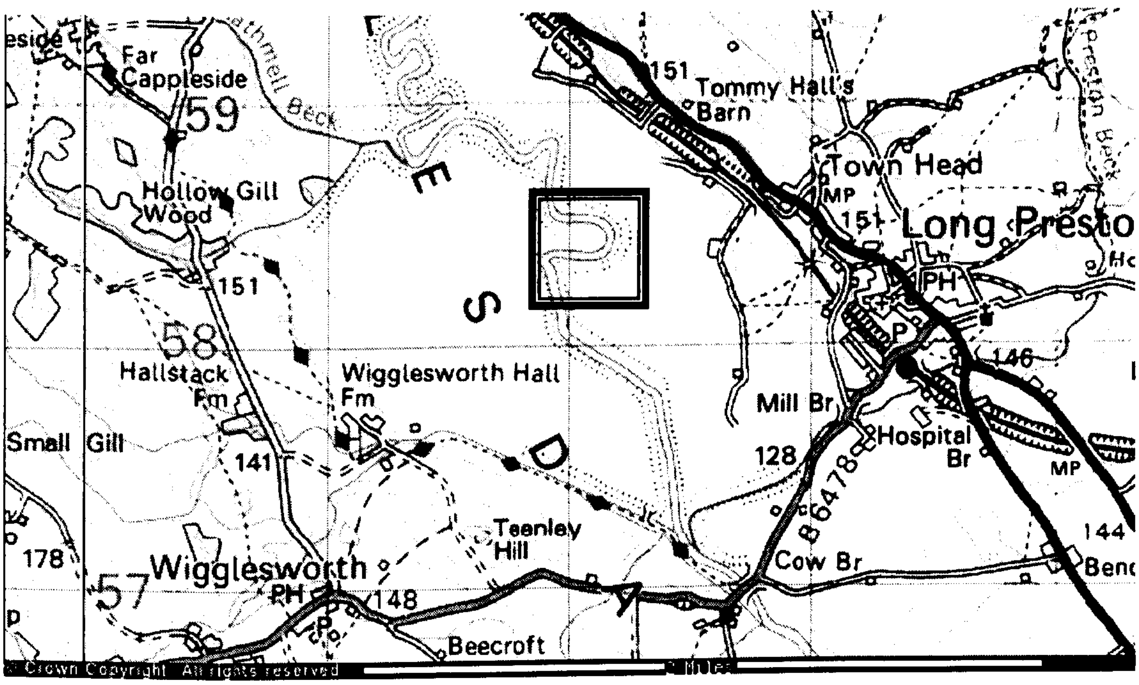

(b)

Fig. 6.11 – Location of the River Ribble Site (MultiMap.Com)

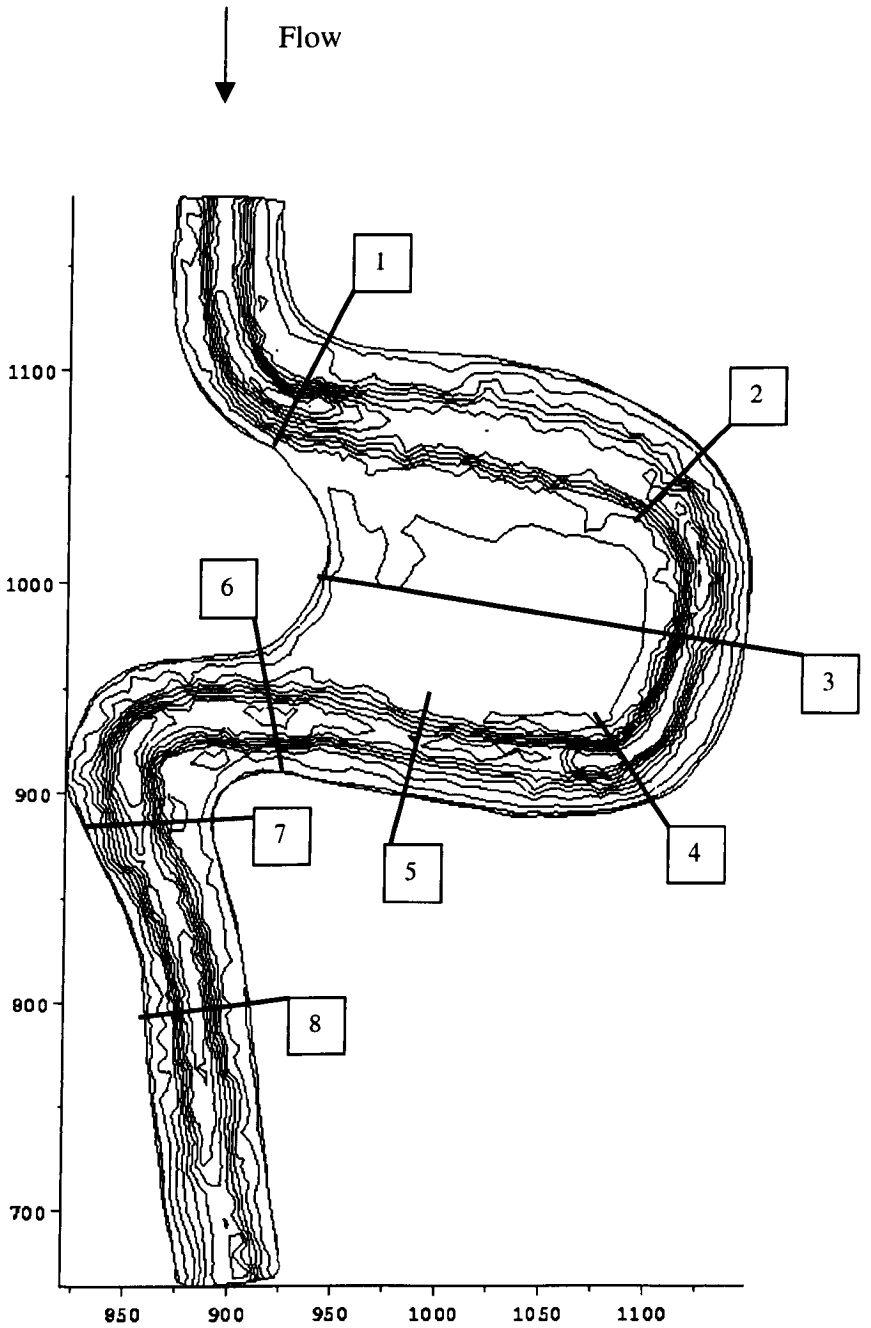

Fig. 6.12 – Plan View of the Ribble and Location of Cross-Sections (Scale in m)

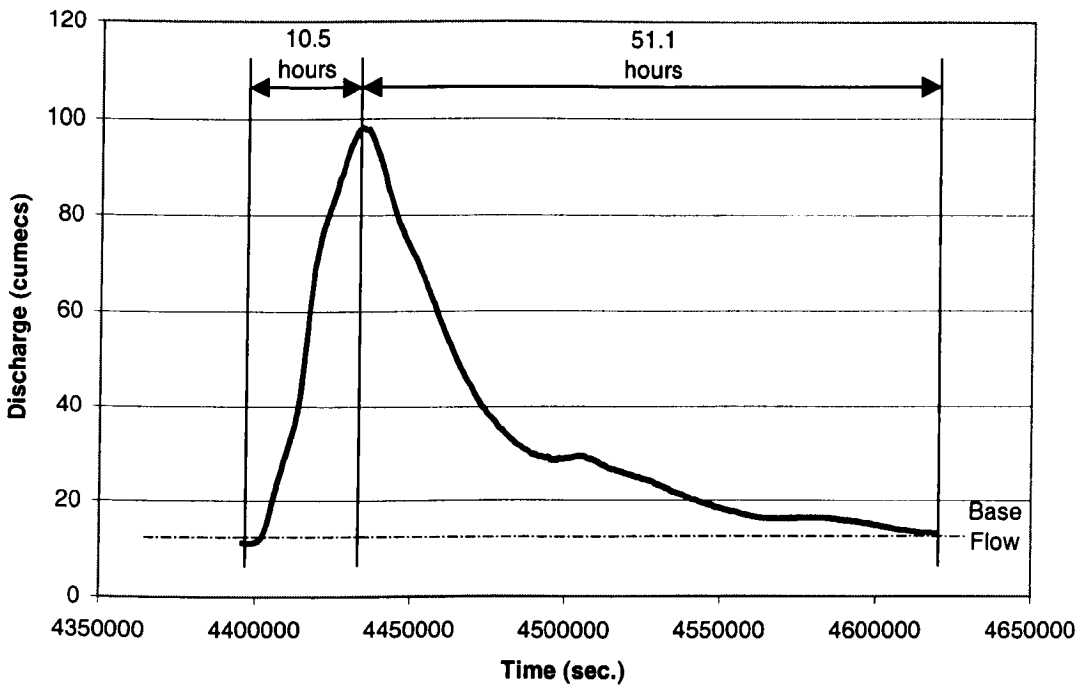

Fig. 6.13 – Peak Flood Hydrograph recorded by the Environmental Agency (EA) upstream of the River Ribble Study Reach over the Winter 1998-1999

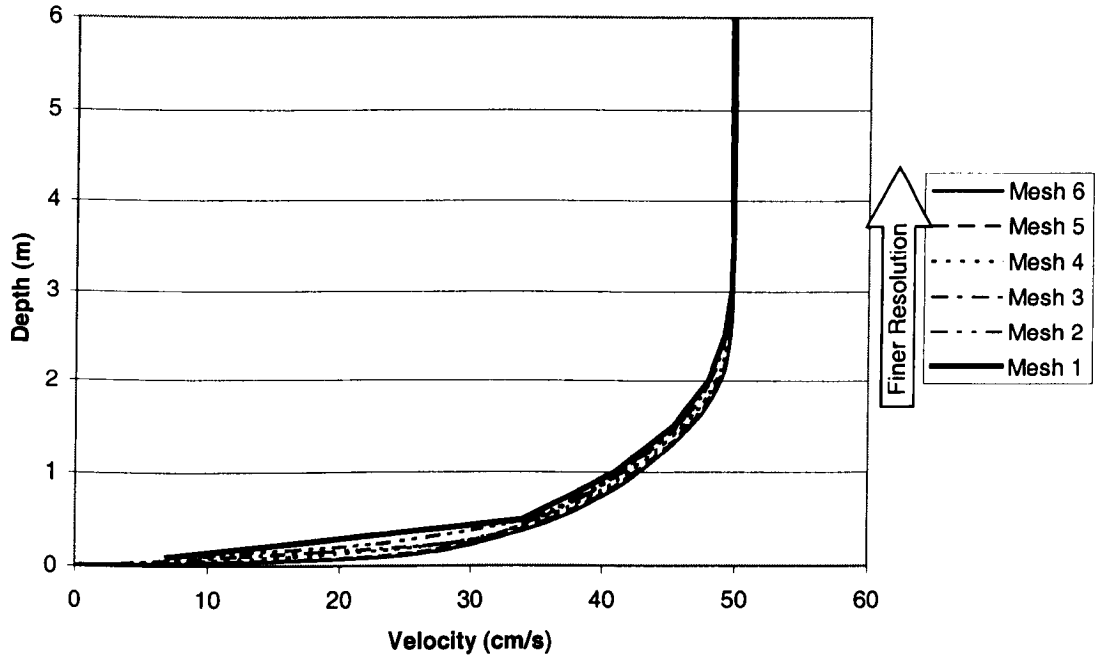

Fig. 6.14 – Large-Scale Problem Grid Resolution: Impact on Velocity

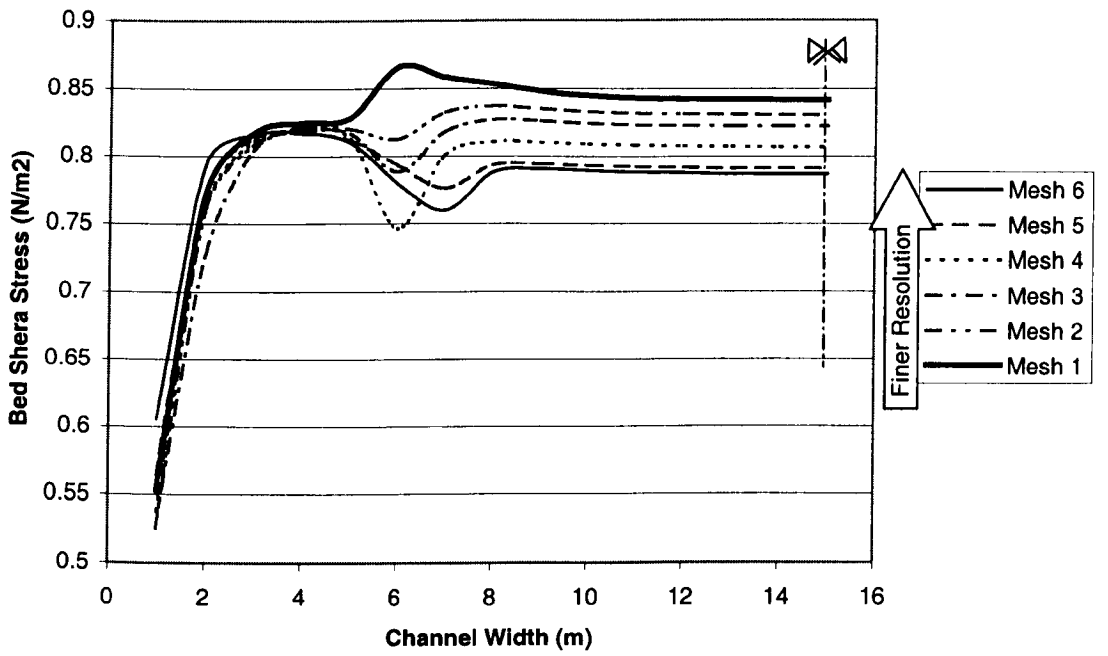

Fig. 6.15 – Large-Scale Problem Grid Resolution: Impact on Bed Shear Stress

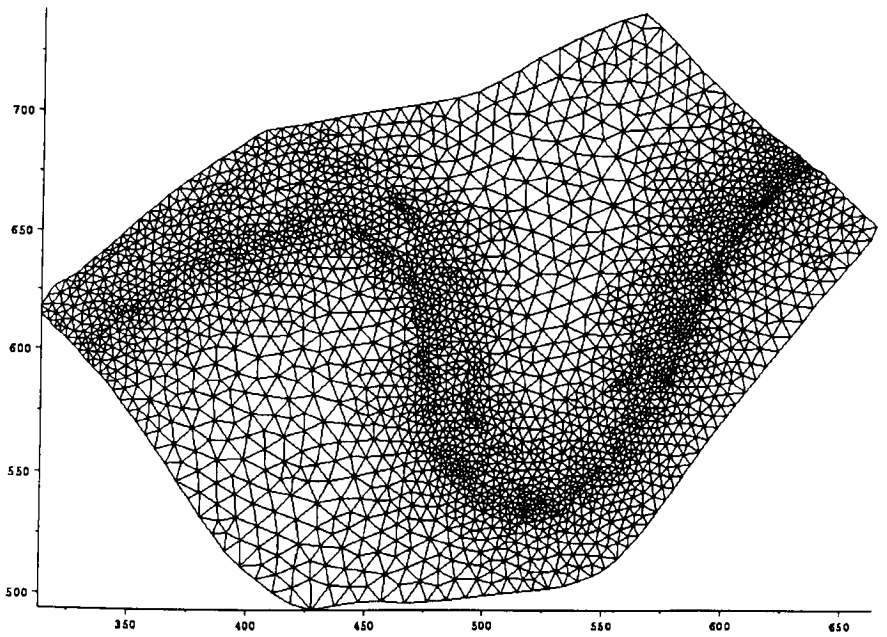

(a)

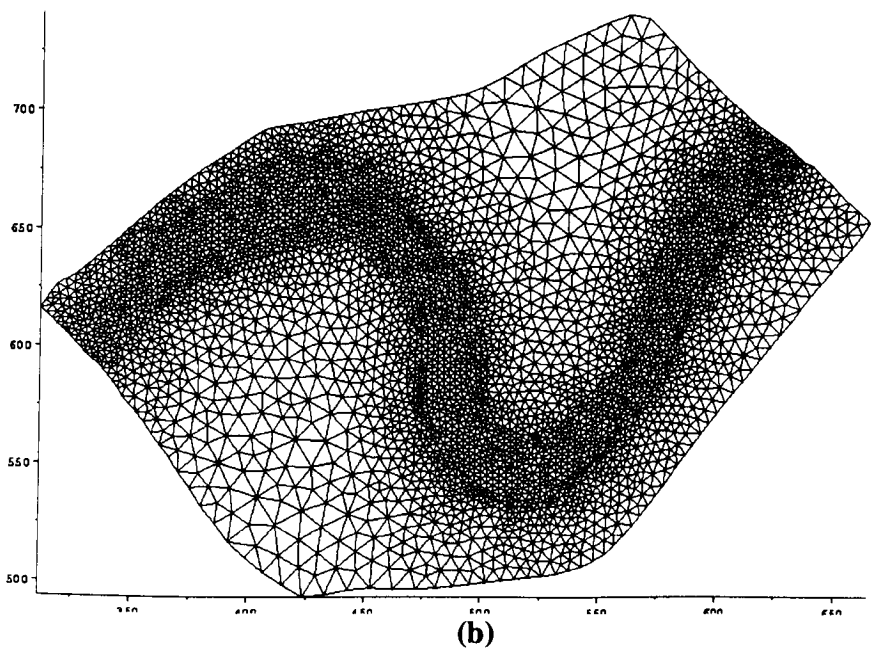

(b)

Fig. 6.16 – Plan View Meshes for TELEMAC Models of the Severn:

(a) Mesh TELEMAC S-1

(b) Mesh TELEMAC S-2

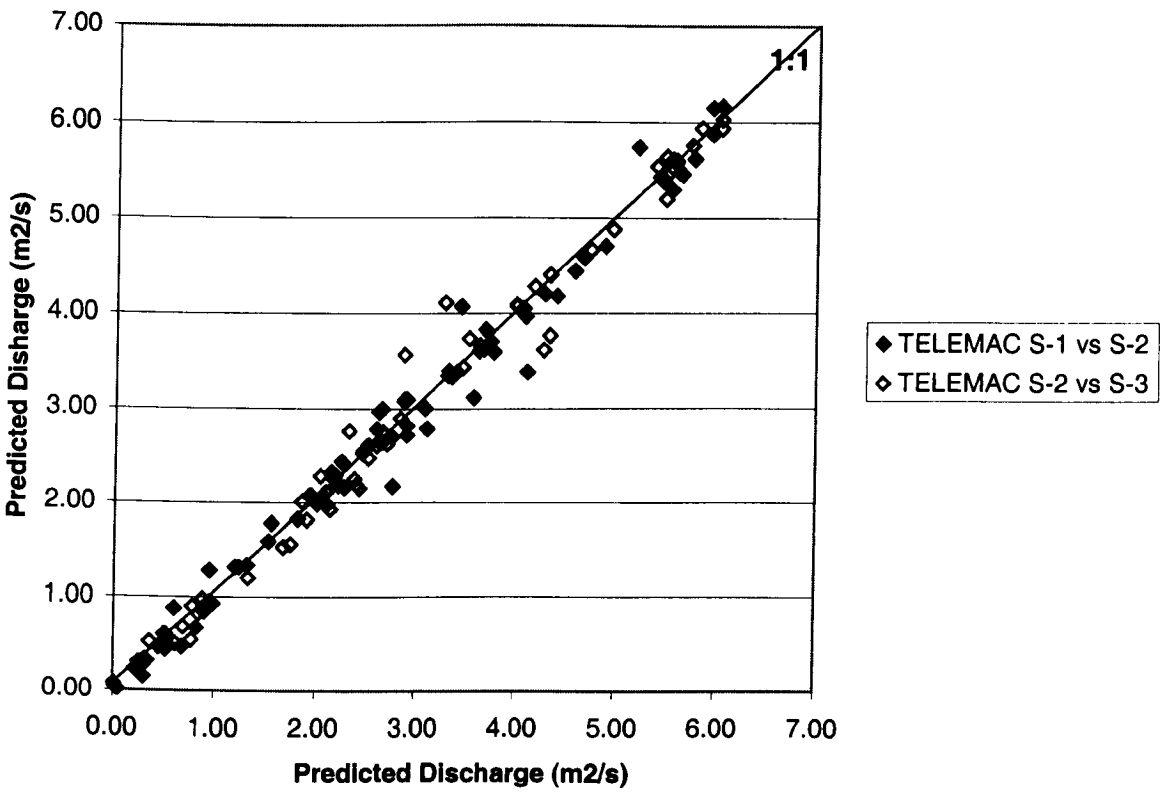

Fig. 6.17 – Mesh Independence for River Severn Models using TELEMAC: Comparison of Calculated Fields at Sections 4, 5, 6 and 7 as well as on the Floodplain and along the Thalweg

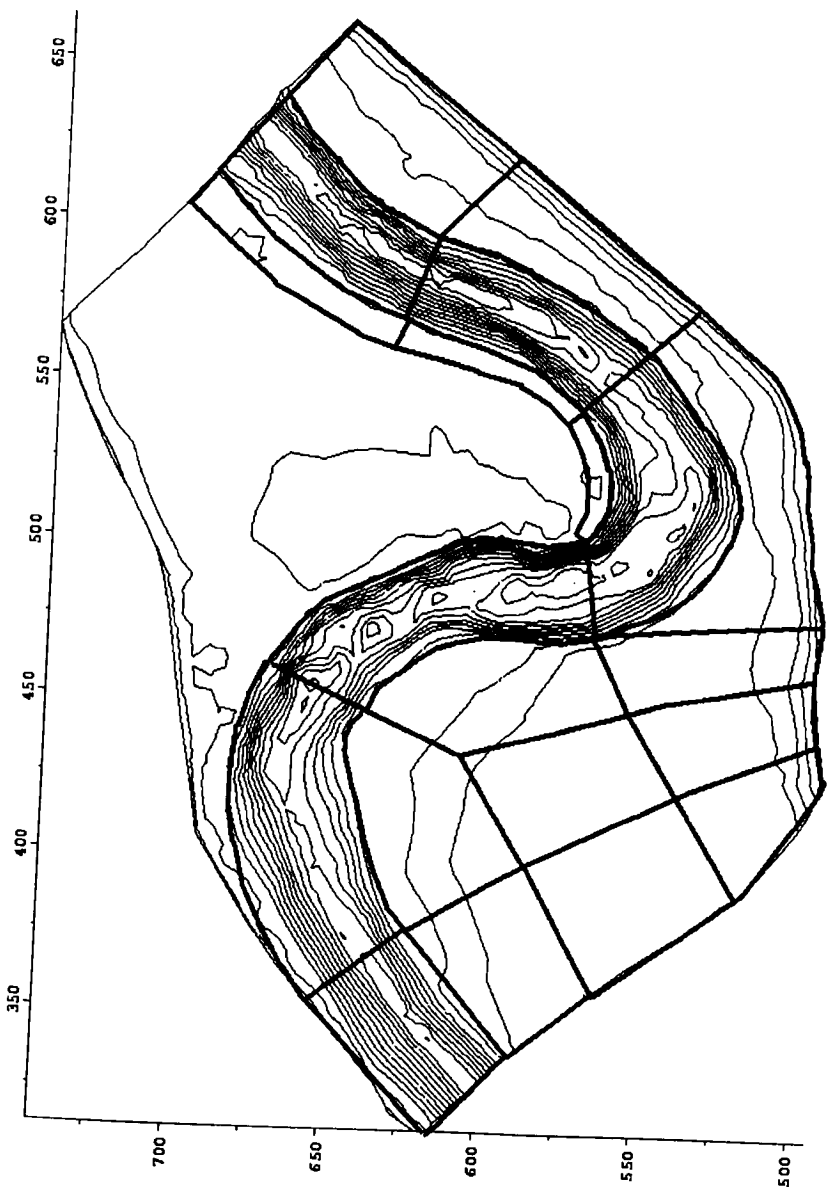

Fig. 6.18 – River Severn Multi-Block Layout in CFX

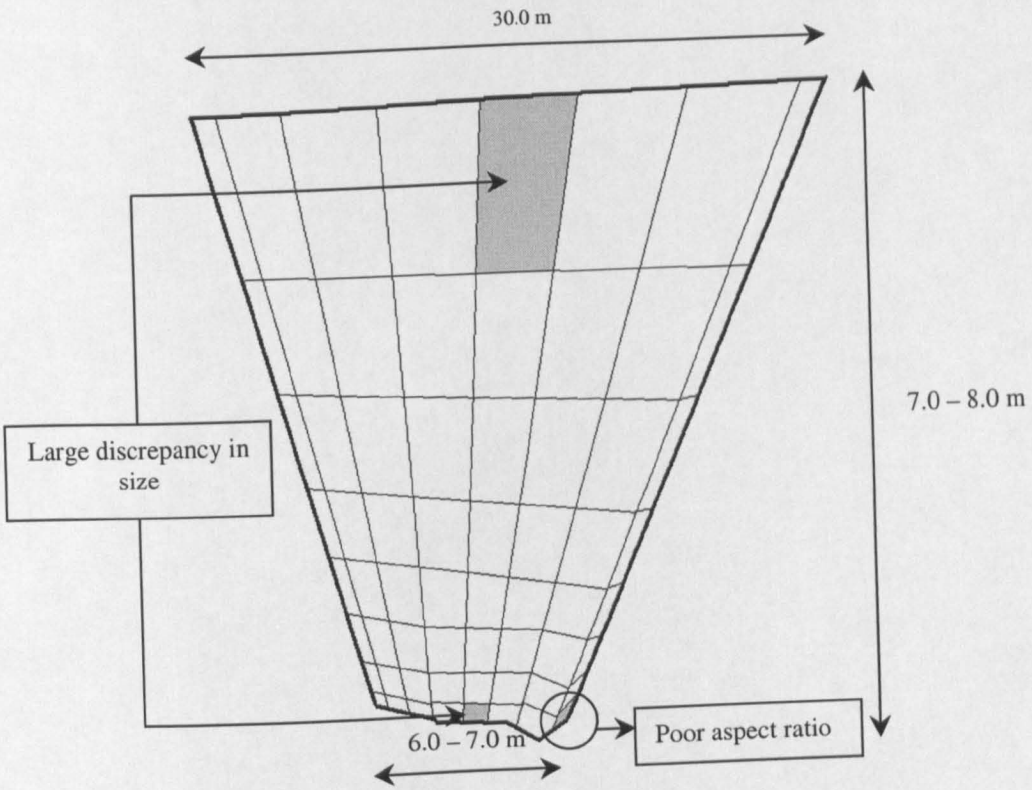

Fig. 6.19 – CFX Main Grid Constraints in the Severn

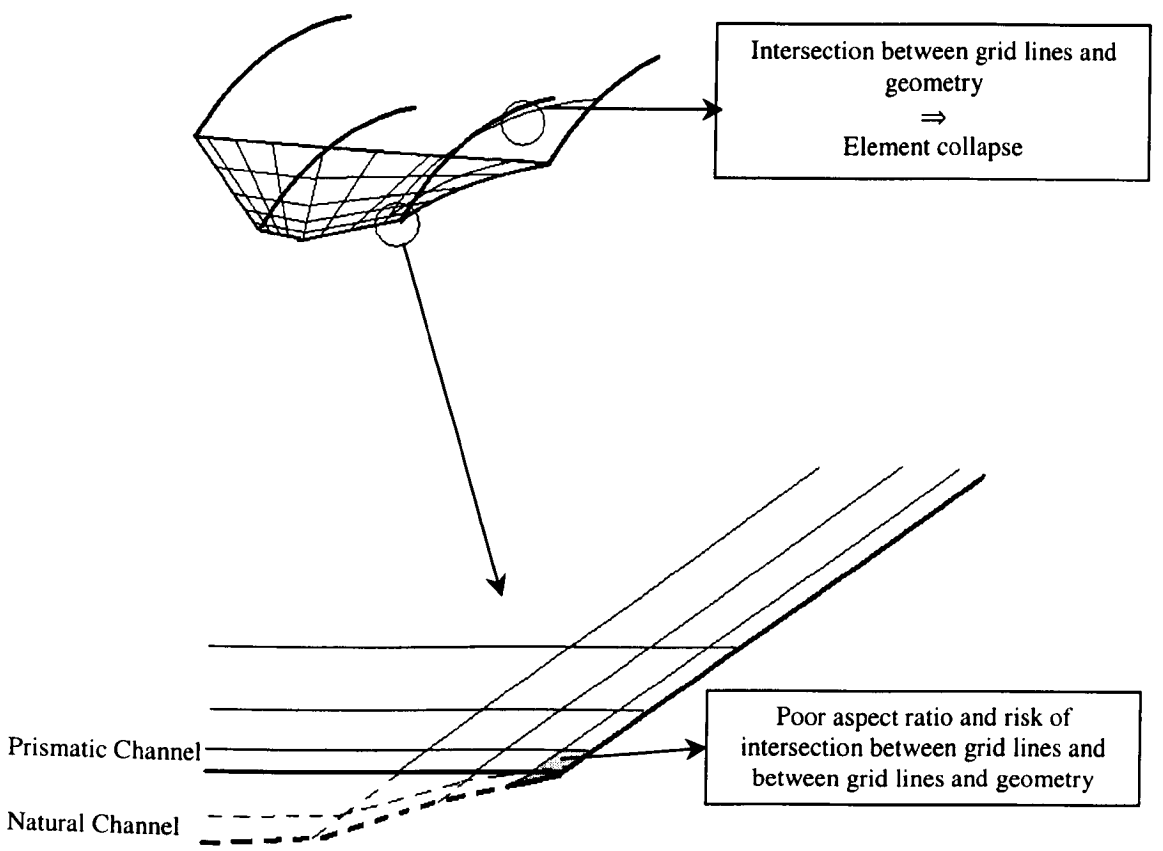

Fig. 6.20 – CFX Main Grid Constraints in the Ribble

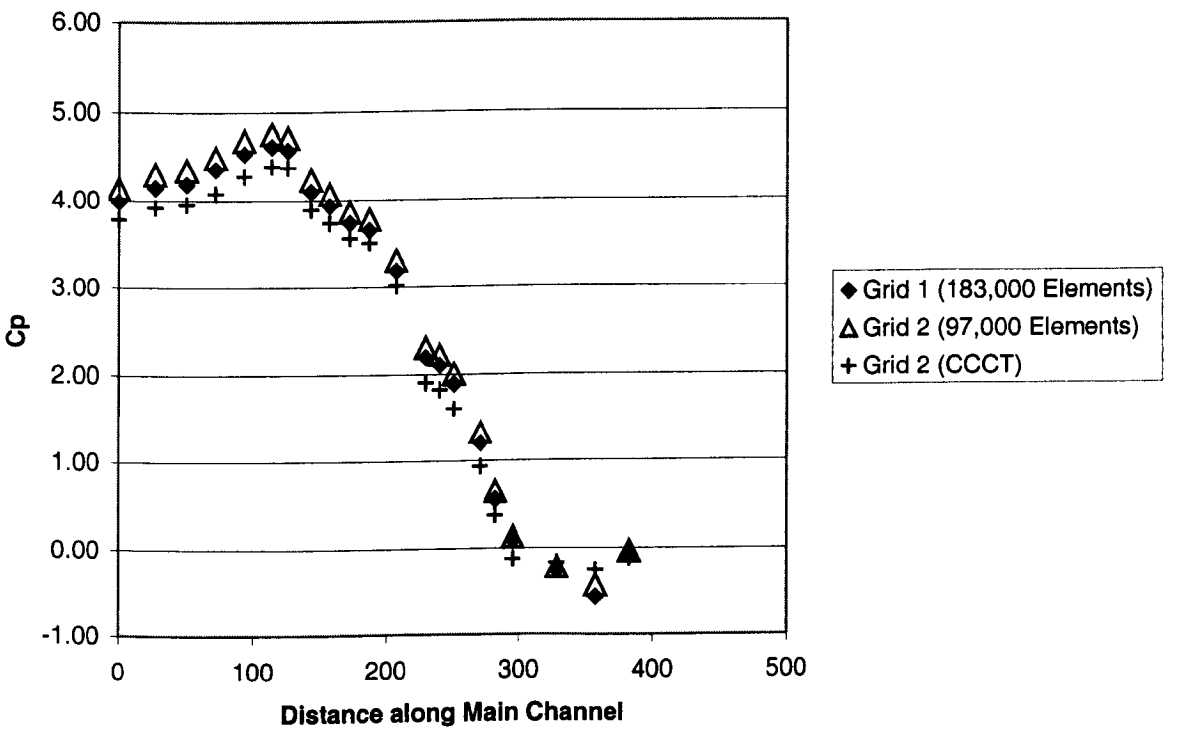

Fig. 6.21 – Mesh Independence Test for River Severn Model using CFX: Comparison of Non-dimensional Pressure along the Main Channel, at the Bed

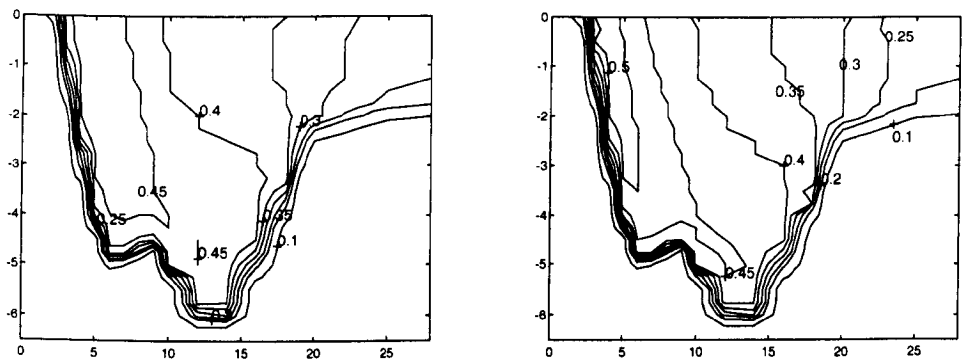

Cross-Section 3

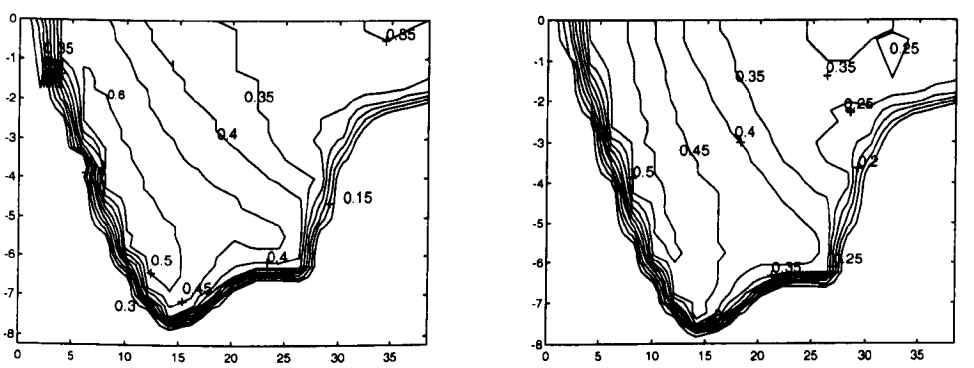

Cross-Section 4

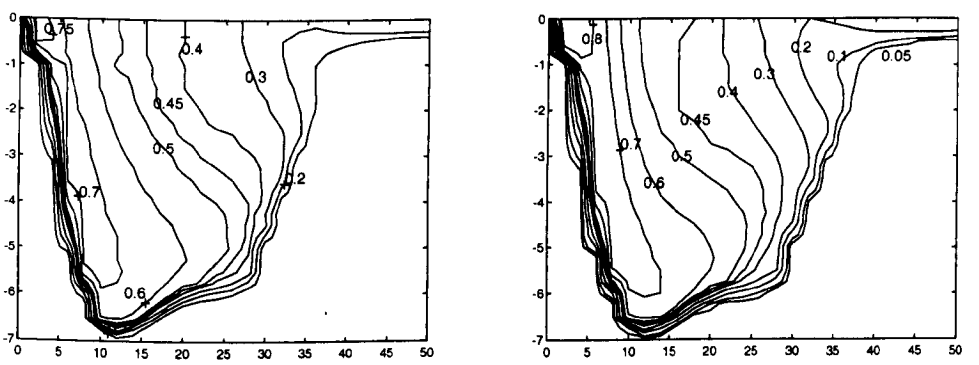

Cross-Section 5

Fig. 6.22 – Comparison between the Results with Hybrid (left) and QUICK-CCCT (right) at Cross-Sections 3, 4 and 5 for the River Severn CFX Model

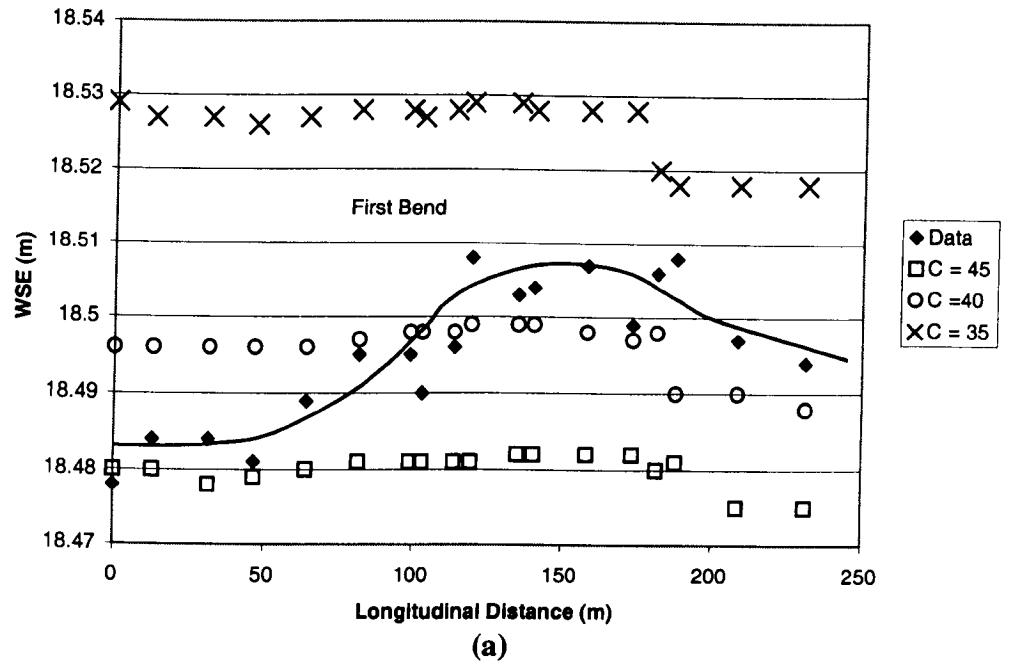

(a)

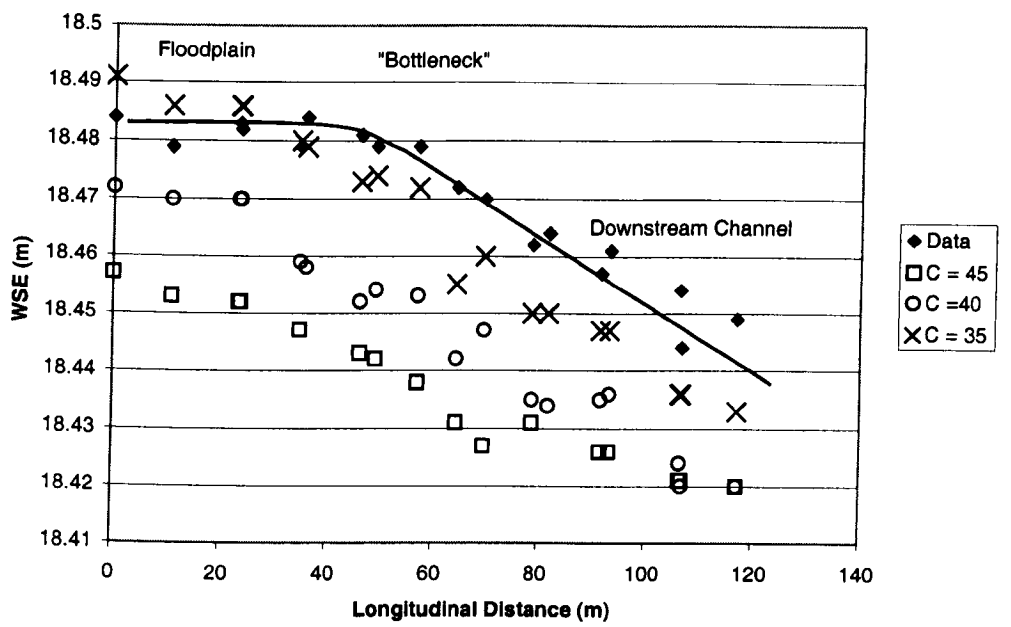

(b)

Fig. 6.23 – Comparison of Water Surface Elevations between TELEMAC Models and Field Data (100 m^3/s Event of Dec. 1999):
(a) along the upstream first bend
(b) along the right embankment

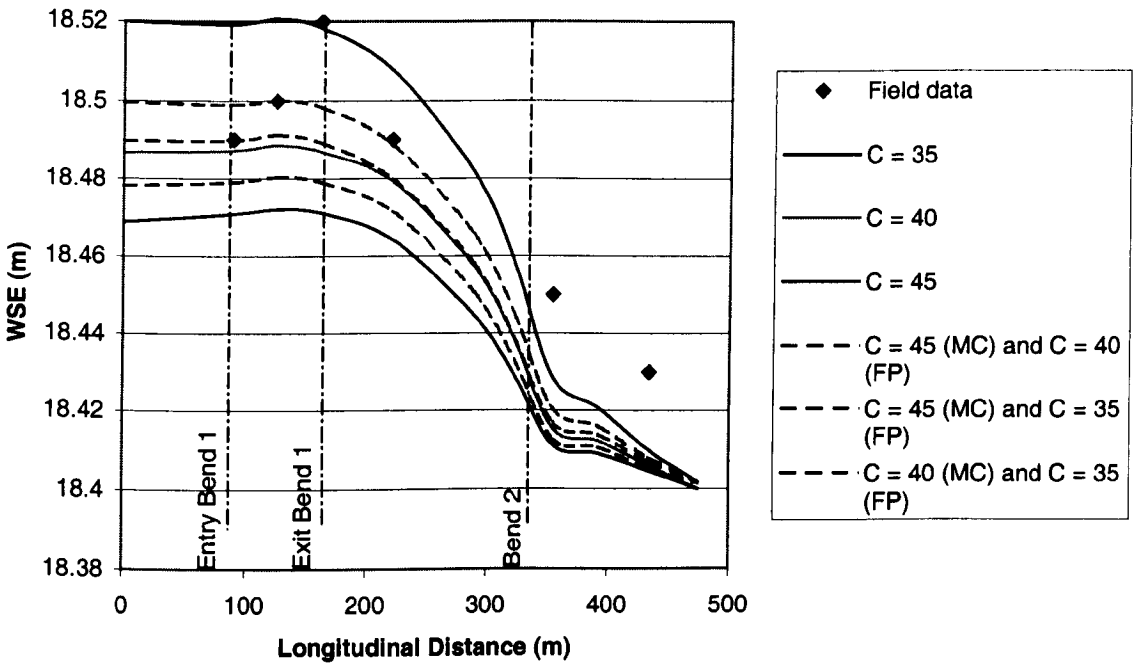

Fig. 6.24 – TELEMAC Model of the Severn: Sensitivity Analysis of the Free Surface to Roughness

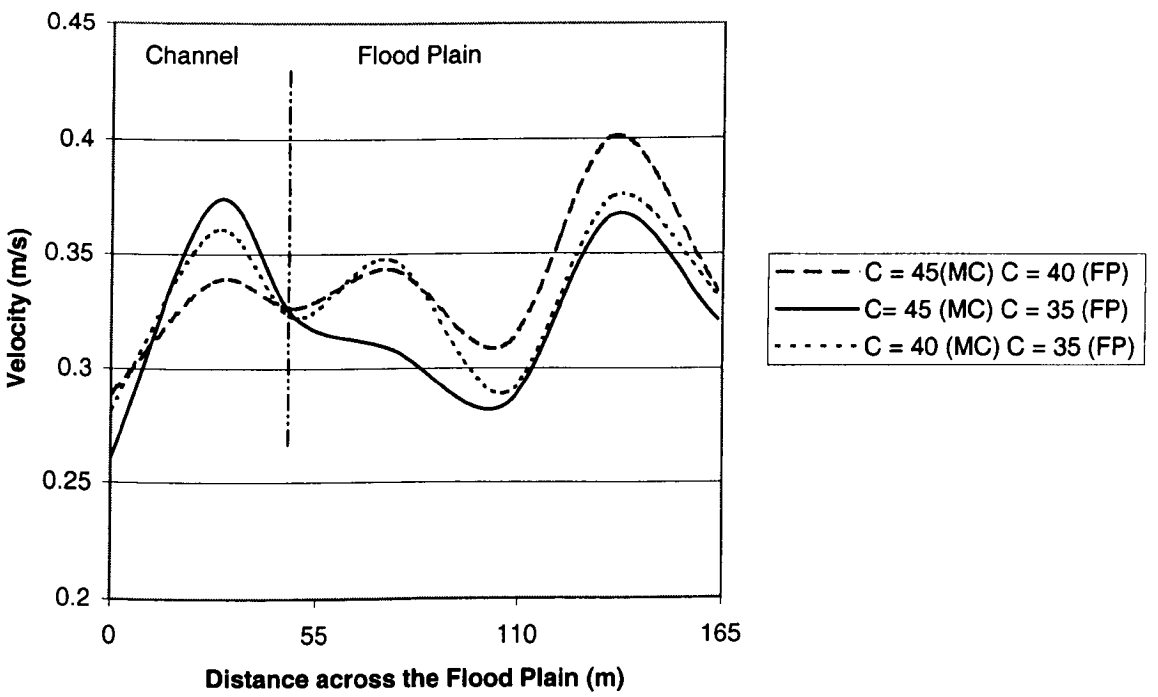

Fig. 6.25 – TELEMAC Model of the Severn: Impact of Roughness on Velocity Distribution across the Upstream Part of the Reach

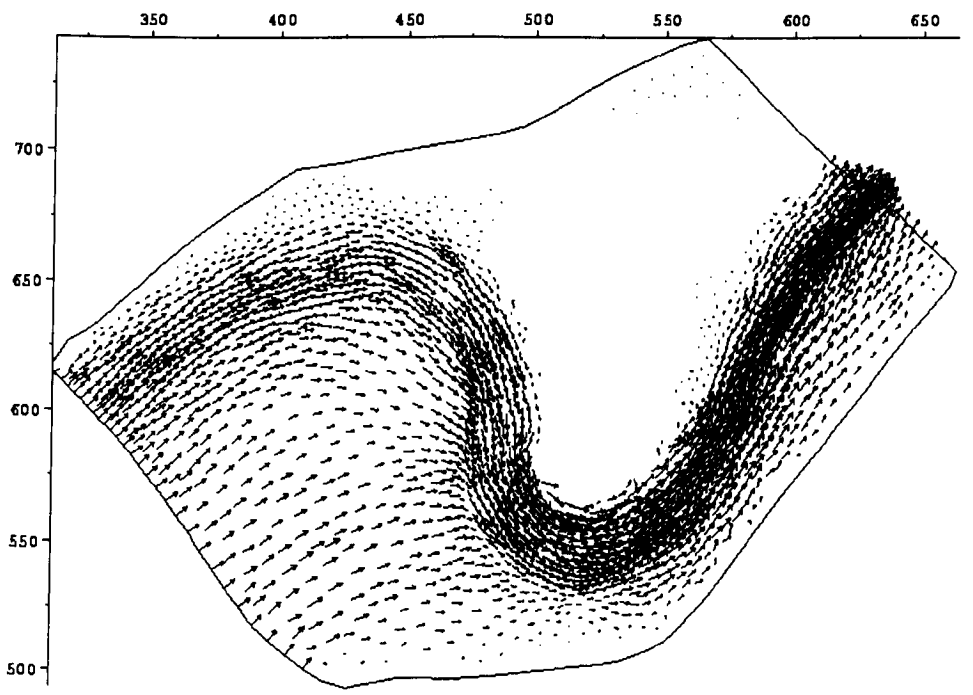

Fig. 6.26 – River Severn TELEMAC Depth-Averaged Velocity Vectors for a Flow of 100 m^3/s

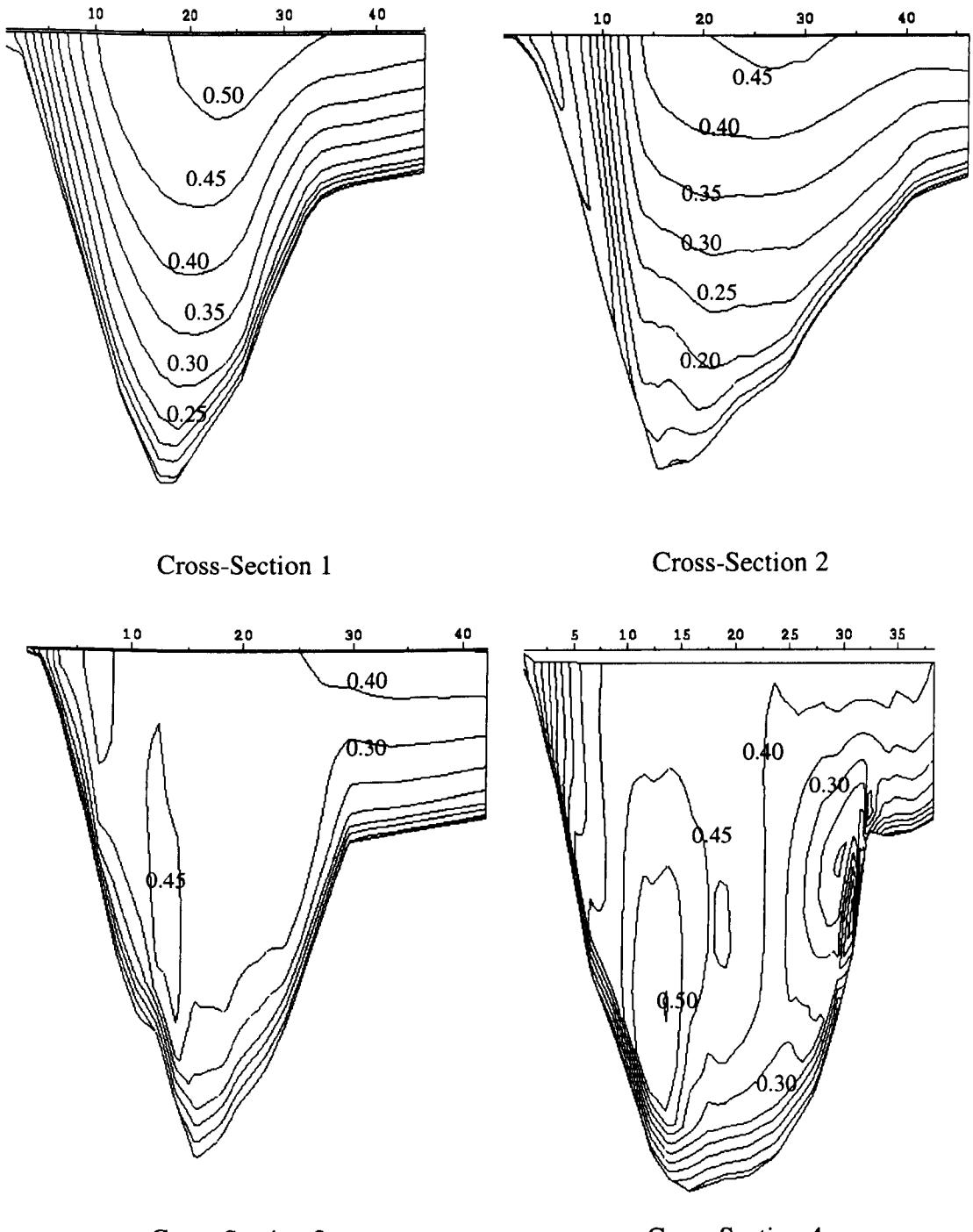

Fig. 6.27 – River Severn TELEMAC Velocity Profile (m/s) at Cross-Sections 1, 2, 3 and 4 (C = 45 $m^{1/2}/s$ (MC) and 35 $m^{1/2}/s$ (FP); Mesh S-2; Mixing-Length Model)

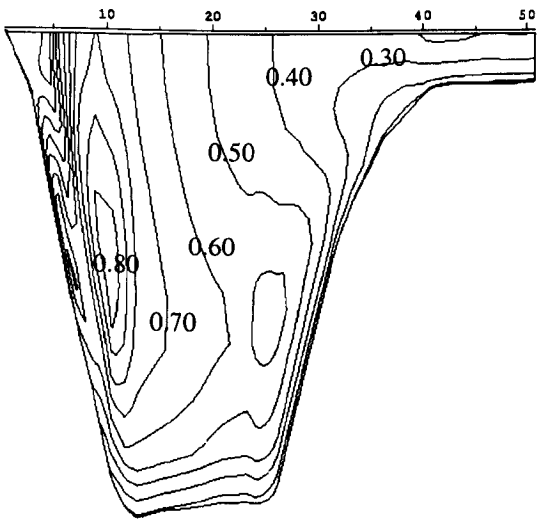

Cross-Section 5

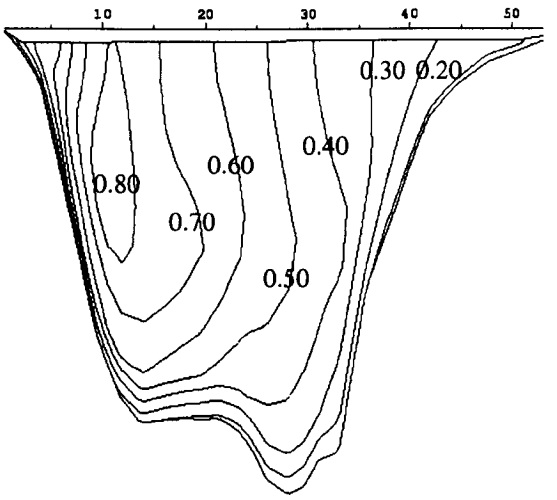

Cross-Section 6

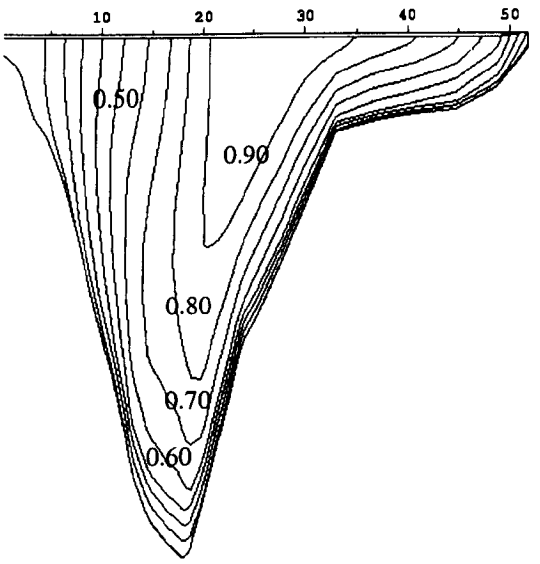

Cross-Section 7

Fig. 6.28 – River Severn TELEMAC Velocity Profile (m/s) at Cross-Sections 5, 6, and 7 (C = 45 $m^{1/2}/s$ (MC) and 35 $m^{1/2}/s$ (FP); Mesh S-2; Mixing-Length Model)

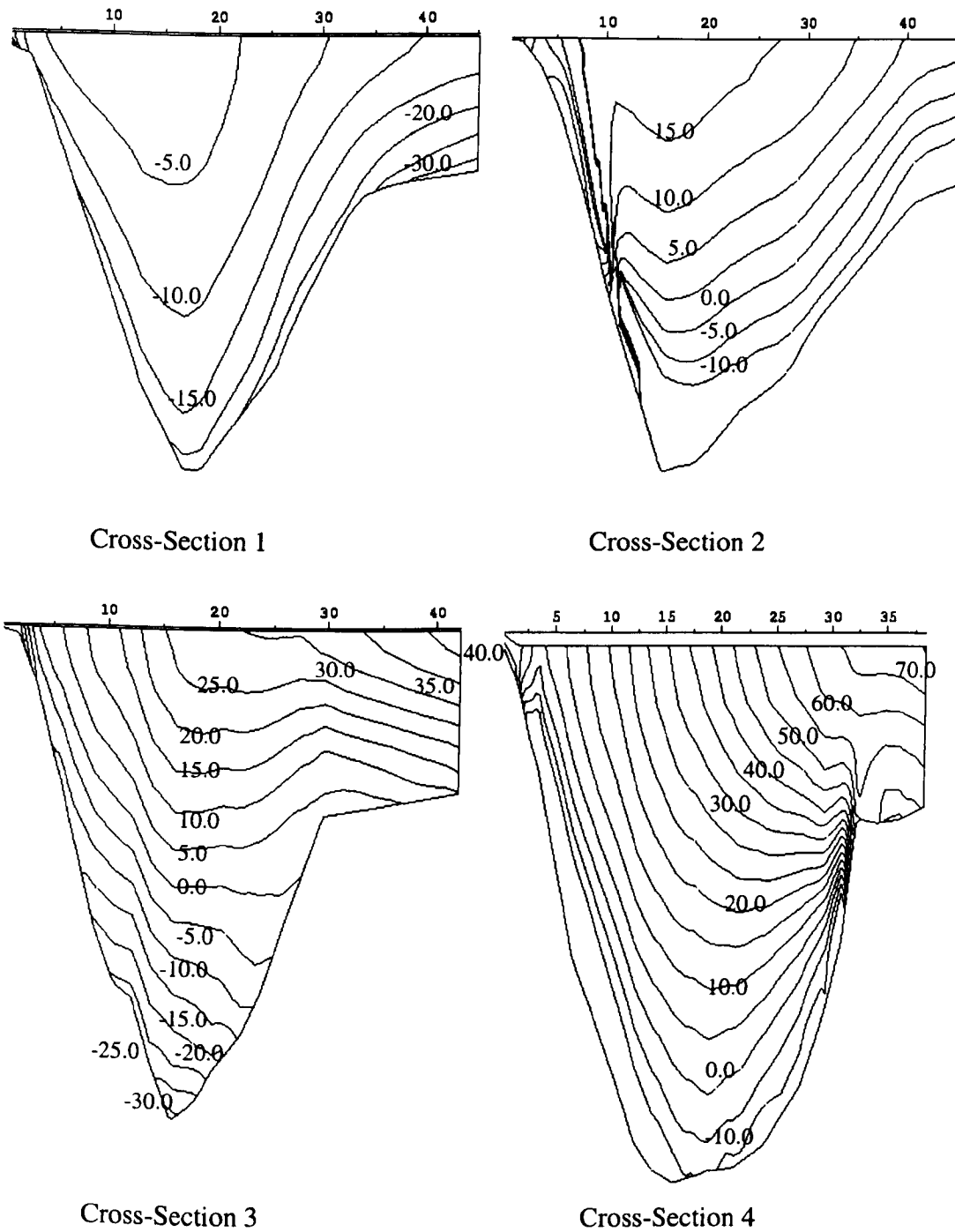

Fig. 6.29 – River Severn TELEMAC Velocity Direction (deg.) at Cross-Sections 1, 2, 3 and 4 (C = 45 $m^{1/2}/s$ (MC) and 35 $m^{1/2}/s$ (FP); Mesh S-2; Mixing-Length Model)

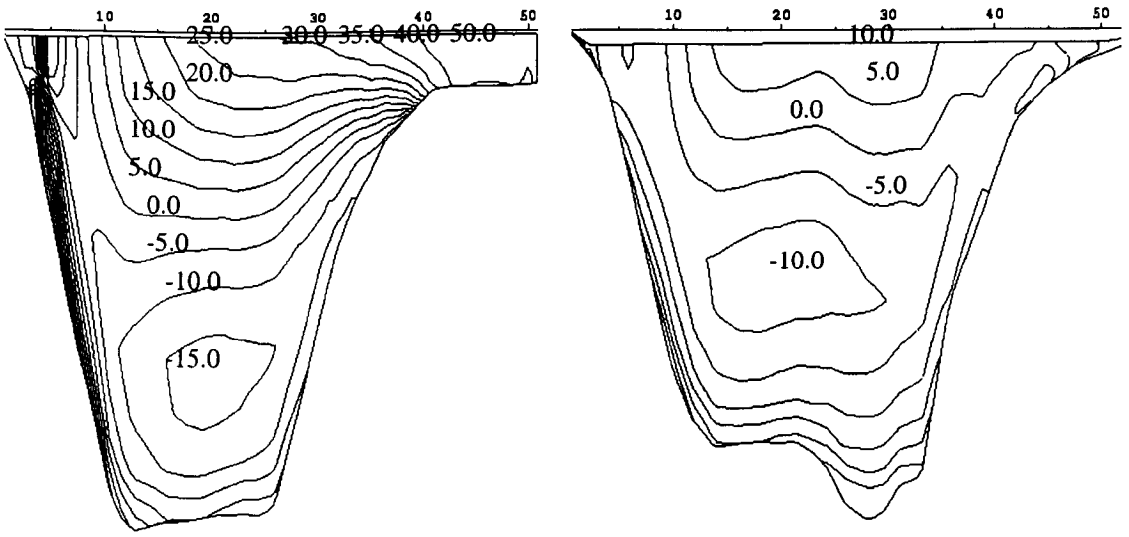

Cross-Section 5

Cross-Section 6

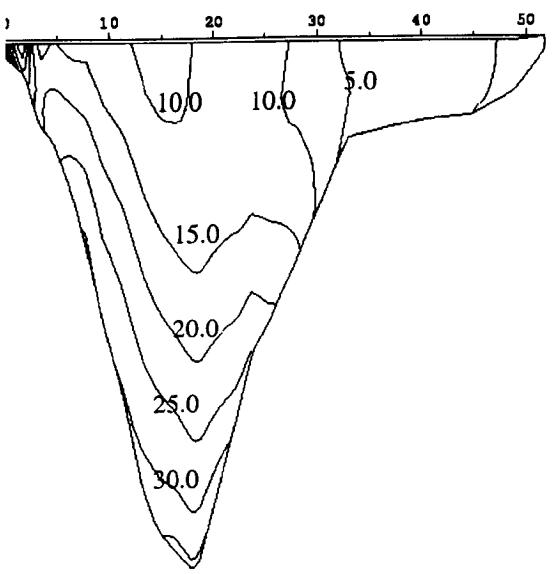

Cross-Section 7

Fig. 6.30 – River Severn TELEMAC Velocity Direction (deg.) at Cross-Sections 5, 6, and 7 (C = 45 $m^{1/2}/s$ (MC) and 35 $m^{1/2}/s$ (FP); Mesh S-2; Mixing-Length Model)

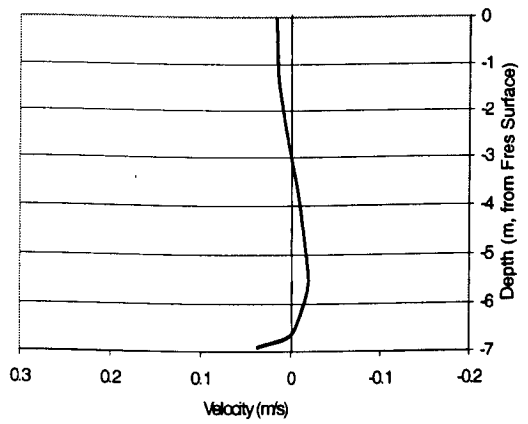

Cross-Section 1

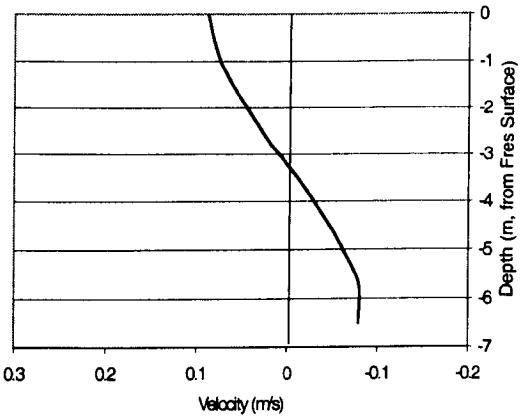

Cross-Section 2

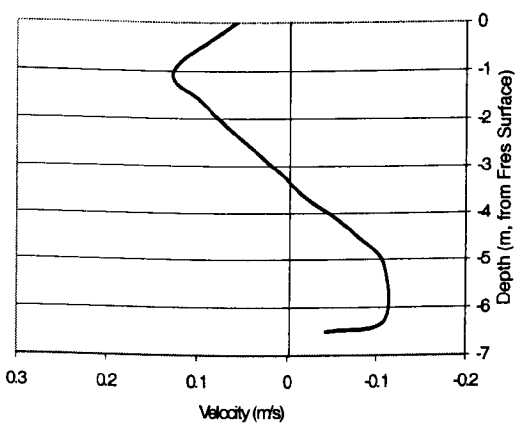

Cross-Section 3

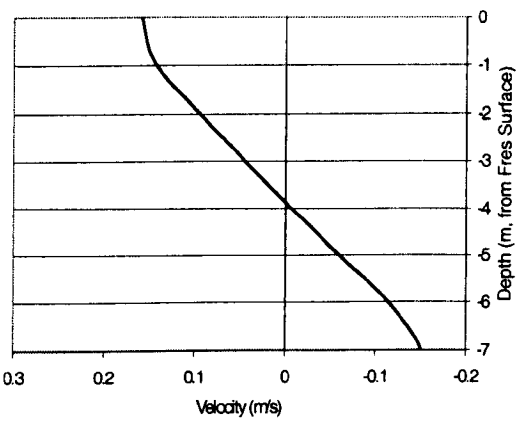

Cross-Section 4

Fig. 6.31 – River Severn TELEMAC Model: Recirculation at Cross-Sections 1 to 4

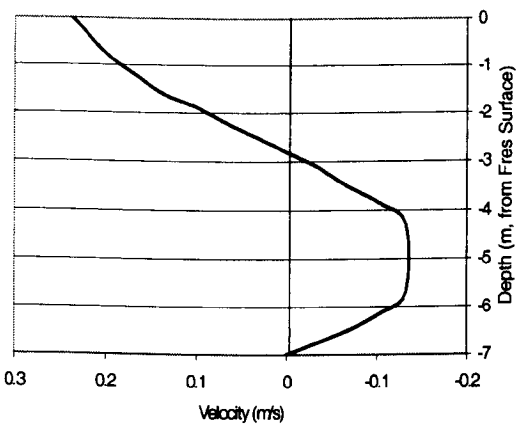

Cross-Section 5

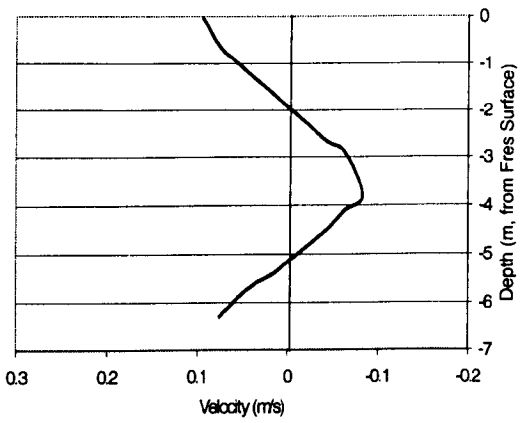

Cross-Section 6

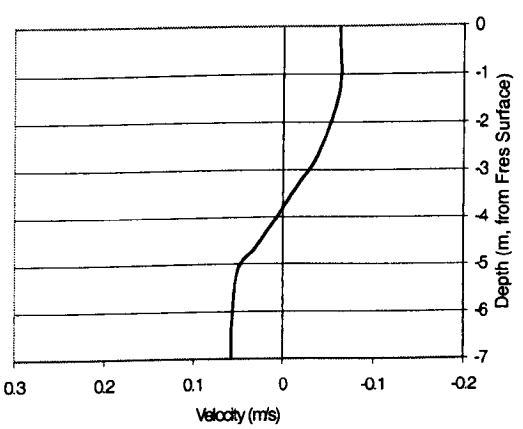

Cross-Section 7

Fig. 6.32 – River Severn TELEMAC Model: Recirculation at Cross-Sections 5 to 7

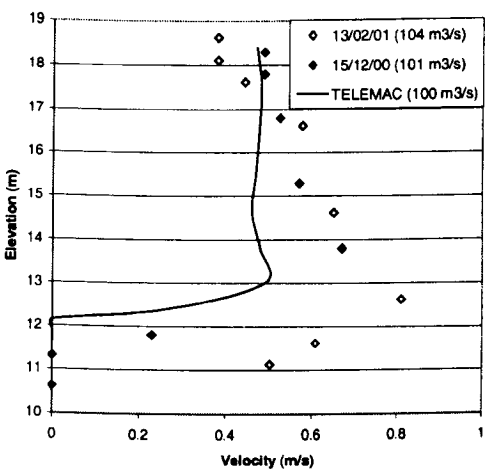

Left

(At 9.00 m from the Left Bank)

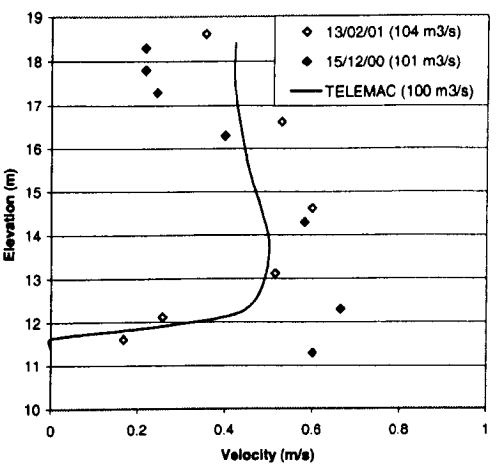

Centre

(At 19.00 m from the Left Bank)

Fig. 6.33 – River Severn: Comparison between Field Data and TELEMAC Predictions at Cross-Section 4

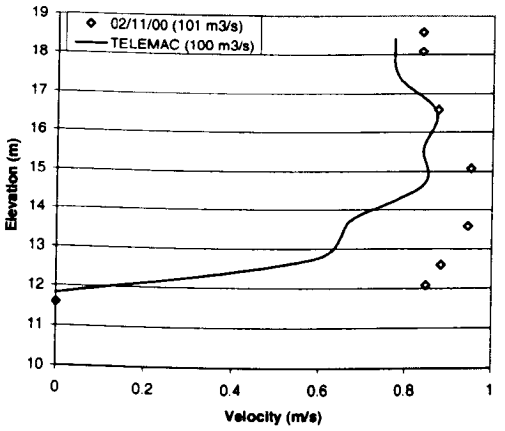

Left
(At 8.00 m from the Left Bank)

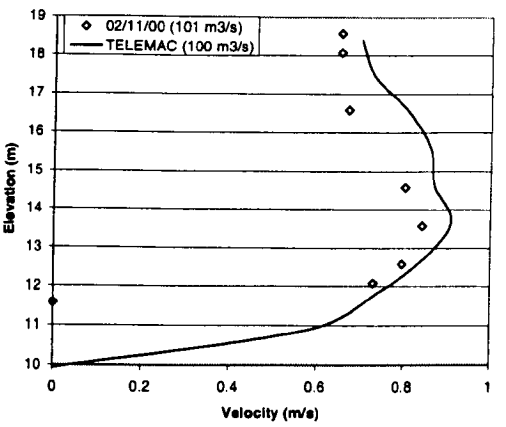

Left
(At 12.00 m from the Left Bank)

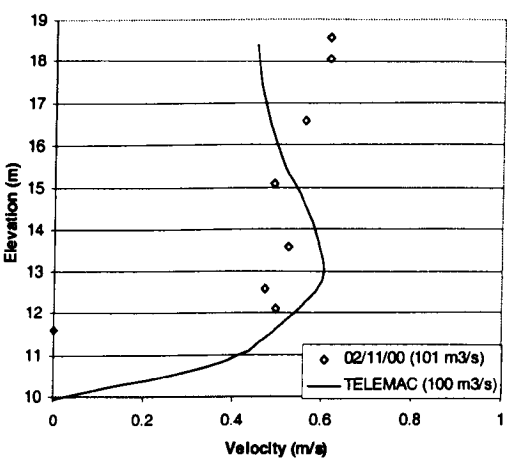

Channel Centre
(At 22.00 m from the Left Bank)

Fig. 6.34 – River Severn: Comparison between Field Data and TELEMAC Predictions at Cross-Section 5

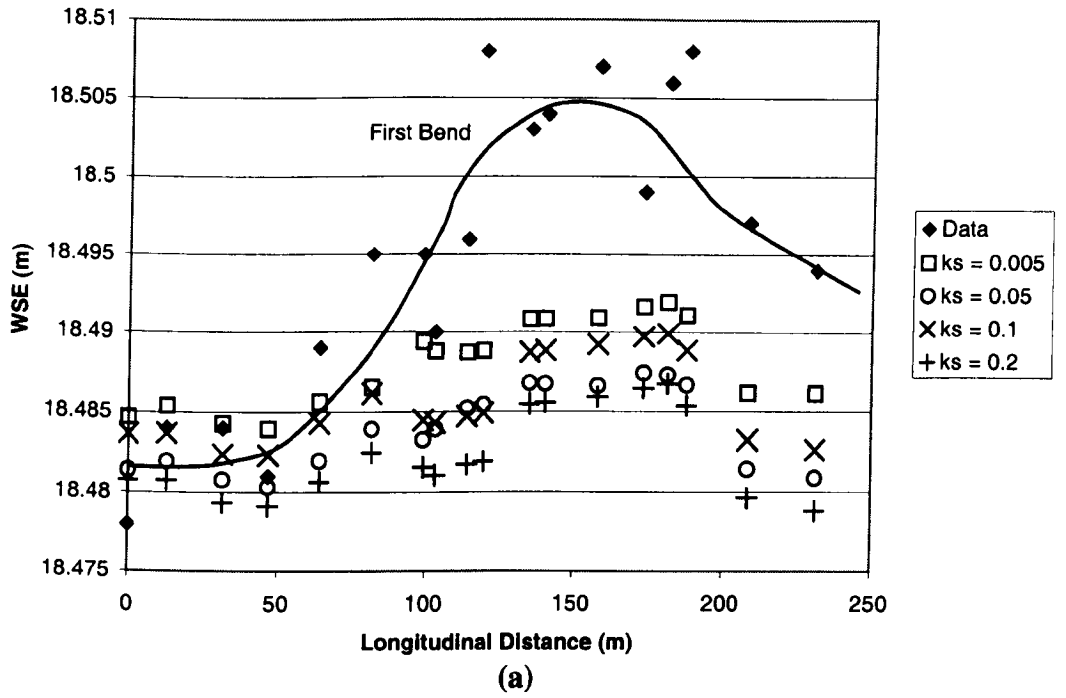

(a)

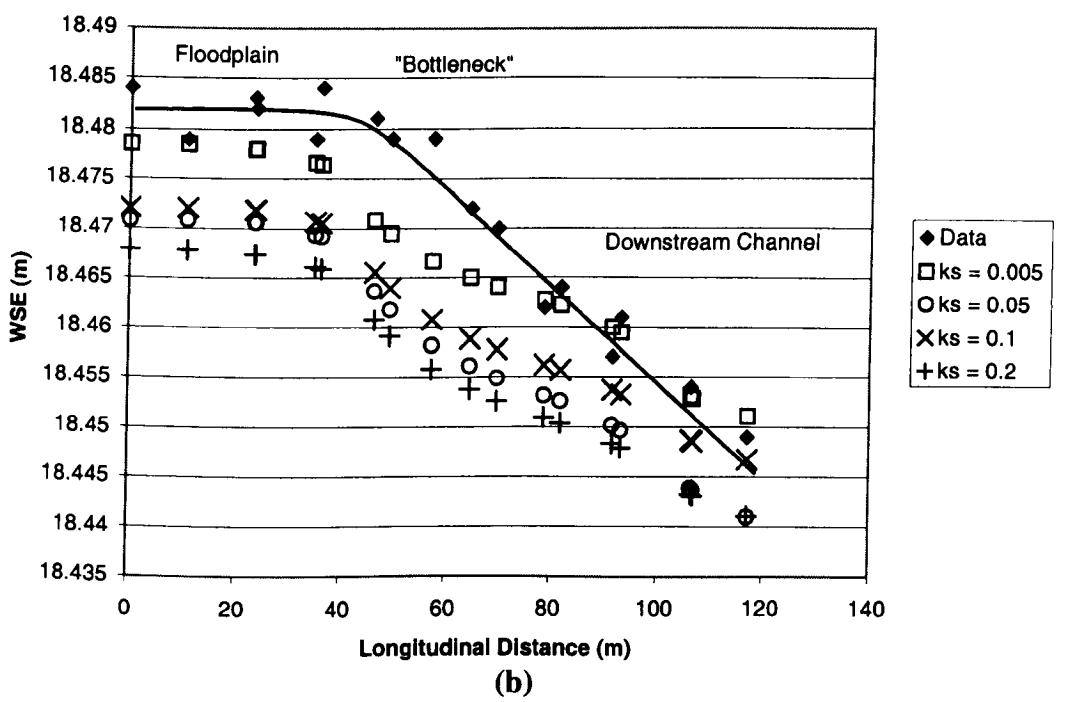

(b)

Fig. 6.35 – Comparison of Water Surface Elevation between CFX Models and Field Data (100 m^3/s Event of Dec. 1999)
(a) along the upstream first bend
(b) along the right embankment

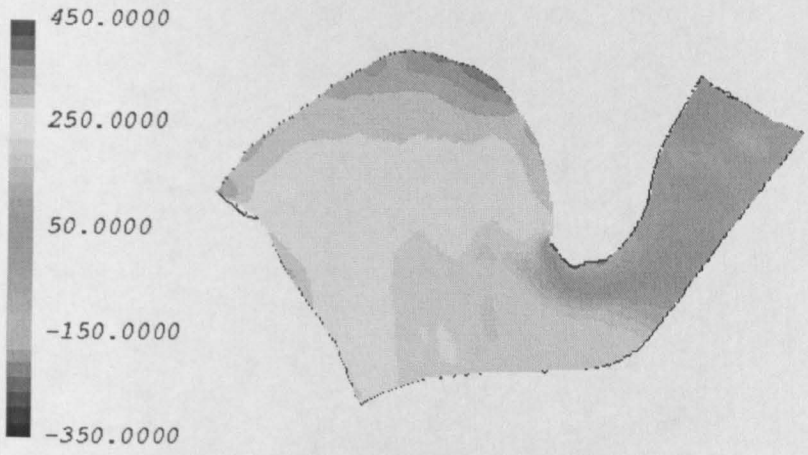

k_s = 0.100 m

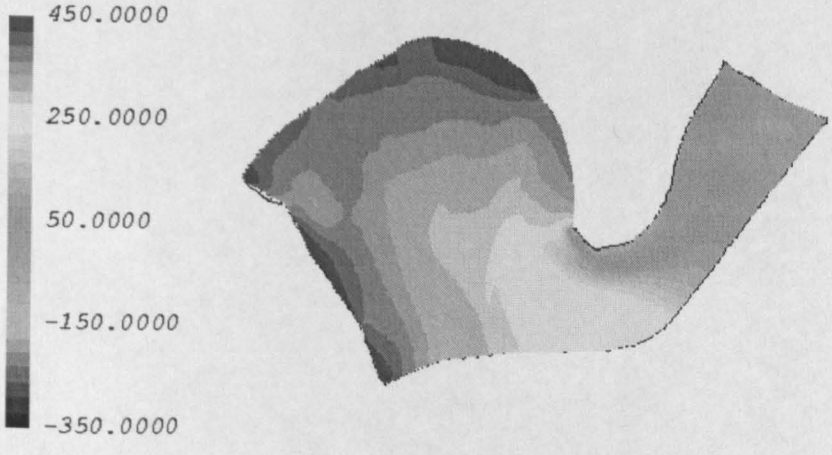

k_s = 0.300 m

Fig. 6.36 – Calculated CFX Pressure Field (Pa) on the Lid for Varying Roughness Values

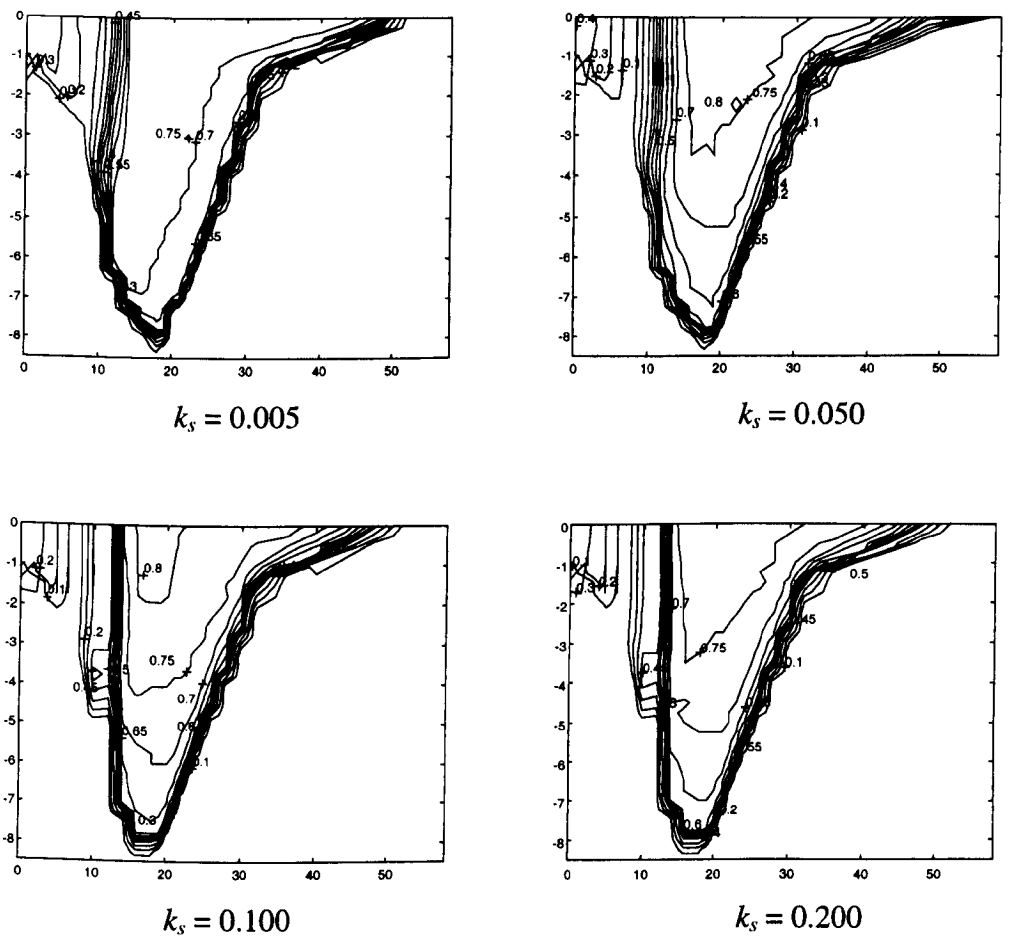

Fig. 6.37 – River Severn CFX Velocity Profiles at Cross-Section 7 for Varying Roughness Values

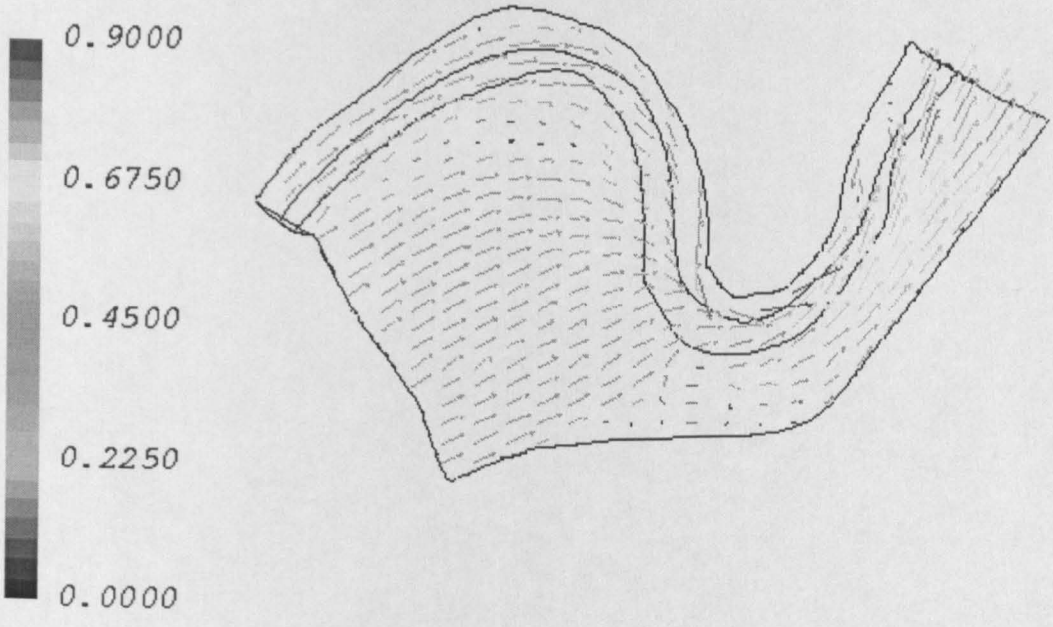

Fig. 6.38 – River Severn CFX Velocity Vectors close to the Free Surface for a Flow of 100 m^3/s

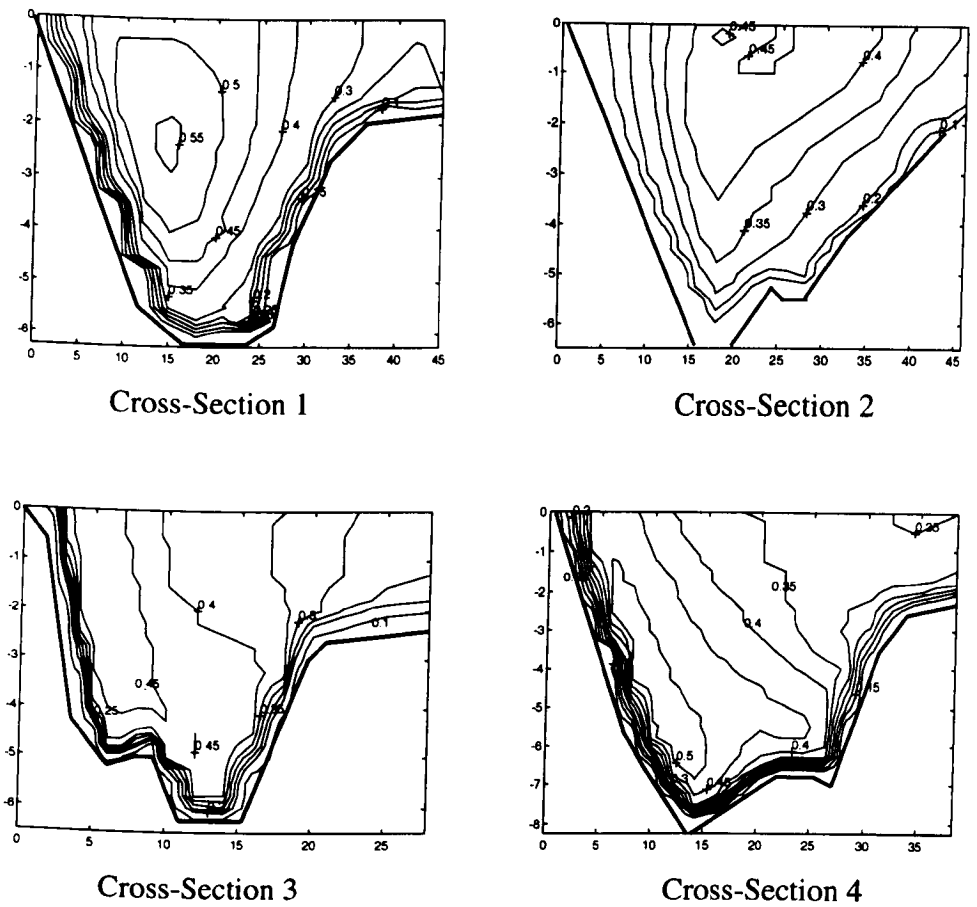

Fig. 6.39 – River Severn CFX Velocity Profile (m/s) at Cross-Sections 1, 2, 3 and 4 (k_s = 0.100 m, Grid CFX S-1, k-ε model)

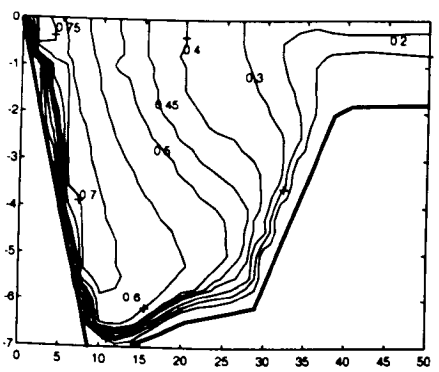

Cross-Section 5

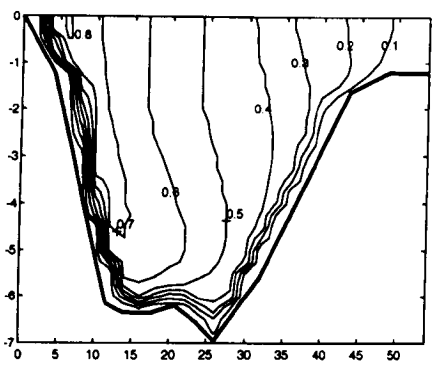

Cross-Section 6

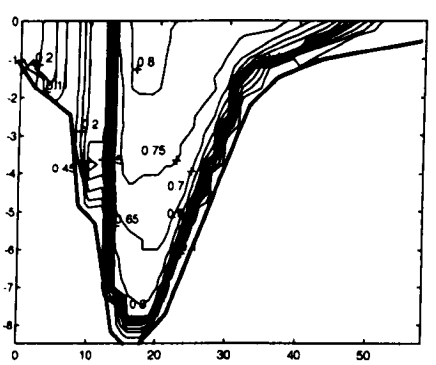

Cross-Section 7

Fig. 6.40 – River Severn CFX Velocity Profile (m/s) at Cross-Sections 5, 6 and 7 (k_s = 0.100 m, Grid CFX S-1, k-ε model)

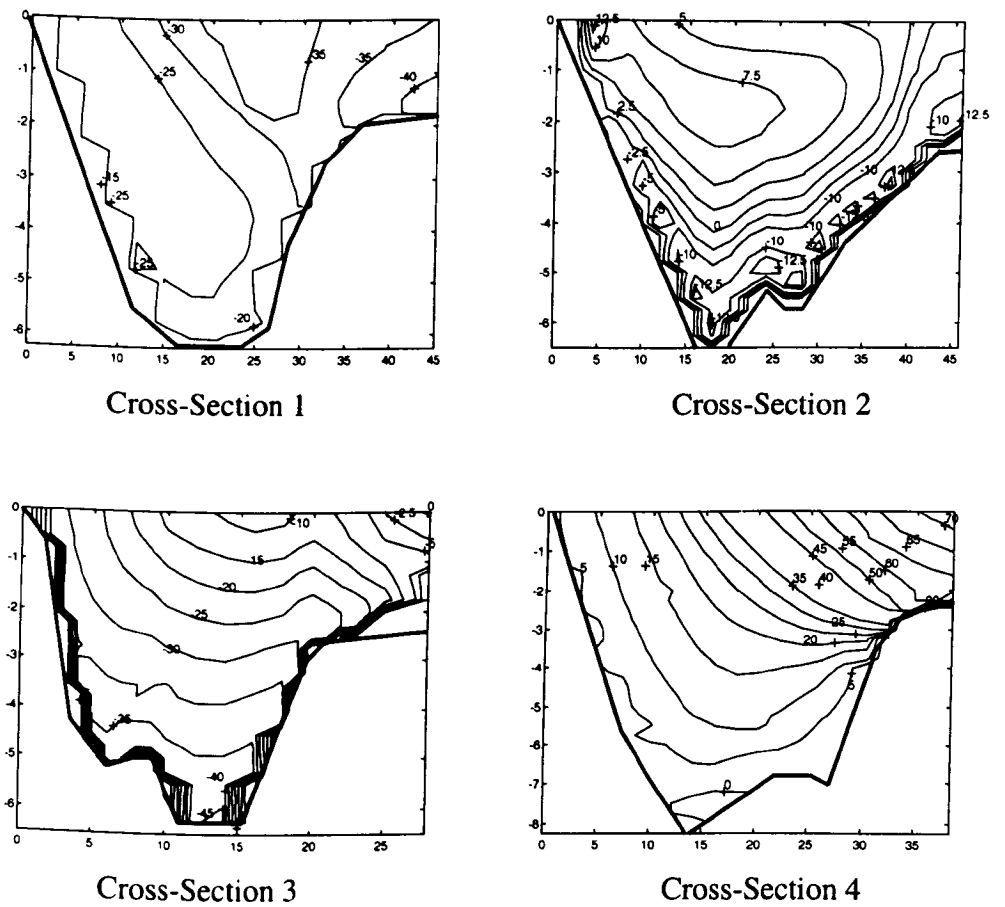

Fig. 6.41 – River Severn CFX Velocity Direction (deg.) at Cross-Sections 1, 2, 3 and 4 (k_s = 0.100 m, Grid CFX S-1, k-ε model)

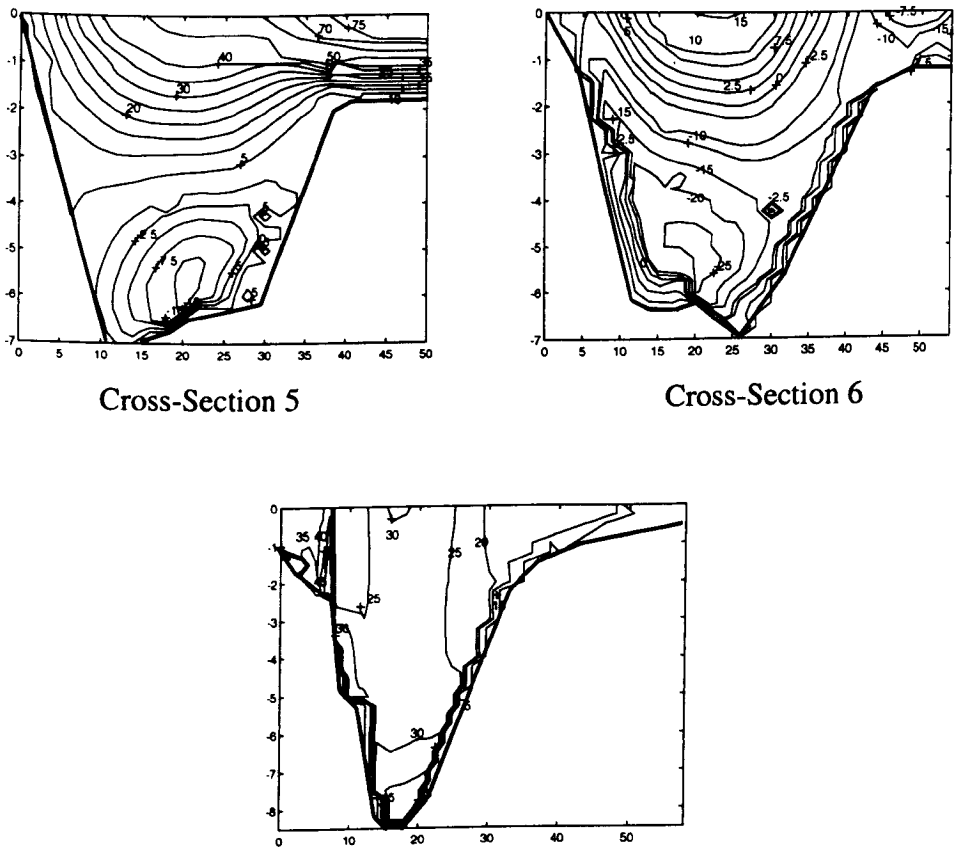

Fig. 6.42 – River Severn CFX Velocity Orientation (deg.) at Cross-Sections 5, 6 and 7 (k_s = 0.100 m, Grid CFX S-1, k-ε model)

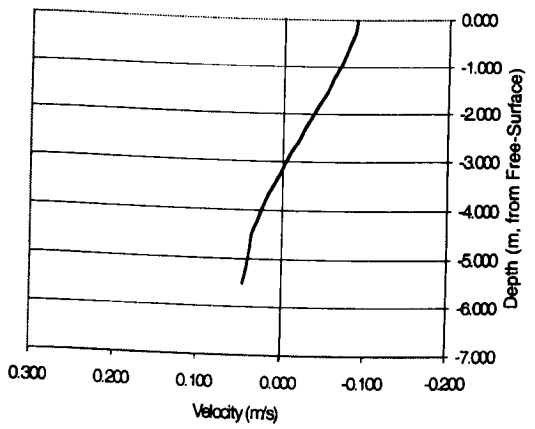

Cross-Section 1

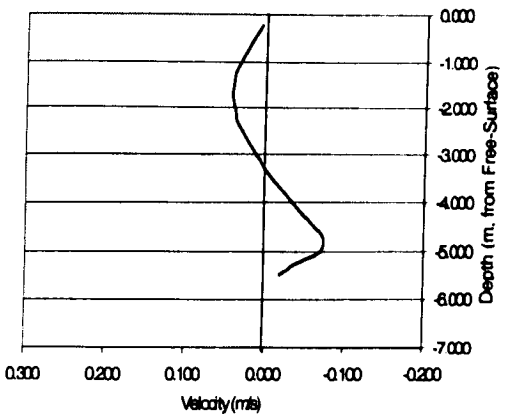

Cross-Section 2

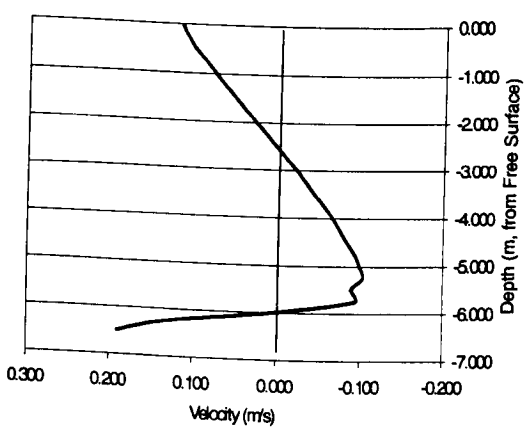

Cross-Section 3

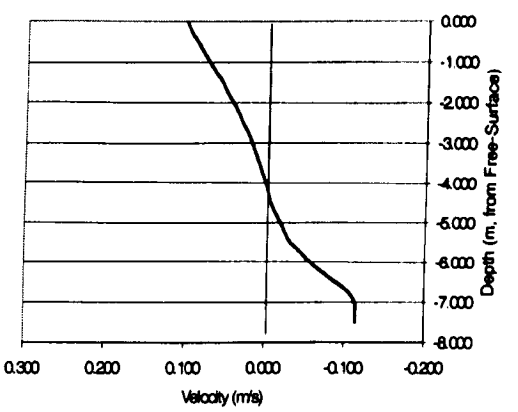

Cross-Section 4

Fig. 6.43 – River Severn CFX Model: River Severn CFX Model: Calculated Recirculation (m/s) at Sections 1, 2, 3 and 4

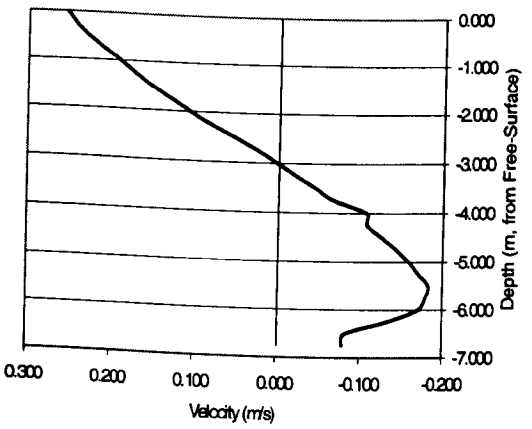

Cross-Section 5

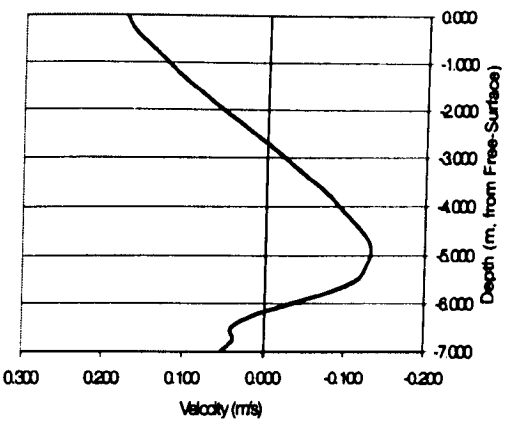

Cross-Section 6

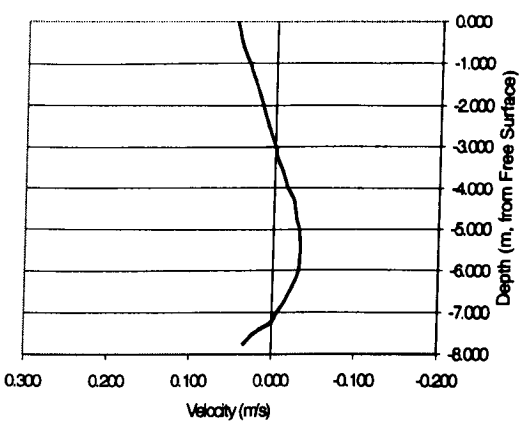

Cross-Section 7

Fig. 6.44 – River Severn CFX Model: River Severn CFX Model: Calculated Recirculation (m/s) at Sections 5, 6 and 7

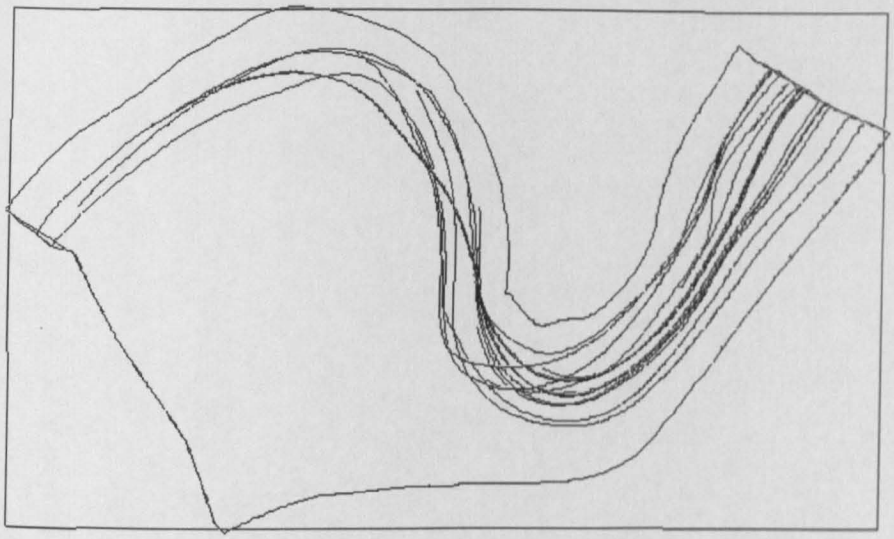

(a)

(b)

Fig. 6.45 – CFX Numerical Tracer Release at Elevation 13.0 m in the Severn:
(a) Tracer Route
(b) Rotational Effects and Velocity

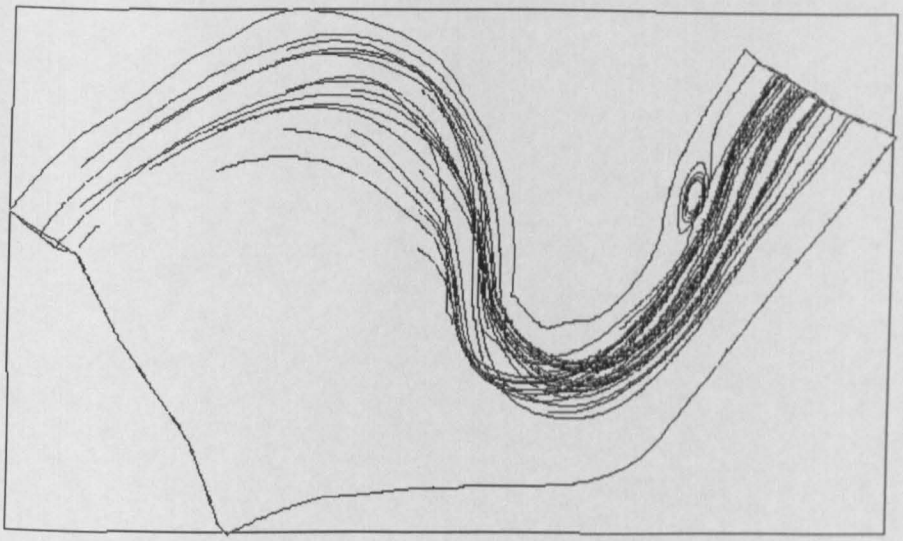

(a)

(b)

Fig. 6.46 – CFX Numerical Tracer Release at Elevation 16.5 m in the Severn:
(a) Tracer Route
(b) Rotational Effects and Velocity

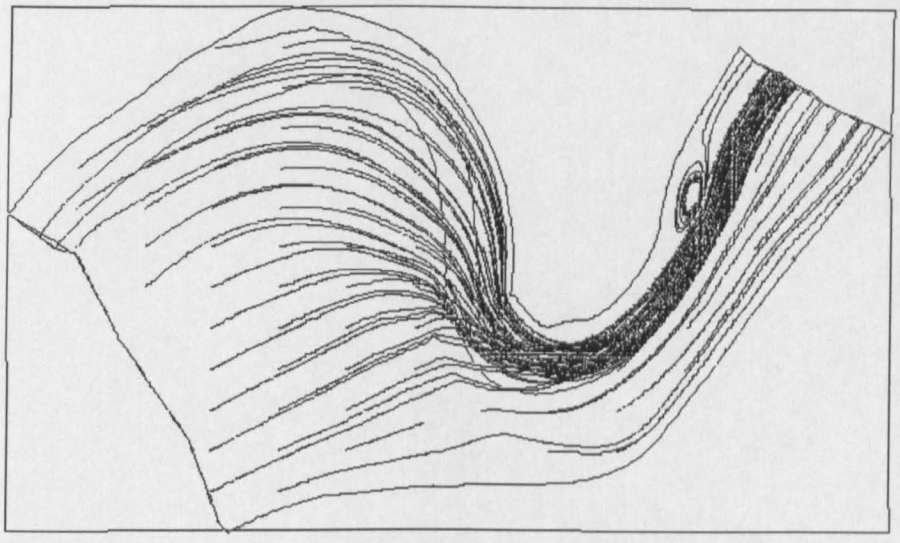

(a)

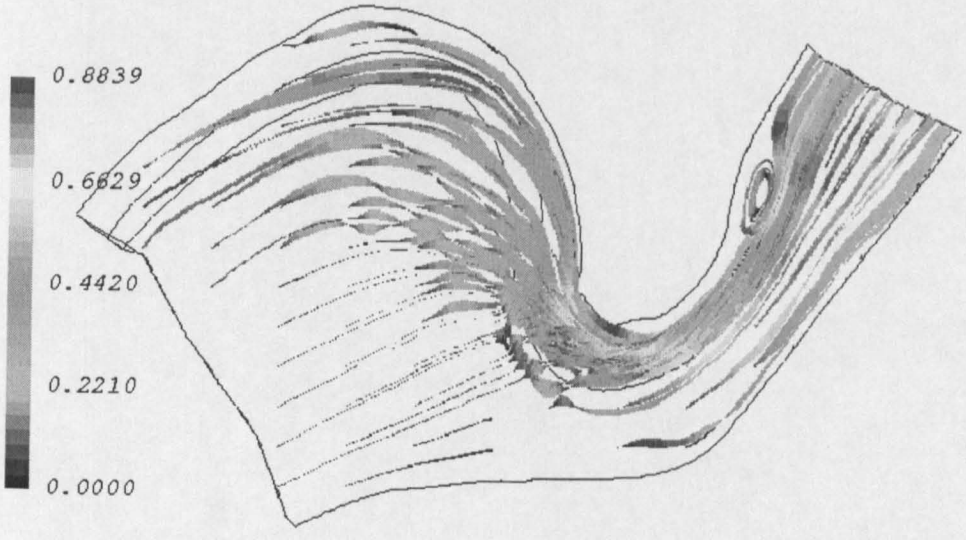

(b)

Fig. 6.47 – CFX Numerical Tracer Release at Elevation 17.9 m in the Severn:
(a) Tracer Route
(b) Rotational Effects and Velocity

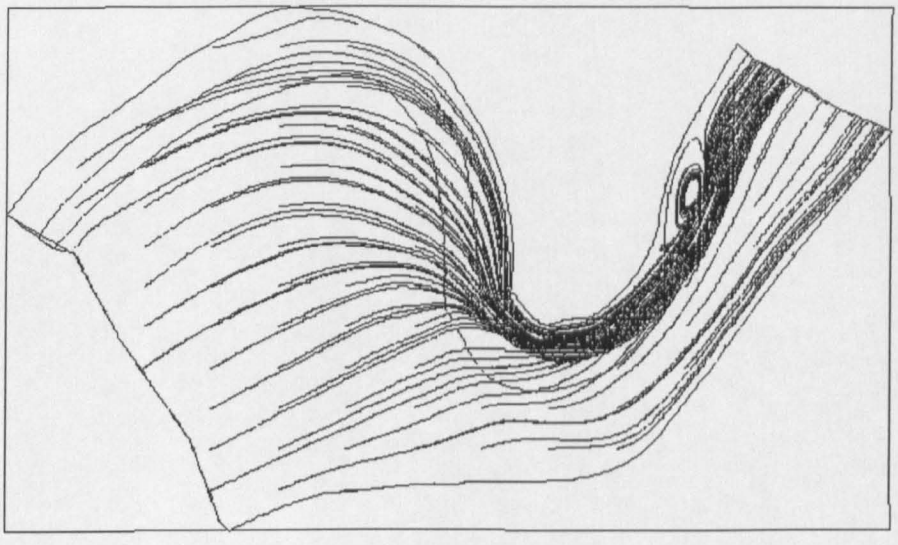

(a)

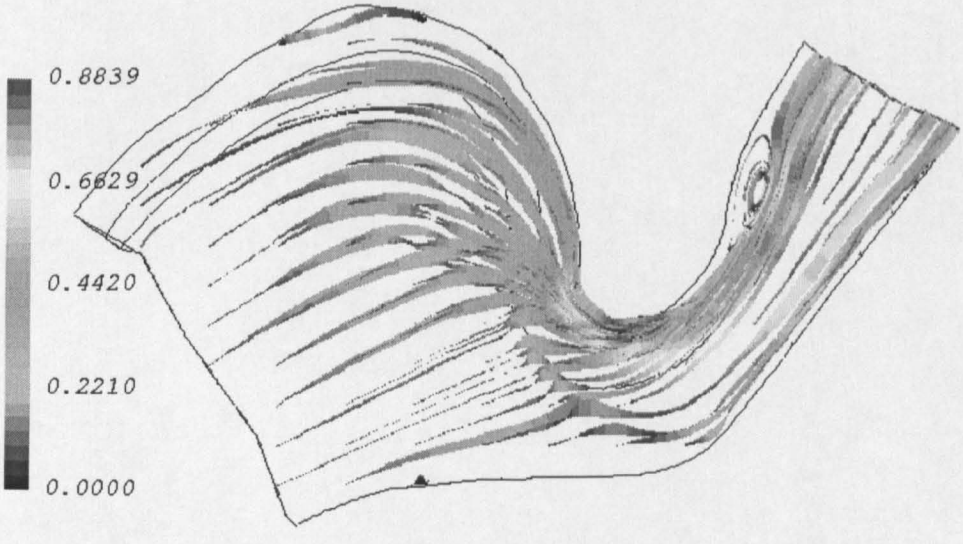

(b)

Fig. 6.48 – CFX Numerical Tracer Release at Elevation 18.3 m in the Severn:
(a) Tracer Route
(b) Rotational Effects and Velocity

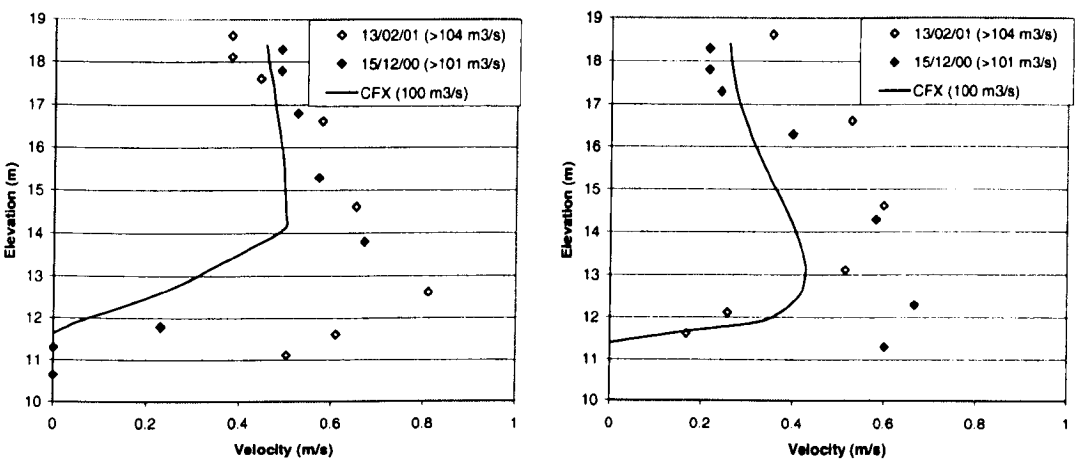

At 9.00 m from the Left Bank

At 19.00 m from the Left Bank

Fig. 6.49 – Comparison between Field Data and River Severn CFX Model Predictions at Cross-Section 4

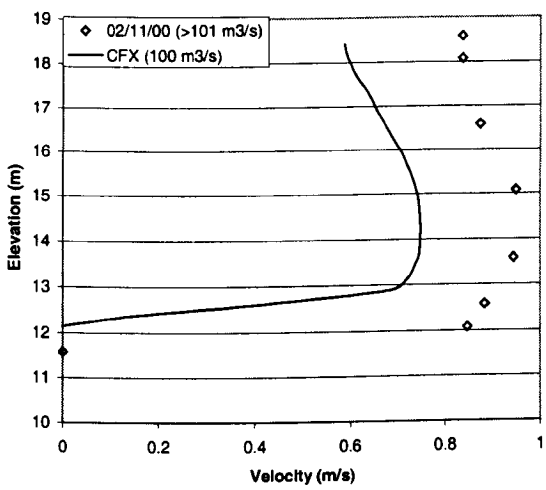

At 8.00 m from the Left Bank

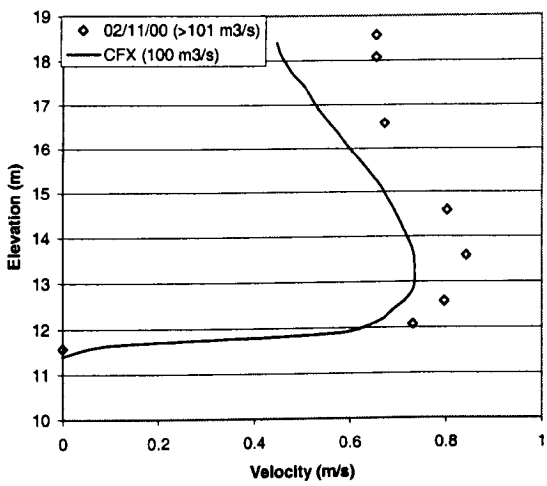

At 12.00 m from the Left Bank

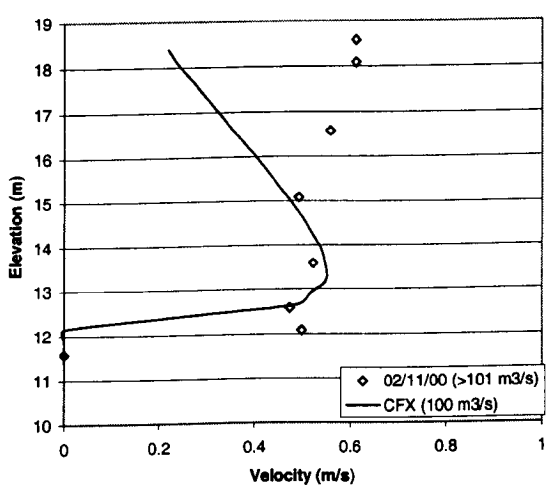

At 22.00 m from the Left Bank

Fig. 6.50 – Comparison between Field Data and River Severn CFX Model Predictions at Cross-Section 5

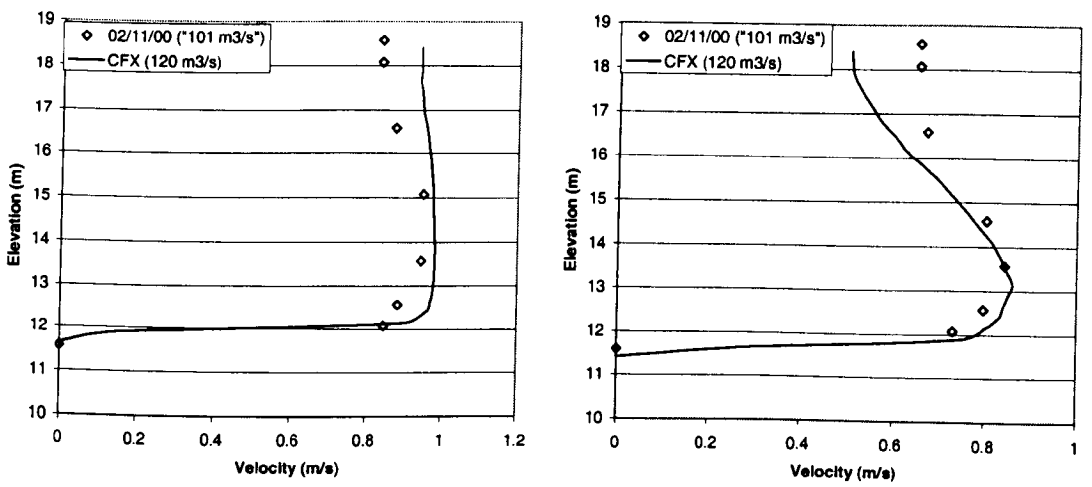

At 8.00 m from the Left Bank

At 12.00 m from the Left Bank

Fig. 6.51 – Comparison between Field Data and River Severn CFX Model Predictions at Cross-Section 5 for a Flow of 120 m^3/s (Discharge + 20%)

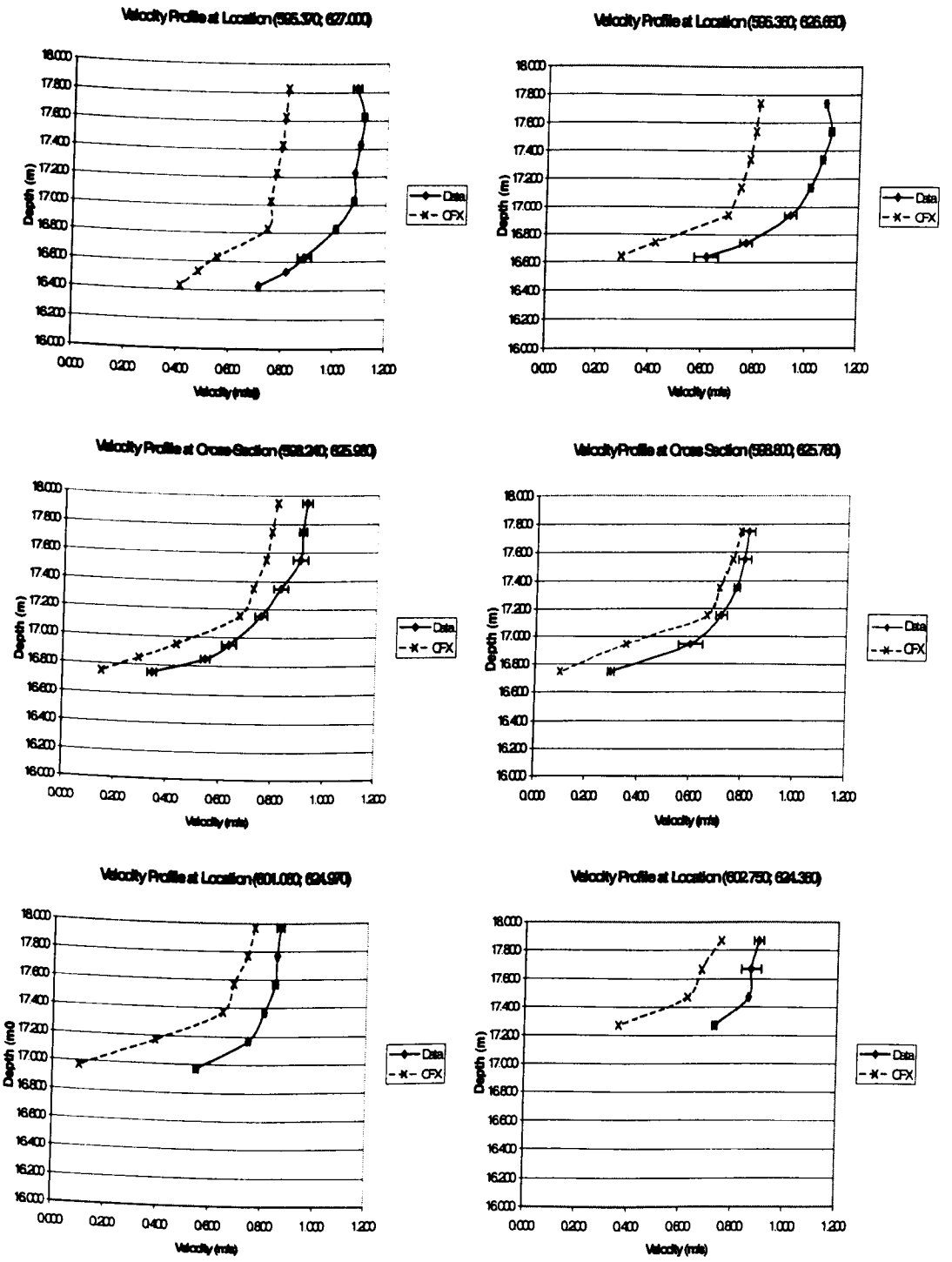

Fig. 6.52 – Comparison between Measured and Predicted Velocity Profiles along the Severn Main Channel Right Bank, at the Tower (m/s; March 2000)

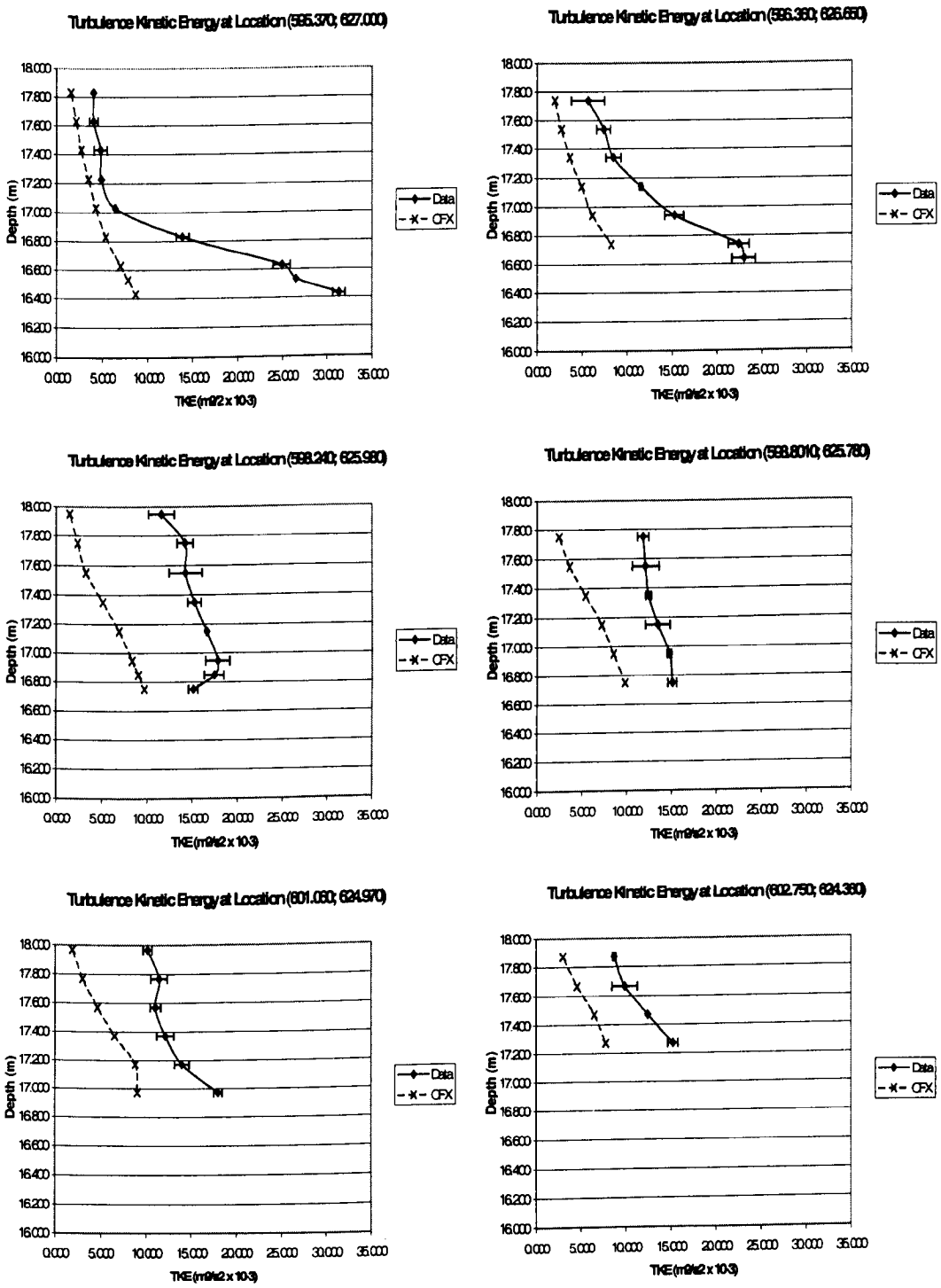

Fig. 6.53– Comparison between Measured and Predicted Turbulence Kinetic Energy along the Severn Main Channel Right Bank, at the Tower (m^2/s^2; March 2000)

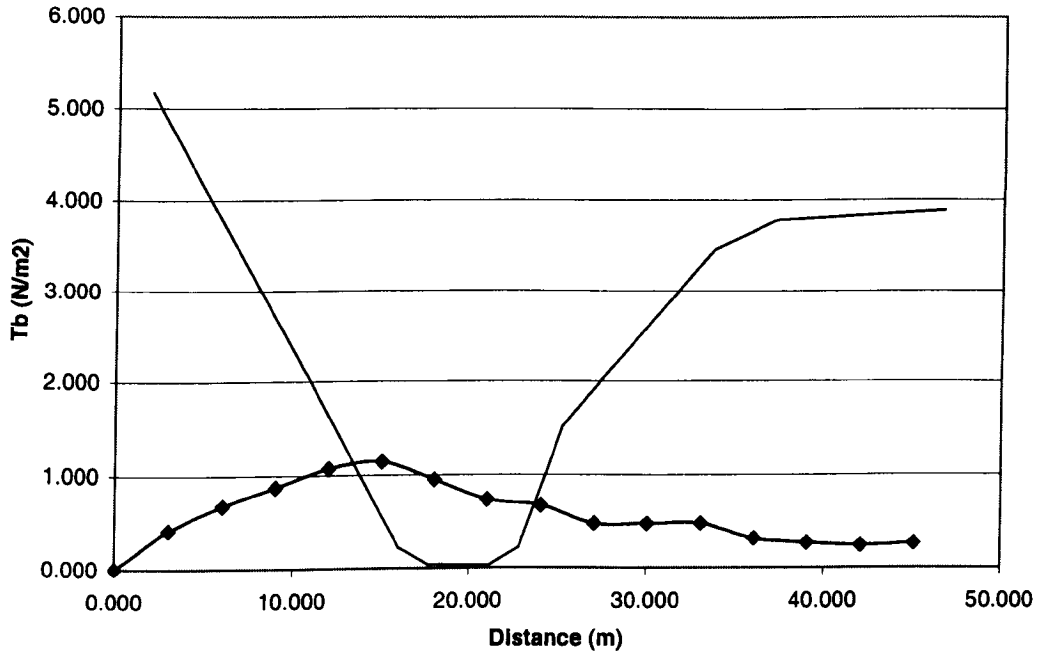

Fig. 6.54 – Calculated Bed Shear Stresses at Section 1 from CFX River Severn Model (k-ε model)

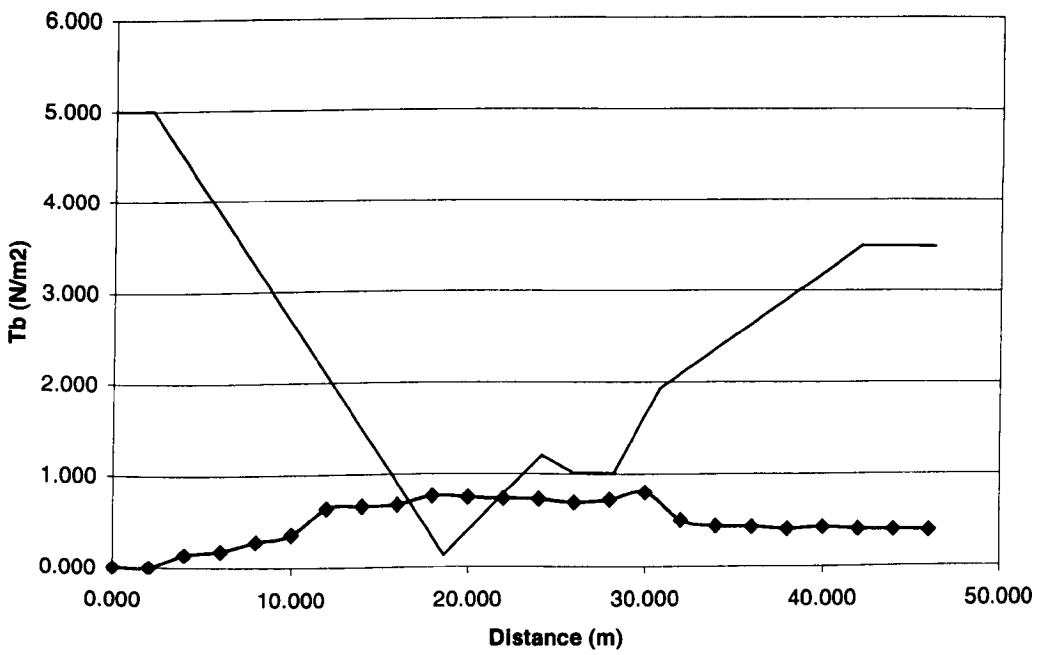

Fig. 6.55 – Calculated Bed Shear Stresses at Section 2 from CFX River Severn Model (k-ε model)

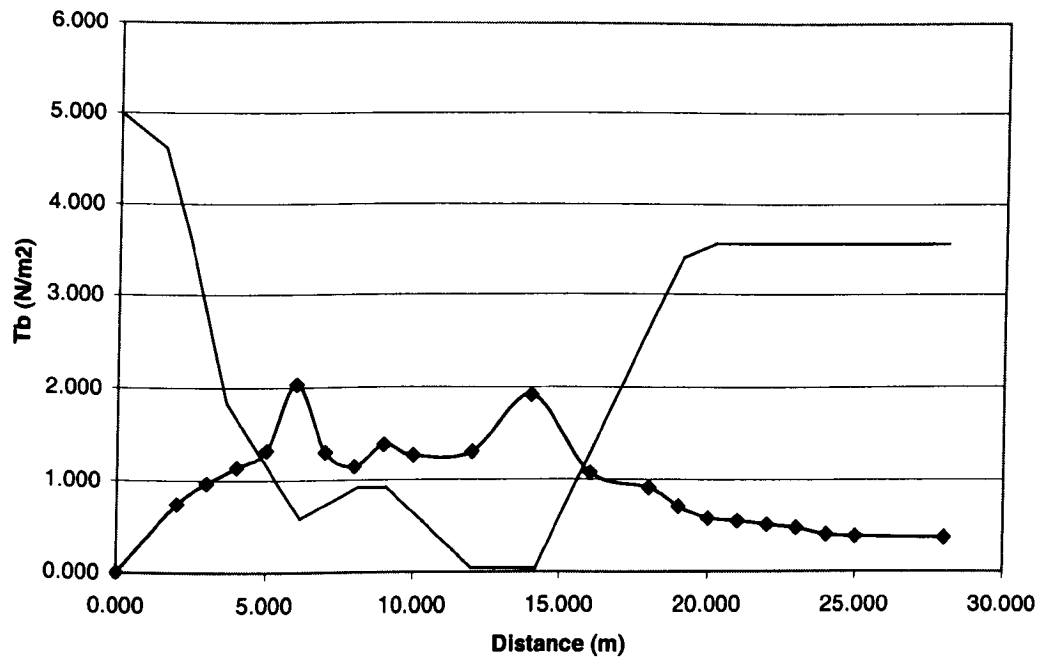

Fig. 6.56 – Calculated Bed Shear Stresses at Section 3 from CFX River Severn Model (k-ε model)

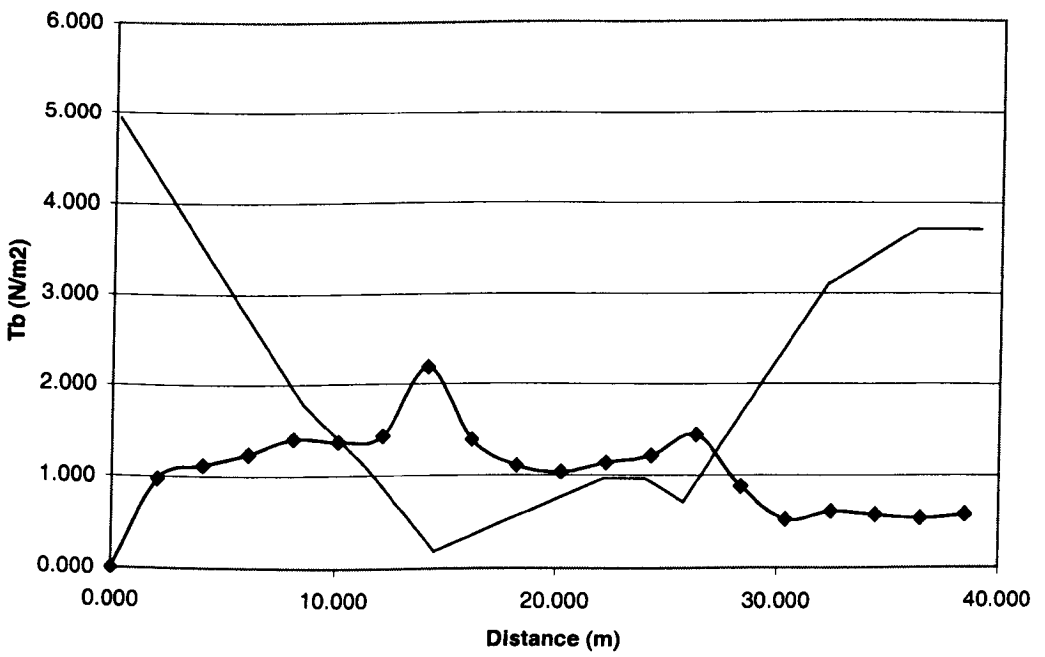

Fig. 6.57 – Calculated Bed Shear Stresses at Section 4 from CFX River Severn Model (k-ε model)

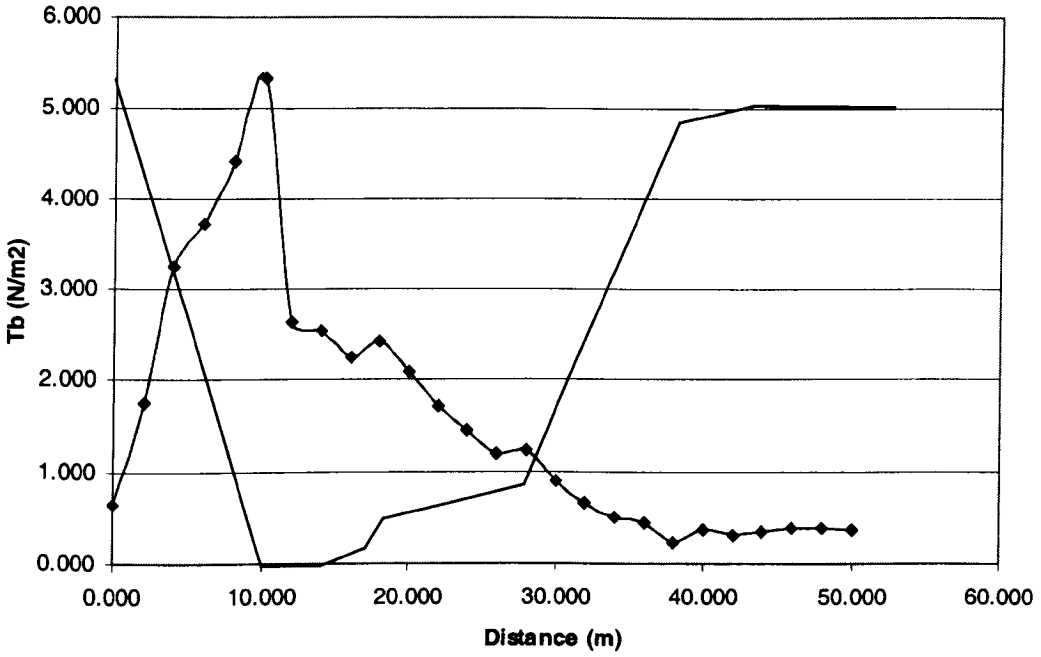

Fig. 6.58 – Calculated Bed Shear Stresses at Section 5 from CFX River Severn Model (k-ε model)

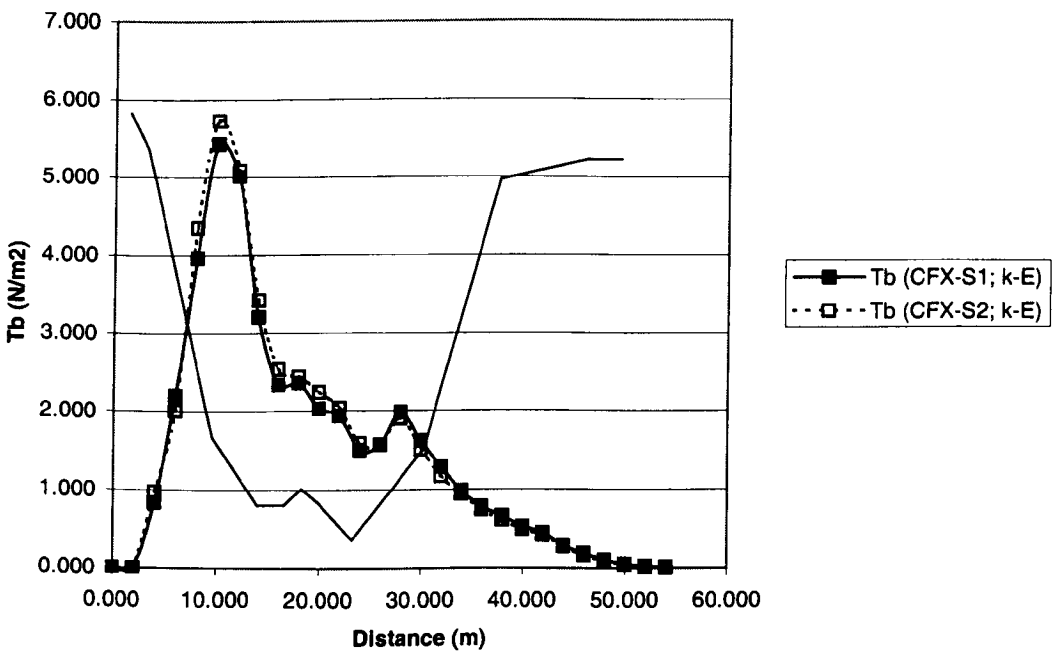

Fig. 6.59 – Calculated Bed Shear Stresses at Section 6 from CFX River Severn Model for the Two CFX Grids (k-ε model)

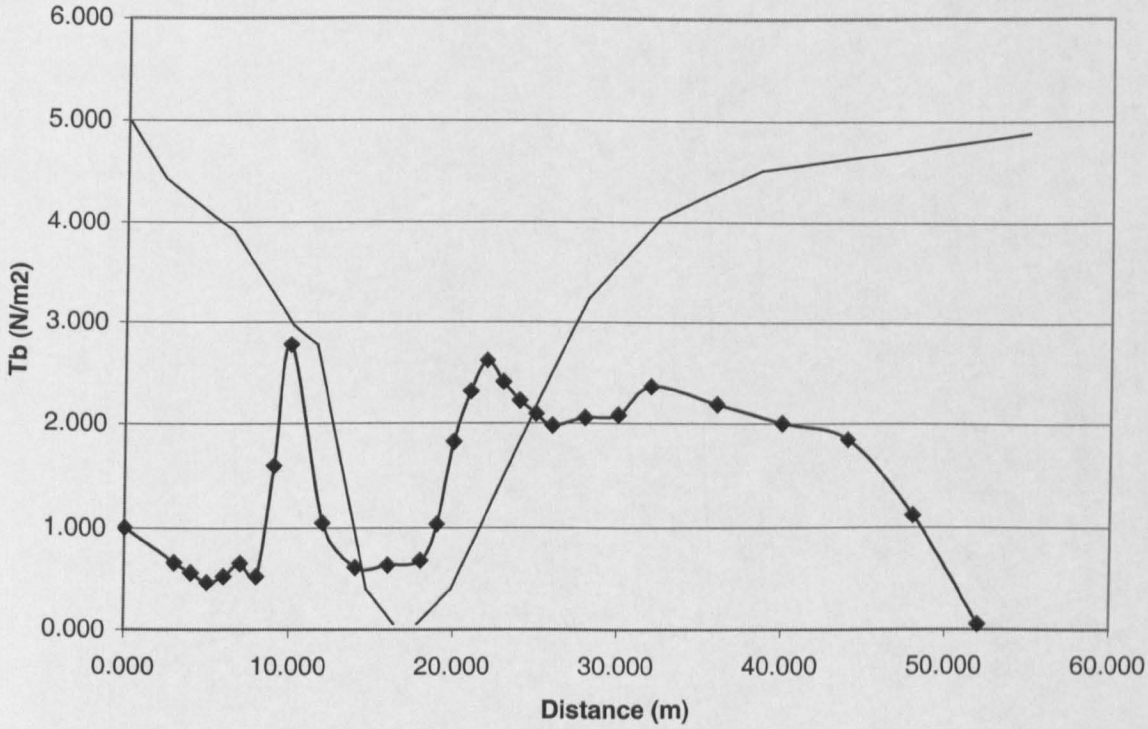

Fig. 6.60 – Calculated Bed Shear Stresses at Section 7 from CFX River Severn Model (k-ε model)

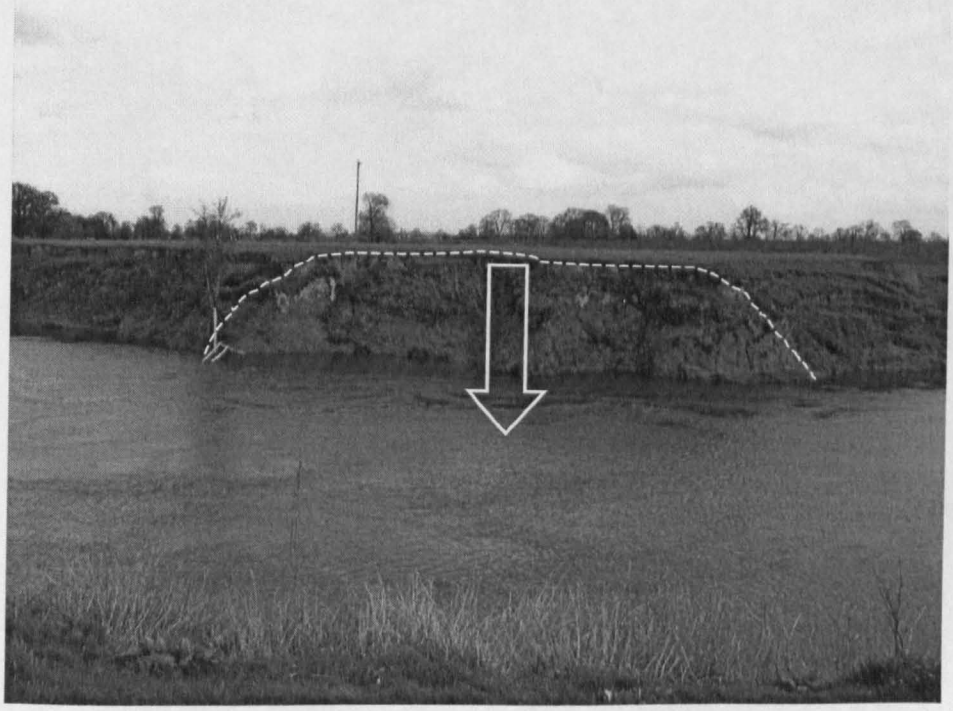

Fig. 6.61 – River Severn: Bank Collapse at the Inner Bank of the Second Meander

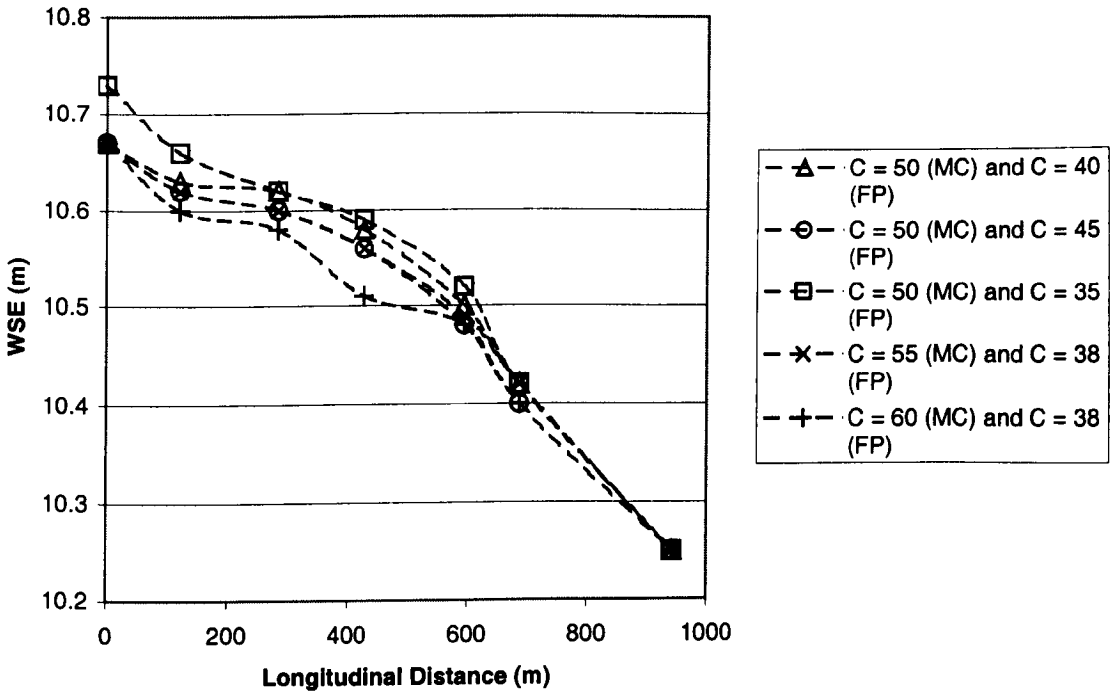

Fig. 6.62 – TELEMAC Model of the Ribble: Sensitivity Analysis of the Free Surface to Roughness

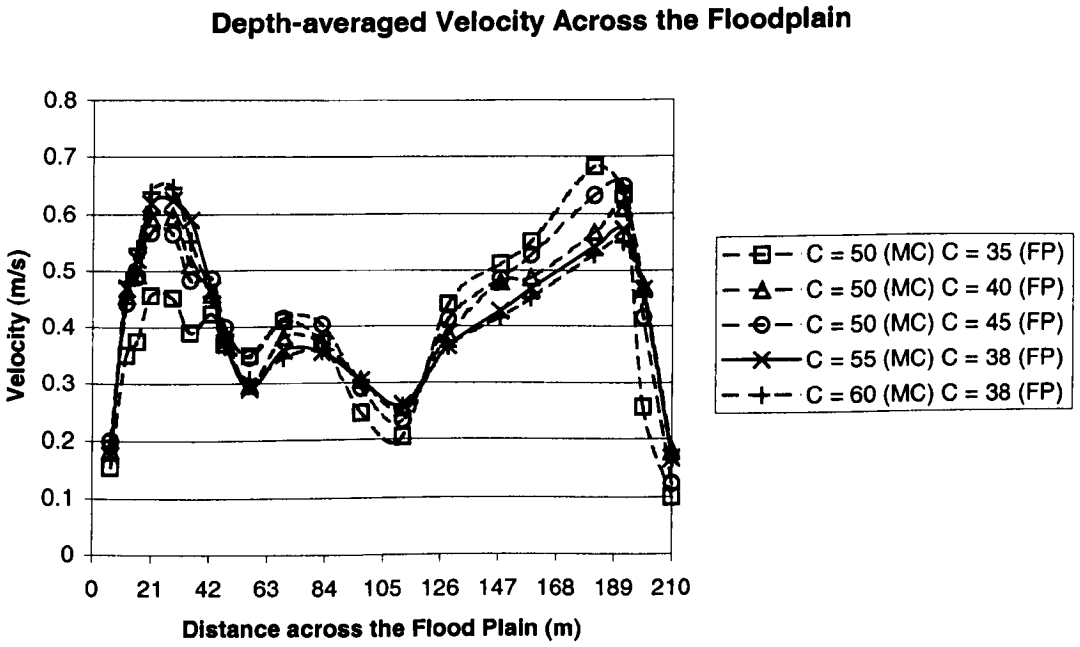

Fig. 6.63 – TELEMAC Model of the Ribble: Impact of Roughness on Velocity Distribution across the Flood Plain

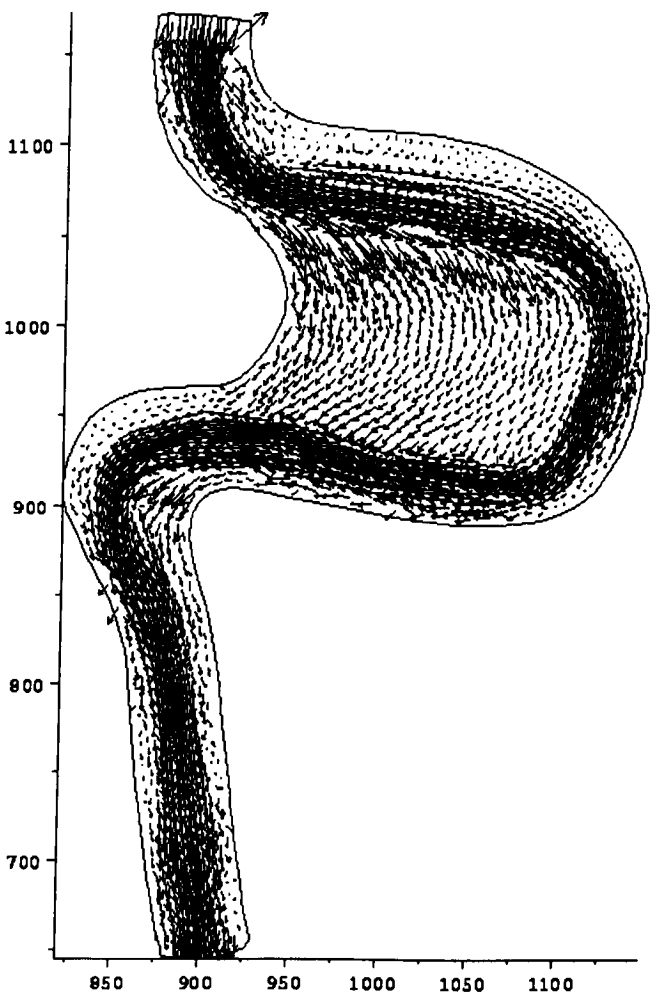

Fig. 6.64 – River Ribble TELEMAC Depth-Averaged Velocity Vectors for a Flow of 98 m^3/s

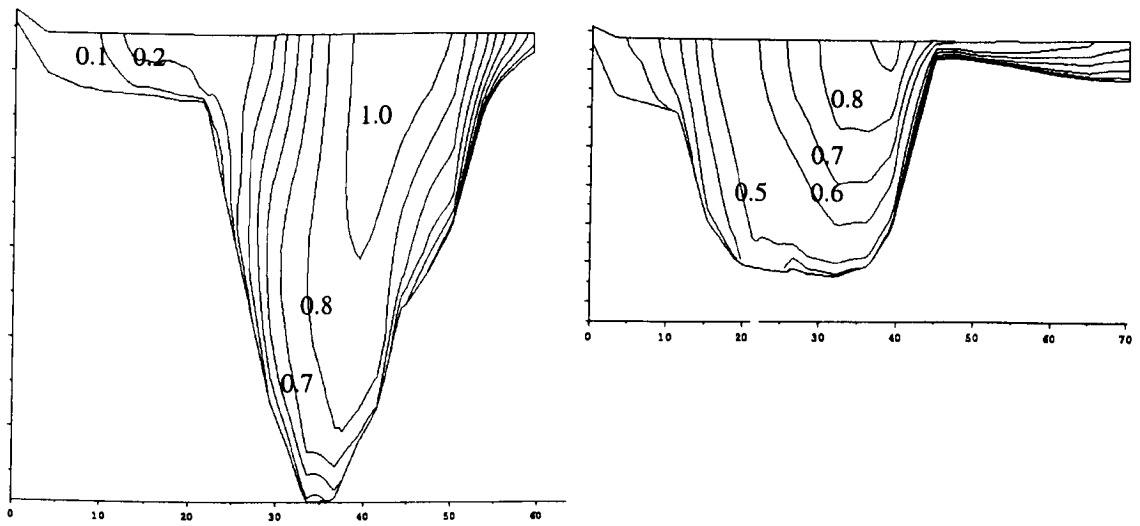

Cross-Section 1

Cross-Section 2

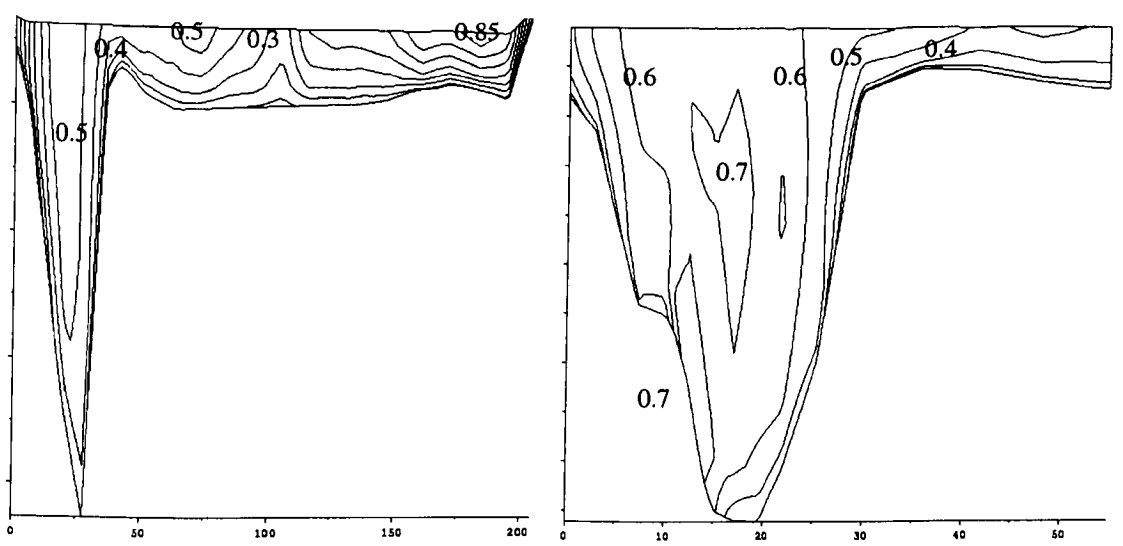

Cross-Section 3

Cross-Section 4

Fig. 6.65 – River Ribble TELEMAC Velocity Profile (m/s) at Cross-Sections 1, 2, 3 and 4 (C = 38 $m^{1/2}/s$ on the flood plain, C = 50 $m^{1/2}/s$ in the main Channel, mixing-length model)

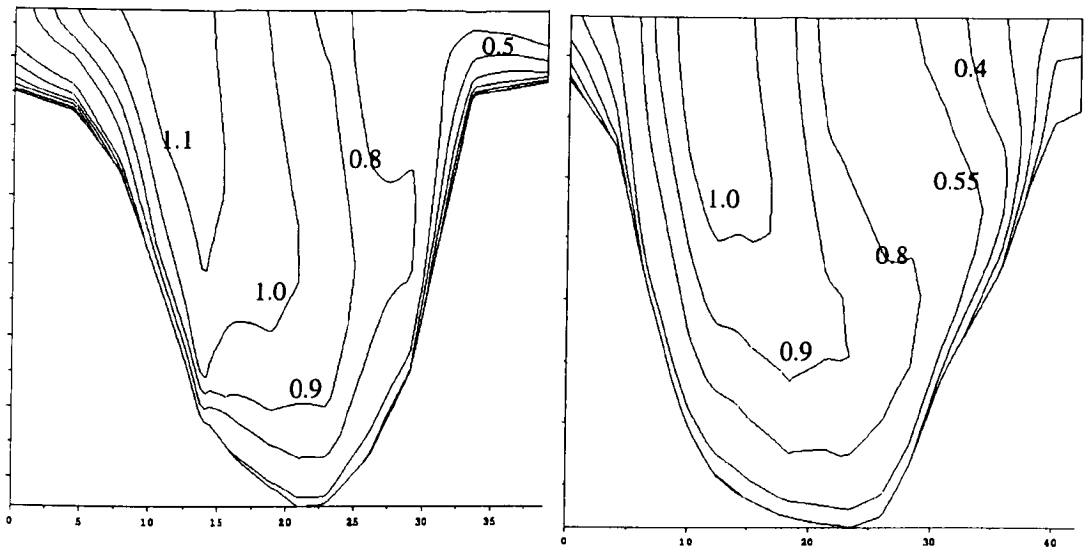

Cross-Section 5 Cross-Section 6

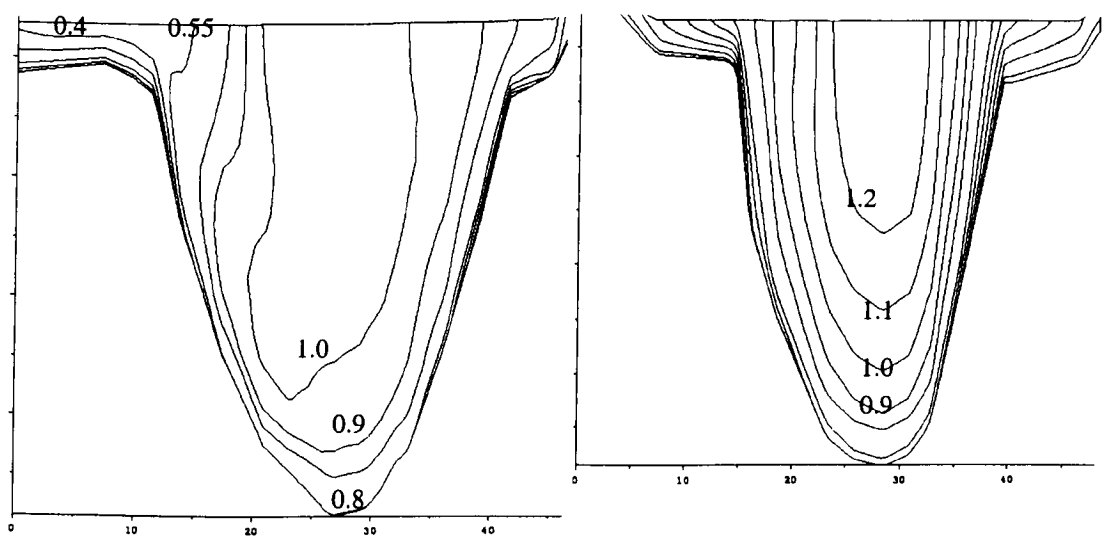

Cross-Section 7 Cross-Section 8

Fig. 6.66– River Ribble TELEMAC Velocity Profile (m/s) at Cross-Sections 5, 6, 7 and 8 (C = 38 $m^{1/2}/s$ on the flood plain, C = 55 $m^{1/2}/s$ in the main Channel, mixing-length model)

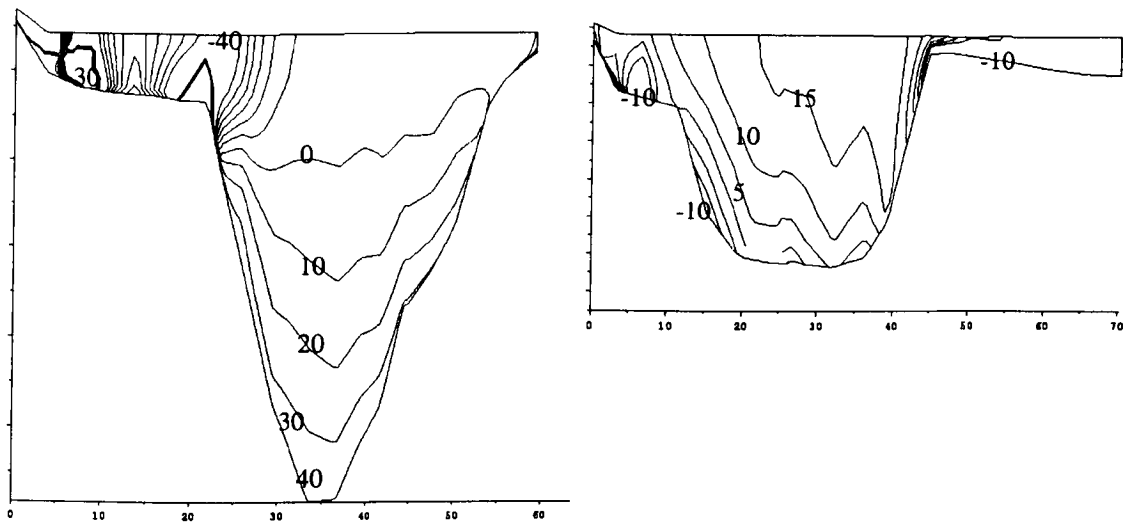

Cross-Section 1

Cross-Section 2

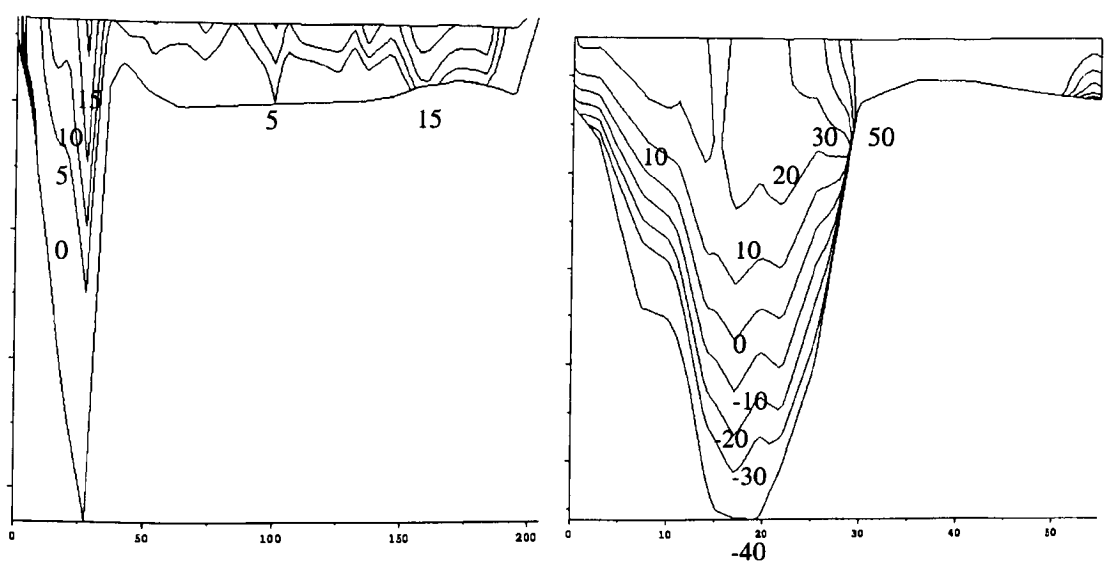

Cross-Section 3

Cross-Section 4

Fig. 6.67 – River Ribble TELEMAC Velocity Orientation (deg.) at Cross-Sections 1, 2, 3 and 4 (C = 38 $m^{1/2}/s$ on the flood plain, C = 55 $m^{1/2}/s$ in the main Channel, mixing-length model)

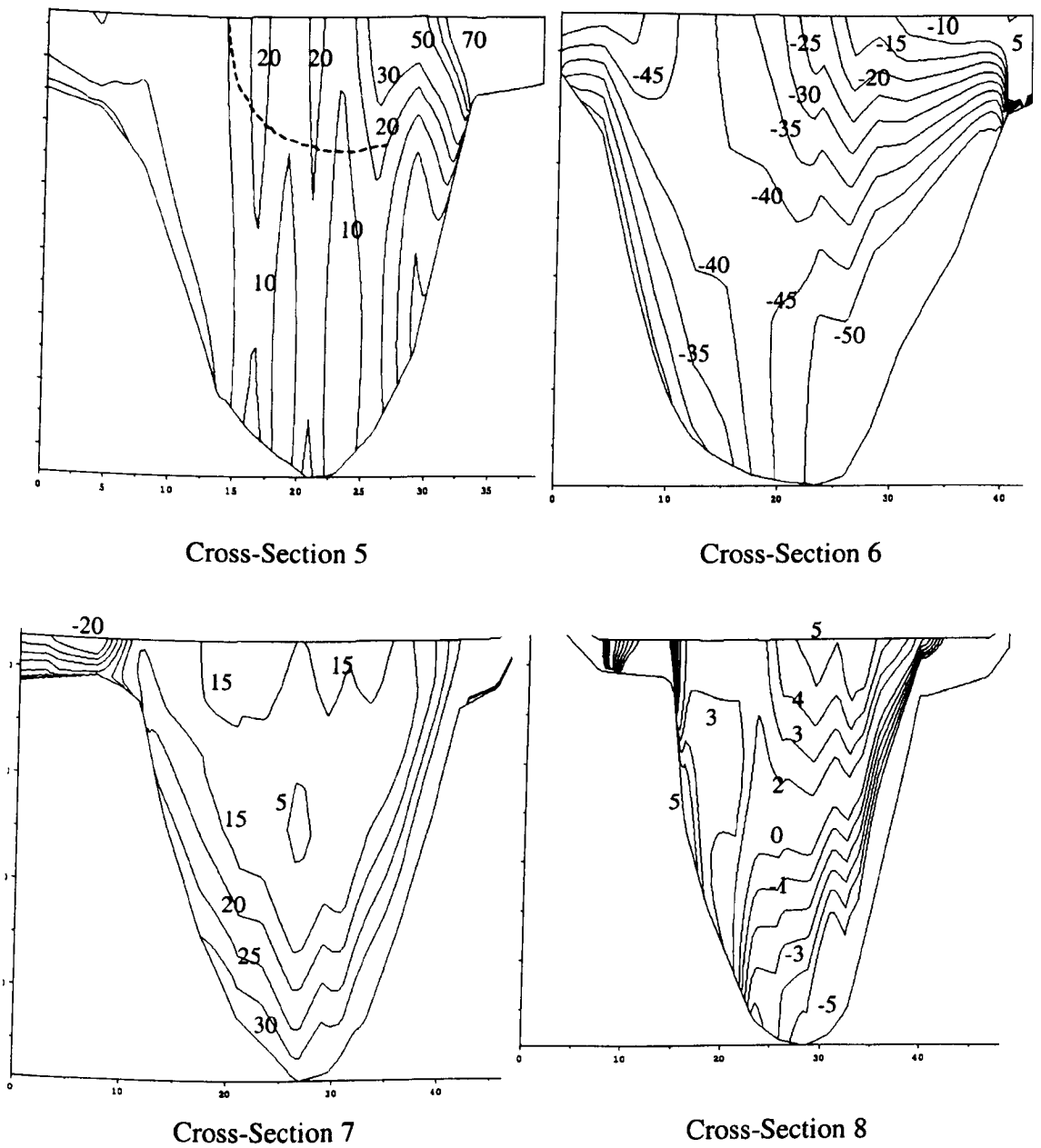

Fig. 6.68 – River Ribble TELEMAC Velocity Orientation (deg.) at Cross-Sections 5, 6, 7 and 8 (C = 38 $m^{1/2}/s$ on the flood plain, C = 55 $m^{1/2}/s$ in the main Channel, mixing-length model)

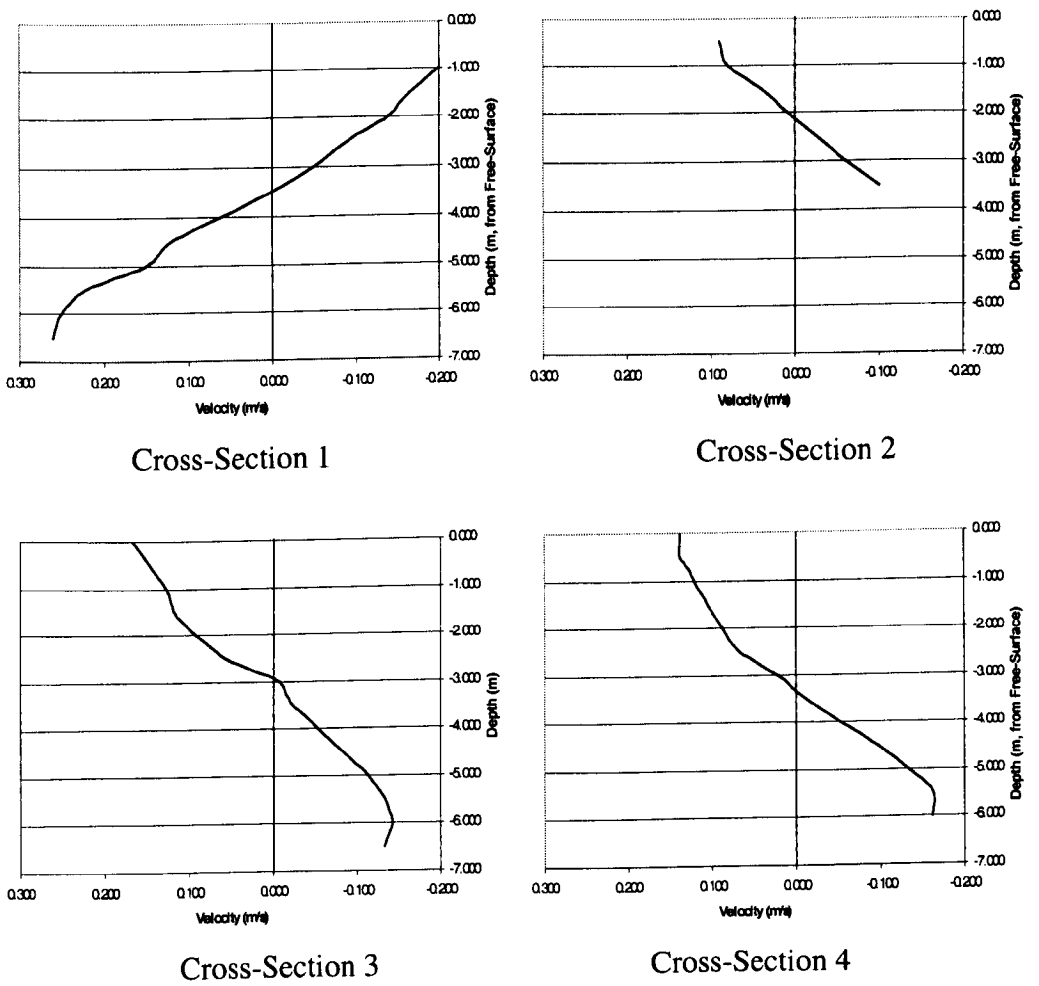

Fig. 6.69 – River Ribble TELEMAC Model: Recirculation at Cross-Sections 1 to 4

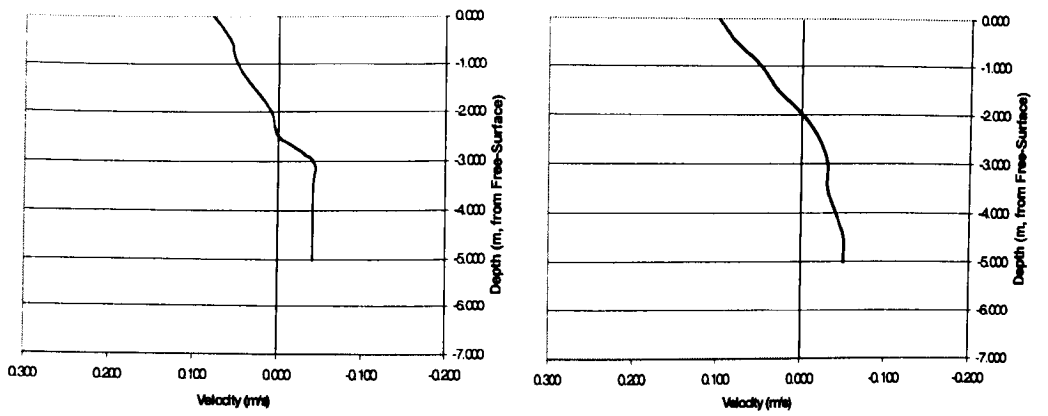

Cross-Section 5

Cross-Section 6

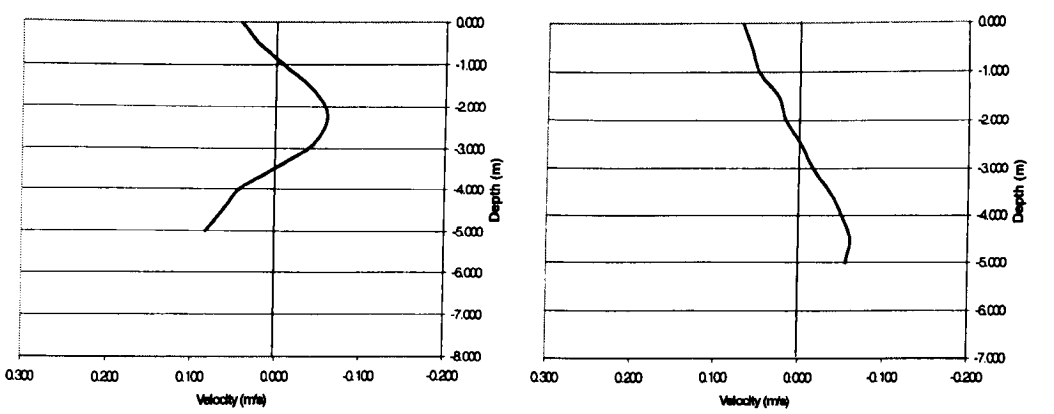

Cross-Section 7

Cross-Section 8

Fig. 6.70 – River Ribble TELEMAC Model: Recirculation at Cross-Sections 5 to 8

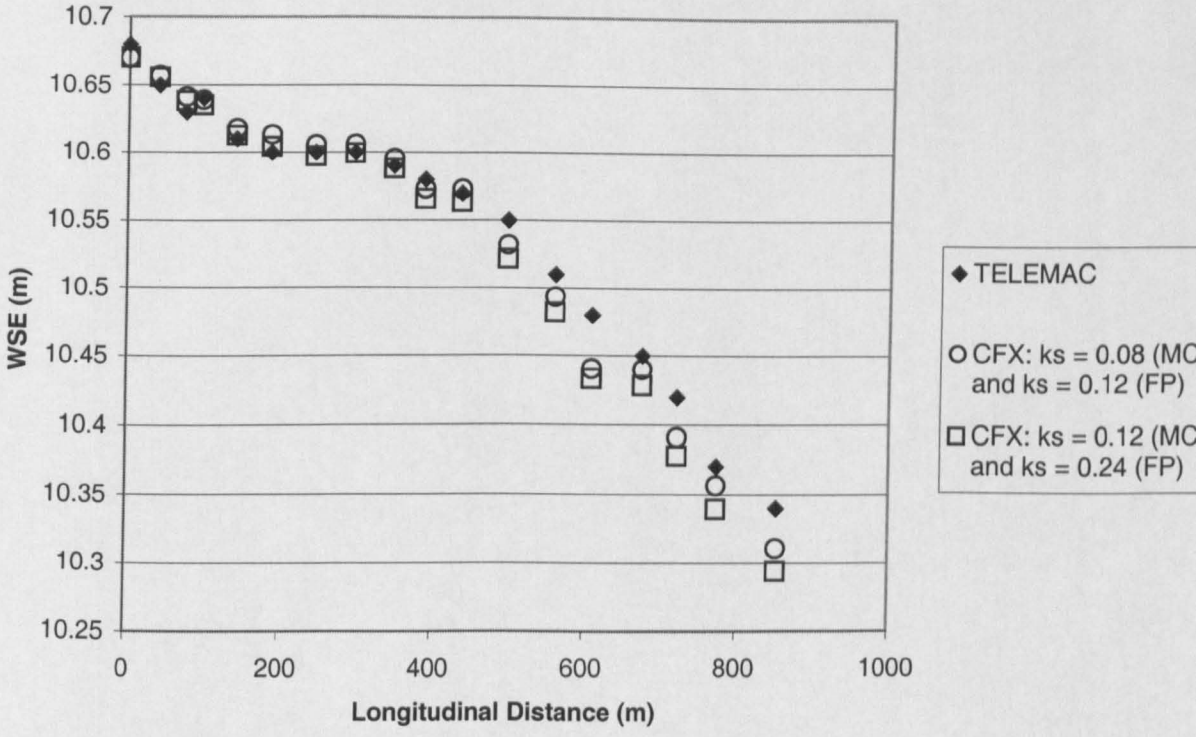

Fig. 6.71 – River Ribble: Comparison between Water Surface Elevation Predicted by TELEMAC and CFX (98 m^3/s)

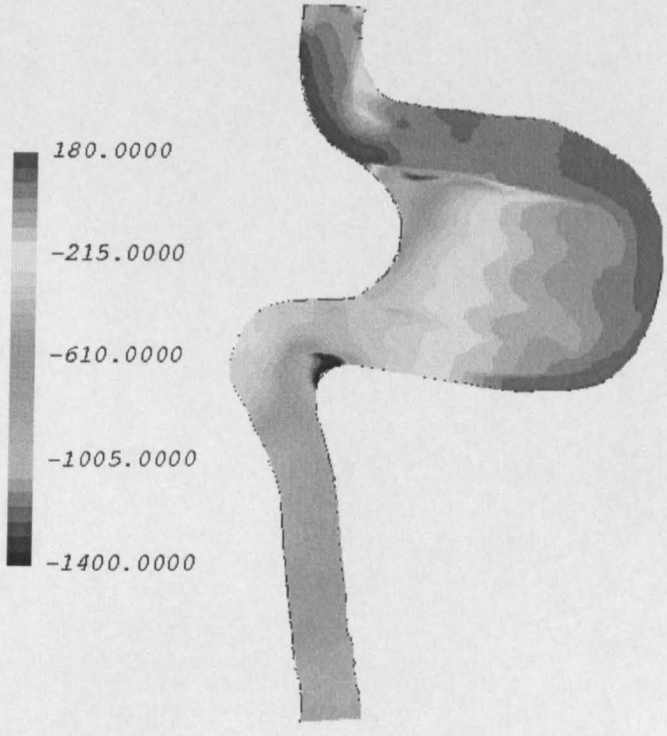

Fig. 6.72 – Calculated CFX Pressure Field (Pa) on the Lid

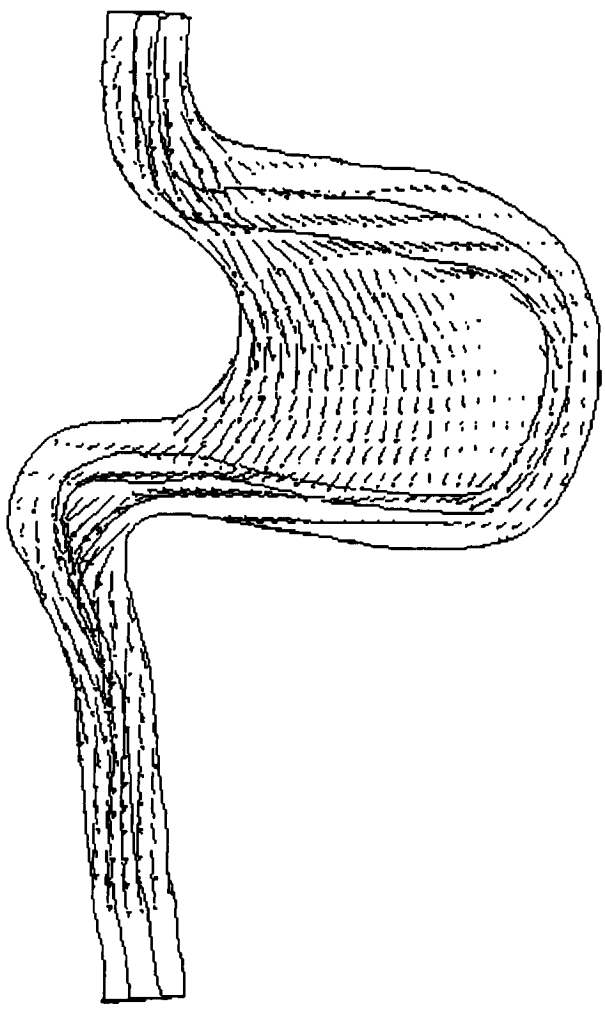

Fig. 6.73 – River Ribble CFX Velocity Vectors close to the Free Surface for a Flow of 98 m^3/s (k_s = 0.08 m in the main channel, k_s = 0.12 m on the floodplain)

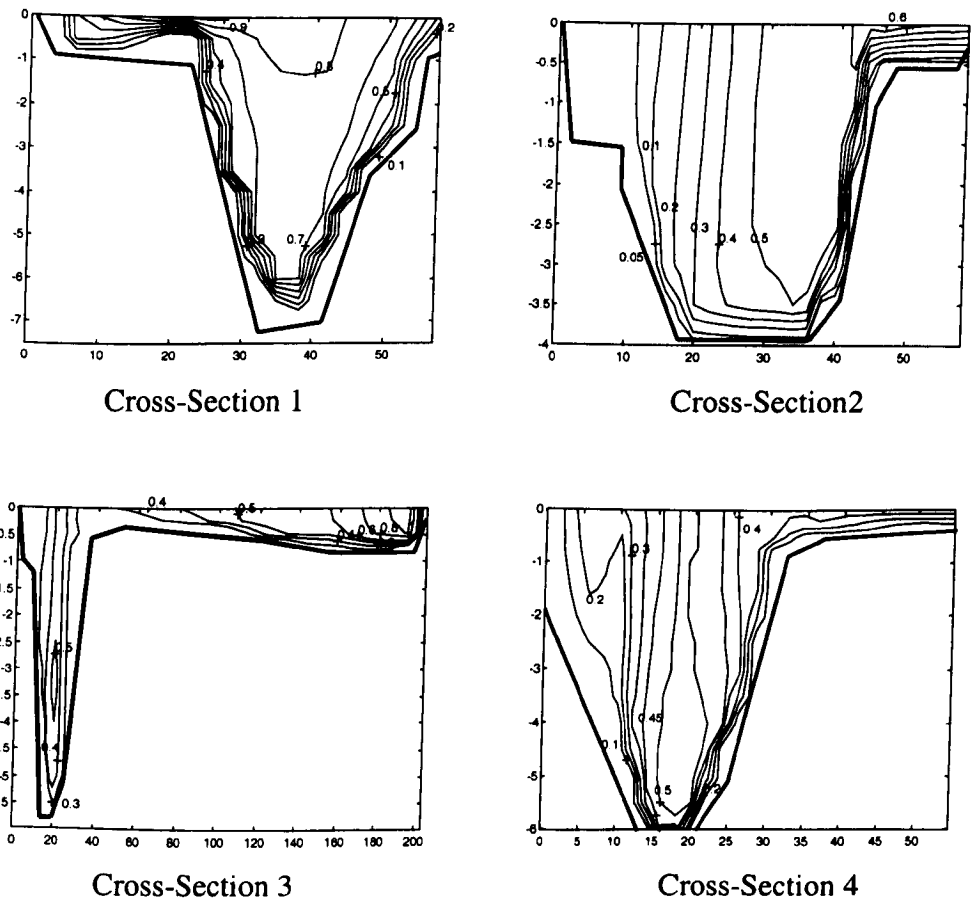

Fig. 6.74 – River Ribble CFX Velocity Profile (m/s) at Cross-Sections 1,2, 3 and 4 (k_s = 0.12 m on the flood plain, k_s = 0.08 m in the main channel, mesh R-1, k-ε model)

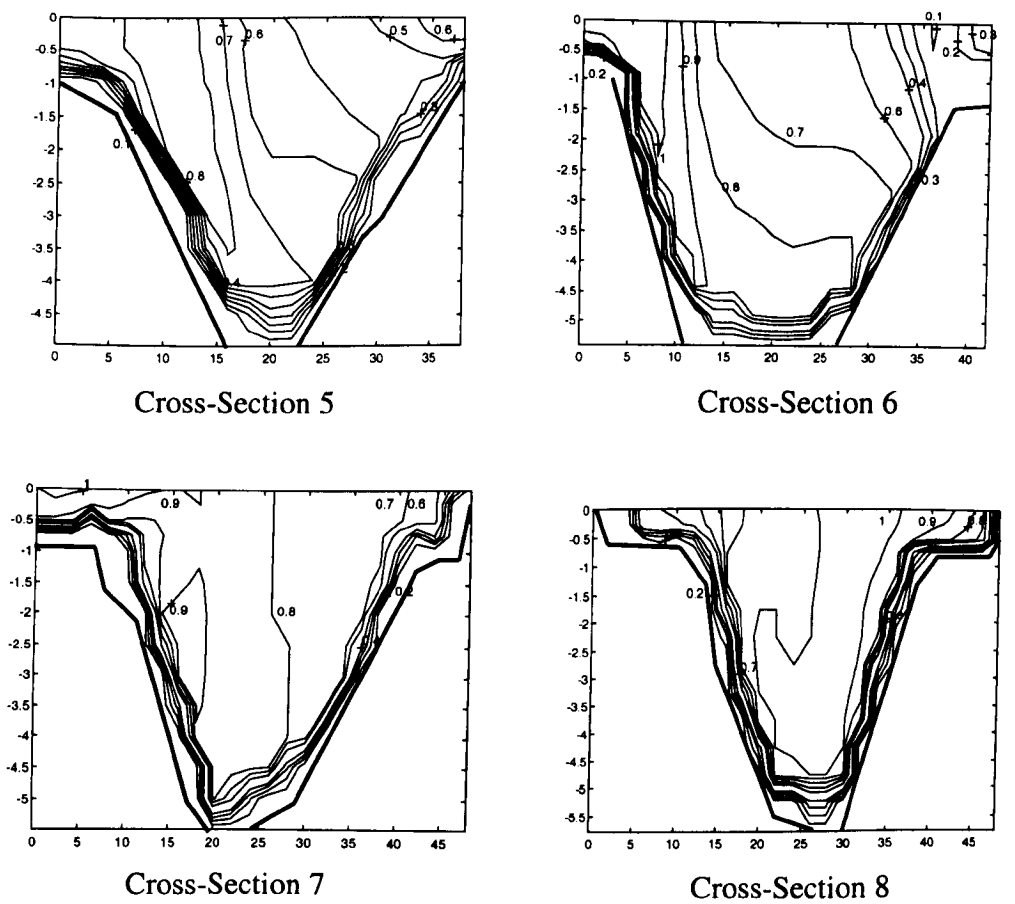

Fig. 6.75 – River Ribble CFX Velocity Profile (m/s) at Cross-Sections 5, 6, 7 and 8 (k_s = 0.12 m on the flood plain, k_s = 0.08 m in the main channel, mesh R-1, k-ε model)

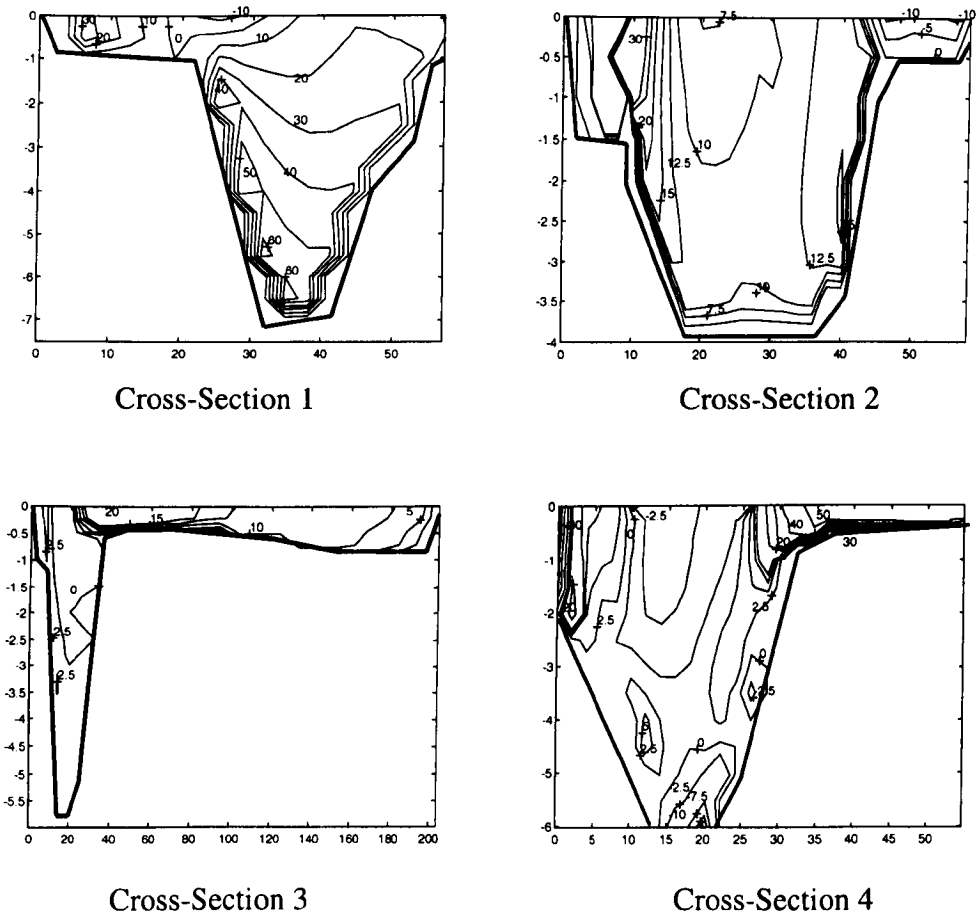

Fig. 6.76 – River Ribble CFX Velocity Orientation (deg.) at Cross-Sections 1, 2, 3 and 4 (k_s = 0.12 m on the flood plain, k_s = 0.08 m in the main channel, mesh R-1, k-ε model)

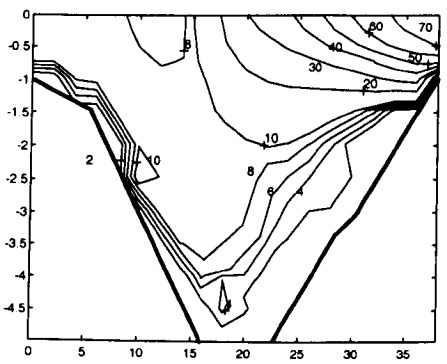

Cross-Section 5

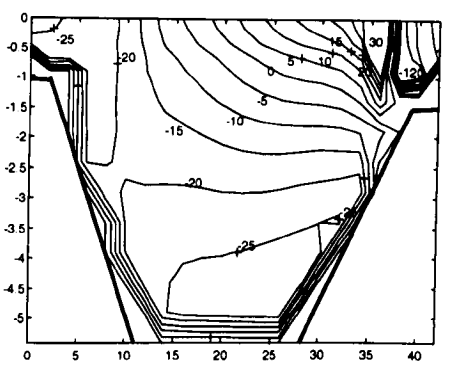

Cross-Section 6

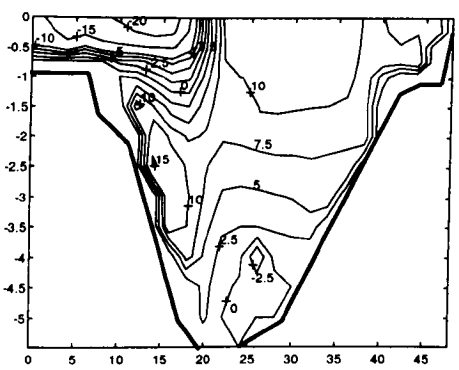

Cross-Section 7

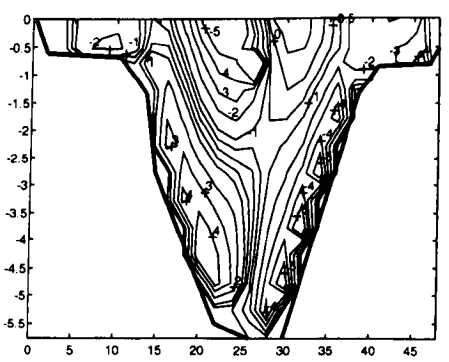

Cross-Section 8

Fig. 6.77 – River Ribble CFX Velocity Orientation (deg.) at Cross-Sections 5, 6, 7 and 8 (k_s = 0.12 m on the flood plain, k_s = 0.08 m in the main channel, mesh R-1, k-ε model)

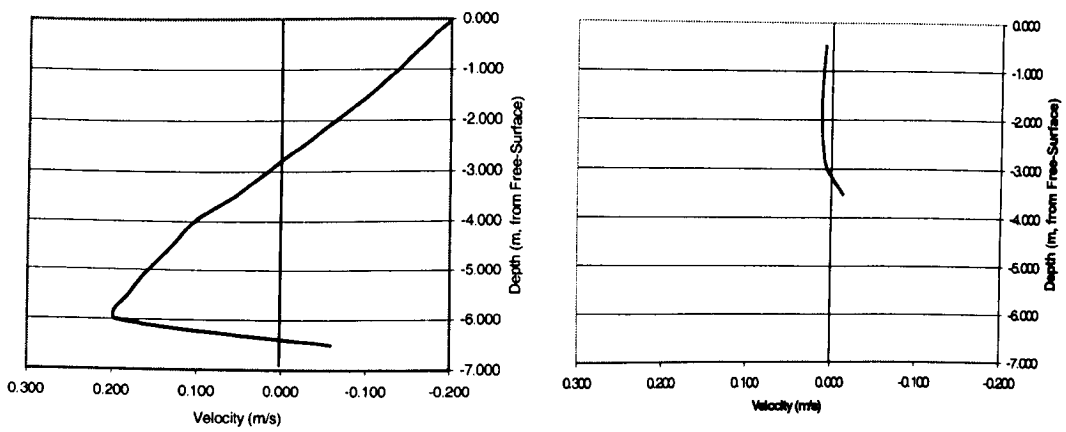

Cross-Section 1

Cross-Section 2

Cross-Section 3

Cross-Section 4

Fig. 6.78 – River Ribble CFX Model: Recirculation (m/s) at Sections 5, 6 and 7

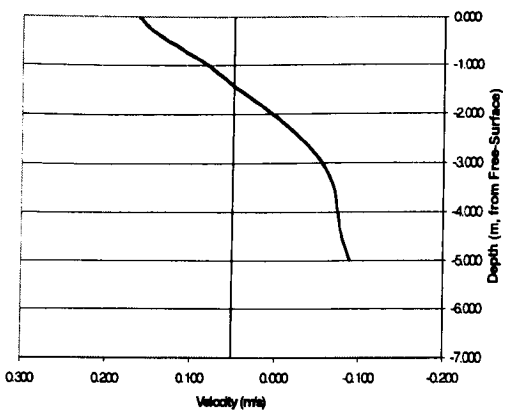

Cross-Section 5

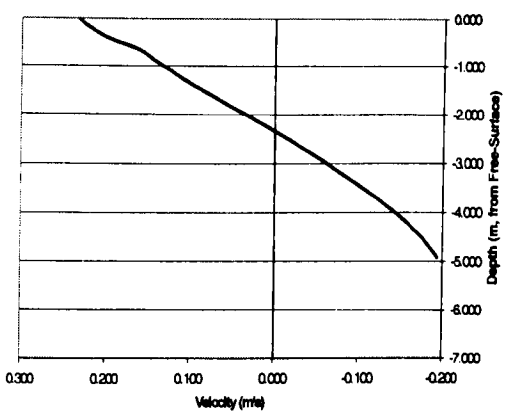

Cross-Section 6

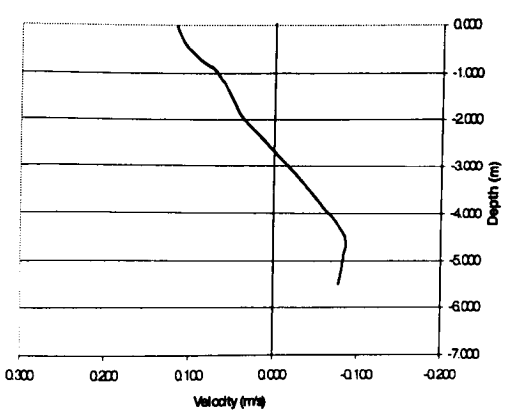

Cross-Section 7

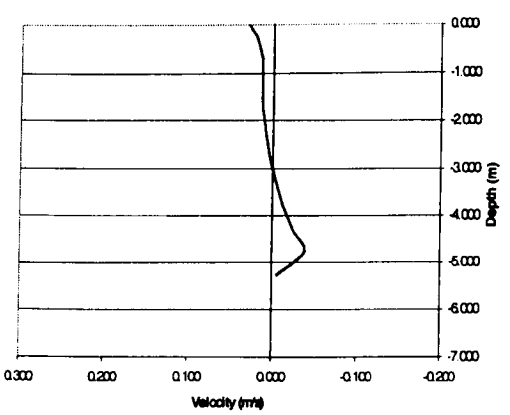

Cross-Section 8

Fig. 6.79 – River Ribble CFX Model: Recirculation (m/s) at Sections 5, 6, 7 and 8

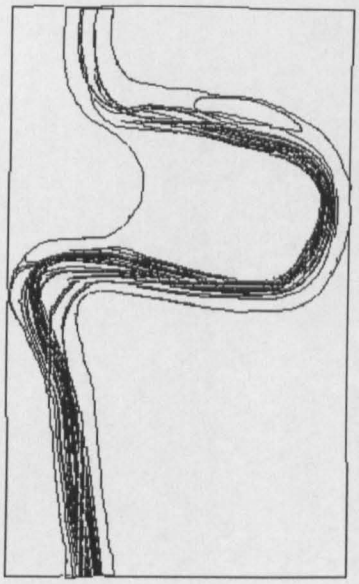

(a)

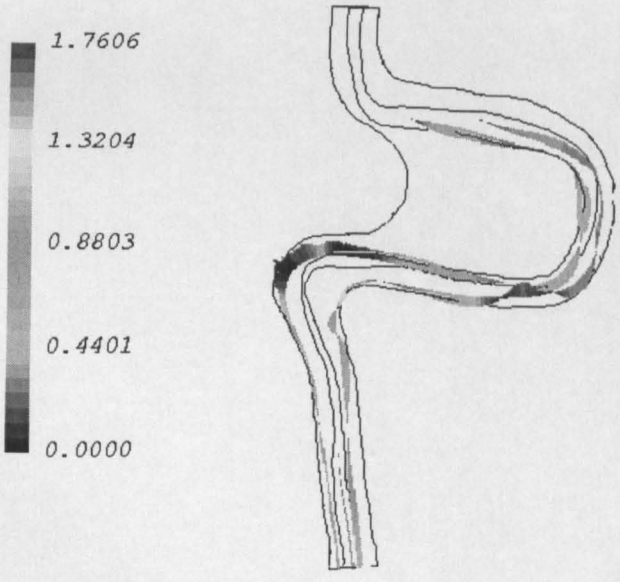

(b)

Fig. 6.80 – CFX Numerical Tracer Release at Elevation 7.0 m in the Ribble :
(a) Tracer Route
(b) Rotational effects and Velocity

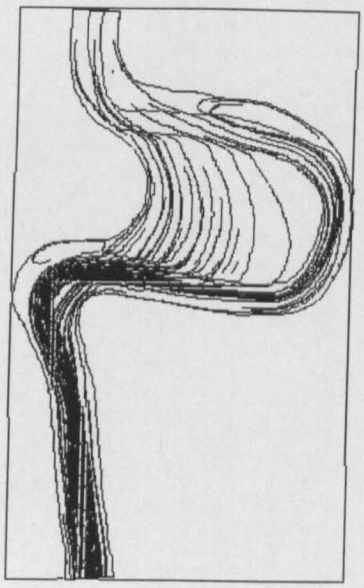

(a)

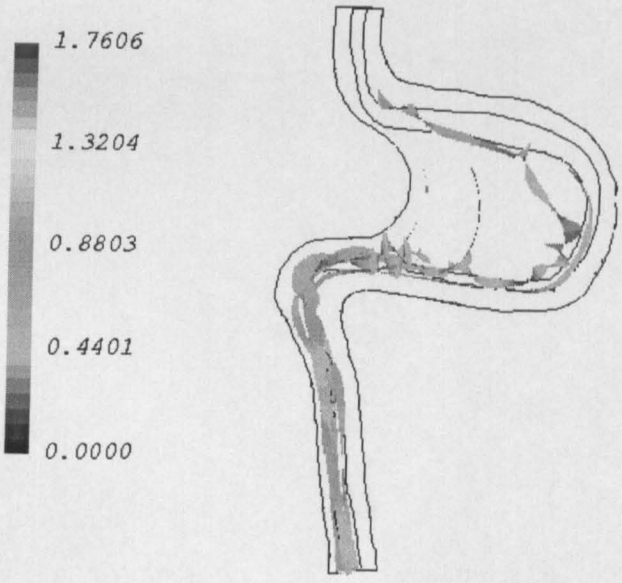

(b)

Fig. 6.81 – CFX Numerical Tracer Release at Elevation 10.0 m in the Ribble:
(a) Tracer Route
(b) Rotational effects and Velocity

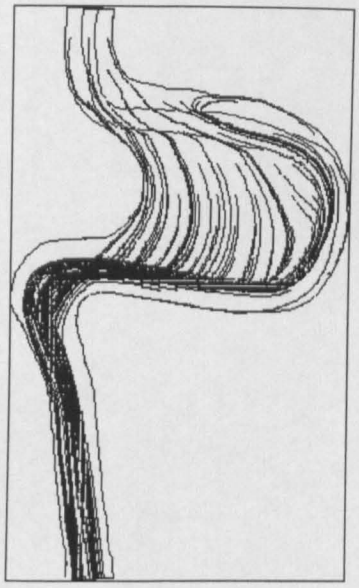

(a)

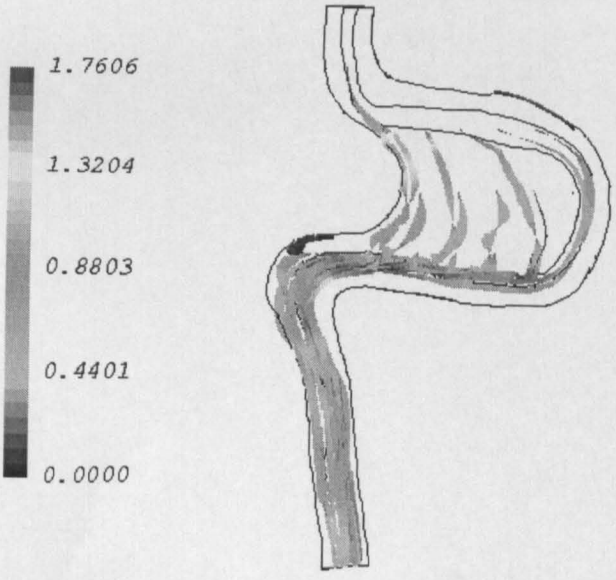

(b)

Fig. 6.82 – CFX Numerical Tracer Release at Elevation 10.5 m in the Ribble:
(a) Tracer Route
(b) Rotational effects and Velocity

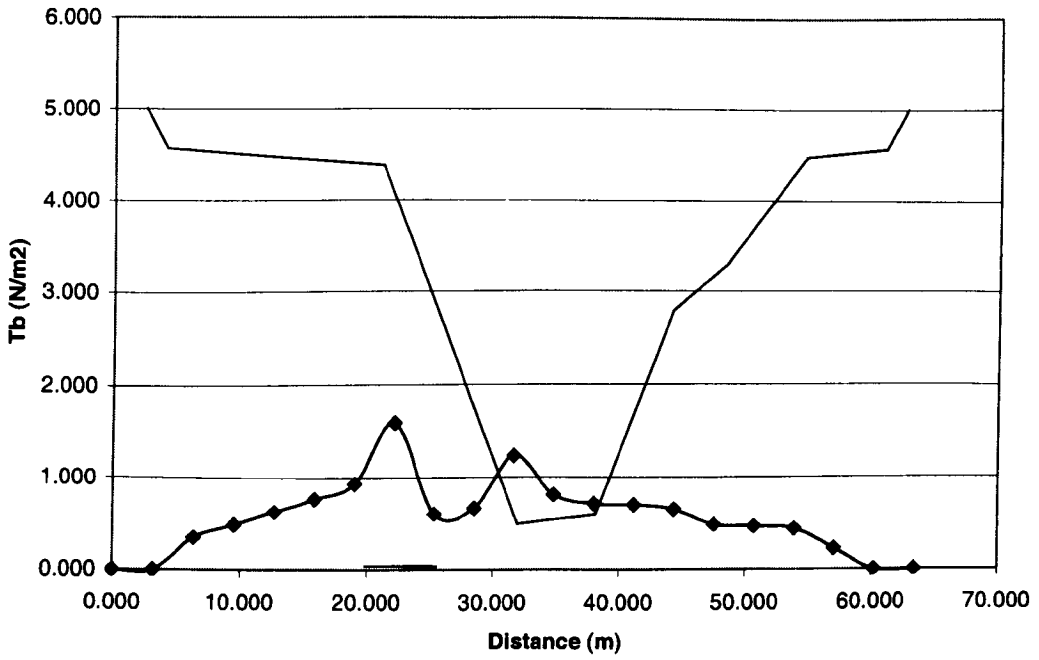

Fig. 6.83 – Calculated Bed Shear Stresses at Section 1 from River Ribble Model (k-ε model)

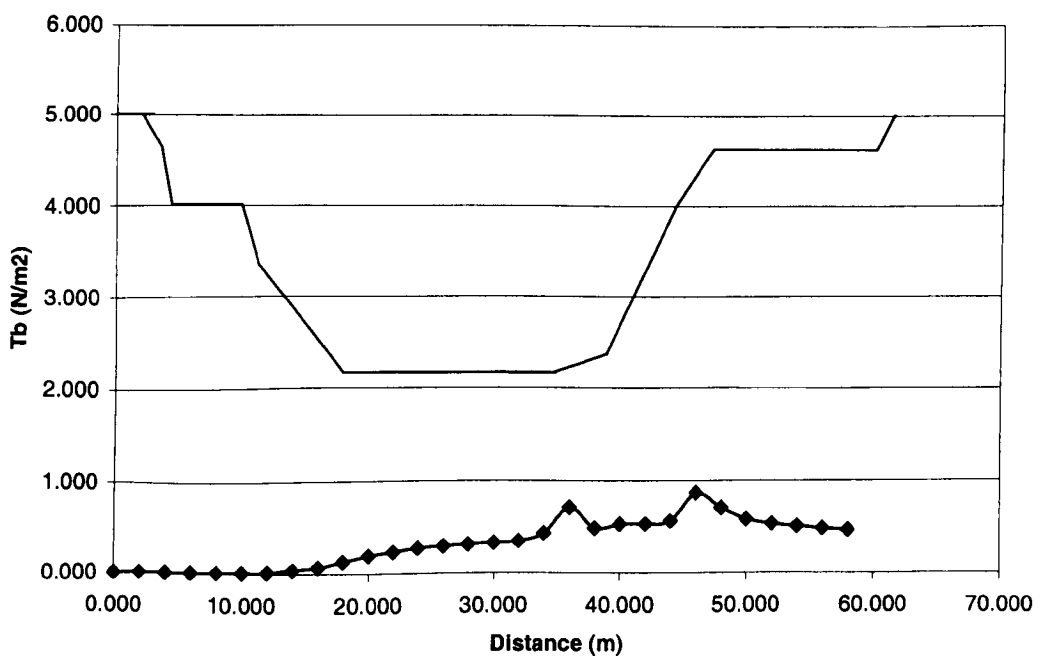

Fig. 6.84 – Calculated Bed Shear Stresses at Section 2 from River Ribble Model (k-ε model)

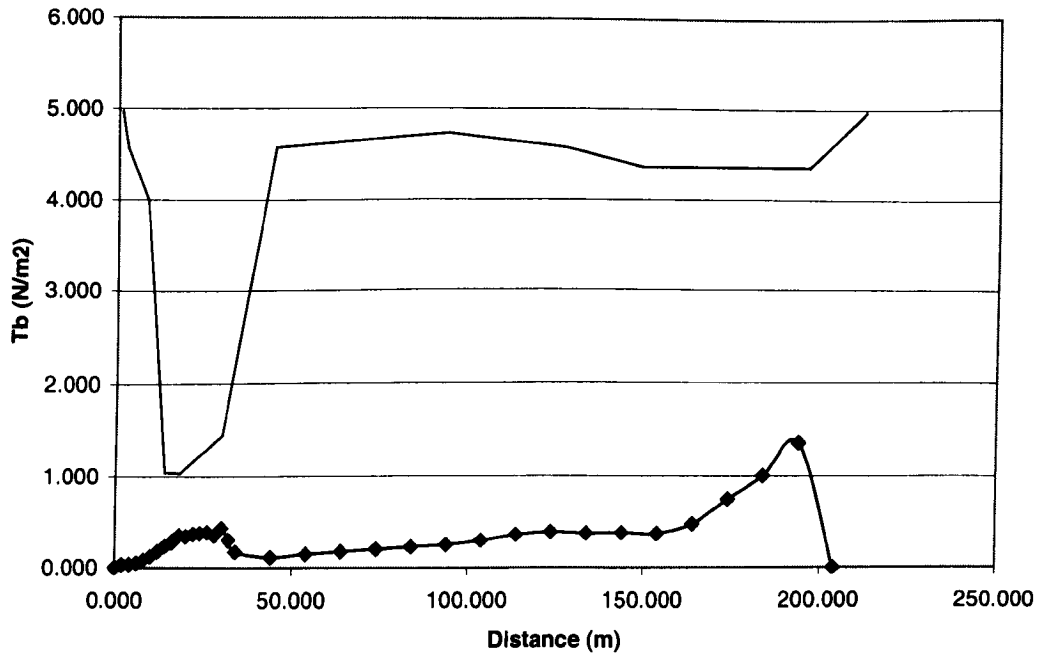

Fig. 6.85 – Calculated Bed Shear Stresses at Section 3 from River Ribble Model (k-ε model)

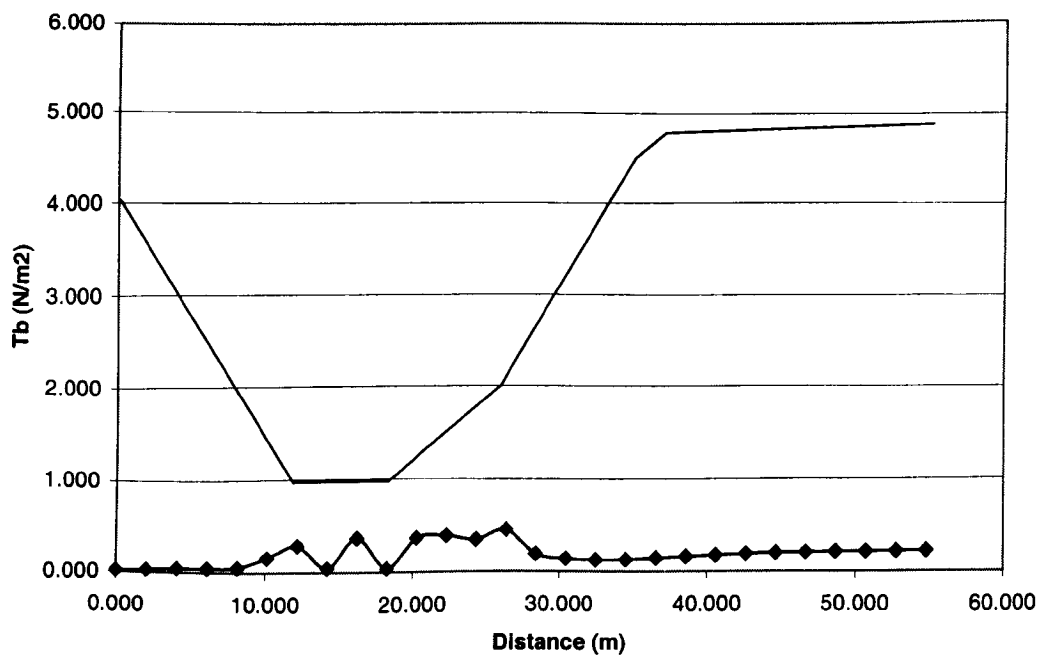

Fig. 6.86 – Calculated Bed Shear Stresses at Section 4 from River Ribble Model (k-ε model)

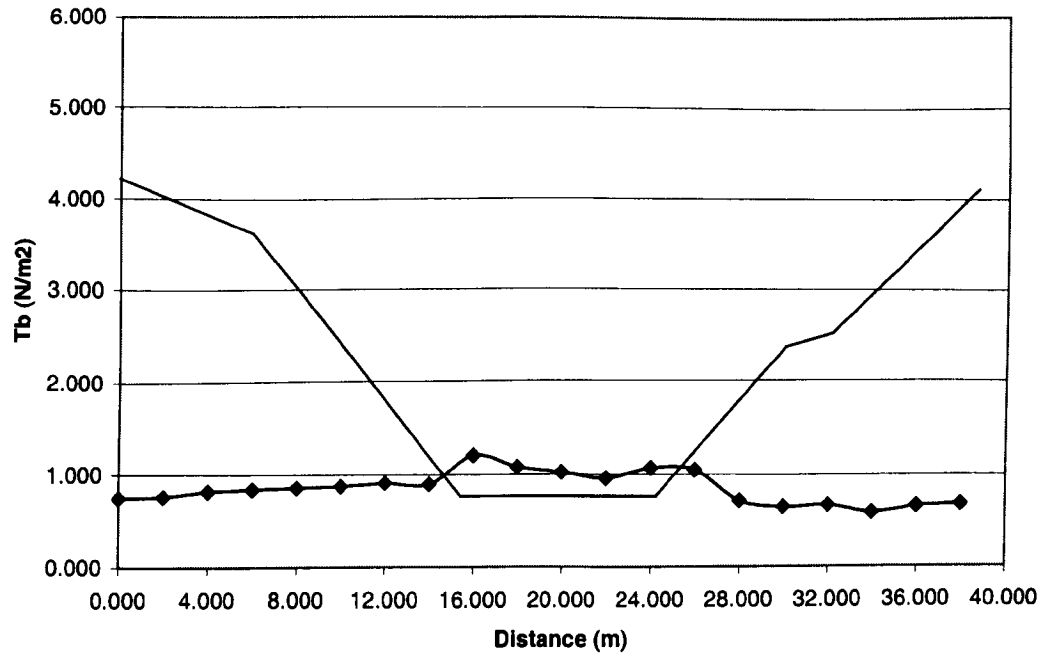

Fig. 6.87 – Calculated Bed Shear Stresses at Section 5 from River Ribble Model (k-ε model)

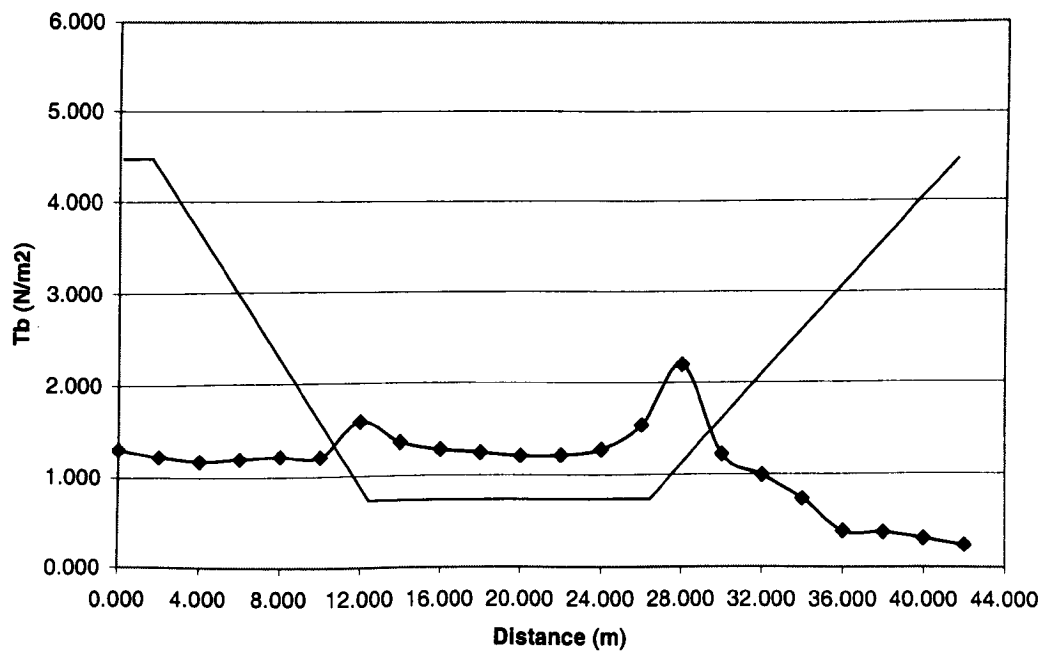

Fig. 6.88 – Calculated Bed Shear Stresses at Section 6 from River Ribble Model (k-ε model)

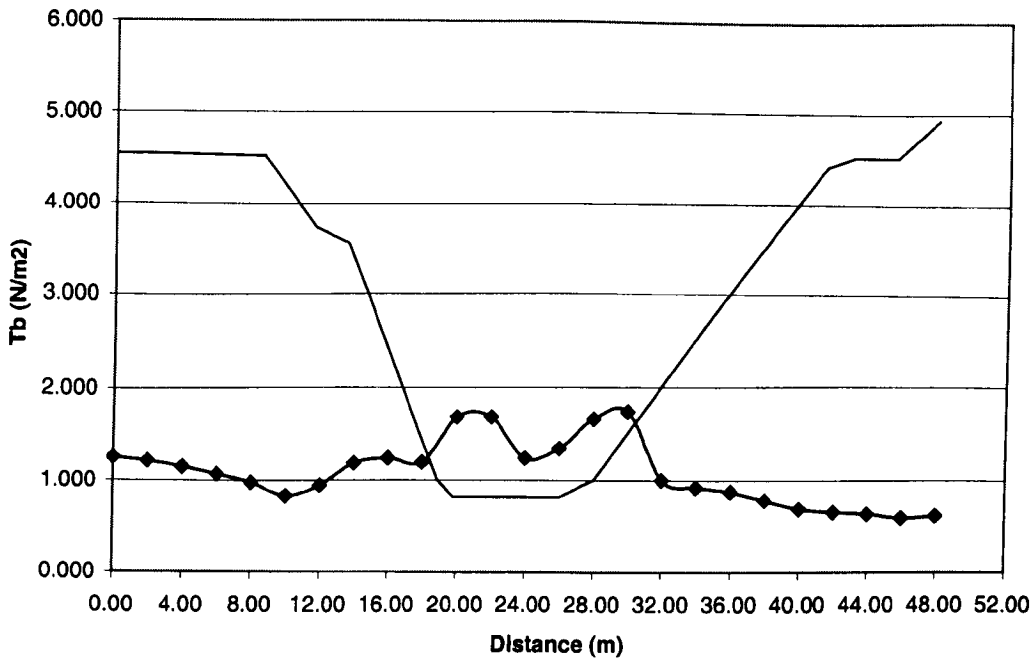

Fig. 6.89 – Calculated Bed Shear Stresses at Section 7 from River Ribble Model (k-ε model)

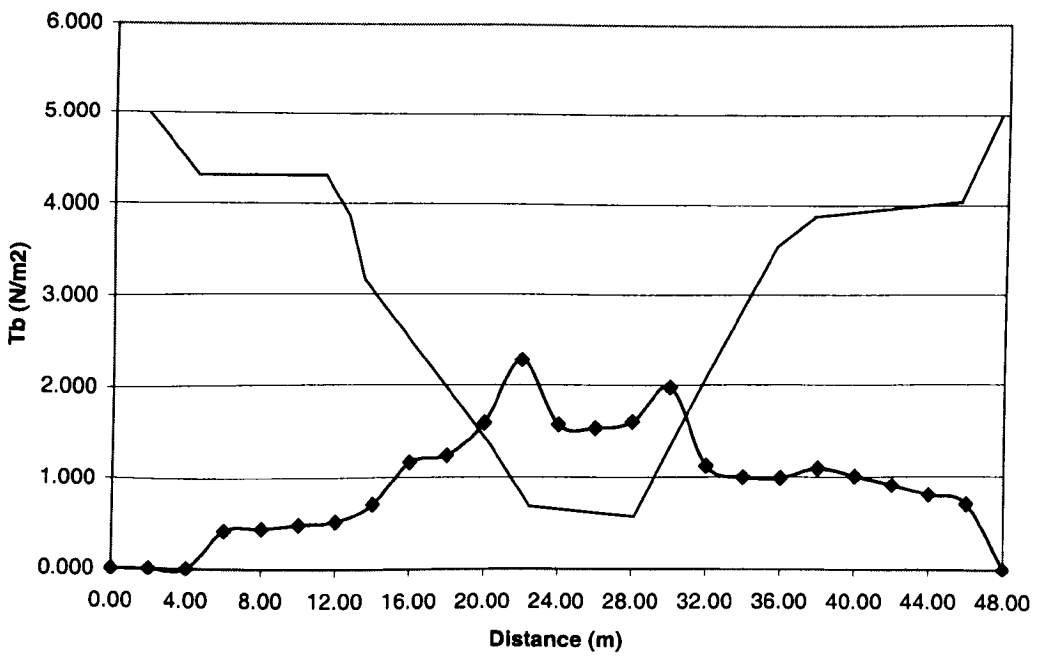

Fig. 6.90 – Calculated Bed Shear Stresses at Section 8 from River Ribble Model (k-ε model)

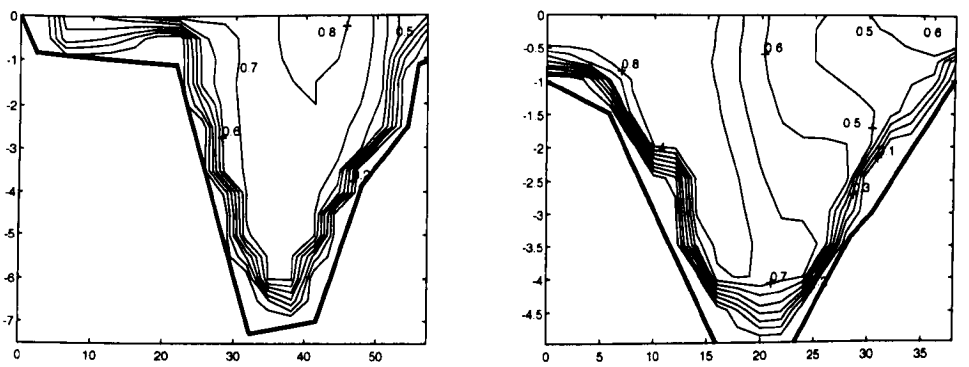

Cross-Section 1

Cross-Section 5

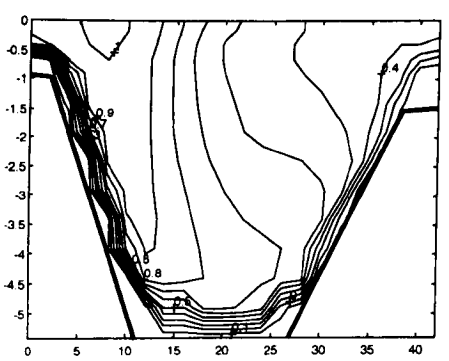

Cross-Section 6

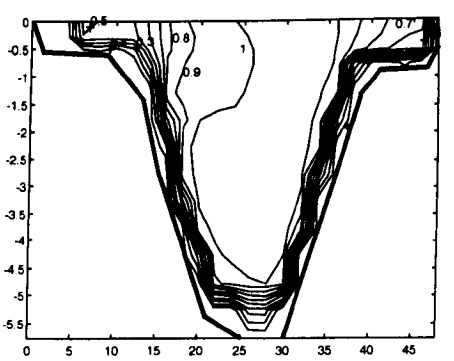

Cross-Section 8

Fig. 6.91 – River Ribble CFX Velocity Profile (m/s) at Cross-Sections 1, 5, 6 and 8 (k_s = 0.12 m on the flood plain, k_s = 0.08 m in the main channel, mesh R-1, RSM)

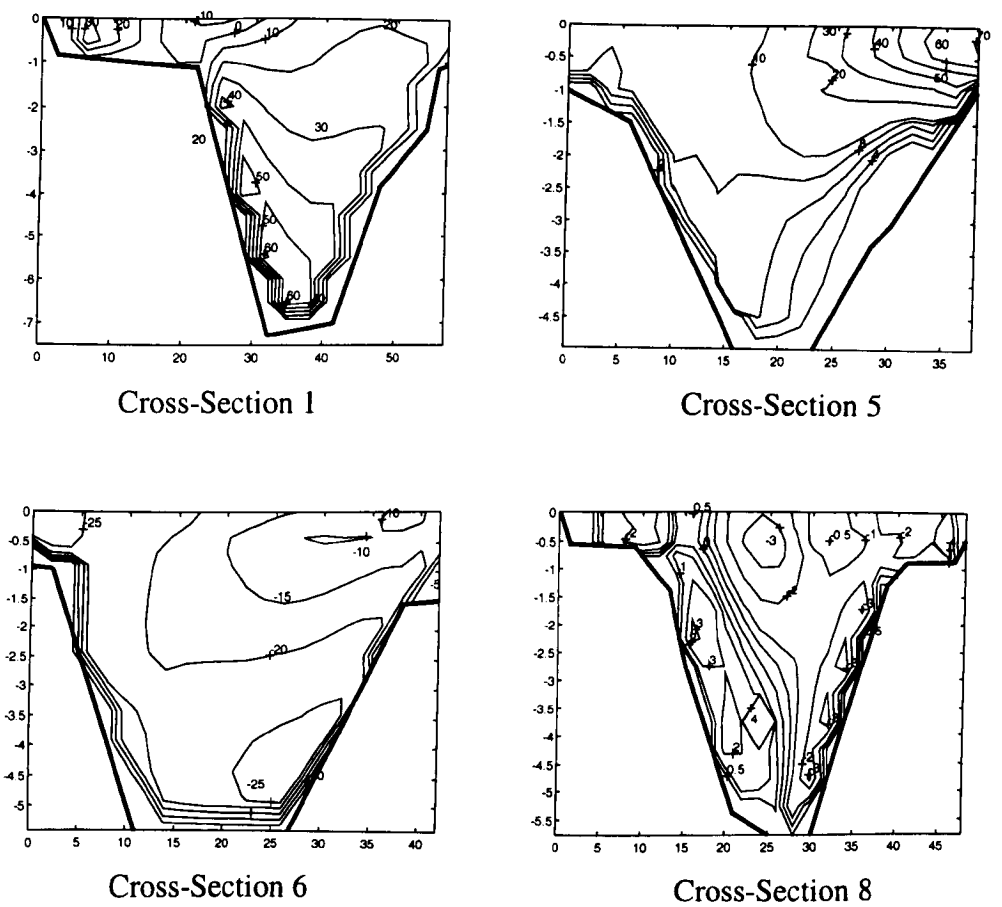

Fig. 6.92 – River Ribble CFX Velocity Orientation (deg.) at Cross-Sections 1, 5, 6 and 8 (k_s = 0.12 m on the flood plain, k_s = 0.08 m in the main channel, mesh R-1, RSM)